

e-ISSN : 2320-0847  
p-ISSN : 2320-0936



# American Journal of Engineering Research (AJER)

Volume 4 Issue 9– September 2015

[www.ajer.org](http://www.ajer.org)

[ajer.research@gmail.com](mailto:ajer.research@gmail.com)

## Editorial Board

### American Journal of Engineering Research (AJER)

**Dr. Moinuddin Sarker,**

Qualification :PhD, MCIC, FICER,  
MInstP, MRSC (P), VP of R & D  
Affiliation : Head of Science / Technology  
Team, Corporate Officer (CO)  
Natural State Research, Inc.  
37 Brown House Road (2nd Floor)  
Stamford, CT-06902, USA.

**Dr. June II A. Kiblasan**

Qualification : Phd  
Specialization: Management, applied  
sciences  
Country: PHILIPPINES

**Dr. Jonathan Okeke  
Chimakonam**

Qualification: PHD  
Affiliation: University of Calabar  
Specialization: Logic, Philosophy of  
Maths and African Science,  
Country: Nigeria

**Dr. Narendra Kumar Sharma**

Qualification: PHD  
Affiliation: Defence Institute of Physiology  
and Allied Science, DRDO  
Specialization: Proteomics, Molecular  
biology, hypoxia  
Country: India

**Dr. ABDUL KAREEM**

Qualification: MBBS, DMRD, FCIP, FAGE  
Affiliation: UNIVERSITI SAINS Malaysia  
Country: Malaysia

**Prof. Dr. Shafique Ahmed Arain**

Qualification: Postdoc fellow, Phd  
Affiliation: Shah Abdul Latif University  
Khairpur (Mirs),  
Specialization: Polymer science  
Country: Pakistan

**Dr. Sukhmander Singh**

Qualification: Phd  
Affiliation: Indian Institute Of  
Technology, Delhi  
Specialization : PLASMA PHYSICS  
Country: India

**Dr. Alcides Chaux**

Qualification: MD  
Affiliation: Norte University, Paraguay,  
South America  
Specialization: Genitourinary Tumors  
Country: Paraguay, South America

**Dr. Nwachukwu Eugene Nnamdi**

Qualification: Phd  
Affiliation: Michael Okpara University of  
Agriculture, Umudike, Nigeria  
Specialization: Animal Genetics and  
Breeding  
Country: Nigeria

**Dr. Md. Nazrul Islam Mondal**

Qualification: Phd  
Affiliation: Rajshahi University,  
Bangladesh  
Specialization: Health and Epidemiology  
Country: Bangladesh

<b>S.No.</b>	<b>Manuscript Title</b>	<b>Page No.</b>
<b>01.</b>	Borehole Drilling, Usage, Maintenance and Sustainability in Ado- Ekiti, Nigeria Oluwadare Joshua OYEBODE    Sunday Olakunle OYEGOKE    Kayode Olufemi OLOWE    Phillip ONOH    Victor Babafemi ADEBAYO	01-12
<b>02.</b>	A Budget Based Optimization of Preventive Maintenance in Maritime Industry Akpan, W. A .    Ogunsola, T.M.	13-20
<b>03.</b>	Analysis of Fractional Order Prey - Predator Interactions A.George Maria Selvam    R.Janagaraj    D. Abraham Vianny	21-25
<b>04.</b>	Estimation Technique of the number of nodes in underwater wireless communication network Eng. Md. Ismail Haque    Eng. Md. Nurul Anwar Tarek    Eng. Md. Ar Rafiul Faisal	26-30
<b>05.</b>	Applicability of Path Loss Prediction in Macrocellular Environment Using Artificial Neural Networks in Hyderabad City Syed Mudassar Ali    Mohammed Mouzam Ali	31-34
<b>06.</b>	Design of a Settling Basin for Small Scale Water Treatment Plant in Borno State, Nigeria Hussaini A Abdulkareem    Mahmud Awwal Tanimu    Ishaq T Muhammad    Sani M Suleiman	35-39
<b>07.</b>	To study the effect of temperature using pretreated rice straw to generate biogas S.Vivekanandan    S.Sathish	40-46
<b>08.</b>	Effect of Gate Length on the DC and RF Performance of GaN HEMT Devices Ahmet Toprak    Ozlem A. Sen    Ekmel Ozbay	47-53
<b>9.</b>	Extraction of Soluble Sodium Silicate using Corn Cob Ash as a Silica Source B.A. Ajayi    S.S. Owoeye	54-56
<b>10.</b>	Existence of Solution of Fractional Impulsive Delay Integrodifferential Equation in Banach Space R. P. Pathak    Piyusha S. Somvanshi	57-62
<b>11.</b>	Evaluation and Critical Technical Study of Li-Fi Compared with Wi-Fi and WiMax Technology Md. Biplob Hossain    Md. Selim Hossain    Md. Mahasin Ali    Md. Toufikur Rahman    Rupam Chandro    Farhana Matin    Md. Dulal Haque	63-71
<b>12.</b>	Broadening of Omnidirectional Photonic Band Gap in Graphene Based one Dimensional Photonic Crystals Neetika Arora    Rakhi Agrawal	72-75

## CONTENTS

<b>13.</b>	3D Design & Simulation of Printed Dipole Antenna Protap Mollick    Amitabh Halder    Mohammad Forhad Hossain    Anup Kumar Sarker	76-80
<b>14.</b>	Institutional and specialized Distance learning program accreditation Mehzabul Hoque Nahid	81-86
<b>15.</b>	Effects, Evaluation and Corrosion of Heat Exchangers Performance in Seawater Robert Poku    Bebetoidoh O. Lucky    Ezenwa A. Ogbonnaya	87-95
<b>16.</b>	Design and Development of Sound Control Door Lock System. Elechi Promise	96-107
<b>17.</b>	Quali-quantitative evaluation for the definition of antiseismic recovery interventions in historical buildings. D. Colapietro    M. Pinto    A. Fiore    F. Fatiguso    G.C. Marano	108-119
<b>18.</b>	Numerical Integration and a Proposed Rule Md.Amanat Ullah	120-123
<b>19.</b>	Adaptive Sliding Mode Control of Mobile Manipulator Welding System for Horizontal Fillet Joints Tran Duy Cuong    Nguyen Thanh Phuong	124-138
<b>20.</b>	OKUMURA-HATA: A PERFECT MODEL FOR DRIVING ROUTE UHF INVESTIGATION Omohimire P. Omolaye    Gabriel A. Igwue    Godfrey A. Akpakwu	139-147
<b>21.</b>	The Effect of Packaging Materials on the Quality Attributes of Crayfish During Cold Storage Ajala, A.S.    Abiola, T.A.	148-152
<b>22.</b>	ORGANIC LIGHT EMITTING DIODE (OLED) Aririguzo Marvis Ijeaku    Madu Hilary Chidubem    Emerole Kelechi Chukwunonyerem    Nwogu Uchenna Obioma	153-159
<b>23.</b>	Fluid Flow through Woven Fabrics by the Lattice-Boltzmann Method Mohammad Miyan    Pramod Kumar Pant	160-167
<b>24.</b>	The Effect Of Chemical Treatment On Tensile Properties Of Soil Retted Entada Mannii Fibres. O.P. Balogun    J.A. Omotoyinbo    K.K. Alaneme    I.O. Oladele    B.J. Babalola	168-175
<b>25.</b>	Determination of traffic delay at selected intersection within Ilorin Metropolis OladelePopoola    JohnWasiu    Abimbola Owolabi	176-180

## CONTENTS

26.	Power Flow Analysis for Elastic Coupling Plates. Fei Han, Min-qing Wang	181-187
27.	Security and Architectural Patterns for Securing the Cloud Architecture Golajapu Venu Madhava Rao    Venu Madhav Kuthadi    Rajalakshmi Selvaraj	188-191
28.	Influence of microwave pre-treatment on the flotation of low-grade sulphide ore Omoyemi Ola-Omole    B.O Adewuyi    J.O. Borode    P.A. Olubambi	192-197
29.	A Feasibility Study on Sustainable Management of Municipal Wastes in Ogbomoso Olatunde Ajani Oyelaran    Ibrahim Rufai	198-204
30.	Data-Collection using Clustering Approach in Wireless Sensor Network Design based on Heuristic Algorithms Vishwaja B    Mrs. Geetha	205-211

## Borehole Drilling, Usage, Maintenance and Sustainability in Ado- Ekiti, Nigeria

Oluwadare Joshua OYEBODE<sup>1</sup>, Sunday Olakunle OYEGOKE<sup>2</sup>, Kayode Olufemi OLOWE<sup>3</sup>, Phillip ONOH<sup>4</sup>, Victor Babafemi ADEBAYO<sup>5</sup>  
*Civil Engineering Department, College of Engineering, Afe Babalola University, Ado- Ekiti, Nigeria.*

**Abstract:** Boreholes are an effective way of tapping into the water bearing aquifer below the ground and pumping the water to the surface. Boreholes for extracting water consist essentially of a vertically drilled shaft, a strong lining (casing) to prevent collapse of the walls, which includes a means of allowing clean water to enter the borehole space (screen), surface protection, and a means of extracting water. This study examines the common drilling techniques, usage, maintenance and sustainability of water boreholes in Ado-Ekiti. Pumping tests were carried on several boreholes in Ado-Ekiti to acquire a general idea of the yield of boreholes in order to proffer viable solution. Hydro geological maps of the area are studied to help in the understanding of the sub surface formation of the region. Questionnaires were also developed and administered in the assessment of borehole usage and maintenance. The study area is characterized by crystalline basement complex rock of low porosity and permeability. Boreholes have to be properly designed, professionally constructed and carefully drilled. It has been discovered that the area generally has low groundwater potential and that there is a high dependence on groundwater as a source for potable water.

### I. Introduction

With rising utility costs and water bills, installing a borehole is fast becoming a viable way to obtain 'cheaper' water for many people. Depending on water usage, boreholes are capable of generating a rapid investment payback, often cutting costs by up to 80% over a metered mains supply. A borehole is basically a narrow vertical shaft bored in the ground. A borehole may be constructed for many different purposes, including the extraction of water or other liquids such as natural petroleum or gases such as natural gas. This brings us to the aim of this study, which is to analyse borehole drilling techniques, borehole maintenance, problems encountered while drilling, borehole usage and sustainability in Ado Ekiti. The exploitation of ground water is a complicated process which involves sinking a narrow shaft into the ground to reach the aquifer by using a drilling rig. Failure is sometimes experienced when carrying out borehole drilling operations or when using installed borehole systems. These failures are caused by several complications which may arise from poor maintenance and rehabilitation of boreholes, lack of expertise poor choice of technology, and poor supervision of the drilling project. In order to prevent these complications, the following measures must be taken: proper maintenance and rehabilitation of bore hole, proper pump installation and maintenance, proper supervision of borehole projects, the use of appropriate drilling technology and the standardization of borehole design and drilling process. Water is a regional resource and it is not always readily available. This has led to shortage of potable water in some parts of the world. Water shortage is becoming a global issue due to increasing population, economic growth and climate change. Development of new sources of new water sources together with conservation measures should be an important component of any country's national water plan.

The construction of a well, using manual and mechanical drilling techniques is a complicated process. Before drilling starts a good drilling site has to be selected, where experience suggests that there will be an adequate quantity of good quality groundwater. During the drilling process there are a lot of different aspects which require attention to prevent things from going wrong. Besides the practical drilling skills which are executed at ground level, at the same time attention has to be paid to important processes which are happening below ground level during drilling. Water used in drilling (working water) could flow away or worse; the borehole could collapse, burying part of the drilling equipment. And finally, once the hole has been drilled, the well casing, screen and sanitary seals have to be installed at the right depth, preventing contaminated water from entering, and ensuring a sufficient yield. In many countries manual drilling teams experience problems with site selection, loss of working water, soil determination, logging, well installation, well development, water quality

and well yield (flow rate of the well). These problems may occur when the drilling process is not completely understood and important steps are missed. Figure 1 and 2 shows the map and Hydro geological map of Ekiti state. With the information provided we will be able to understand what takes place beneath the surface during drilling. This will enable us to construct high quality water wells.

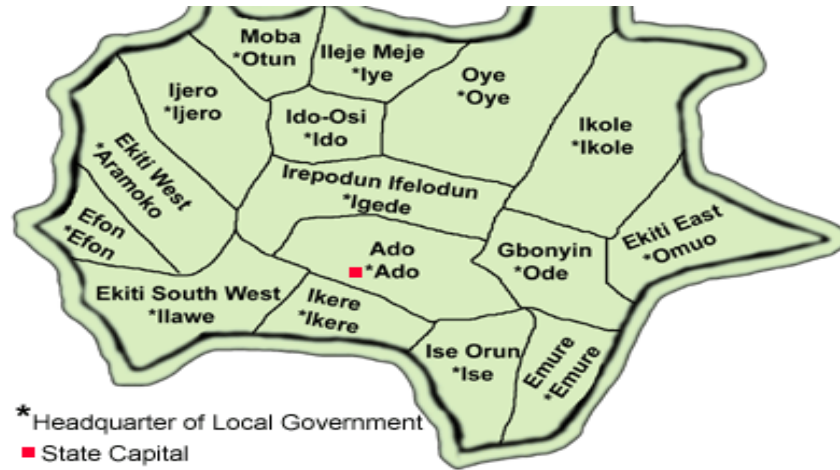


Figure 1: Map of Ekiti State

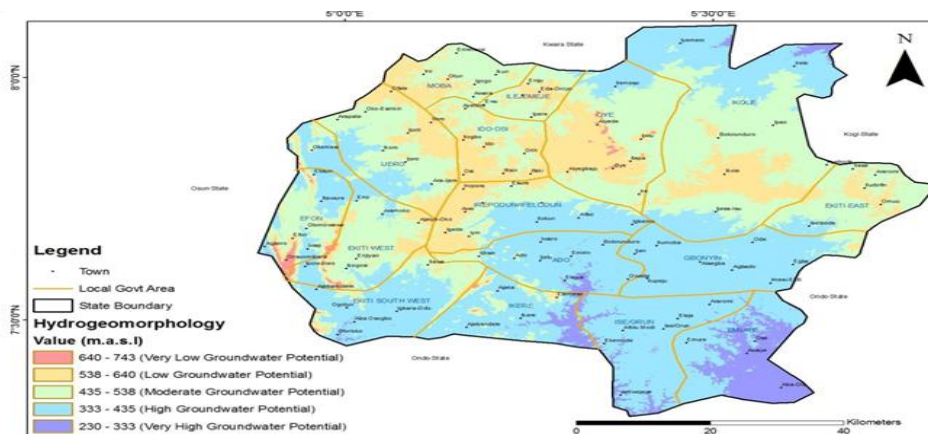


Figure 2: Hydro geological map of Ekiti state

## II. Methodology

### Project activities

Table 1: Project activities

S/N	Work done	Contribution to knowledge
1.	Development of questionnaire	To evaluate the usage and maintenance of boreholes in ado Ekiti
2.	Survey of the population of ado Ekiti	To determine water demand of ado Ekiti
3.	Conduct pumping tests on various boreholes in the study area	To determine the rate of discharge, rate of recharge, transmissivity, storativity and permeability of the aquifer.
4.	Study geophysical investigations carried out on the groundwater potential of ado Ekiti	This will enable me have a better understanding of the characteristics of the sub surface layers beneath the study area.
5.	Observe and help in the planning and construction of boreholes in ado Ekiti	This will help me acquire information on the common drilling methods used and problems encountered before, during and after the drilling of boreholes.

### 2.1 Population of area

The population of Ado-Ekiti has increased tremendously in the last decade. This is due to its new status of being the capital of Ekiti-State, carved out of the old Ondo State in 1996. As a result of this, there has also been corresponding increase in demand for potable water by the inhabitants for both domestic and industrial usages. However, public water supply has been inadequate in spite of efforts of government and the water

corporation. The shortfall in water demand has been partly met by groundwater development through hand dug wells, springs and the available boreholes. According to Ekiti State Rural Water Supply and Sanitation Agency, the failure rate in the previously drilled boreholes in the State is around 54%. This is probably due to lack of detailed hydro geological and pre-drilling geophysical investigation or poor understanding of the hydro geological characteristics of the Basement complex environment. The study area is underlain by Precambrian basement complex rocks. These rocks are characterized by low porosity and near negligible permeability. The highest groundwater yield in basement terrains is found in areas where thick overburden overlies fractured zones. These zones are often characterized by relatively low resistivity values. (Olorunfemi and Fasuyi, 1993).

## 2.2 Cost analysis for a borehole

The cost of a borehole is largely dependent upon the depth and amount of casing that the borehole will require. Geology (the type of rock formations) that has to be drill through does have some influence as do the actual ground conditions. Many people expect the easiest drilling to be into soft and loose geologies; however the opposite is generally true. One of the main difficulties with drilling is keeping the borehole open during the drilling process; this is made more difficult if the hole is collapsing owing to the ground being loose and unstable. Many methods could be employed to prevent this from happening, including the use of drilling additives and fluids and the installation of temporary steel casing. All these factors affect the cost of a borehole.

**Cost of mobilization to and from site:** This is the cost of getting all drilling equipment from the storage yard to home or site of the client. The cost is usually depends on whether the equipment is wheeled or tracked and on the distance travelled to reach the site.

**Cost of drilling:** The cost for drilling is determined per meter for different diameters. The borehole usually starts at a larger diameter of about 203mm and this is drilled into the solid rock to allow for the casing to be installed through the soft upper portions and prevent collapse. The bore is then continued at a diameter of 165mm through the solid rock to the target depth or the saturated region. Most rock types are drilled at the same rate, however quartzite which is very abrasive is charged at a higher price because it wears the drill bit down quickly. Typical costs for drilling in ado-Ekiti are between N5, 000–N8, 000 per meter.

**Cost for casing and gravel packing of borehole:** This is the cost per meter for the supply and installation of casing. Most boreholes only require steel casing through the soft weathered overburden (12-24m) to secure the upper parts of the borehole from collapse, however some boreholes are drilled into highly weathered rock which extends a lot deeper down than usual. These types of boreholes require the installation of screens and casing from surface to the end of the hole. We use PVC casing and screens in these. A gravel filter pack is placed around the outside of the screens to keep sand out of the well and allow the water through. Typically costs for casing are around N7, 000 per meter for PVC casing and screens.

**Cost of installation of well head:** The well head is installed over the head of the borehole to allow access to the borehole and protect it from contamination. The well head should be made of reinforced concrete so as to withstand load. The cost of installation is around N22,000.

**Cost of developing and flushing of the borehole:** Developing and flushing of borehole is one of the most important procedures undertaken once the borehole has been drilled. This procedure helps remove rock fragments which could get caught up in the aquifer cracks and thereby blocking water from entering the borehole. All boreholes that reach water should be developed until they are sand free. The cost of developing a borehole is around N25, 000.

**Cost of cleaning up the site:** Borehole drilling can be messy. All the soil, mud and rock fragments which come out of the hole accumulate on the surface making a huge mess. The drill cuttings should be cleaned up and taken away from the site. The final clean up happens when the rig moves off the borehole. Cleaning of the site is usually the obligation of the drillers.

**Water analysis:** If the water is to be used in the home then it recommended that a potable water analysis of the borehole be undertaken by a registered water lab. It is important that the water sample be taken after some time of pumping and that the sample gets to the lab and is analysed for pathogens within 6 hours of sampling. This test costs about N65, 000.



**Cost of pumping system:** The cost for the supply, installation and commissioning of a pumping system largely depends on the depth of the borehole, piping, amount of water to be pumped and the pressure requirements of the system. Typical costs for an average home water supply pump range from N850, 000 – 1,085,000.

**Table 2:** Cost Analysis for a Borehole

S/N	TASKS	COST
1.	mobilization to and from site	Depends on distance
2.	Drilling operation	N5, 000 to 8, 000 per meter
3.	installation casing and gravel packing of borehole	About N7, 000 per meter
4.	installation of well head	About N22,000
5.	Developing and flushing of the borehole	About N25,000
6.	Cleaning up of site	Depends on the volume of materials removed from well
7.	Water analysis	Around N65,000
8.	Supply, installation and commissioning of pumping system	N850,000 – N1,085,000
9.	Payment for service (workmanship)	Depends on negotiation between client and company

### 2.3 Site investigation

In order to carry out this project successfully, Investigations were carried out on five boreholes in the following regions of Ado Ekiti; Ado Ekiti North, Ado Ekiti South, Ado Ekiti West, Ado Ekiti East and Ado Ekiti Central. The geophysical survey was carried out on the borehole construction site beside Afe Babalola University, Ado-Ekiti in order to determine the ground water potential of the area. The method used in geophysical survey for the proposed water boreholes was the electrical resistivity sounding. The electrical resistivity sounding method is the most common method used to carry out geophysical surveys in the state.

The site selection strategy is to maximize the probability of successfully completing the borehole, at a site with favorable geological, hydro geological, and geochemical conditions, within budgetary and schedule constraints.

#### Site Description

The survey site is Afe Babalola secondary school proposed site ado-Ekiti. There are no structures on the site. The compound is well fenced and the topography is relatively level. The area is characterized by short dry season and long wet season and has high rainfall of about 160mm and peak rainfall between August and September. The area has high temperature ranging between with relatively high humidity during the wet season and low humidity during the dry season.

The area is characterized by dense ever green forest. The basement complex rocks are crystalline rocks of low porosity and permeability. In this geologic environment groundwater accumulation depends on:

1. Degree of weathering and thickness of the overburden
2. Degree and nature of fracturing of the rocks
3. The presence and absence of clays above the weathered zone and its effect on rate of infiltration of water into the aquifer
4. The hydrological continuity (permeability) of the weathered zone.

Source of recharge in the area include stream and precipitation, cracks, fractures bedrock depression and weathered basement. The sources of recharge mentioned above are the geologic subsurface structure in basement terrain that can favour groundwater accumulation. Porosity, permeability and transmissivity are the parameters of an aquifer. A good aquifer must have high porosity, high permeability and transmissivity.

#### Electrical resistivity soundings

The electrical resistivity test was started by putting two iron pins (called ‘current electrodes’) into the ground.

1. The current electrodes were then subjected to electricity. The electricity flows through the ground from one current electrode to the other, in a half circle (see below).
2. The resistance that the electricity finds on its way is measured by two other electrodes, the ‘potential electrodes’. The resistance depends on the distance between the two current electrodes, the soil formation through which the current flows and the humidity in this formation.
3. The electrical Resistivity sounding is used to determine the resistivity at different depths in the underground.
4. The current electrodes are placed each time further apart from each other in the ground and each time the resistance is measured. The further the current electrodes are placed apart, the deeper the electricity flow will reach. This way of working is often used when a suitable location for one borehole needs to be determined.

5. In case information is required over a larger area of which the approximate depth of the aquifer is known, electrical resistivity soundings are done at different points, each time at the same depth. In that way the resistivity is measured at a certain depth at different locations in an area. This is done by having for each measurement a fixed distance between the current electrodes while repeating the measurements along a number of traverses over an area in a grid pattern.
6. The outcome will make it possible to plot the resistivity values on a map, indicating zones of high and low resistivity (meaning zones of different groundwater potential) at a certain depth in the underground.
7. All the information obtained is entered into a computer that analyses the measurements with special software.

The idea is that if there is water underground the electricity will flow more easily through it because the resistance in wet ground against a flow of electricity is lower than such resistance in dry ground. Therefore the computer can predict based on the measurements where water will probably be. However, good skills are required to interpret the outcome of the computer program. The resistance measured also depends on the type of soil, which makes it difficult to interpret the outcome properly. In other words, the software cannot tell you just like that whether there is water in the underground formation and how deep it is. It requires someone who knows how to interpret the outcome of the computer analysis to predict this by analysing the outcome of the computer program along with knowledge about the soil and soil layers in the underground formation, information about other boreholes in the area.

#### 2.4 Causes of Borehole Failures

According to Ekiti State Rural Water Supply and Sanitation Agency, the failure rate in the previously drilled boreholes in the State is around 54%. This is probably due to lack of detailed hydro geological and pre-drilling geophysical investigation or poor understanding of the hydro geological characteristics of the Basement complex environment. Borehole failure is defined as a situation when a borehole which was recorded as successful, or productive immediately after drilling, subsequently fails to deliver a sufficient yield of safe as follows:

- Drilling of crooked boreholes which affect installation of casing, screens and pumps
- Poor collection of samples, and essential data like penetration rate log, lithological log during drilling operation. This can lead to poor design and subsequently well failure.
- Use of drilling fluid in such proportion that will lead to sealing of the intake portion of the well with mud cake or cause excessive mud invasion into the aquifer system
- Use of substandard casings and screens in an attempt to save cost. This can result into causing an incursion of soil or formational materials into the well
- Use of inappropriate gravel packs materials like rock chippings
- Lack of placement of sanitary seal or grout.

Borehole failure is defined as a situation when a borehole which was recorded as successful, or productive immediately after drilling, subsequently fails to deliver a sufficient yield of safe water throughout the year. Problems associated with water well drilling result from many causes including equipment failure, depletion of the aquifer, corrosive qualities of the water and improper well design and construction.

#### 3.0 Borehole drilling

Once the water requirements are known and an assessment either by a hydrogeologist or an examination of geological maps has been undertaken, the borehole can be drilled according to the information found. Typically, a borehole used as a water well is completed by installing a vertical pipe (casing) and well screen to keep the borehole from caving in. Drilled wells are typically created using either top-head rotary style, table rotary, or cable tool drilling machines, all of which use drilling stems that are turned to create a cutting action in the formation, hence the term 'drilling'. Boreholes can vary in depth and design depending upon the level of the water table, quantity of water stored in the ground and the requirements of the customer but typically are between 60-120 vertical metres. Normally the inner pipe is at least 4" in diameter to accommodate a 3" or 4" borehole pump and must be surrounded by gravel to prevent dirt clogging up the plastic pipe then sealed near the surface using a special grout. This grout usually goes down as far as the impermeable layer and is designed to prevent contamination from surface water entering the borehole. The outer metal casing pipe is usually at least 6" diameter to accommodate all this.



Figure 3: Typical borehole drilling showing water flow

**Ado Ekiti east (Afe Babalola university talent discovery centre) Boreholes 1**

S/N	Depth (m)	Lithology
1.	0.00 – 1.00	Rusty red lateritic sand, coarse
2.	1.00 – 2.00	Rusty red lateritic gravel
3.	2.00 – 3.00	Rusty lateritic mud, coarse sand, gravel
4.	3.00 – 4.00	Mud greyish brown, gravel
5.	4.00 – 6.00	Light greyish brown weathered base complex
6.	6.00 – 8.00	Greyish granite base complex
7.	8.00 – 35.00	Dark- grey – greenish horn blends
8.	35.00 – 40.00	Dark grey mica schist – gneissic basement complex
9.	40.00 – 46.00	Dark grey granite basement complex
10.	46.00 – 50.00	Dark grey granite basement complex
11.	50.00 – 70.00	Dark grey mica schist

**Ado Ekiti north (EKSU campus) Borehole**

S/N	DEPTH (m)	LITHOLOGY
1.	0.00 – 6.00	Weathered basement
2.	6.00 – 89.00	Fresh fractured basement

**Ado Ekiti west (better life) borehole**

S/N	DEPTH (m)	LITHOLOGY
1.	0.00 – 3.50	Top soil
2.	3.50 – 70.00	Granite basement

**Ado Ekiti central (Christ school) Borehole**

S/N	DEPTH (m)	LITHOLOGY
1.	0.00 – 1.00	Rusty yellow mud, very coarse sand
2.	1.00 – 4.00	Yellowish grey micaceous coarse sand
3.	4.00 – 6.00	Grey micaceous, very coarse sand gravel
4.	6.00 – 9.00	White – yellow, large gravel, very coarse
5.	9.00 – 11.00	Shale dark grey, whitish gravel, sand
6.	11.00 – 12.00	Sand brown coarse, gravel silty shale
7.	12.00 – 14.00	Dark grey, grey silty sand, gravel
8.	14.00 – 17.00	Grey granitic base complex
9.	17.00 – 20.00	Grey gneissic base complex
10.	20.00 – 27.00	Greyish – black micascist base
11.	27.00 – 56.00	Black – grey hornblende / micashist
12.	56.00 – 68.00	Black – grey hornblende / micashist base complex

**Ado Ekiti south (Mary Assumption Hospital) Borehole**

S/N	DEPTH (m)	LITHOLOGY
1.	0.00 – 1.00	Dark brownish top sandy soil, fine grain
2.	1.00 – 2.00	Poorly sorted, angular, brownish coarse grained sand
3.	2.00 – 7.00	Moderately sorted fine to medium grained, yellowish to brownish sand, light brown lay.
4.	7.00 – 8.00	Light brown clay
5.	8.00 – 9.00	Moderate well sorted light gneissic base complex.

**III. TESTING, RESULTS AND DISCUSSION OF RESULTS**

**Total water demand for Ekiti state**

Assuming water requirement/head/day = 100liters  
 Total population of state from table = 2,384,212  
 Total water demand = total population × water requirement/head/day  
 =2,384,212 × 100liters  
 =238,421,200liters/day  
 =238,421.2 m<sup>3</sup>/day

**Total water demand for ado Ekiti**

Assuming water requirement/head/day = 100liters  
 Total population of Ado Ekiti from table = 308,621  
 Total water demand = total population × water requirement/head/day  
 =308,621 × 100liters  
 =30,862,100liters/day  
 =30,862.1 m<sup>3</sup>/day

**Pump test analysis**

The purpose of the following pump test analysis is to determine the aquifer characteristics for various boreholes in ado Ekiti thereby assessing the viability and possible use of groundwater in conjunction with supply based on the assumptions of pumping tests (Kruseman and ridder, 1970)

**Assumptions**

1. Flow into well is radial and there are no entrance losses
2. Instantaneous release of water from storage upon lowering of the draw-down curve (no lag) when pumping.
3. There is no seepage or leakage from or to the aquifer
4. Prior to pumping the piezometric surface is horizontal
5. There is complete penetration of the aquifer by well.
6. Aquifer is homogenous, isotropic, uniform and of infinite areal extent.
7. Well radius is infinitesimal and pumping rate is constant.

The determination of the following parameters below indicates the viability of the aquifer and their pumping.

T= transmissivity (ability of aquifer to permit groundwater)

S<sub>c</sub>= storage coefficient (storage capacity of the aquifer)

E = well efficiency

S<sub>p</sub>= specific capacity of borehole or well.

**II Method of Analysis**

Almost all the aquifers investigated in the study area behave as confined aquifer in which water is present in weathered portions of the basement crystalline complex and the flows fit the non-steady state conditions.

The possible methods of analysis are

1. Theis recovery method
2. Jacob’s approximate method
3. Brereton step drawdown pumping test method
4. Eden and hazel method

Equation of drawdown

$$S = \frac{Q}{4\pi T} \cdot W(u)$$

Brereton’s method, based on equal time duration in the steps in pumping, is similar to lewis clark’s explanation for computing the total drawdown in step drawdown step tests.

$$S_m = a(Q_m \log bt + D_m) + CQ^2 \dots\dots\dots (i) \text{ Brereton’s equation}$$

$$S_{wt} = (a + b \log t)QLCQ^2 \dots\dots\dots (ii) \text{ Lewis Clark’s equation}$$

Where

$W(u)$  = well function with  $u = \frac{r^2 s}{4Tt}$

$a$  = Aquifer coefficient =  $\frac{2.30}{4\pi T}$

$b$  = Aquifer coefficient =  $\frac{2.25T_t}{rw^2 S_c}$

$e$  = Well loss coefficient

$Q_m$  = Pumping rate at the  $n^{th}$  step

$S_{wt}$  = Drawdown at start time  $t$

$S_m$  = Drawdown at the end of the  $n^{th}$  step

$$D_m = (Q_m - 1 \log 2 + Q_m - 2 \log \frac{3}{2} + Q_1 \log \frac{m}{m-1})$$

The two equations are best suited for short duration step pumping say 90mins each (Brereton1979) and show no immediate movement towards steady state or equilibrium. In any case, they require more than three steps for their effective use.

The recommended and modified their recovery method is suitable for the state's aquifer analysis. Transmissivity is calculated as

$$T = \frac{2.3Q_{av}}{4\pi \Delta s} \dots \dots \dots (iii)$$

The maximum storage coefficient of the aquifer is calculated from eden and hazel's expression for the drawdown in a confined aquifer using the step method.

$$st = \frac{2.3Q_{av}}{4\pi T} \cdot \log_{10} \frac{2.25Tt}{rw^2 S_c} \dots \dots \dots (v)$$

**Borehole characteristics in ado Ekiti**

Well location	Theis (modified)	Logan	Max yield $m^3/day$	Storage coefficient
Ado ekiti	0.84	1.8	115	$4.7 \times 10^{-2}$
Ado Ekiti east	4.5	4.1	129.6	$2.5 \times 10^{-4}$
Ado Ekiti west	3.8	4.8	260	$1.6 \times 10^{-2}$
Ado central	1.9	1.4	320	$2.5 \times 10^{-6}$
Ado south	35.7	10.0	288.5	$5.2 \times 10^{-10}$

Ado Ekiti borehole characteristics (Watson,1999)

**Pumping tests**

**LOCATION:** Ado Central (Christ school)

**DEPTH OF WELL:** 68.00M

**WELL DIAMETER:** 120mm

Time since pumping stopped. $t'$ (minutes)	Time since pumping started. $t = t' + 4320$	$\frac{t}{t'}$	Residual drawdown $S$ (meters)
1	4321	4321	17.80
2	4322	2161	15.11
5	4325	1442	13.32
10	4330	433	11.62
20	4340	217	10.33
50	4370	87.7	9.35
100	4420	44.2	8.78
200	4520	22.6	8.34
400	4720	11.8	7.72
800	5120	6.40	7.42
1000	5320	5.32	6.58
1200	5520	4.60	6.23

$$Transmissivity T = \frac{2.3}{4\pi \Delta s} = \frac{2.3 \times 20.75}{4\pi(2)} = 3m^3/day$$

$$S_t = \frac{2.3}{4\pi T} \log \frac{2.25Tt}{r_w S_c}$$

$$17.8 = \frac{2.3 \times 20.75}{4\pi \times 1.9} \log \frac{2.25 \times 1.9 \times 3}{0.08^2 S_c}$$

$$\text{storage capacity } S_c = 2.5 \times 10^{-6}$$

Comment: values of *Transmissivity* *T* and *storage capacity* *S<sub>c</sub>* indicate poor quality of aquifer  
 Comment: values of *T* and *S<sub>c</sub>* indicate poor quality of aquifer.

**LOCATION:** ado Ekiti south (Mary assumption hospital)

**DEPTH OF WELL:** 43.00M **WELL DIAMETER:** 120mm

Time since pumping stopped. <i>t'</i> (minutes)	Time since pumping started. <i>t = t' + 4320</i>	$\frac{t}{t'}$	Residual drawdown <i>S</i> (meters)
1	4321	4321	25.87
2	4322	2161	25.06
5	4325	1442	24.44
10	4330	433	22.59
20	4310	217	21.08
50	4370	87.7	18.71
100	4420	44.2	16.60
200	4520	22.6	13.17
400	4720	11.8	8.05
800	5120	6.40	6.43
1000	5320	5.32	4.56
1200	5520	4.60	4.01

$$\text{Transmissivity } T = \frac{2.3}{4\pi \Delta s} = \frac{2.3 \times 92.2}{4\pi (3.75)} = 4.5 \text{ m}^3/\text{day}$$

$$S_t = \frac{2.3}{4\pi T} \log \frac{2.25 T_t}{r_w S_c}$$

$$17.8 = \frac{2.3 \times 92.2}{4\pi \times 4.5} \log \frac{2.25 \times 4.5 \times 2}{0.08^2 S_c}$$

$$S_c = 2.5 \times 10^{-4}$$

Comment: *S<sub>c</sub>* value is too low. Pumping rate is believed to be excessive for this type of aquifer.

**LOCATION:** Ado West (Better Life)

**DEPTH OF WELL:** 70.00m

**WELL DIAMETER:** 115mm

Time since pumping stopped. <i>t'</i> (minutes)	Time since pumping started. <i>t = t' + 4320</i>	$\frac{t}{t'}$	Residual drawdown <i>S</i> (meters)
1	4321	4321	37.87
2	4322	2161	36.73
5	4325	1442	33.41
10	4330	433	29.32
20	4340	217	25.56
50	4370	87.7	23.65
100	4420	44.2	21.42
200	4520	22.6	18.07
400	4720	11.8	13.77
800	5120	6.4	8.75
1000	5320	5.32	7.45
1200	5520	4.6	6.43

$$T = \frac{2.3}{4\pi \Delta s} = \frac{2.3 \times 154.1}{4\pi (7.5)} = 3.8 \text{ m}^3/\text{day}$$

$$S_t = \frac{2.3}{4\pi T} \log \frac{2.25 T_t}{r_w S_c}$$

$$17.8 = \frac{2.3 \times 154.1}{4\pi \times 4.5} \log \frac{2.25 \times 3.8 \times 3}{0.08^2 S_c}$$

$$S_c = 1.6 \times 10^{-2}$$

**LOCATION:** Ado East (Afe Babalola university talent discovery)

**DEPTH OF WELL:** 70.00M

**WELL DIAMETER:** 125mm

RECOVERY TIME (ELAPSED TIME IN MINUTES)	RECOVERY WL READING FROM TOC (M)	RECOVER Y WL (M)	DRAWDOWN OR RESIDUAL (M)	PUMPING RATE/DISCHARGE (M <sup>3</sup> /Hr)
0	27.03	26.12	15.36	
0.5	25.99	25.08	14.32	
1	25.33	24.42	13.66	
1.5	24.81	23.90	13.14	
2	24.63	23.72	12.96	
2.5	24.54	23.63	12.84	
3	23.50	22.59	11.83	
3.5	21.70	20.79	10.03	
4	21.46	20.55	9.79	
4.5	20.76	19.85	9.09	
5	20.09	19.18	8.42	
6	18.93	18.02	7.26	
7	18.11	17.20	6.44	
8	17.44	16.53	5.77	
9	17.35	16.44	5.68	
10	16.62	15.71	4.95	
12	16.22	15.31	4.55	
14	16.04	15.13	4.37	
16	15.73	14.82	4.06	
18	15.52	14.61	3.85	
20	15.32	14.41	3.65	
22	15.13	14.22	3.46	
24	15.00	14.09	3.33	
26	14.91	14.00	3.24	
28	14.85	13.94	3.18	
30	14.76	13.85	3.09	
35	14.58	13.67	2.91	
40	14.45	13.54	2.78	
45	14.31	13.40	2.64	
50	14.15	13.24	2.48	
55	14.00	13.09	2.33	
60	13.91	13.00	2.24	

**By 5minutes since pumping was stopped 45% Recovery was achieved.**

RECOVERY TIME (ELAPSED TIME IN MINUTES)	RECOVERY WL READING FROM TOC (M)	RECOVERY WL (M)	DRAWDOWN OR RESIDUAL (M)	PUMPING RATE/DISCHARGE (M <sup>3</sup> /Hr)	COMMENTS
70	13.68	12.77	2.01		
80	13.50	12.59	1.83		
90	13.00	12.09	1.33		
100	12.50	11.59	0.83		
110	12.33	11.42	0.66		
120	12.25	11.34	0.58		
135	11.67	10.76	0.00		
150	11.67	10.76	0.00		
165	11.67	10.76	0.00		

**By 5 minutes since pumping stopped 45% Recovery was achieved.**

Transmissivity (T)

$$T = 0.183Q/\Delta S_w$$

$\Delta S_w$  = Slope of Time – Drawdown graph

$$\Delta S_w = 0.072$$

$$T = 0.183 \times 108/0.072$$

$$= 274.5m^2/day$$

Permeability (K)  
 $K = (0.306Q/LS) \times \log(1.321/R)$   
 L = Length of screen equivalent to thickness of aquifer = 12m  
 S = Max. drawdown = 15.36m  
 R = Radius of screen = 0.062m  
 $K = (0.306 \times 108/12 \times 15.36) \times \text{Log}(1.321/0.062)$   
 $= 0.238$   
 Storativity ( $S_o$ )  
 $S_o = 0.117\sqrt{K}$   
 $= 0.117\sqrt{0.238}$   
 $= 0.057$   
 Specific Capacity (q)  
 $q = Q/S$   
 $Q = 4.5\text{m}^3/\text{hr} = 108\text{m}^3/\text{day}$   
 S = Max. drawdown = 15.36m  
 $= 108/15.36$   
 $= 7.03\text{m}^2/\text{day}$   
 If drawdown (S) is 5m:  
 $Q = Sq$   
 $= 5 \times 7.03\text{m}^3/\text{day}$   
 $= 35.15\text{m}^3/\text{day}$   
 Entrance velocity (V)  
 $V = Q/\pi RLP$   
 $Q = 4.5\text{m}^3/\text{hr} = 0.00125\text{m}^3/\text{sec}$   
 R = 0.062m  
 L = 12m (Length of screen)  
 P = % of opening in the screen (0.2)  
 $V = 0.00125/3.14 \times 0.062 \times 12 \times 0.2$   
 $= 2.7 \times 10^{-3}\text{m/s}$   
 Range of cone of depression ( $R_c$ )  
 $R_c = 10S \times \sqrt{k}$   
 S = 15.36m (max. drawdown)  
 K = 0.238  
 $R_c = 10 \times 15.36\sqrt{0.238}$   
 $= 74.93\text{m}$

**Pumping test**

**LOCATION:** ado north (EKSU campus)

**DEPTH OF WELL:** 89.00M

**WELL DIAMETER:** 120mm

Time since pumping stopped. $t'$ (minutes)	Time since pumping started. $t = t' + 4320$	$\frac{t}{t'}$	Residual drawdown S (meters)
1	4321	4321	17.80
2	4322	2161	15.11
5	4325	1442	13.32
10	4330	433	11.62
20	4340	217	10.33
50	4370	87.7	9.35
100	4420	44.2	8.78
200	4520	22.6	8.34
400	4720	11.8	7.72
800	5120	6.40	7.42
1000	5320	5.32	6.58
1200	5520	4.60	6.23

$$T = \frac{2.3}{4\pi\Delta s} = \frac{2.3 \times 113}{4\pi(26)} = 0.84\text{m}^3/\text{day}$$



$$S_t = \frac{2.3}{4\pi T} \log \frac{2.25T_t}{r_w S_c}$$

$$17.8 = \frac{2.3 \times 113}{4\pi \times 0.84} \log \frac{2.25 \times 0.84 \times 2}{0.08^2 S_c}$$

$$S_c = 4.7 \times 10^{-2}$$

#### IV. CONCLUSION AND RECOMMENDATIONS

##### Conclusion

In conclusion, the study area is characterized by crystalline basement complex rock of low porosity and permeability. The various pumping tests that were carried out indicate that the area generally has low groundwater potential. This research gives better understanding of the common drilling methods used in drilling water wells in the study area, borehole yields and the problems faced before during and after drilling. I discovered that there is a high dependence on groundwater as a source for potable water. It has also been discovered that in the study area that the practice of borehole maintenance is very poor.

##### Recommendation

Borehole maintenance should be taken more seriously and borehole owners should develop the habit of carrying out regular maintenance on their borehole wells so as to ensure that they reach their serviceability life. It is necessary that borehole drilling should be monitored by a certified agency and that drilling license be issued to qualified water well drillers so as to reduce the infiltration of inexperienced drillers into the water well drilling sector and to reduce the drilling of sub-standard water wells. Owners of boreholes should consider rehabilitating boreholes instead of abandoning them. Rehabilitation of wells can save money and prevent the sub surface layers from losing stability as a result of excessive well drilling.

##### References

- [1]. Adekile, D. and Olabode, O 2008 *Hand drilling in Nigeria RWSN/UNICEF Field note.*
- [2]. Adekile, D and Olabode, O. 2009 *Study of Public and Private Borehole Drilling in Nigeria*
- [3]. Samad Valipour Shokouhi<sup>1</sup>, Agnar Aamodt<sup>2</sup> and Pål Skalle<sup>1</sup>, Frode Sørmo, 2006 *drilling techniques for boreholes*
- [4]. Managing director of midlands pumps cc, water supply specialists inkwazulu-natal. 2004. *Overcoming incrustation on borehole screens.*
- [5]. Abiola O, Enikanselu, P. A, Oladapo, M.I. 2004 *Groundwater potential and aquifer protective capacity of overburden units in Ado-Ekiti, south-western Nigeria,*
- [6]. Olayinka, A. I. 2004 *Statistical evaluation of groundwater potential of ado-Ekiti, southwest, Nigeria* oyedele, e. a. a, physics department, university of ado – Ekiti, Nigeria Geology Department, University of Ibadan, Ibadan.
- [7]. Bayowa G.O. Olorunfemi M.O. and Ademilua O.L. 2014. *A geoelectric Assessment and Classification of the aquifer systems in a Typical Basement Complex Terrain: Case study of Ekiti State, Southwestern Nigeria.*
- [8]. Bayowa O.G, Olorunfemi, M.O, and Ademilua, O.L. 2014 *Preliminary Geomorphologic, Geological, Hydrogeological Assessment of the Groundwater potential of Ekiti State, South-western Nigeria.*
- [9]. WATSON 1999 *Ado Ekiti borehole characteristics.*
- [10]. Kruseman and ridder 1970 *Assumptions of pumping tests.*
- [11]. Morgan W.T 1983. *Classification of ado Ekiti under a massive crystalline platform of south western Nigeria.*
- [12]. Tomando, borehole *drilling company cost analysis for borehole drilling operation 2011.*
- [13]. Ekiti state government portfolio, *Ekiti state population figures.*
- [14]. Roscoe Moss Company, *A guide to water well casing and screen selection*
- [15]. Ekiti State Rural Water Supply and Sanitation Agency
- [16]. Carruthers and Smith 1992, Olorunfemi, 2008 *Fieldwork Experience*

## A Budget Based Optimization of Preventive Maintenance in Maritime Industry

<sup>1</sup>Akpan, W. A . , <sup>2</sup>Ogunsola, T.M.

<sup>1</sup>Mechanical Engineering Department, University of Uyo (234) P.M.B 1017 Uyo, Akwa Ibom State, Nigeria

<sup>2</sup>Boat and Shipbuilding Department, Maritime Academy of Nigeria, Oron

**Abstract :** This research work investigates preventive maintenance management of diesel engine generators at the Maritime Academy of Nigeria, Oron. A budget based optimization methodology taking cognisance of the age of the equipment was applied on failure data of diesel engine generators obtained from the institution maintenance data base to provide cost effective maintenance management / replacement programme for critical components of diesel engine generators. The results were analyzed using Matlab. The results provide effective cost and reliability template which can be used to perform a budget based maintenance planning programme in the Maritime Industry.

**Keywords:** Budget; optimization; maintenance; modeling;; reliability; diesel engines; maritime industry.

### I. Introduction

The Maritime Academy of Nigeria Oron in Akwa Ibom State Nigeria started as Nautical college of Nigeria in 1979 with a mandate to train shipboard officers, ratings and shore-based management personnel (Wikipedia, 2014). In 1988 the college was upgraded to the present status and the mandate was expanded to training all levels and categories of personnel for all facets of the Nigerian maritime industry.

The poor power supply in Nigeria country has prompted the academy to generate its electricity for the administrative activities of the institution using the diesel engine generators. The diesel engine is popular in maritime industries. This can be attributed to its high performance. It has high reliability and a better fuel economy than gasoline engine and is more efficient at light and full loads. The diesel generator emits fewer harmful exhaust pollutants and is inherently safer because diesel fuel is less volatile than gasoline. However, diesel engines can be ineffective with poor maintenance method.

Maintenance is all actions which have the objective of returning a system back to another state. According to Moubray, (1995) and Tsang et al. (1999) maintenance has the ability to bring back the system quickly to its normal functional state and reduces equipment down time. Paz, (1994) categorized maintenance into two: corrective maintenance and preventive maintenance. Maintenance is very important in the life of any physical asset. The fundamental basis of any planned maintenance system is deciding in advance.

- The individual items of the plant and equipment to be maintained;
- The forms, method and details of how each item is to be maintenance;
- The tools, replacements, spares, tradesmen and time that will be required to carry out this Maintenance;
- The frequency at which these maintenance operation must be carried out;
- The method of administering the system and;
- The method of analyzing the results.

I

The introduction of planned maintenance scheme in an organization involve time, money and considerable amount of work. It has been shown that the benefits obtained from planned maintenance are numerous Koboia-Aduama (1991).

Maintenance provides freedom from breakdown during operations. Maintenance of equipment is essential in order to: keep the equipment at their maximum operating efficiencies; keep equipment in a satisfactory condition for safe operations; and reduce to a minimum, maintenance cost consistent with efficiency and safety (Koboia-Aduma (1991).

Studies on imperfect maintenance can be found in Pharm and Wang (1996) and Nakagawa (1987). The Maritime Academy of Nigeria Oron has 500KVA, 600KV and 800KVA diesel engine generators to generate power for the administrative needs of the academy. The maintenance costs of diesel engine generators in the academy is rising daily. This is caused by lack of clear maintenance methodology by the institution to maintain these generators. The objective of this research is to conduct a budget based maintenance methodology on 500KVA, 600KVA and 800KVA diesel engine generators own by the academy and to suggest ways maintenance and replacement actions should be performed on the generators with the objective of reducing the cost of maintenance with the required reliability of the generators given any stipulated budget.

### II. Methodology

Data for this research work were collected from both primary and secondary sources. The primary information was obtained from maintainers, supervisors, engineers and managers. This information include: maintenance cost, failure cost and replacement cost of each part. The main data were obtained from the log book for a period of five years. This data include the time of failure of the diesel engine generator, the components causing the failure and also when the failed components were repaired or replaced.. Ten critical parts were selected for the study. This data formed input into a maintenance and replacement model developed by Kamran (2008). The information was used to predict future maintenance planning for the three diesel generators in the next five years with a given budget and the objective of reducing maintenance cost and increasing the reliability of the diesel generators used by the institution. The methods used in solving the problem are generalized reduced gradient (GRG) and simulating annealing (SA).

### III. Optimization model

The model by Kamran (2008) provides a general framework that was applied on the study. In the reliability maximization equation, the constraints for the solution of the equation are as follows:

- (i) Constraints that address the initial age of each component at the beginning of planning horizon.

Thus;  

$$X_{ij} = 0; \quad i = 1 \dots N \tag{1}$$

where  $i$  = component,  $j$  = period &  $N$  = No of components

- (ii) Effective age of the components based on preventive maintenance activities recursively.

$$X_{i,j} = (1 - m_{i,j-1})(1 - r_{i,j-1})X_{i,j+1} + m_{j+1}(\alpha X'_{j,j+1}) \tag{2}$$

$$i = 1 \dots N \text{ and } j = 2 \dots T$$

$$X'_{i,j} = X_{i,j} + \frac{T}{J} \quad i = 1, N \text{ and } j = 1 \dots T \tag{3}$$

$$m_{i,j} + r_{i,j} \leq 1; \quad i = 1 \dots N \text{ and } j = 1 \dots T$$

Where:  $X_{i,j}$  Effective age of component  $i$  at the start of period  $j$ ,  $X'_{i,j}$ : Effective age of component  $i$  at the end of period  $j$ .

$T$  = No. of periods,  $J$  = No. of intervals,  $m_{i,j} : \begin{cases} 1 \\ 0 \end{cases}$  if component  $i$  at period  $j$  is maintained, otherwise.

$r_{i,j} : \begin{cases} 1 \\ 0 \end{cases}$  if component  $i$  at period  $j$  is replaced, otherwise,  $\alpha i$ : Improvement factor of component  $i$

- (iii) Condition/constraint preventing occurrence of simultaneous maintenance and replacement actions on the components.

$$\prod_{i=1}^N \prod_{j=1}^T e^{-(\lambda_i (X'_{i,j})^{\beta_i} - (X_{i,j})^{\beta_i})} \gg RR_{series} \tag{4}$$

$$m_{i,j}, r_{i,j} = 0 \text{ or } 1; \quad i = 1 \dots N \text{ and } j = 1 \dots T \tag{5}$$

$$X_{i,j}, X'_{i,j} \geq 0; \quad i = 1, N \text{ and } j = 1 \dots T \tag{6}$$

$\lambda i$ : Characteristic life (scale) parameter of component  $i$

$\beta i$ : Shape parameter of component,  $i$ ,  $RR_{series}$ : Required reliability of the series system of components.

Consider the case where component  $i$  is maintained in period  $j$ . For simplicity, it is assumed that the maintenance activity occurs at the end of the period. The maintenance action effectively reduces the age of component  $i$  at the beginning of the next period. That is:

$$X_{i,j+1} = \alpha X'_{i,j} \text{ for } i = 1, \dots, N; j=1, \dots, T \text{ and } (0 \leq \alpha \leq 1) \tag{7}$$

The term  $\alpha$  is an “improvement factor”, similar to that proposed by Malik (1979), Jayabalan (1992). This factor allows for a variable effect of maintenance on the aging of a system. When  $\alpha = 0$ , the effect of maintenance is to return the system to a state of “good-as new”. When  $\alpha = 1$ , maintenance has no effect, and the system remains in a state of “bad-as-old”.

The maintenance action at the end of period  $j$  results in an instantaneous drop in the ROCOF of component  $i$ . Thus at the end of period  $j$ , the ROCOF for component  $i$  is  $v_i(X'_{i,j})$ . At the start of period  $j + 1$  the ROCOF drops to  $v_i(0)$

If component  $i$  is replaced at the end of period  $j$ , the following applies:

$$X'_{i,j+1} = 0 \text{ for } i = 1, \dots, N; j=1, \dots, T \tag{8}$$

i.e., the system is returned to a state of “good-as-new”. The ROCOF of component  $i$  instantaneously drops from  $v_i(X'_{i,j})$  to  $v_i(X'_{i,j})$

If no action is performed in period  $j$ , there is no effect on the ROCOF of component  $i$  and thus :

$$X'_{i,j} = X_{i,j} + \frac{T}{J} \text{ for } i = 1, \dots, N; j=1, \dots, T \tag{9}$$

$$X'_{i,j+1} = X_{i,j} \text{ for } i = 1, \dots, N; j=1, \dots, T \tag{10}$$

$$v_i(X_{i,j+1}) = v_i(X_{i,j}) \text{ for } i = 1, \dots, N; j=1, \dots, T \tag{11}$$

$T =$  No. of periods,  $J =$  No. of intervals, ROCOF = Rate of Occurrence of Failure

For a new system, the cost associated with all component levels of maintenance and replacement actions in period  $j$ , remains as a function of all the actions taken during that period.

The expected number of failures of component  $i$  in period  $j$ ,  $i$

$$E[N_{i,j}] = \int_{X_{i,j}}^{X'_{i,j}} v_i(t) dt \text{ for } i = 1, \dots, N; j = 1, \dots, T \tag{12}$$

Under the Non- homogenous poisson process assumption (NHPP) the expected number of component  $i$  failures in period  $j$  is

$$E[N_{i,j}] = \lambda_i(X'_{i,j})^{\beta} - \lambda_i(X_{i,j})^{\beta} \text{ for } i = 1, \dots, N; j = 1, \dots, T \tag{13}$$

If the cost of each failure is  $F_i$  (in units of #/failure event), which in turn allows the computation of,  $F_{ij}$ , the cost of failures attributable to component  $i$  in period  $j$  is:

$$F_{ij} = F_i E[N_{i,j}] \text{ for } i = 1, \dots, N; j = 1, \dots, T \tag{14}$$

Hence regardless of any maintenance or replacement actions (which are assumed to occur at the end of the period) in period  $j$ , there is still a cost associated with the possible failures that can occur during the period.

If maintenance is performed on component  $i$  in period  $j$ , a maintenance cost constant  $M_i$  is incurred at the end of the period. Similarly If component  $i$  is replaced, in period  $j$ , the replacement cost is the initial purchase price of the component  $i$ , denoted by  $R_i$ .

For a multi-component system, the cost structure is defined as stated above, the problem can be reduced to a simple problem of finding the optimal sequence of maintenance, replacement, or do-nothing for each component, independent of all other components. That is, one could simply find the best sequence of actions for component 1 regardless of the actions taken on component 2 and so on. This would result in  $N$  independent optimization problems. Such a model seems unrealistic, as there should be some overall system cost penalty when an action is taken on any component in the system. It would seem that there should be some logical advantage to combine maintenance and replacement actions, e.g., while the system is shutdown to replace one component, it may make sense to go ahead and perform maintenance/replacement of some other components, even if it is not at its individual optimum point where maintenance or replacement would ordinarily be performed. Under this scenario, the optimal time to perform maintenance/replacement actions on individual components is dependent upon the decision made for other components. As such, a fixed cost of “downtime”,  $Z$ , is charged in period  $j$  if any component (one or more) is maintained or replaced in that period. Consideration of this fixed cost makes the problem much more interesting, and more difficult to solve, as the optimal sequence of actions must be determined simultaneously for all components.

From the vantage point, at the start of period  $j = 0$ , it is good to determine the set of activities, i.e., maintenance, replacement, or do nothing, for each component in each period such that total cost is minimized. In order to have  $X_{i,j}$  age of component  $i$  at the end of period  $j$  by using equation 2. First, define  $m_{i,j}$ , and  $r_{i,j}$ , as binary variables of maintenance and replacement actions for component  $i$  in period  $j$  as:

$$m_{i,j} \begin{cases} 1 \\ 0 \end{cases} \text{ if component } i \text{ at period } j \text{ is maintained, otherwise.} \quad (15)$$

$$r_{i,j} \begin{cases} 1 \\ 0 \end{cases} \text{ if component } i \text{ at period } j \text{ is replaced, otherwise.} \quad (16)$$

The following recursive function of  $X_{i,j}, X'_{i,j}, m_{i,j}, r_{i,j}, \alpha$ , with a constraint are constructed:

$$\begin{cases} X_{i,j} = (1 - m_{i,j-1})(1 - r_{i,j-1})X'_{i,j-1} + m_{i,j-1} + (\alpha X_{i,j-1}) \end{cases} \quad (17)$$

$$\begin{cases} X'_{i,j} = X'_{i,j} + \frac{T}{J} \end{cases} \quad (18)$$

$$m_{i,j} + r_{i,j} \leq 1 \quad (19)$$

In addition, the initial age for each component is equal to zero:

$$X_{i,j} = 0 \text{ for } i = 1, \dots, N \quad (20)$$

If component replacement occurs in the previous period then,

$$r_{i,j-1} = m_{i,j-1} = 0, \quad (21)$$

$X_{i,j}$ . If a component is maintained in the previous period then

$$r_{i,j-1} = m_{i,j-1} = 1 \quad (22)$$

$$X_{i,j} = \alpha X'_{i,j-1} \quad (23)$$

and finally if nothing is done,

$$r_{i,j-1} = 0, m_{i,j-1} = 0 \text{ and } X_{i,j} = X'_{i,j+1} \quad (24)$$

The formulation of a budget constraint, GB is introduced. The objective of this model is to maximize the system reliability, through our choice of maintenance and replacement decisions, such that we do not exceed the budgeted total cost. This model is formulated as:

$$\text{Max Reliability} = \prod_{i=1}^N \prod_{j=1}^T e^{-[li(x'_{i,j}) \beta_i - li(x_{i,j}) \beta_i]} \quad (25)$$

Subject to

$$X_{ij} = 0; \quad i = 1 \dots N \quad (26)$$

$$X_{ij} = (1 - m_{i,j-1})(1 - r_{i,j-1})X'_{i,j-1} + m_{i,j-1}(\alpha X'_{i,j-1}) \quad (27)$$

$$i = 1 \dots N \text{ and } j = 2 \dots T \quad (28)$$

$$X'_{i,j} = X_{i,j} + \frac{T}{j}; \quad i = 1 \dots N; \text{ and } j = 1 \dots T \tag{29}$$

$$m_{i,j} + r_{i,j} \leq 1; \quad i = 1 \dots N; \text{ and } j = 1 \dots T \tag{30}$$

$$\sum_{i=1}^N \sum_{j=1}^T [F_i \alpha_i ((X'_{i,j})^{\beta_i}) - (X_{i,j})^{\beta_i}) + M_{i,j} \cdot m_{i,j} + R_i \cdot r_{i,j}] + \sum_{j=1}^T [Z(1 - \prod_{i=1}^N (1 - (m_{i,j} + r_{i,j})))] \leq GB \tag{31}$$

$$m_{i,j}, r_{i,j} = 0 \text{ or } 1 \quad i = 1 \dots N \text{ and } j = 1 \dots T \tag{31}$$

$$X_{i,j}, X'_{i,j} \geq 0 \quad i = 1 \dots N \text{ and } j = 1 \dots T \tag{32}$$

$$M_{i,j}, r_{i,j} = 0 \text{ or } 1; \quad i = 1 \dots N \text{ and } j = 1 \dots T \tag{33}$$

$$X'_{i,j} = X_{i,j} \geq 0; \quad i = 1, N \text{ and } j = 1 \dots T \tag{36}$$

Where:  $X_{i,j}$ : Effective age of component  $i$  at the start of period  $j$ ,

$X'_{i,j}$ : Effective age of component  $i$  at the end of period  $j$ .  $T$  = No. of periods,  $J$  = No. of intervals

$m_{i,j}$ :  $\begin{cases} 1 \\ 0 \end{cases}$  if component  $i$  at period  $j$  is maintained, otherwise.,  $r_{i,j}$ :  $\begin{cases} 1 \\ 0 \end{cases}$  if component  $i$  at period  $j$  is replaced, otherwise

$\lambda_i$ : Characteristic life (scale) parameter of component  $i$   $\beta_i$ : Shape parameter of component,  $i$

$RR_{series}$ : Required reliability of the series system of components.  $\alpha_i$ : Improvement factor of component  $i$

$\sum$ : Summation,  $\Pi$ : Multiplication,  $F_i$ : Unexpected failure cost of component  $i$  in period  $j$

$N$ : No. of components,  $M_i$ : maintenance cost of component  $i$ ,  $R_i$ : Replacement cost of component  $i$ ,  $Z$ : Fixed cost of the system

Decision variables

$M_{i,j}$ :  $\begin{cases} 1 \\ 0 \end{cases}$  if component  $i$  at period  $j$  is maintained, otherwise.

$r_{i,j}$ :  $\begin{cases} 1 \\ 0 \end{cases}$  if component  $i$  at period  $j$  is replaced, otherwise.

This objective function computes the maximum reliability subject to a given budget cost with stated constraints and input parameters from tables 1, 2 and 3.

The generalized reduced gradient and the simulated annealing algorithms were used to solve the cost minimization using Matlab software and the results presented in tables 4, 5 and 6. Tables 1, 2 and 3 were generated based on data obtained from maintenance log book and information from maintenance engineers.

#### IV. Results and discussion

The characteristic life  $\lambda$ , shape factor  $\beta$ , maintenance factor  $\alpha$ , failure cost, maintenance cost, and replacement cost are presented in tables 1, 2 and 3 for 500KVA, 600KVA and 800KVA diesel generators respectively for the selected components shown in tables 1.2 and 3.

Table :1. Parameters for 500KV a diesel generator

Month	Component	$\lambda$ (Days)	$\beta$	$\alpha$	Failure Cost (₹)	Maintenance Cost (₹)	Replacement Cost (₹)
1.	Injector Pump	950	0.0005	0.00025	128,000.00	68,000.00	91,000.00
2.	Calibration of Valve	1080	0.0007	0.00025	340,000.00	32,000.00	180,000.00
3.	Cutting of Ring	1090	0.0004	0.00025	210,000.00	80,000.00	170,000.00
4.	Top Gasket Cylinder Replacement	1170	0.0004	0.00025	260,000.00	80,000.00	183,000.00
5.	Radiator	1050	0.0004	0.00025	96,000.00	16,000.00	36,000.00
6.	Oil Pump	1005	0.0004	0.00025	80,000.00	16,000.00	80,000.00
7.	Injector Nozzle	900	0.0005	0.00025	270,000.00	80,000.00	270,000.00
8.	Air Filter	1160	0.0004	0.00025	120,000.00	40,000.00	80,000.00
9.	Alternator	250	0.0006	0.00025	154,000.00	46,000.00	85,000.00
10.	Water Pump	1050	0.0005	0.00025	87,000.00	40,000.00	70,000.00

The characteristics life and shape factors were calculated from failure data while the failure costs, maintenance costs and replacement costs data were obtained from maintenance engineers. The maintenance factors were assumed based on the frequency of failure of components.

**Table: 2.** Parameters for 600KV a diesel generator

Month	Component	$\lambda$ (Days)	$\beta$	$\alpha$	Failure Cost (₦)	Maintenance Cost (₦)	Replacement Cost (₦)
1.	Injector Pump	1100	0.0007	0.00010	128,000.00	68,000.00	91,000.00
2.	Calibration of Valve	800	0.0006	0.00010	340,000.00	32,000.00	180,000.00
3.	Cutting of Ring	470	0.0003	0.00010	240,000.00	80,000.00	190,000.00
4.	Top Gasket Cylinder Replacement	1020	0.0005	0.00010	310,000.00	80,000.00	189,000.00
5.	Radiator	1020	0.0004	0.00010	96,000.00	16,000.00	36,000.00
6.	Oil Pump	800	0.0005	0.00050	80,000.00	16,000.00	80,000.00
7.	Injector Nozzle	900	0.0005	0.00050	270,000.00	80,000.00	270,000.00
8.	Air Filter	1200	0.0006	0.00050	160,000.00	40,000.00	110,000.00
9.	Alternator	990	0.0006	0.00050	210,000.00	76,000.00	115,000.00
10.	Water Pump	780	0.0007	0.00050	87,000.00	40,000.00	70,000.00

The failure cost is higher than replacement cost which in the same vain higher than the maintenance cost. The costs of components in 500KVA, 600KVA and 800KV generators are different in some cases or similar in others.

**Table: 3.** Parameters for 800KV a diesel generator engine

Month	Component	$\lambda$ (Days)	B	$\alpha$	Failure Cost (₦)	Maintenance Cost (₦)	Replacement Cost (₦)
1.	Injector Pump	900	0.0005	0.00022	128,000.00	68,000.00	91,000.00
2.	Calibration of Valve	1050	0.0004	0.00035	340,000.00	32,000.00	180,000.00
3.	Cutting of Ring	1050	0.0005	0.00038	210,000.00	80,000.00	170,000.00
4.	Top Gasket Cylinder Replacement	980	0.0007	0.00034	33,600.00	6,720.00	28,800.00
5.	Radiator	1010	0.0003	0.00032	310,000.00	80,000.00	189,000.00
6.	Oil Pump	1015	0.0003	0.00028	96,000.00	16,000.00	36,000.00
7.	Injector Nozzle	1020	0.0003	0.00015	80,000.00	16,000.00	80,000.00
8.	Air Filter	1030	0.0005	0.00012	270,000.00	80,000.00	170,000.00
9.	Alternator	1010	0.0003	0.00025	270,000.00	80,000.00	170,000.00
10.	Water Pump	1110	0.0006	0.00020	120,000.00	40,000.00	80,000.00

In tables 4, 5 and 6 the given budget with maximum reliability is presented in the third and sixth columns by the decision maker, while a search algorithm of generalized reduced gradient and simulated annealing calculate the total optimized cost function for each component and the optimum reliability in the sixth column using Matlab software. A gap analysis shows the effectiveness of each algorithm. At 98.21% reliability and a given cost of 800,000.00 naira, six number periods at ten months per period for the 60 months prediction has a total cost of 800,000.00 naira and 792,027.2 naira as shown in table 4. From periods of 36 and above , the calculated total cost is less than the given budget. The optimized reliability lies between 46.96% and 84.71% for simulated annealing algorithm and 55.42% and 95.06% for generalized reduced gradient method.

**Table: 4.** Budget Algorithm and Optimized function value (OFV) for 500KVA

No. of components	Number of periods	Given Budget (₦)	Algorithm	Optimized Function Value (OFV) Reliability %	Total cost (₦)	OFV Gap (%)
10 For 500KVA	6	800,000.00	GRG	98.21	800,000.00	-
			SA	97.09	792,027.2	1.15%
	12	480,000.00	GRG	90.32	480,000.00	-
			SA	85.81	464,187.2	4.99%
	18	640,000.00	GRG	81.24	640,000.00	-
			SA	71.36	636,337.60	12.16%
	24	800,000.00	GRG	73.11	800,000.00	-
			SA	69.37	800,030.40	5.12%
	30	960,000.00	GRG	64.96	960,000.00	-
			SA	58.31	970,774.40	10.24%
	36	1,120,000.00	GRG	55.42	1,120,000.00	-
			SA	46.96	1,112,390.00	15.27%
	42	1,685,654.4	GRG	95.06	1,320,000.00	-
			SA	84.71	1,042,416.00	10.89%
	48	2,061,760.0	GRG	75.64	1,280,000.00	-
			SA	74.15	1,277,782.40	1.97%
	54	2,198,049.6	GRG	63.49	1,600,000.00	-
			SA	58.93	1,609,659.20	7.18%
60	2,918,223.78	GRG	52.15	1,920,000.00	-	
		SA	50.47	1951,516.80	3.22%	

For the 600KVA and 800KVA diesel engine generators, the same trend is followed. However, the allocated given budgets are much more higher than that of the 500KVA generator

**Table :5.** Budget Algorithm and Optimized function value (OFV) for 600KVA

No. components of	Number of periods	Given Budget (₹)	Algorithm	Optimized Function Value (OFV) Reliability %	Total cost (₹)	OFV Gap (%)
10 For 600KVA	6	1,600,000.00	GRG	97.53	1,600,000.00	-
			SA	97.43	1603,318.40	0.10%
	12	960,000.00	GRG	85.06	960,000.00	-
			SA	84.71	942,416.00	0.41%
	18	1,280,000.00	GRG	75.64	1,280,000.00	-
			SA	74.15	1,277,782.40	1.97%
	24	1,600,000.00	GRG	63.49	1,600,000.00	-
			SA	58.93	1,609,659.20	7.18%
	30	1,920,000.00	GRG	52.15	1,920,000.00	-
			SA	50.47	1951,516.80	3.22%
	36	2,400,000.00	GRG	49.91	2,400,000.00	-
			SA	46.93	2,425,304.00	5.97%
	42	2,355,771.2	GRG	98.21	800,000.00	-
			SA	97.09	792,027.2	1.15%
	48	3,432,178.10	GRG	90.32	480,000.00	-
			SA	85.81	464,187.2	4.99%
	54	2,207,536.00	GRG	64.96	960,000.00	-
			SA	58.31	970,774.40	10.24%
	60	3,732,178.10	GRG	55.42	1,120,000.00	-
			SA	46.96	1,112,390.00	15.27%

**Table: 6.** Budget Algorithm and Optimized function value (OFV) for 800KVA

No. components of	Number of periods	Given Budget (₹)	Algorithm	Optimized Function Value (OFV) Reliability %	Total cost (₹)	OFV Gap (%)
10 For 800KVA	6	480,000.00	GRG	90.32	480,000.00	-
			SA	85.81	464,187.2	4.99%
	12	960,000.00	GRG	85.06	960,000.00	-
			SA	84.71	942,416.00	0.41%
	18	640,000.00	GRG	81.24	640,000.00	-
			SA	71.36	636,337.6	12.16%
	24	1,600,000.00	GRG	63.49	1,600,000.00	-
			SA	58.93	1,609,659.2	7.18%
	30	1,920,000.00	GRG	52.15	1,920,000.00	-
			SA	50.47	1951,516.8	3.22%
	36	1,120,000.00	GRG	55.42	1,120,000.00	-
			SA	46.96	1,112,390.00	15.27%
	42	1,280,000.00	GRG	90.32	480,000.00	-
			SA	85.81	464,187.2	4.99%
	48	1,600,000.00	GRG	81.24	640,000.00	-
			SA	71.36	636,337.60	12.16%
	54	1,061,760.0	GRG	52.15	1,920,000.00	-
			SA	50.47	1951,516.80	3.22%
	60	2,198,049.6	GRG	49.91	2,400,000.00	-
			SA	46.93	2,425,304.00	5.97%

**V. Conclusions**

The results presented from the study show that the formulation is quite effective in maintenance decision making for diesel engine generators. The research shows that shorter maintenance interval is effective allowing budget surplus for the decision maker. The generalized reduced gradient gives a lower cost than the simulated annealing. This methodology is therefore recommended to the Maritime Academy Oron for effective budget based maintenance management programme for the diesel engine generators.

**References**



- [1] Kamran, S. M.(2008) Preventive Maintenance and Replacement Scheduling: Models and algorithms. Ph.D thesis, University of Louisville, Kentucky, USA.
- [2] Kobo-Aduma, B. (1991) "Maintenance Management of Small scale Industries", in the Proceedings of the International Conference Workshop on Engineering for Accelerated Rural Development (Eds) Anazodo, U. G. N. Chukwuma. G. O. and Chukwueze, H. O.; Faculty of Engineering, University of Nigeria, Nsukka. 243
- [3] Jabayalan, V.; Chaudhuri, D. (1992) Sequential Imperfect Preventive Maintenance Policies: a case study , microelectronics and reliability, V 32, n 3 September pp 223-229
- [4] Malik, M. A.K.(1979) Reliable Preventive Maintenance Scheduling, AIIE Transaction, V11, N 3 September, pp 221-228
- [5] Moubray, J. (1995) Maintenance Management – A New Paradigm. (Online serial) Available: [www.thealadonnetwork.com/PDFs/PartUK.pdf](http://www.thealadonnetwork.com/PDFs/PartUK.pdf) [June 18, 2013].
- [6] Nakagawa, T. and Yusui, K, (1987) "Optimum Policies for System with Imperfect Maintenance", *IEEE Transaction on Reliability*. Vol. R-36, No. 5, pp. 631-633.
- [7] Paz, N. M. (1994) "Maintenance Scheduling: Issues, Results and Research Needs". *International Journal of Operations and Production Management*. Vol. 14, No. 8, pp. 47-69.
- [8] Pharm, H. and Wang, H. (1996) "Imperfect Repair", *European Journal of Operational Research* Vol. 94, pp 423-438.
- [9] Tsang, A. H. C., Jardine, A. K. S., Kolodry, H. C. (1999) "Measuring Maintenance Performance: A Holistic Approach" *International Journal of Operations and Production Management*. Vol. 19. Issue 1, pp. 691-715.
- [10] Wikipedia (2014) Maritime Academy of Nigeria: Available [Online] <http://en.wikipedia.org>.

## Analysis of Fractional Order Prey - Predator Interactions

A.George Maria Selvam<sup>1</sup>, R.Janagaraj<sup>2</sup> and D. Abraham Vianny<sup>3</sup>

<sup>1</sup> Sacred Heart College, Tirupattur - 635 601, S.India

<sup>2</sup> Kongunadu College of Engineering and Technology, Thottiam - 621 215, S.India.

<sup>3</sup> Knowledge Institute of Technology, Kakapalayam-637 504, S.India

**ABSTRACT:** The dynamical behavior of a Fractional order Prey - Predator model is investigated in this paper. The equilibrium points are computed and stability of the equilibrium points is analyzed. The phase portraits are obtained for different sets of parameter values. Numerical simulations are performed and they exhibit rich dynamics of the fractional model.

**Keywords** – Fractional Order, differential equations, Prey - Predator, stability.

### I. INTRODUCTION

Fractional order integral and derivative operators have found several applications in large areas of research during the last decade. The concept of fractional calculus was raised in the year 1695 by Marquis de L'Hopital to Gottfried Wilhelm Leibniz regarding solution of non-integer order derivative. On September 30<sup>th</sup> 1695, Leibniz replied to L'Hopital "This is an apparent paradox from which one day, useful consequences will be drawn". Between 1695 and 1819 several mathematicians (Euler in 1730, Lagrange in 1772, Laplace in 1812, and soon..) mentioned it. The question raised in 1695 was only partly answered 124 years later in 1819, by S. F. Lacroix. The real journey of development of fractional calculus started in 1974 when the first monograph on fractional calculus was published by academic press [7]. Recently theory of fractional differential and its applications has attracted much attention.

### II. FRACTIONAL DERIVATIVES AND INTEGRALS

In this section, we present important definitions of fractional calculus which arise as natural generalization of results from calculus [2, 5].

**Definition 1.** The Riemann - Liouville fractional Integral of order  $0 \leq \alpha \leq 1$  is defined as

$$J^\alpha f(t) = \frac{1}{\Gamma(\alpha)} \int_0^t (t-u)^{\alpha-1} f(u) du, t > 0$$

**Definition 2.** The Riemann - Liouville fractional derivative is defined as

$$D_t^\alpha f(t) = \frac{d}{dt} J^{1-\alpha} f(t)$$

**Definition 3.** The Caputo fractional derivative is defined as

$$D_t^\alpha f(t) = J^{1-\alpha} \frac{d}{dt} f(t)$$

When  $m$  and  $n$  are integers such that  $m > n$ , then,  $n^{\text{th}}$  - order derivative of  $t^m$  (using Euler's Gamma Function) is

$$\frac{d^n}{dt^n} t^m = \frac{\Gamma(m+1)}{\Gamma(m-n+1)} t^{m-n}.$$

Recently, fractional calculus was introduced to the stability analysis of nonlinear systems. The following lemmas are useful in the discussion of dynamical properties of the fractional order predator - prey system.

**Lemma 4.** [1] The following linear commensurate fractional - order autonomous system

$$D^\alpha x = Ax, \quad x(0) = x_0$$

is asymptotically stable if and only if  $|\arg \lambda| > \alpha \frac{\pi}{2}$  is satisfied for all eigenvalues ( $\lambda$ ) of matrix A. Also, this system is stable if and only if  $|\arg \lambda| > \alpha \frac{\pi}{2}$  is satisfied for all eigenvalues ( $\lambda$ ) of matrix A, and those critical eigenvalues which satisfy  $|\arg \lambda| = \alpha \frac{\pi}{2}$  have geometric multiplicity one, where  $0 < \alpha < 1, x \in R^n$  and  $A \in R^{n \times n}$ .

**Lemma 5.**[1] Consider the following autonomous system for internal stability definition

$$D^\alpha x(t) = Ax(t), \quad x(0) = x_0$$

with  $\alpha = [\alpha_1, \alpha_2, \dots, \alpha_n]^T$  and its n-dimensional representation:

$$\begin{aligned} D^{\alpha_1} x_1(t) &= \alpha_{11} x_1(t) + \alpha_{12} x_2(t) + \dots + \alpha_{1n} x_n(t) \\ D^{\alpha_2} x_2(t) &= \alpha_{21} x_1(t) + \alpha_{22} x_2(t) + \dots + \alpha_{2n} x_n(t) \\ &\dots \dots \\ D^{\alpha_n} x_n(t) &= \alpha_{n1} x_1(t) + \alpha_{n2} x_2(t) + \dots + \alpha_{nn} x_n(t) \end{aligned} \tag{1}$$

where all  $\alpha_i$ 's are rational numbers between 0 and 2. Assume  $m$  to be the LCM of the denominator  $u_i$ 's of  $\alpha_i$ 's, where  $\alpha_i = \frac{u_i}{v_i}, u_i, v_i \in Z^+$  for  $i = 1, 2, \dots, n$  and we set  $\gamma = \frac{1}{m}$ .

Define:

$$\det \begin{bmatrix} \lambda^{m\alpha_1} - a_{11} & -a_{12} & \dots & -a_{1n} \\ -a_{21} & \lambda^{m\alpha_2} - a_{22} & \dots & -a_{2n} \\ \vdots & \vdots & \dots & \vdots \\ -a_{n1} & -a_{n2} & \dots & \lambda^{m\alpha_n} - a_{nn} \end{bmatrix} = 0 \tag{2}$$

The characteristic equation (4) can be transformed to integer - order polynomial equation if all  $\alpha_i$ 's are rational number. Then the zero solution of system (3) is globally asymptotically stable if all roots  $\lambda_i$ 's of the characteristic (polynomial) equation (4) satisfy:

$$|\arg(\lambda_i)| > \gamma \frac{\pi}{2} \forall i.$$

### III. MODEL DESCRIPTION

The dynamic relationship between predator and prey has long been and will continue to be one of the dominant themes in both ecology and mathematical ecology. It is well known the Lotka-Volterra prey-predator model is one of the fundamental population models, a predator -prey interaction has been described firstly by two pioneers Lotka and Volterra in two independent works [6]. Recently great considerations have been made to the fractional order models in different area of researches. The most essential property of these models is their non local property which does not exist in the integer order differential operators. We mean by this property that the next state of a model depends not only upon its current state but also upon all of its historical states. Several authors formulated fractional order systems and analyzed the dynamical and qualitative behavior of the systems [3, 4, 8, 9, 10]. In this paper, we introduce the following fractional order system of prey-predator interactions. The model for our investigation is as follows:

$$\begin{aligned} D^{\alpha_1} x(t) &= rx(t)[1 - x(t)] - \frac{ax(t)y(t)}{a + x(t)} \\ D^{\alpha_2} y(t) &= \frac{bx(t)y(t)}{a + x(t)} - cy(t) \end{aligned} \tag{3}$$

where the parameters  $r, a, b, c$  are positive and  $\alpha_1, \alpha_2$  are fractional orders.

### IV. EQUILIBRIUM POINTS, STABILITY AND NUMERICAL SOLUTIONS

Numerical solution of the fractional - order Prey - Predator system is given as follows [1]:

$$\begin{aligned} x(t_k) &= (rx(t_{k-1})[1 - x(t_{k-1})] - ax(t_{k-1})y(t_{k-1}))h^{\alpha_1} - \sum_{j=v}^k c_j^{(\alpha_1)} x(t_{k-j}) \\ y(t_{k-1}) &= (bx(t_{k-1})y(t_{k-1}) - cy(t_{k-1}))h^{\alpha_2} - \sum_{j=v}^k c_j^{(\alpha_2)} y(t_{k-j}) \end{aligned}$$

where  $T_{sim}$  is the simulation time,  $k = 1, 2, 3, \dots, N$ , for  $N = [T_{sim}/h]$ , and  $(x(0), y(0))$  is the initial conditions. To evaluate the equilibrium points, we consider

$$D^{\alpha_1} x(t) = 0$$

$$D^{\alpha_2} y(t) = 0$$

The fractional order system has three equilibria  $E_0 = (0,0)$  (trivial),  $E_1 = (1,0)$  (axial) and  $E_2 = \left(\frac{ac}{b-c}, br \left[\frac{1}{b-c} - \frac{ac}{(b-c)^2}\right]\right)$ . The equilibrium point  $E_2$  is interior which corresponds to the existence of both prey and predator species provided  $\frac{b}{a+1} > c$ .

The Jacobian matrix of the system (3) for equilibrium  $E^* = (x^*, y^*)$  is

$$J(x,y) = \begin{bmatrix} r(1-2x) - \frac{a^2 y}{(a+x)^2} & -\frac{ax}{a+x} \\ \frac{aby}{(a+x)^2} & \frac{bx}{a+x} - c \end{bmatrix} \quad (4)$$

From (4), Jacobian matrix for  $E_0$  is

$$J(E_0) = \begin{bmatrix} r & 0 \\ 0 & -c \end{bmatrix}$$

and the eigenvalues of matrix  $J(E_0)$  are  $\lambda_1 = r$  and  $\lambda_2 = -c$ . Using lemma (5), the characteristic equation of the linearized system (3) at the equilibrium point  $E_0$  is

$$(\lambda^{0.99} - r)(\lambda^{0.99} + c) = 0$$

Jacobian matrix for  $E_1$  is

$$J(E_1) = \begin{bmatrix} -r & -\frac{a}{a+1} \\ 0 & \frac{b}{a+1} - c \end{bmatrix}$$

The eigen values of matrix  $J(E_1)$  are  $\lambda_1 = -r$  and  $\lambda_2 = \frac{b}{a+1} - c$ .

Most of the fractional order differential equations do not have exact analytic solutions. Hence we seek numerical techniques to analyze the behavior of the system (3). In the following examples, we illustrate the stability properties of the model by providing time plots and phase portraits.

**Example 1.** Let us consider the parameter values  $r = 0.2$ ;  $a = 1$ ;  $b = 2$ ;  $c = 1.3$  and the derivative order  $\alpha_1 = \alpha_2 = 0.99$ . For these parameter the corresponding eigenvalues are  $\lambda_1 = -0.2$  and  $\lambda_2 = -0.3$  for  $E_1$ , which satisfy conditions  $|\arg \lambda| > \alpha \frac{\pi}{2}$ . It means the system (1) is stable, Fig-1. Also using lemma (5) the characteristic equation of the linearized system (3) at the equilibrium point  $E_1$  is

$$(\lambda^{0.99} - 0.2)(\lambda^{0.99} + 0.3) = 0$$

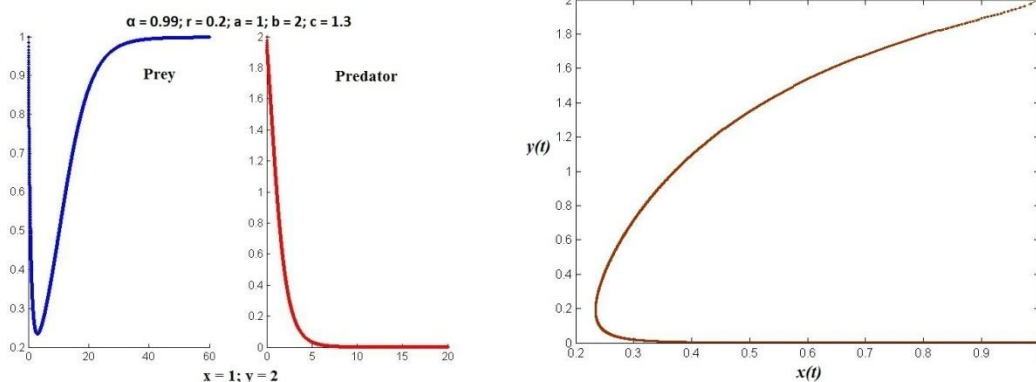


Fig1. Time plot and Phase diagram of Equilibrium point  $E_1$

Jacobian matrix for  $E_2$  is

$$J(E_2) = \begin{bmatrix} cr \left(1 - \frac{a(b+c)}{b(b-c)}\right) & -\frac{ac}{b} \\ \frac{r(b-c)}{a} - cr & 0 \end{bmatrix}$$

Here Trace of  $J = cr \left( 1 - \frac{a(b+c)}{b(b-c)} \right)$  and Det of  $J = \frac{cr}{b} [b - c(a + 1)]$ .

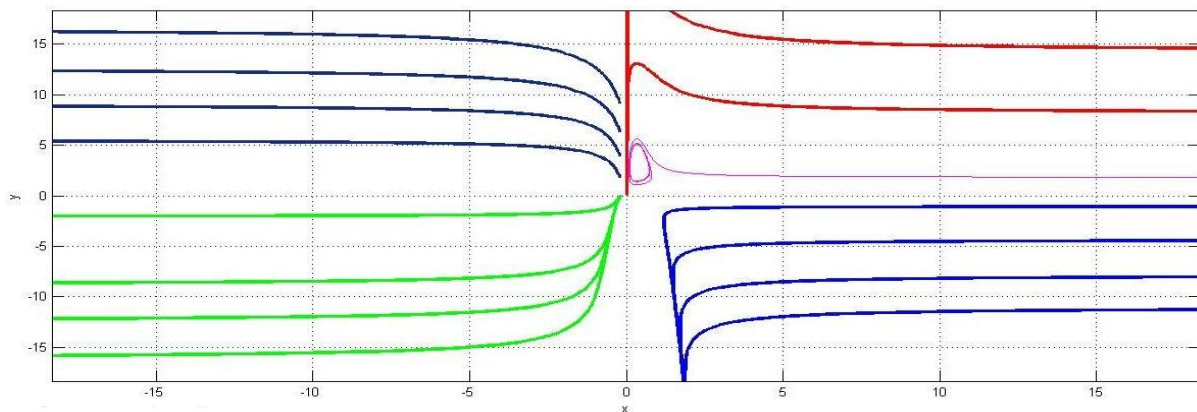


Fig 2. Phase diagram of Prey Predator Model of system (3)

**Example 2.** Let us consider the parameters with values  $r = 1.99$ ;  $a = 0.2$ ;  $b = 2$ ;  $c = 1.25$  and the derivative order  $\alpha_1 = \alpha_2 = 0.9$ . For these parameter the corresponding eigenvalues are  $\lambda_{1,2} = 0.7048 \pm i0.3537$  for  $E_2$ , which satisfy conditions  $|\arg \lambda| > \alpha \frac{\pi}{2}$ . It means the system (3) is stable, see Fig-3. Also using lemma (5) the characteristic equation of the linearized system (3) at the equilibrium point  $E_2$  is  $\lambda^{180} - 1.4096\lambda^{90} + 0.6219 = 0$ .

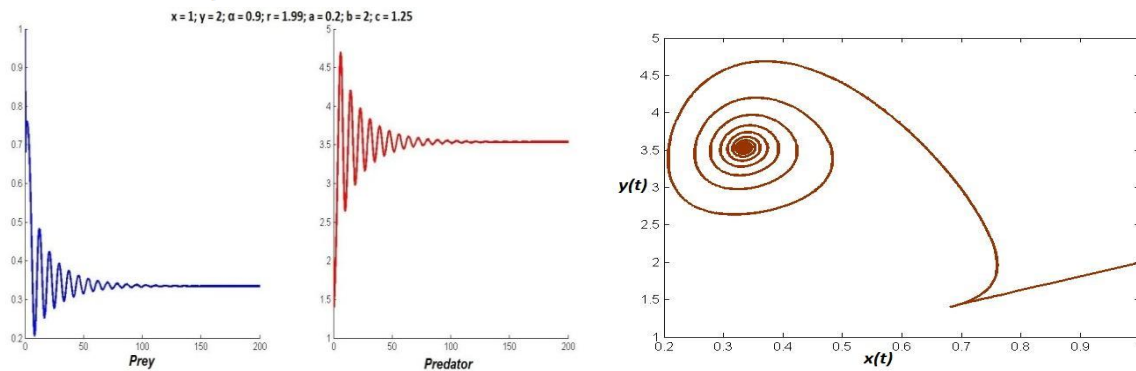


Fig 3. Time plot and Phase diagram of Equilibrium point  $E_2$  with Stability

**Example 3.** Let us consider the parameters with values  $r = 1.99$ ;  $a = 0.1$ ;  $b = 2$ ;  $c = 1.5$  and the derivative order  $\alpha_1 = \alpha_2 = 0.99$ . For these parameter the corresponding eigenvalues are  $\lambda_1 = 1.6172$  and  $\lambda_2 = 0.3230$  for  $E_2$ , which not satisfy conditions  $|\arg \lambda| > \alpha \frac{\pi}{2}$ . It means the system (3) is unstable, see fig-4. Also using lemma (5) the characteristic equation of the linearized system (3) at the equilibrium point  $E_2$  is  $\lambda^{198} - 1.9402\lambda^{99} + 0.5224 = 0$ .

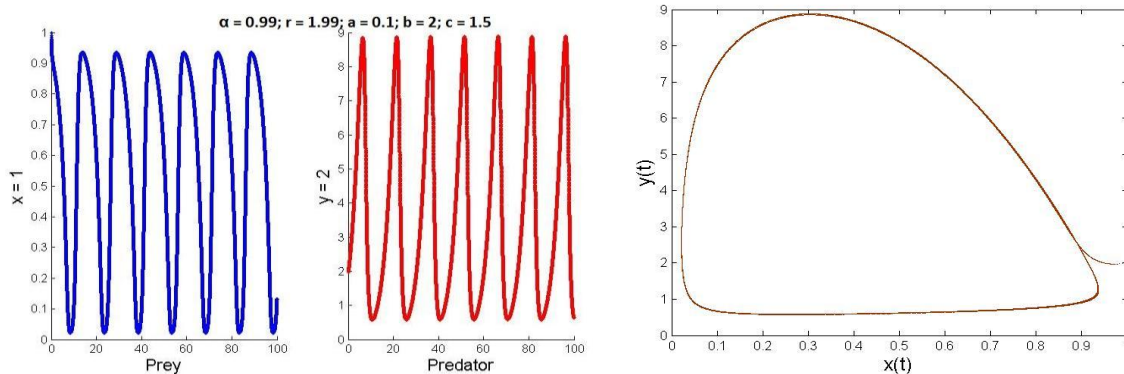


Fig4. Time plot and Phase diagram of Equilibrium point  $E_2$  with Unstability

**Example 4.** Let us consider the parameters with values  $r = 1.99$ ;  $a = 0.17$ ;  $b = 2$ ;  $c = 1.3$  and the derivative order  $\alpha_1 = \alpha_2 = 0.9$ . For these parameter the corresponding eigenvalues are  $\lambda_{1,2} = 0.1789 \pm i0.7665$  for  $E_2$ , which satisfy conditions  $|\arg \lambda| > \alpha \frac{\pi}{2}$ . It means the system (3) is Unstable, see fig-5. Also using lemma (5) the characteristic equation of the linearized system (3) at the equilibrium point  $E_2$  is

$$\lambda^{1.80} - 0.3579\lambda^{0.90} + 0.6169 = 0.$$

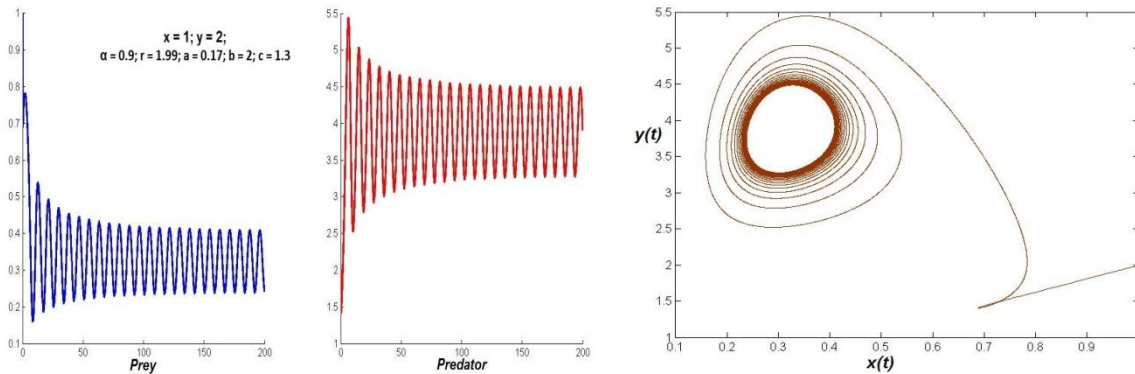


Fig 5. Time plot and Phase diagram of Equilibrium point  $E_2$  with Limit Cycle

## V. CONCLUSION

In this paper, we considered and investigated the fractional-order predator-prey model. The stability of equilibrium points is studied. Also we provided numerical simulations exhibiting dynamical behavior and stability around equilibria of the system.

## REFERENCES

- [1] Ivo Petras, *Fractional order Nonlinear Systems - Modeling, Analysis and Simulation*, (Higher Education Press, Springer International Edition, April 2010.)
- [2] A. A. Kilbas, H. M. Srivastava and J. J. Trujillo, "Theory and applications of fractional differential equations", Elsevier, Amsterdam, 2006.
- [3] Leticia Adriana Ramirez Hernandez, Mayra Guadalupe Garcia Reyna and Juan Martinez Ortiz, *Population dynamics with fractional equations (Predator-Prey)*, Vol. 23 (NE-2) *Clculo fraccionario* Noviembre 2013.
- [4] Margarita Rivero, Juan J. Trujillo, Luis Vzquez, M. Pilar Velasco, *Fractional dynamics of populations*, *Applied Mathematics and Computation* 218 (2011) 1089 - 1095.
- [5] K. S. Miller and B. Ross, *An Introduction to The Fractional Calculus and Fractional Differential Equations*, (John Wiley & Sons, INC 1993)
- [6] Murray JD. *Mathematical biology*. (2nd ed. Berlin: Springer-Verlag; 1993)
- [7] Oldham K. and Spanier J., *The fractional calculus: Theory and applications of differentiation and integration to arbitrary order*, (Academic Press, 1974)
- [8] H.A.A. El-Saka, *The fractional-order SIS epidemic model with variable population size*, *Journal of the Egyptian Mathematical Society* (2014) 22, 50 - 54.
- [9] Xueyong Zhou, Qing Sun, *Stability analysis of a fractional-order HBV infection Model*, *Int. J. Adv. Appl. Math. And Mech.* 2(2) (2014) 1 - 6 (ISSN: 2347-2529).
- [10] A. George Maria Selvam, R. Janagaraj and D. Abraham Vianny, *Dynamics in a Fractional Order Prey - Predator Interactions*, *Mathematical Modelling and Applied Computing*. ISSN 0973-6093 Volume 6, Number 1 (2015), pp. 1-6.

## Estimation Technique of the number of nodes in underwater wireless communication network

Eng. Md. Ismail Haque<sup>1</sup>, Eng. Md. Nurul Anwar Tarek<sup>2</sup>, Eng. Md. Ar Rafiul Faisal<sup>3</sup>

<sup>1</sup>(EEE, International Islamic University Chittagong, Chittagong, Bangladesh)

<sup>2</sup>(EEE, International Islamic University Chittagong, Chittagong, Bangladesh)

<sup>3</sup>(Instrument Tx Testing, Energypac Engineering Ltd, Rangpur, Bangladesh)

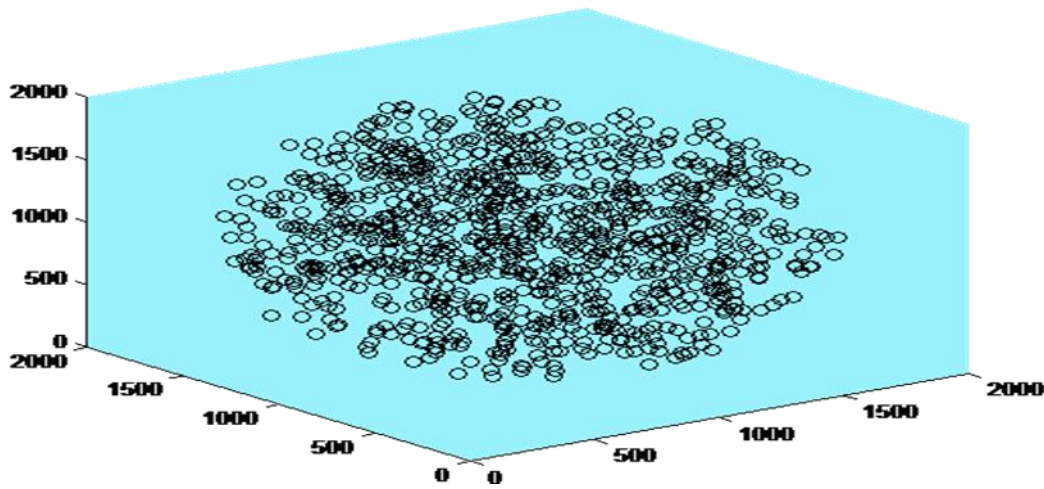
**ABSTRACT :** Node estimation is very essential for a network's proper operation. It is so complicated to estimate in underwater soundings using conventional techniques. An alternative method of node estimation based on cross correlation of the signals from the nodes has proposed in this paper. It can be applied to any environment networks, from underwater to space. But in this paper, underwater wireless communication network (UWCN) is most significant network. 3D space has considered in this experimental phenomena. For estimating the number of node, two sensors are used as receiver. In this method, different number of bin has been used for node estimation. A relative parameters have been discussed which leads us to select the suitable estimation of network.

**Keywords -** Bin, Wireless Sensor Network (WSN), Cross-Correlation Function (CCF), Underwater Communication network (UCN), Node- Estimation

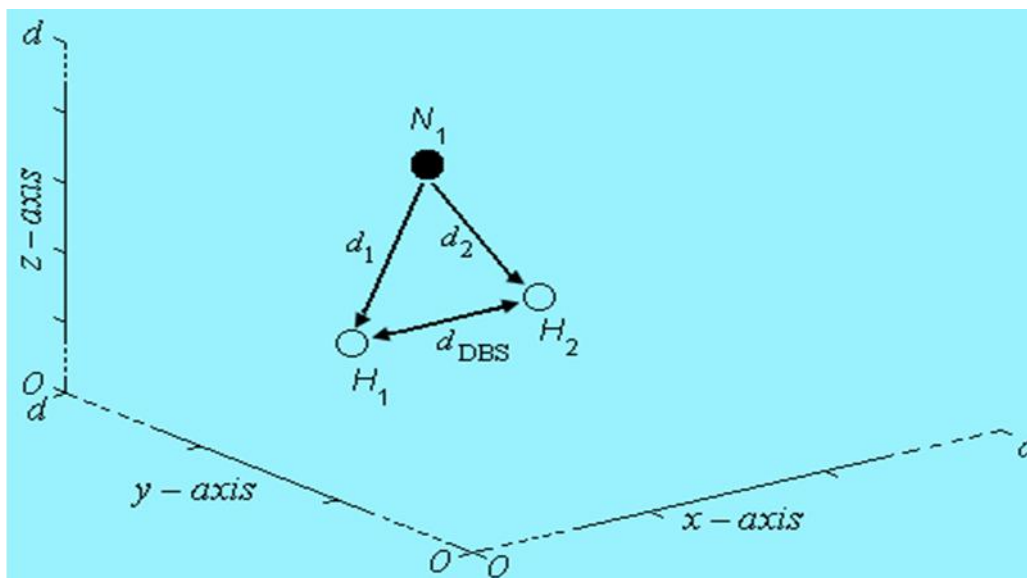
### I. INTRODUCTION

The technique of cross-correlation is an essential statistical tool in various fields of interest. It has been used in communication networks to identify and localize nodes, and for angle of arrival (AOA) estimations of signals from the nodes in a WSN. Some researchers have used it for the detection of weak signals in the field of cardiology. In this paper, the use of the cross-correlation function is to estimate the number of signal sources (nodes in WCN). It begins with the formulation of the cross-correlation of random signals, which is the starting material and method for estimating the number of nodes in a network. In ad hoc networks where a node needs to know the number of neighbors, cross-correlation is performed by a computer associated with the node. In other networks, cross-correlation is performed by a remote computer controlled by testing personnel. All the signals transmitted are received by the receiving node and recorded in the associated computer, in which the cross-correlation is performed. Transmission and reception of the signals are performed for a time frame which is called signal length throughout this thesis. The received signals are the delayed copy of the transmitted signals. The proposed method does not require any time synchronization and thus the time stamp is not a performance factor. The communication requirement that need to be satisfied is that the transmitters and the receivers need to be capable of transmitting and receiving signals for the specified recorded time without becoming overheated.

II. FORMULATION OF RANDOM SIGNAL CROSS-CORRELATION



(a)



(b)

Figure 1 Distributions of underwater network nodes in 3D space:

(a)  $N$  nodes; and (b) only one node

Consider two receiving nodes surrounded by  $N$  transmitting nodes in a 3D space, as shown in Figure 1 (a). In this figure red color indicates sensor and others indicate nodes. Assume that the transmitting nodes are the sources of white Gaussian signals and are uniformly distributed over the volume of a large sphere, the Centre of which lies halfway between the receiving nodes, because only a sphere provides equal amounts of signals from every direction. The propagation velocity is assumed to be constant which, in our case, is the sound velocity,  $S_p$ , in the medium. To make the distinction between the receiving and transmitting nodes easily understandable, we call them the *sensor/receiver* and *node*, respectively.

To formulate the random signal cross-correlation problem in this analysis, the two sensors,  $H_1$  and  $H_2$ , and a node,  $N_1$ , are taken at locations  $(x_1, y_1, z_1)$ ,  $(x_2, y_2, z_2)$  and  $(x_3, y_3, z_3)$ , respectively, somewhere inside the sphere, as shown in Figure 1 (b). The distance between the sensors,  $d_{DBS}$  is then

$$d_{DBS} = \sqrt{(x_1 - x_2)^2 + (y_1 - y_2)^2 + (z_1 - z_2)^2} .$$

Consider  $N_1$  emits a signal,  $S_1(t)$ , which is infinitely long. So the signals received by  $H_1$  and  $H_2$  are, respectively:



$$S_{r_{11}}(t) = \alpha_{11} S_1(t - \tau_{11})$$

$$S_{r_{12}}(t) = \alpha_{12} S_1(t - \tau_{12})$$

where,  $\alpha_{11}$  and  $\alpha_{12}$  are the respective attenuations due to the absorption and dispersion present in the medium,  $\tau_{11} = \frac{d_{11}}{S_p}$  and  $\tau_{12} = \frac{d_{12}}{S_p}$  the respective time delays for the signal to reach the sensors, and  $S_p$  is the speed of wave propagation.

Assuming  $\tau$  is the time shift in the cross-correlation, and then the CCF is:  $C_1(\tau) = \int_{-\infty}^{+\infty} S_{r_{11}}(t) S_{r_{12}}(t - \tau) dt$

Which takes the form of a delta function as it is a cross-correlation of two white Gaussian signals where one signal essentially is a delayed copy of the other.

The final CCF between the signals at the sensors is:

$$\begin{aligned} C(\tau) &= \int_{-\infty}^{+\infty} S_{r_{11}}(t) S_{r_{12}}(t - \tau) dt \\ &= \int_{-\infty}^{+\infty} \sum_{j=1}^N \alpha_{j1} S_j(t - \tau_{j1}) \sum_{j=1}^N \alpha_{j2} S_j(t - \tau_{j2} - \tau) dt \end{aligned}$$

Which takes the form of a series of delta functions as it is a cross-correlation of two signals which are the summations of several white Gaussian signals.

### III. CCF FOR INFINITELY LONG SIGNAL

If a source emits an infinitely long unity strength Gaussian signal, which is recorded at two sensors with the corresponding time delays and attenuations, the cross-correlation function of these two signals can be expressed by a delta function, whose amplitude depends on the attenuations and position will be the delay difference of the signals from the Centre of the CCF.

Thus, the CCF for such a source is

$$C_1(\tau) = \alpha_{11} \alpha_{12} \delta\left(\tau - \left[\frac{d_{11} - d_{12}}{S_p}\right]\right)$$

The CCF for  $N$  source is summation of  $N$  numbers of deltas with their corresponding positions which are determined by the delay differences of the signals in the sensors.

$$C(\tau) = \sum_{j=1}^N \delta\left(\tau - \left[\frac{d_{j1} - d_{j2}}{S_p}\right]\right)$$

It is intuitive that if  $N$  is larger than the number of bins,  $b$ , which is usually the case, the bins are occupied by more than one delta due to the same delay differences. This increases the amplitude of the deltas in the bins, and thus the CCF is expressed in terms of bins as

$$C(\tau) = \sum_{i=1}^b P_i \delta_i$$

Where  $P_i$  is the amplitude or peak of the Dirac delta  $\delta_i$  in the  $i^{\text{th}}$  bin.

The above analytical expression is verified by simulation in the following Figure 2. Here we have used 50 nodes and 29 bins. The nodes are the sources of equal unity power signal. It is shown that some bins are occupied by only one, some of them by more than one, and rest of them is empty due to the delay differences in the cross-correlation process. The results follow the expression where the  $P_i$  values are as follows.

$P_1 = P_{21} = P_{24} = 3, P_2 = P_5 = P_9 = P_{19} = 1, \dots$  and so on.

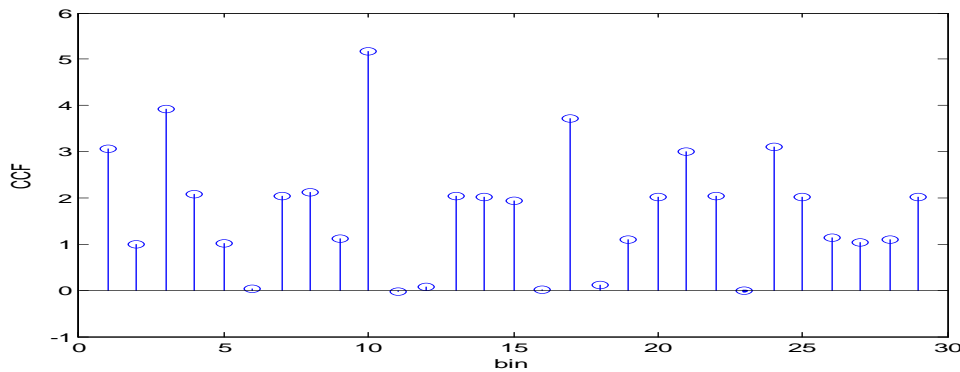


Figure 2 CCF in case:  $N=50$ , and  $b=29$

#### IV. THEORETICAL ESTIMATION

The cross-correlation problem has been reframed into a probability problem where it is shown that it follows the binomial probability distribution in which the parameters are the number of nodes,  $N$ , and the inverse of the number of bins,  $b$ .

The expected value of the first moment (the mean) of the CCF is:

$$E(X) = \text{mean}, \mu = \langle C(\tau) \rangle = np \tag{1}$$

$$= N \div b$$

Where  $b$  is twice the number of samples between the sensors (NSBS),  $m$  minus one, as we cross-correlate two vectors of length  $m \times 1$ ; and the second moment is:

$$E(X^2) = \text{second moment} = \langle C^2(\tau) \rangle \tag{2}$$

$$= (np)^2 + npq$$

From (1) and (2), we can obtain the variance:

$$\sigma^2 = E(X^2) - E(X)^2 = npq$$

$$= N \times (1/b) \times (1 - 1/b)$$

Then, the standard deviation is:

$$\sigma = \sqrt{E(X^2) - E(X)^2}$$

$$= \sqrt{N \times (1/b) \times (1 - 1/b)}$$

Thus, the ratio of the standard deviation to the mean,  $R$ , is:

$$R = \sigma \div \mu = \sqrt{\frac{q}{np}} = \sqrt{\frac{(1-1/b)}{N \times (1/b)}} = \sqrt{\frac{(b-1)}{N}} \tag{3}$$

This is the relationship between the number of nodes,  $N$ , and the ratio of the standard deviation to the mean,  $R$ , of the CCF. Since we know  $b$  and can measure  $\sigma$  and  $\mu$  (and, therefore, determine  $R$ ) from the CCF, we can readily determine the number of nodes,  $N$ . Figure 3 shows the theoretical result derived from (3) for  $b$  (Figure 3 for 29 bins).

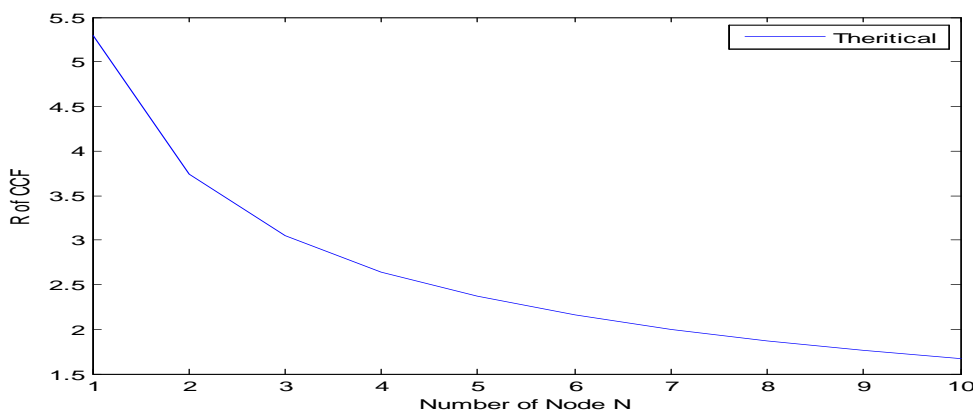


Figure 3 Theoretical  $R$  versus  $N$ : for  $b = 29$

It is clear from (3) that the ratio,  $R$ , is also dependent on  $b$ . Recalling (3),  $R = \sqrt{\frac{b-1}{N}}$  and, assuming  $b \gg 1$ , i.e.,  $b-1 \approx b$ :

$$R = \sqrt{\frac{b}{N}}$$

## V. ESTIMATION FROM SIMULATION

After cross-correlating signals received at two sensors from a number of random Gaussian signal sources, the CCF, which is a rectangular pulse over the space between the sensors, can be obtained. Then, it is easy to estimate the mean and standard deviation of this CCF and, therefore, the ratio,  $R$ , as the sampling rate and  $d_{DBS}$  are known. In the particular case in which the sampling rate, speed of propagation and  $d_{DBS}$  are fixed, (3) tells us that the ratio,  $R$ , is inversely proportional to the square root of the number of nodes,  $N$ . Thus, (3) becomes:

$$R \propto \frac{1}{\sqrt{N}} \quad \text{or} \quad R = \frac{c}{\sqrt{N}}$$

Where  $c (= \sqrt{b-1})$  is a known constant. Thus, from the simulation, we can readily estimate the number of nodes by knowing only the ratio of the standard deviation to the mean of the CCF.

## VI. CONCLUSION

Estimation of the number of nodes is investigated here with theory (obtained from statistical property of CCF) and simulation. So,  $R$  of CCF is the suitable estimation parameter for fast and efficient size estimation of underwater network using cross-correlation based technique. It can be seen from the results that the proposed technique is good enough for estimation. This simple and novel technique might be an effective alternate of the protocol techniques.

## REFERENCES

- [1] M. S. Anower, S. A. H. Chowdhury, J. E. Giti, A. S. M. Sayem, M. I. Haque, "Underwater network size estimation using crosscorrelation:selection of estimation parameter", The 9th International Forum on Strategic Technology (IFOST), October 21 - 23, 2014, Cox's Bazar, Bangladesh.
- [2] C. B. Li, H. Li, and P. W. Wang, "Forward predicting and backward verifying tags number estimation in RFID system," *Applied Mechanics and Materials*, vol. 321-324, pp. 2902-2905, 2013
- [3] C. Yihong, F. Quanyuan, Z. Ma, and T. Liu, "Multiple-bits-slot reservation aloha protocol for tag identification," *IEEE Transactions on Consumer Electronics*, vol. 59, no. 1, pp. 93-100, February 2013
- [4] J M. H. Nazir, S. Mehmood, N. Sheriff, and A. Adeel, "Improved efficient RFID tag estimation scheme," *International Journal of Computer Applications*, vol. 47, no. 17 pp. 16-19, 2012.
- [5] M. S. A. Howlader, M. R. Frater, M. J. Ryan, "Estimating the Number and Distribution of the Neighbors in an Underwater Communication Network", *Proceedings of Second International Conference on Sensor Technologies and Applications (SENSORCOMM'08), 25-31 Aug, 2008, France*

## Applicability of Path Loss Prediction in Macrocellular Environment Using Artificial Neural Networks in Hyderabad City

Syed Mudassar Ali<sup>1</sup>, Mohammed Mouzam Ali<sup>2</sup>

<sup>1</sup>(Department of Information Technology, Deccan College of Engineering/ Osmania University,India)

<sup>2</sup>(Department of Information Technology, Deccan College of Engineering/ Osmania University,India)

**ABSTRACT:-**This paper investigates the applicability of Artificial Neural Networks in predicting the propagation path loss in the wireless environment. The proposed path loss prediction model composed of Feed Forward Neural Network trained with measured data using levenberg-marquardt algorithm. The system consists of a GUI application for predicting path loss using various models suitable for different environments. A comparative analysis of measured path loss and predicted path loss is done.

**Keywords:** -Path loss prediction, artificial neural networks, measured path loss, predicted path loss

### I. INTRODUCTION

Path loss is the degradation in received power of an Electromagnetic signal when it propagates through space. Path loss is due to several effects such as free space path loss, refraction, diffraction, reflection, coupling and cable loss, and absorption. Path loss depends on several factors such as type of propagation environments, distance between transmitter and receiver, height and location of antennas. Propagation models are used extensively in network planning, particularly for conducting feasibility studies and during initial deployment. Radio engineers carried out signal strength measurement for a specific area and compared the observed output with that of predicted outputs from different widely accepted propagation models so as to find out which model best predict the path loss for the given scenario. Many propagation models are available for path loss predictions. These models can be broadly classified into two models deterministic and empirical models. Deterministic models are based on the laws of electromagnetic wave propagation whereas Empirical models are based on extensive collection of data for specific case [1,2].

To encompass the benefits of both models Artificial Neural Network models are proposed. As ANN models can easily comply with different environments and it has high processing power. ANN models can be built according to the type of model depending on the scenario required. Artificial neural networks (ANNs) have also been proposed to obtain prediction models that are more accurate than standard empirical models while being more computationally efficient than deterministic models. ANNs have been shown to successfully perform path loss predictions in urban environments [4, 5, 6]. Therefore, to obtain an ANN model that is accurate and generalizes well, measurement data from many different environments had been used in the training process. The trained ANN model consist of inputs that contain information about the transmitter and receiver locations, surrounding buildings, frequency, etc. while the output gives the propagation loss for those inputs. The feasibility analysis of different models has been done for macrocellular propagation environments in Hyderabad city by taking four different areas namely: Amber Nagar, Osmania University, Vidya Nagar and Zamistanpur and Field Strength Measurements offers a better means to understand what path loss model to use in certain propagation environments. Field strength measurements were conducted on the existing GSM (948.2, 951.4, 949.8, and 948.8) MHz Network of BSNL Telecom on the locations of interest.

### II. ARTIFICIAL NEURAL NETWORKS

Artificial Neural Networks (ANNs) are relatively adaptive models based on the neural structure of the brain. The brain learns from experience. Artificial neural networks try to mimic the functioning of brain. An ANN is configured for a specific application, such as pattern recognition or data classification, through a learning process.

The network is composed of a large number of highly interconnected processing elements (neurons) working in parallel to solve a specific problem. Neural networks learn by example. By examples ANN can create its own model [4,5].

In this work the ANN are trained using the measured field data to create its own model of behavior. Later on this model can be used for predicting path loss values by observing the measured values. With this generalization is achieved. There are many types of network architectures used. In this work feed forward network is used for simplicity. This network (Figure 1) consists of one or more hidden layers, whose computation nodes are called hidden neurons or hidden units. The function of hidden neurons is to interact between the external input and network output in some useful manner and to extract higher order statistics. The source nodes in input layer of network supply the input signal to neurons in the second layer (1st hidden layer). The output signals of 2nd layer are used as inputs to the third layer and so on. The set of output signals of the neurons in the output layer of network constitutes the overall response of network to the activation pattern supplied by source nodes in the input first layer [5,7].

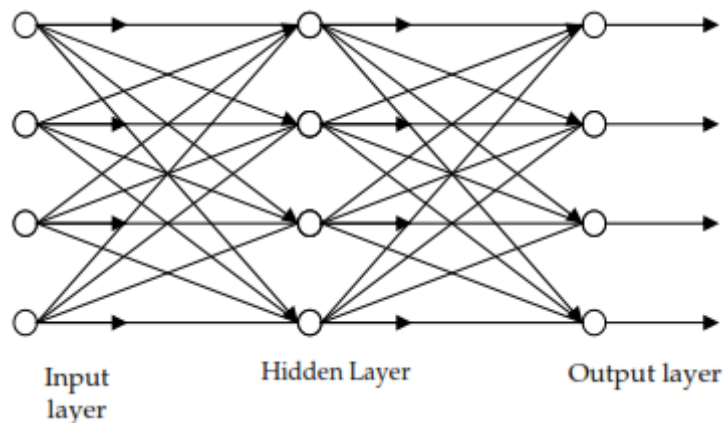


Figure 1: A Multi-layer feedforward network

### Training of Artificial Neural Networks

Once a network has been structured for a particular application, it is ready for training. At the beginning, the initial weights are chosen randomly and then the training or learning begins using training algorithms. There are many algorithms available for training a neural network but the simplest one is gradient descent method. Levenberg Marquardt (LM) training algorithm is used for the project.

Levenberg Marquardt algorithm is one of the fastest training algorithm for moderate sized networks [5,8].

The LM algorithm is a combination of gradient descent method and the Gauss Newton method. LM algorithm was designed to approach 2nd order training speed without having to compute the hessian matrix. Hence the Hessian matrix is computed as,

$$H=J^T J \quad (1)$$

Where the gradient is computed as,

$$g=J^T e \quad (2)$$

Where,

J is the Jacobian matrix that contains first derivatives of the network errors

e is a vector of network errors

The LM algorithm uses this approximation to the Hessian matrix in the following Newton like update is given

as,

$$X_{k+1} = X_k - [J^T J + \mu I]^{-1} J^T e \quad (3)$$

When the scalar  $\mu$  is zero, it will act like Newton's method using the approximate Hessian matrix. When  $\mu$  is large, it acts like gradient descent with a small step size. Newton's method is faster and accurate near an error minimum, so the aim is to shift toward Newton's method as quickly as possible. Thus  $\mu$  is decreased after each successful step and is increased only when a tentative step would increase performance function. In this way, the performance function is always reduced at every iteration of the algorithm [5,8].

LM algorithm was found to be one of the fastest algorithms that fits for the optimal configuration of the proposed ANN model.

### III. METHODOLOGY

Measured data was collected to train and tune neural network model, so that it can create its own behavior of radio waves. GSM base station data was provided by the Bharat Sanchar Nigam Limited (BSNL) which is a telecom company owned by Government of India. The base station data sheet consists of the location, cell identity, transmitted power, height of all the base stations near the Osmania University where the experiments were done. GSM module was mainly used to capture received signal strengths from the base stations. GSM data sheet is in the form of +CCED format.

The receiving antenna was held on the top of the car. The experiment setup consists of GSM modem (Wavecom WM01-G900) and a laptop with suitable interface installed on it. The car was driven starting from the main base station to the neighboring base stations. At all instants Received signal strength were captured. Four parameters namely distance, frequency, mobile station height, base station height were considered as input parameters and a 4-4-1 network was created.

A set of path loss data recorded at distances of 100m to 1km for the three different base stations were taken and was used for training. 400 measurement samples of each were used. 75% of data was used for training, 15% was used for validation, and 15% was used for performance evaluation. Training was continued as long as it decrease the network's error on the validation samples.

During the training phase weights were adjusted and modified in order to obtain minimal error so that the error between the actual output and the desired output is minimized.

### IV. RESULTS

The main aim was to develop an ANN model that accurately predicts the propagation path loss. This paper presents the path loss prediction made using free space path loss, Egli, Hata, Cost-231, Walfisch-Ikegami and Neural network model. Path loss exponent is calculated for all the models and the neural network model was found to be the best suited prediction model. The path loss exponents computed for the prediction models of the three base stations are tabulated in Table1.

Table 1: Path loss exponent values of all the models.

Base Stations	Measured Path loss	Free Space Path loss	Egli	Hata	Cost 231	Walfisch Ikegami	Neural Network
Amber Nagar	5.3	2.0	4.0	3.6	3.6	2.6	5.0
Osmania University	4.7	2.0	4.0	3.5	3.5	2.6	4.6
Vidya Nagar	4.6	2.0	4.0	3.6	3.6	2.6	4.6

The performance of the ANN model was evaluated by making a comparison between expected and the measured values using error metrics. The error metric used here is mean square error (mse). The mse values computed for the ANN model are tabulated in Table 2.

Table 2: Mean square error values of the ANN model.

Distance	0.2km	0.4km	0.6km	0.8km	1.0km	Average
mse(dB)	2.77	2.73	2.68	2.63	2.58	2.67

Table 3 presents the mse values for all the models to show the better accuracy of the ANN model.

Table 3: Mean square error values of the ANN model.

Free space	Egli	Hata	Cost 231	Walfisch Ikegami	Neural Network
14.77	10.73	3.68	4.63	10.58	2.67

From the above statistics it is noted that the ANN model has an average of 2.67dB mse value. This value falls below 6dB which is better for good signal propagation [2].

Below figures show the best performance obtained during the training process and also regression plot.

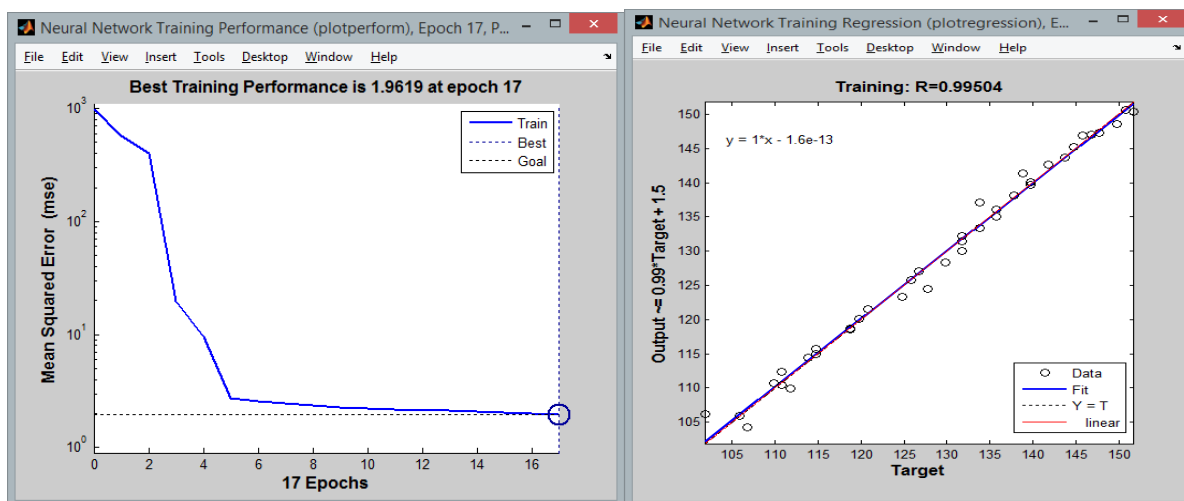


Figure 2 : Training performance and regression plott of the proposed ANN model.

## V. CONCLUSION

The proposed ANN model for path loss prediction gives better performance compared to the empirical models. As ANN's are capable of best function approximation they are useful for the propagation loss modeling. ANN model was found to be more accurate than empirical models and computationally efficient than deterministic models. A test bed is provided for validating the loss for each scenarios by considering different models. The GUI system developed makes easier to plan the best value of parameters for the specified path loss based on the need. ANN model can be used to take account of various types of environments based on measured data taken in the desired environment.

## VI. RECOMMENDATIONS

The ANN model provides transcription for new models. For better path loss prediction, by introducing of additional parameters during the training process such as buildings, trees, mountains, road orientation makes it more feasible and efficient. This is to make sure that the path loss calculated indicates overall obstacles. The outcome of this model can be used for interference estimation and frequency assignment planning for new network. Telecommunication companies in Hyderabad can use this model for realistic planning of GSM networks, intelligent placement of base stations, link budget analysis, and frequency re-use, better coverage predictions and interference reduction. Path loss and received signal strength can be used to estimate user position.

## REFERENCES

- [1] Rappaport T.S, "Wireless Communications", second edition, printed in India, 2010.
- [2] Simon R. Saunders and Alejandro Aragon-Zavala, "Antennas and Propagation for Wireless Communication System", 2007.
- [3] Joseph M.Mom, Callistus O. Mgbe and Gabriel A. Igwe, "Application of Artificial Neural Network for Path loss prediction in urban macrocellular environment", AJER, VOL 3, pp-270-275, 2014.
- [4] Erik Ostlin, Hans-Jurgen Zepernicka and Hajime Suzuki, "Macrocell path-loss prediction using Artificial Neural Networks", IEEE Transactions on Vehicular Technology, vol. 59, no 6, July 2010.
- [5] M. T. Hagan, H. B. Demuth and M. H. Beale Neural Network Design, 2002 :PWS
- [6] M. T. Hagan and M. B. Menhaj "Training feedforward networks with the Marquardt algorithm", IEEE Trans. Neural Network., vol. 5, no. 6, pp.989 -993 1994.
- [7] H. Demuth and M. Beale Neural Network Toolbox, 2014 : MATLAB.
- [8] M. T. Hagan, H. B. Demuth and M. H. Beale Neural Network Design, 1996 :PWS

## Design of a Settling Basin for Small Scale Water Treatment Plant in Borno State, Nigeria

Hussaini A Abdulkareem, Mahmud Awwal Tanimu, Ishaq T Muhammad, and Sani M Suleiman

Department of Mechanical Engineering, School of Industrial Engineering, College of Engineering, Kaduna Polytechnic, Nigeria

**Abstract:** A settling basin being one of the major components in any water treatment plant be it small or large scale was design for a small village community with an access river or stream water source. The capacity of the settling basin is taken as  $10m^3$  which is same dimension of the flocculate so as to ease construction and better flexibility of unit to future expansion. The overflow rate of the settlement tank is evaluated to be 51.84m/day with a settlement velocity  $V_s$  of 0.06m/s.

**Key words:** Design, settling basin, settlement velocity, overflow rate

### I. INTRODUCTION

Preliminary settling is the most widely applied method to heavily silted and turbid waters. This makes use of gravity for particles to settle from a suspended state in the water usually from the top to the bottom of the settling tank, the time of settling depends on many factors: which includes the densities of the particles and water, the design of the tank etc. Although a further settling is needed for treatment process, this is employed to reduce the proper settling which occurs later in the stages at a sort of uniform velocity.

Some of the tank designs used is the Horizontal flow or the vertical basins. The Horizontal-flow basins tend to be a better type of pre-settlement basin especially in cases of waters with high amount of silt and turbidities. The vertical flow basins tend to be difficult to operate once the dry silt by weight is 1000mg/1. Where this occurs It is helpful to put in a small, non-chemically assisted horizontal flow basin immediately upstream of the vertical flow, to keep the peaks of suspended solids well below 1000mg/1 [1].

Once the provision of pre-settlement tanks where conditions require them can be assumed, it follows that all water reaching a main settling basin will have suspended solids of less than 1000mg/1 by dry weight and under these conditions any properly designed and operated basin should be able to produce water fit to admit to rapid gravity sand filters. [1]

#### Settling basin:

Settling tank, sedimentation basin are synonymous terms and signify the chamber in which settlement occurs. Such chambers mostly belong to two great families, namely horizontal flow tanks in which the direction of water flow is predominant horizontal and vertical flow tanks in which the water enters the bottom and overflows from the top.

### II. SEDIMENTATION

When silt-laden water is admitted to the still conditions of a sedimentation basin its velocity tends to fail to zero, its capacity to transport solids disappears, and the solids begin to settle.

It has long been established that a discrete particles setting freely through water quickly attains a constant velocity [3].

$$V_s = \left[ \left( \frac{2g}{c} \right) (s - 1) \frac{V}{Ac} \right]^{1/2} \dots \dots \dots (1)$$

Where,

$V_s$  = velocity of settlement cm/s

$g$  = acceleration due to gravity (981cm/s<sup>2</sup>)



$c$  = drag coefficient

$s$  = specific gravity of the particle

$v$  = volume of the particle,  $\text{cm}^3$

$A_c$  = projected area of particle,  $\text{cm}^2$

From the above equation, it can be seen that increases in the size of the particle ( $V$ ) and the drag coefficient ( $c$ ) speeds up and slow down respectively [3]. Most of the spherical particles of concern in water treatment settle in accordance with a modified form of equation (1) known as Stokes Law, in which  $V_s$  can be written as,

$$V_s = \frac{g}{18\mu}(\rho_1 - \rho)d^2 \dots\dots\dots (2)$$

Where,

$\rho_1$  = density of the particle,  $\text{g/cm}^3$

$\rho$  = density of the fluid,  $\text{g/cm}^3$

$\mu$  = dynamic viscosity of the fluid,  $\text{g/cms}$

$d$  = diameter of the particle,  $\text{cm}$

Or in term of the kinematic viscosity i.e  $\nu = \frac{\mu}{\rho} \dots\dots\dots (3)$

$$V_s = \frac{g}{18\nu\rho}(\rho_1 - \rho)d^2 \dots\dots\dots (4)$$

For settling in Stokes Law region, the drag coefficient ( $c$ ) is  $24/\text{Re}$ , where ( $\text{Re}$ ) is the Reynolds number and thus it decreasing as the Reynolds number increases. Reynolds number is also inversely proportional to Kinematic viscosity, which decreases with rising temperature thus; higher water temperature decreases the drag coefficient and increases the rate of settlement [1].

### III. DESIGN CONSIDERATIONS

Pure theory is of very little use in designing a settling basin. For one thing it is difficult to predict the worst condition under which the basin will have to operate. Although laboratory tests on a series of sample will give an indication of the most suitable types of basin and the required doses and of optimum floc formation and settling velocity, general factors of safety have to be allowed before the results can safely be applied in practice. Each of the four functional zones of sedimentation basins and flotation tanks presents special problems of hydraulic and process design that depend on the behavior of the suspended matter within the tank, during removal and after deposition as sludge or scum [3].

Size, density and flocculating properties of the suspended solids, together with their tendency to entrain water, determine the geometry of the settling or rising zone. Their concentration by volume and the contemplated length of storage establish the dimensions of the bottom zone and the scum zone [3].

Putrescence and excessive accumulations are divided by removing sludge more or less continuously. Mechanical removal, it is said, becomes economical when the volume of settle able matter (including entrain water) is more than 0.1% the volume of the transporting liquid. [3] Removal devices affect tank design as well as tank operation. Thermal convection currents and wind-induced currents are held in check by housing or covering the tanks. The proper number of units is a matter of wanted flexibility of operation and economy of design [3].

Horizontal-flow tanks and vertical flow tanks have been constructed in great variety, some of which are Circular, Square or rectangular in plan. They vary in depth from 7 to 15ft, 10ft being a preferred value. Circular tanks are as much as 200ft in diameter, but they are generally held to a 100ft maximum so as to reduce wind effects. Square tanks are generally smaller. A side length of 70ft is common. Rectangular tanks have reached length of almost 300ft but a 100ft limit is generally imposed [2]. Except for steep sided sludge hoppers, the bottom of most settling tanks slopes gently. Common values lie close to 8% for circular or square tank and 1% for rectangular tanks. Foothold on a slippery surface becomes precautions at a slope of  $1\frac{1}{2}$  in. per ft. The slopes of sludge hoppers range from 1.2:1 to 2:1 (vertical: horizontal). They should be steep enough for the solids to slide to the bottom [3].

The laboratory approach for the design of horizontal – flow basins are as follows.

Tests should be made to determine the period required for the water to settle naturally in a cylinder equal in depth to the basin without the addition of coagulants or stirring. In many quite heavily turbid waters the samples quickly show a clear dividing line between the upper clarified zone and the lower zone of settled silt. If this period is short and the line of demarcation is well defined, flocculation is probably not necessary. If the period is lengthy and the zone of junction is blurred, colloids are probably present and flocculation is essential. A commonly accepted settling velocity for well-formed floc is about 3m/h [1].

The time it takes for the average suspended solids of the water at all draw-off points above the silt lime to fall to 2mg/l should be multiplied by a factor of safety of 3 to arrive at the nominal retention capacity of the settling zone of the basin. The factor of safety allows for inefficiency of the basin due to streaming.

On the more salty rivers commonly found in the tropics, characterized by high temperatures and heavy silt particles, 4h basins are common, but where conditions are particularly difficult (low temperature, colloids and heavy silt) 6-9h retention is not uncommon and in some of the more difficult cases pre-sedimentation tanks and flocculation are also necessary[1] . If coagulant aids are found to be effective it is probable that the above retention times could be reduced, but these aids need skilled administration and may not be suitable for use in developing countries [1].

The depth of the settling zone is normally about 3m; hence for turbid water one should add 0.6m in which precipitated silt can accumulate while awaiting removal.

Other recent developments in the design of settling basins include the spiral flow basins in which the water follows through an upward spiral path. This originated in Egypt to deal with exceptionally difficult waters. Others include the multi-storey tanks, where it is used when space is limited or structural cheapness, by building structures of two or more storeys. Other types of settling basins include the plated tanks. The plated tanks operate, by allowing the water to pass through plates supported by hangers and dog-legged, such that the silts deposit on the plates and slides down from plate to plate through the gaps, on to a belt scraper and can thus be ejected. Other types of recently developed designs of settling basin includes the lamella separator, the Hopper-bottomed sludge blanket basins and the modified hopper-bottom designs, the accelerator type solid contact clarifiers, the pulsator and the separator are recent developments in settling basins design.

#### IV. SETTLING BASINS DESIGN

A continuous-flow basin can be divided into four zones,

1. Inlet zone, in which influent flow and suspended mater disperse over the cross section at right angle to flow.
2. A settling zone in which the suspended particles settle within the flowing water.
3. A bottom zone in which the removed solids accumulate and from which they are withdrawn as underflow.
4. Outlet zones in which the flow and remaining suspend particles assemble and are carried to the effluent conduit [2].

The paths taken by discrete particles settling in a horizontal flow rectangular or circular basin are almost the same. They are determining by the vectors sums of the settling velocities ( $V_s$ ) displacement velocities ( $V$ ) of the basin [2].

Consider a particle settling with velocity ( $V_s$  cm/s), and being carried horizontally by water flowing at a velocity ( $V$  cm/s).it would follow the inclined path AB. and by comparing similar triangle, the particle would just reach the bottom when  $V_s/V = D/L$ . if,

$Q$  is rate of flow  $m^3/s$ ,

$W$  is width of basin  $m$ ,

$A$  is area ( $=WL$ )  $m^2$

Then,

$$Q = \frac{V}{100} WD \dots\dots\dots(5)$$

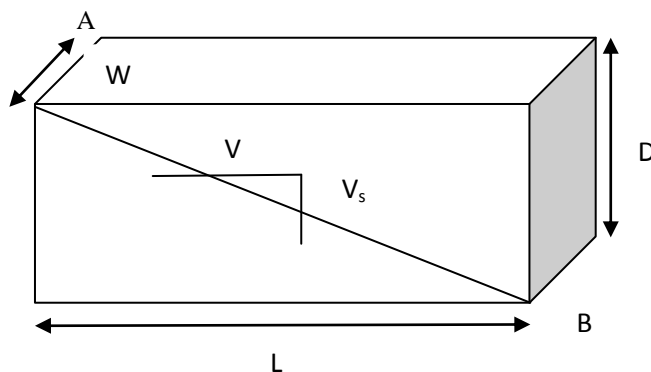
And,

$$V_s = \frac{100}{A} Q \dots\dots\dots (6)$$

The quality  $\frac{Q}{A}$  is known as the overflow rate or velocity. It is generally stated in meters per day [1].

The importance of surface area in the simple theory of settlement is clear and it would logically appear that the depth of the basin and therefore the retention time of the liquid is of little significant [1].

Fig 1.0 below shows the theoretical settlement in a horizontal flow basin.



In upward flow basins settlement in the upper regions is controlled by making the area (A) of the tank sufficiently big, so that  $V < V_s$ , where  $v$  is the upward velocity of the water ( $\frac{Q}{A}$ ) and  $V_s$  is the settling velocity of the particle. When this condition is achieved the particle must be settling through the rising water and clarification must result [1].

In practice, the upward velocity of water is kept down to about half the settling velocity of the floc particles. The normal velocity of settlement of well-formed floc is about 3m/h. if coagulant aids are used this may become 6-10m/h, and where the floc is consolidated pulsing or other devices, it may be somewhat more. In a softening plant the settling velocity of the particle of calcium carbonate is about 8m/h, applying the commonly used factor of 0.5, many upward flow basins are provided with designed to limit the upward velocity of the water [1].

To ease construction and better flexibility of unit to future expansion, the settlement basin is designed to the same dimension as the flocculation tank. In this project a flocculation tank has being design with the follow dimensions 2m X 2m X 2.5m as well.

Natural settlement time of the water as tested is 20min, hence the retention time in basin 3 X natural settlement time. Where, 3 is a factor of safety.

It follows that retention time = 3 X 20 = 60min or 1 hr.

For a well formed floc, in a horizontal flow basin equation (6) gives the settlement velocity  $V_s$  as

$$V_s = 100Q/A = 100 \times 0.003/L \times B$$

Where L and B are the length and breadth respectively, Thus,  $V_s = 100 \times 0.003/2 \times 2.5 = 0.06\text{m/s}$

The settlement velocity of the particles is therefore 0.06m/s. The value Q/A is the overflow rate =  $0.003/2 \times 2.5$

Overflow rate = 0.0006m/s

$$= 0.0006 \times 3600 \times 24 \text{ metres per day}$$

$$= 51.84\text{m/day}$$

## V. MATERIAL SELECTION AND SPECIFICATION

The settlement basin is to be constructed with bricks; the floor should be slanted upwards by 10% of its height, 0.9m from its entry. This is done to facilitate the easy collection of silt at the lowest point of the tank, with a drain plug for sludge removal during maintenance. The drain is a tapered steel material with larger and smaller diameters of 100mm and 60mm respectively, which is fitted to the floor of the tank during construction. A steel rod 2.2m long and 10mm diameter is welded to a similar tapered solid steel (the plug) which is machined to fit into the drain this serves as a valve for the control of sludge removal, The steel rod is bent into a handle and is controlled from the top of the settlement tank.

The top of the settlement tank is covered with a light wood material 15mm thick cover the whole area of the tank.

The entry pipe is 1m long and 100mm diameter, which is provided with a union 0.5m from entry for future expansion. See diagram for necessary details.

## VI. CONCLUSION

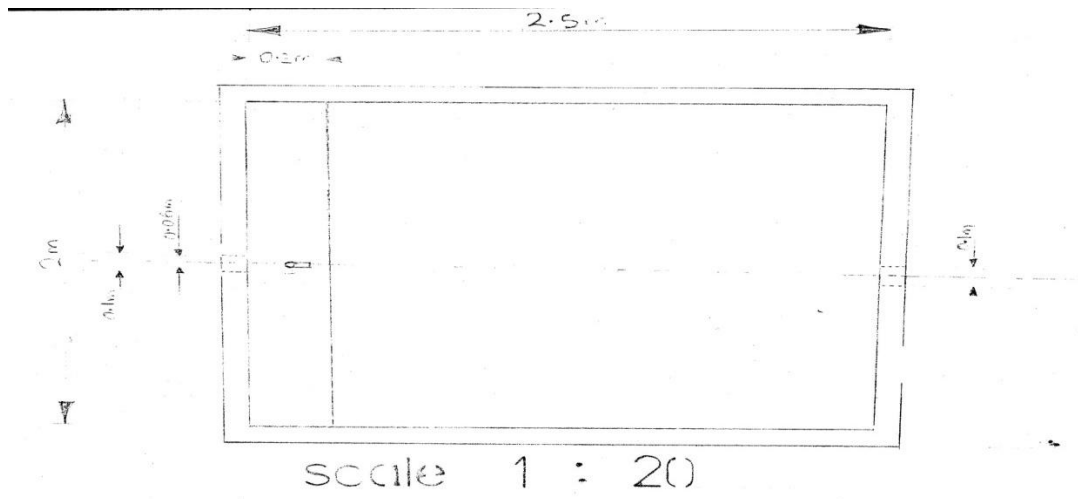
Great simplicity and economy was taken into account in the course of the design, this is necessary for a water treatment plant to be located in the villages where skilled maintenance personnel may not be readily available. However, the simplicity does not in any way compromises the required standard and safety consideration needed.

The sedimentation tank were both designed to the required purpose and made of materials appropriate for their efficient performance.

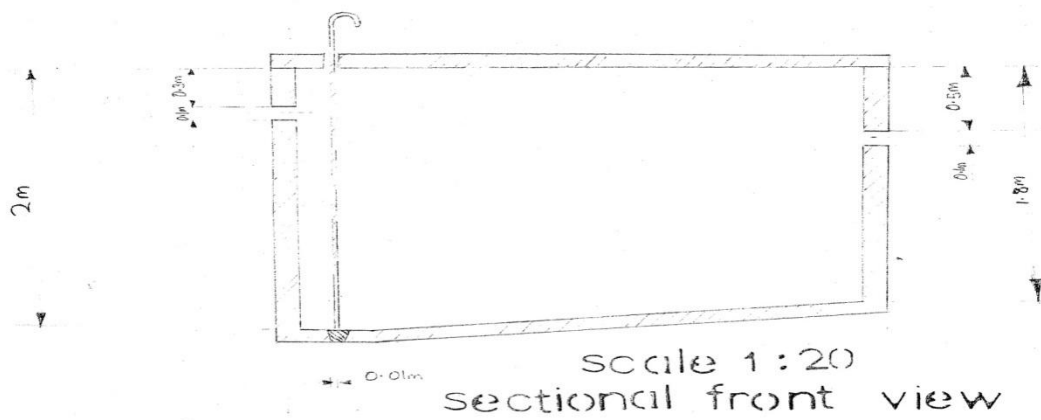
## REFERENCES

- [1] *Smsrthurst G. 1979, Basic Water Treatment; Thomas Telford Ltd, London.*
- [2] *M. Fair, Gordon/C. Geyer, John/A. Okun, Daniel. Water and Waste water Engineering Vol.1, 1968, John Willey and Sons Inc.*
- [3] *Mogarr, F: Water and Waste water utilization in Hot climate*
- [4] *Gary Fornshell:, Settling Basin Design, Western Regional Aquaculture Center*
- [5] *Alaska . Arizona . California . Colorado . Idaho . Montana . Nevada . New Mexico . Oregon . Utah . Washington . Wyoming*
- [6] *Settling Basin Design and Performance:, Daniel Stechey, Canadian Aquaculture Systems 1076Tillison Avenue Coboarg, Ontario K9A 5N4 CANADA*

APPENDEIX I



Plan view of settlement tank



sectional front view

## To study the effect of temperature using pretreated rice straw to generate biogas

S.Vivekanandan<sup>1\*</sup> S.Sathish<sup>2</sup>

<sup>1</sup>Associate Professor, Department of Mechanical Engineering, Annamalai University, India

<sup>2</sup>Research Scholar, Department of Mechanical Engineering, Annamalai University, India

**Abstract:** The objective of this study was to investigate the effect of pretreatment and operating temperature during the anaerobic digestion by using rice straw as biomass. The experiment was conducted for 30 days under both for mesophilic 30 to 40°C and thermophilic 45 to 60°C condition by continuous digestion process. Rice straw is a lignocellulosic biomass use as feedstock with to effect of pretreatment by NaOH was investigated for biogas generation. Quantity of biogas yield was reported as 0.73m<sup>3</sup>, hence pH level was 7.2 is obtained at 50°C was achieved in 18<sup>th</sup> day of thermophilic anaerobic digestion with respect 0.58 for mesophilic digestion at 10<sup>th</sup> day of anaerobic digestion, Since the thermophilic anaerobic digestion having higher biogas yield compare to mesophilic anaerobic digestion process.

**Keywords:** Anaerobic digestion, biomass, biogas yield, NaOH, pretreatment, rice straw.

### I. Introduction

The main aim of this research to investigate the performance of thermophilic and mesophilic anaerobic digestion using pretreated rice straw used to produce biogas yield. Lignocellulosic biomass and composition was selected in this study. Hence in India, lignocellulosic materials such as agricultural residues are abundant but most of them are not applied efficiently for energy purpose. While biogas production from rice straw is obtain a very good response due to its economical and eco-friendly usage of agricultural residues. [Zheng, i et al, 2014] is reported that the lignocelluloses is a plant biomass, primarily consists of three major elements such as cellulose, hemicelluloses and lignin. The other constituents such as water and proteins do not participate in organizing the structure of the material. The conversion of agricultural wastes to energy and application of biogas had been widely accepted by household digestion process. The biogas anaerobic digestion of rice straw converted into life fuel and also transformed to high quality of organic fertilizer reported by [Sathish S et al, 2015].

In the agricultural wastes, particularly rice straws having high lignocellulosic, hemicelluloses and cellulose are penetrating with the rigidifying binding material is known as lignin. The polysaccharides are not usable for bioconversion process. Hence pretreatment is involved to overcome the physical block of lignin and case sugar available for the microorganisms' indicated by [Mette Hedgard et al, 2005].

Due to the unmanageable properties of lignocellulosic biomass, alkaline pretreatments can be conducted on this research since the lignocellulosic biomass to enhance the specific biogas production (sbp) in anaerobic digestion. [Mtui, God et al, 2009] was suggested the characteristic of the lignocellulosic biomass is presented in Table 1. Since that the rice straws contain high lignin delivering its anaerobic digestion delay compare with formal digestion methods so, these rice straws cannot be directly used for biogas generation in this research. So to crack the lignin content using different pretreatment methods can be implemented which include the biological and chemical pretreatment methods in anaerobic digestion technology.

**Table .1** characteristics of the lignocellulosic biomass

S.No	Characteristics	Mean Value (%)
1	Physical characteristics (wet basis )	
	a) Moisture	89.6
	b) Total solid	91.4
	c) Volatile Solid	84.6
	d) Ash	20.30
	e) Specific gravity	20.56

2	Chemical characteristics (dry basis ) (i) Elemental analysis a) Carbon b) Hydrogen c) Nitrogen d) C/N ratio	44.24 05.70 02.16 28.51
	ii) Organic composition a) Hemicellulose b) Cellulose c) Lignin	38.5(0.9) 8.6(0.7) 9.7

Indian government has approached the sustainable rural energy development in the last ten years, and one of the most important issues is to increase the biogas production by promoting pre-treatment of technique for biomass and different temperatures. The idea of biogas production is to alter the physical and chemical structure of lignocelluloses through applying with NaOH pretreatment with different slurry temperature working in this experimental study. These studies proved that maximum biogas yield obtained from when slurry temperature at 50°C. Alkali pretreatment consists in the addition of alkali solution like NaOH, KOH, and Ca (OH)<sub>2</sub> or ammonia to remove lignin and hemicelluloses. The first steps in alkali pretreatment are salvation and saponification. NaOH is one of the more effective alkaline reagents and has been used to treat a variety of lignocellulosic feedstock were used anaerobic digestion process [Zhu, J, et al, 2010].

[Vivekanandan S et al] reported the Among various pretreatment methods, sodium hydroxide (NaOH) has been proved to be capable of releasing digestive material from the cell wall and is suitable for upgrading lignocellulosic materials

It is founded from the present study that biogas yield increased from temperature 50 to 55°C in thermophilic anaerobic digestion process. Since, [Yadvika A et al.2004] is suggested that the temperature of thermophilic anaerobic digestion process is preferred worldwide because, it is very easier to operate and improve the digester efficiency. Thermophilic bacteria are more stable than the mesophilic bacteria. It produced high quality of biogas and methane yield.

previous studies [Santosh y et al, 2004] described that the While rice straw and rice husk materials are reluctant to the impact of temperature, this almost presence of lignin and enhancement of silica (Just about 21-27%) in both the case of agricultural residues.

The reactor curbing lignocellulosic biomass sustained at 55°C produced more gas than the bio-reactor maintained at 45°C [Kim et al, 2006]. In virtually all the cases of biogas generation potential as well as the biogas yield was the highest at 56°C followed by 50 and 45°C respectively reported by [Garba et al, 1996].

## II. Experiments and methods

The cow dung and rice straw used in this study were collected from nearly village at Chidambaram town, the cow dung were used as an inoculum of the digester. The rice straw was grounded into 0.5 to 1.2mm particle by using grinding machine after being air dried. The straws are pretreated with NaOH. First 8% NaOH was dissolved in water to prepare NaOH solution and this solution was added with rice straw (RC) and mixed completely. Alkali pretreatment (Sodium hydroxide) has been studies in many literatures. Therefore Alkali pretreatment requires normal temperature and pressure and it also the dilute NaOH pretreatment makes the substrates (lignocelluloses) swollen, and then the degree of crystalline decreases and structure of lignocellulosic material has been destroyed. The moisture content of the straws is adjusted to 80% by adding water. This procedure is reaped in all 30 days of experiment. Figure 2.1 and 2.2 showed that the Line diagram and photographic view of the experimental setup. In this study the experimental values are compiled using trial and error methods followed by [Montgomery et al 2014].

The pretreated rice straw mixed with water using floating drum anaerobic continues digestion process carried in 1m<sup>3</sup> portable digester. The total volume of the digester was 1000liters with an effective slurry volume of 700liters. For digester loaded with waste by volume 40:60 and waste by water 30:70 and the feeding concentration of 80, 90,100 and 110,120 were used for this study. Feeding concentration was defined as the dry weight of rice straw feed per liter and the effective volume of the digester (kg/l TS). The digester slurry temperature was seeded with a mesophilic 30 to 40°C and thermophilic 45 to 60°C were operated in this study. Figure 2.1and2.2 illustrates the photographic view of the alkaline biomass and anaerobic digester.



**Figure.2.1** photographic view of the Rice Straw



**Figure.2.2** photographic view of the Experimental setup

The experiment was started and the gas volume was monitored daily for 30 days of retention time. The pneumatic stirrer used in the digester, since this device agitates the digester slurry at every 2 to 8 sec for both the digestion periods. The gas production was measured at intervals of about 24 hours by [Air bug gas flow meter] and pressure and temperature of the digester was measured using thermocouples and pressure gauge. The pH formation of the digested slurry was measured using pH redox meter.

### III. Results and Discussion

From the results shown that the biogas production was found to be higher with optimum temperature for methanogenesis bacteria is 50 to 55°C compare to 30 to 45°C mesophilic anaerobic digestion. During the 18<sup>th</sup> day and third week, the rate of digestion was more and biogas yield achieved at 0.73m<sup>3</sup>. The optimum pH level was 7.2 reductions in pH level causes major problem during the mesophilic anaerobic digestion reported by [Sathish S et al 2015]. Figure 3.1 and 3.2 illustrate the biogas yields and different slurry temperature with respect to Retention time.

The results indicate that the gas production stopped at an average 30 days HRT using daily anaerobic digestion process. This is because of the balanced nutrition and proper earlier digestion. When the rice straw was added in

this digester, the flow rate of biogas yield increased with 220 l/day to 320 l/day, which is the most prominent value compared to other agricultural wastes also examined by [Suntikunaporn et al, 2014]. The anaerobic digester working at the optimum temperature for biogas production means increase temperature range, which should not have negative effects in the anaerobic digestion process. Therefore it is suggested to carry out similar experiments to test the effect of temperature production using various agricultural wastes at 50°C. From this result, anaerobic digestion of pretreated rice straw and recorded that the flow of biogas yield by thermophilic anaerobic digestion was higher than that of mesophilic digestion process. It is incurred from the present study that with enhance the temperature from 30 to 60°C, in thirty days of experiment.

The results examine variety of lignocellulosic biomass biogas yield is larger for higher temperatures. The anaerobic digestion carrying lignocellulosic biomass maintained at 50°C. Generate more quantity of biogas than the anaerobic digestion maintained at 40 and 60°C reported by [Kim et al, 2006]. Hence the temperature improves the biogas yield as well as the efficiency of the anaerobic digester. The digester working in thermophilic condition was interesting because it resulted to faster reaction rates and high quantity of biogas production compare to mesophilic condition.

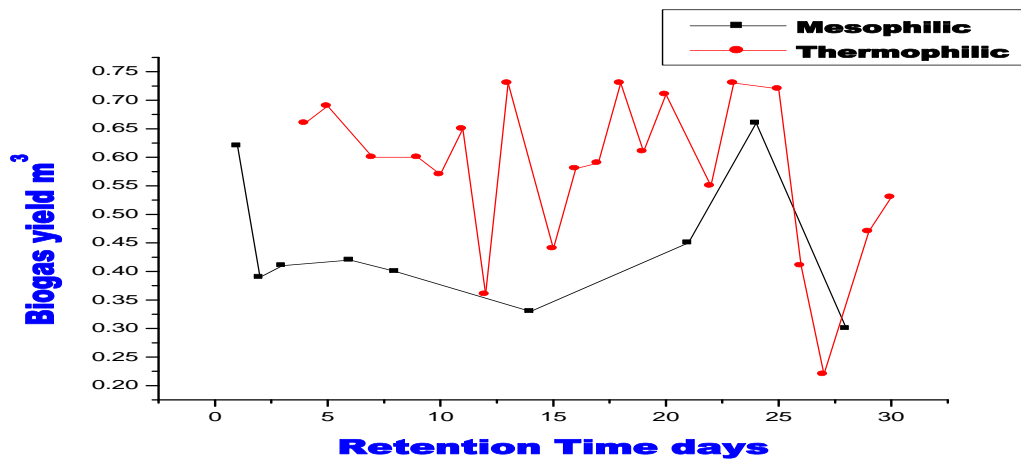


Figure.3.1 Biogas yield with respect to Retention time

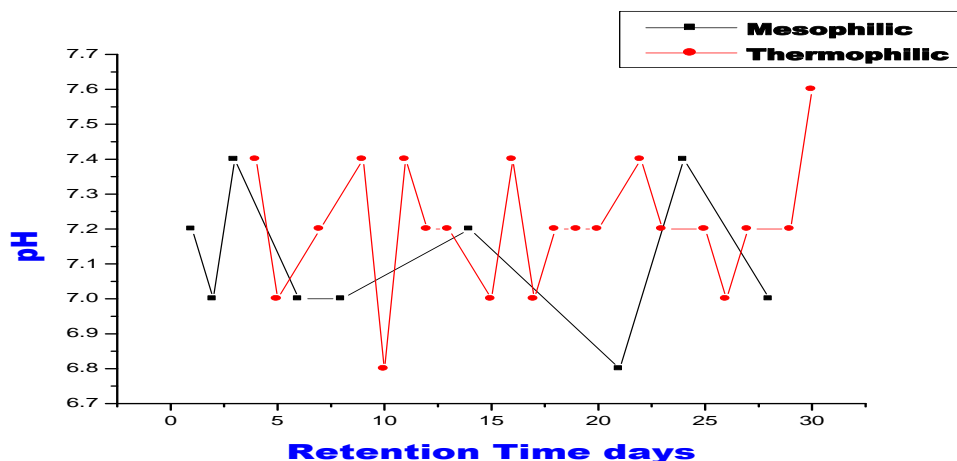


Figure.3.2 Change in pH with respect to Retention time



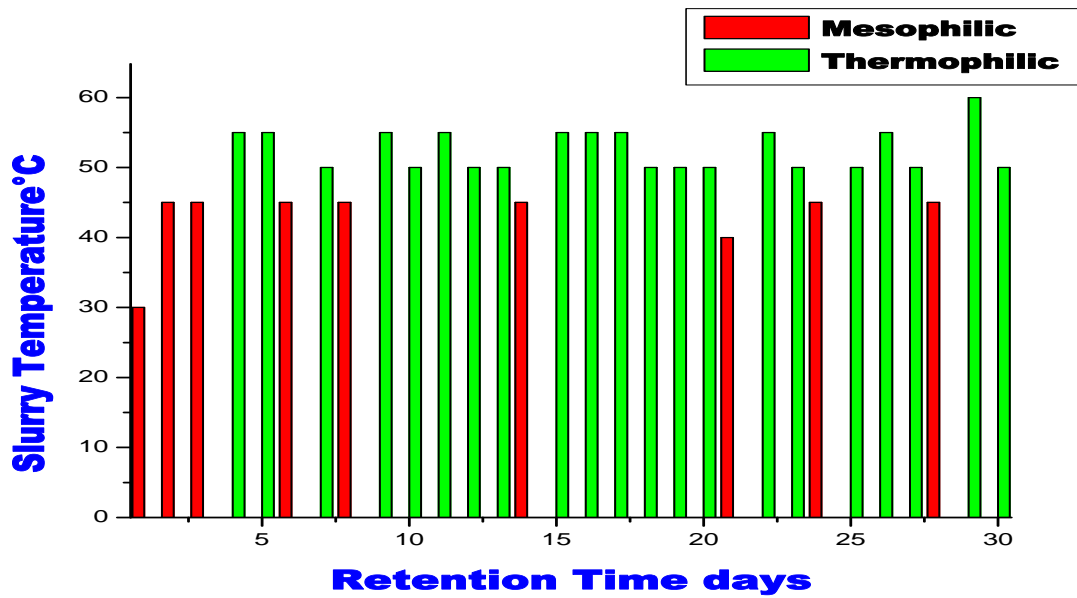


Figure.3.3 Temperature with respect to Retention time

Hence the biogas generation mainly depending on the solids concentration and amount of microorganisms presence in the feeding materials [AOAC, 14TH EDITION 1980]. So pretreatment of rice straw is generally required for biogas generation. The process of pretreatment to eliminate the lignin and hemicelluloses enhance the microorganisms and porousness of materials. Amongst various pretreatment methods NaOH method has been tested to be capable of eliminating material for promoting lignocellulosic biomass [Alriva p et al, 2010]. So from this result alkali pretreatment as well as the NaOH addition can be also extended to the continue digestion tests 8% of NaOH dose was obtained maximum gas production from this research.

This study would provide relevant information about the effect of temperature and these treatments on biogas production from rice straw (lignocellulosic) materials. Figure 3.4 and 3.5 shows the substrate concentration and pressure of the anaerobic digester during the digestion periods. The biogas yield was greatly increased at substrate concentration at 110kg. The average biogas productivity 0.73m<sup>3</sup> was also higher with substrate concentration at 110kg compared with other feeding concentrations.

The anaerobic digestion process is strongly determined by change in pH formation. It is takes place optimum neutral condition of the pH is 7 and optimal value of pH among with 6.8 - 7.5[MonaH et al, 2013].

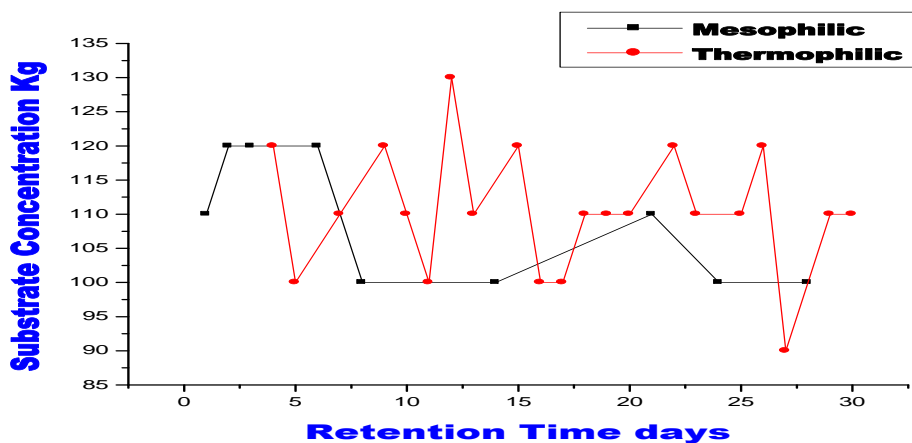


Figure.3.4 Substrate concentration with respect to Retention time

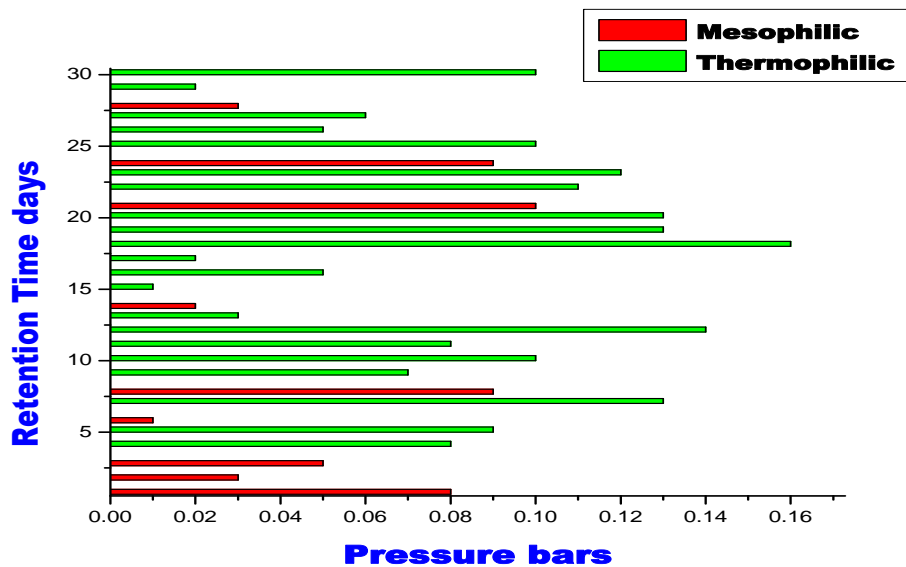


Figure.3.5 Change in pressure with respect to Retention time

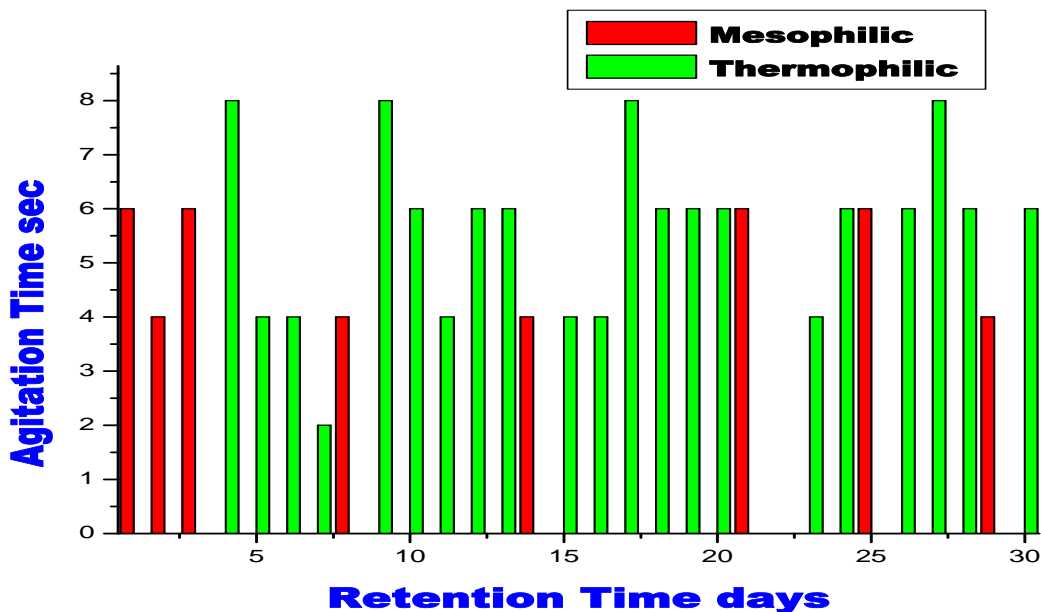


Figure.3.6 Change Agitation time with respect to Retention time

The results indicated that, NaOH pretreatment was attributed to more balanced nutrients and enhance the buffering capacity of the digester. From the results indicates that of NaOH pretreatment is yet another cause for effective biogas yield from the rice straw with abundant rich lignocellulosic rice crop residues. The effect of alkalinity is to improve the biogas yield significantly. Furthermore, pretreatment of straws was proven shorten digestion time by approximately 50% reported by [Ye, J et al 2013]. The digester obtained at a maximum pressure of 0.16 bars in 14<sup>th</sup> day of digestion and 0.59m<sup>3</sup> volume of biogas produced from the digester. When the digester slurry stirred at 6sec that time digester recorded highest biogas yield in 0.62 to 0.73m<sup>3</sup>. The results indicated the potentiality of rice straw, with substrate concentration at 110kg and pH maintained 7.2 in a thermophilic anaerobic condition at 50 to 55°C and also the digested slurry stirred at 6sec in same condition of an anaerobic digestion process. Figure 3.6 illustrates the Agitation time of the digester slurry with respect to Retention time.

Using the constitutional stirrer, the slurry was agitated regularly to circulate and keep up uniformity of temperature, hence the thickening and caking of impurities was prevented by [Onah D.U.2014]. Previous results proved that the NaOH pretreatment is an effective method to improve the biodegradability of corn stover with straws and anaerobic biogas production. The NaOH doses used in this study were 4%, 6%, 8% and 10% on dry basis of corn and straws. The optimal dose of NaOH was 8% and the recommended thermophilic temperature at 50°C to 60°C and loading rate was 120 kg/L. Under these conditions the biogas production achieved was 48.5% more than the control (without pretreatment) with a BioEnergy gain of 71% was obtained by [Pang et al 2008].

#### IV. Conclusion

The experimental results that biogas could be efficiently produced from pretreated rice straw and both the temperature ranges using continuous anaerobic digestion process. The NaOH pretreatment applied to anaerobic digestion contributes to promoting the degradability of the feed stock and increasing the biogas yield. Finally the thermophilic digestion offers advantages over mesophilic digestion by increasing the rate of biogas yield and efficiency of the digester.

#### Reference

- [1] Zheng, Yi, et al. "Pretreatment of lignocellulosic biomass for enhanced biogas production." *Progress in Energy and Combustion Science* 42 (2014): 35-53.
- [2] Mtui, Godliving YS. "Recent advances in pretreatment of lignocellulosic wastes and production of value added products." *African Journal of Biotechnology* 8.8 (2009).
- [3] Mussoline, W., Esposito, G., Lens, P., Garuti, G. and Giordano, A., Design considerations for a farm-scale biogas plant based on pilot-scale anaerobic digesters loaded with rice straw and piggyery wastewater, *Biomass and Bioenergy*. Vol. 46, pp. 469-478, 2012.
- [4] Zhu, J., Wan, C., & Li, Y. (2010a). Enhanced solid-state anaerobic digestion of corn stover by alkaline pretreatment. *Bioresource technology*, 101(19), 7523–8. doi:10.1016/j.biortech.2010.04.060.
- [5] Yadvika, A. (2004). Enhancement of biogas production from solid substrates. *Bioresource Technology* 1-10.
- [6] Mussatto, S.I., Fernandez, M., Milagres, A.M.F., Roberto, I.C.(2008) Effect of hemicelluloses and lignin on enzymatic hydrolysis of cellulose from brewer's spent grain. *Enzyme Microb. Technol.* 43: 124–129.
- [7] Kim, K., Oh, B. R., Chun, Y.N., Si Wouk Kim, S.W.: Effects of temperature and hydraulic retention time on anaerobic digestion of food waste. *Journal of Bioscience and Bioengineering*, 102 (4), 328–332 (2006).doi: 10.1263/jbb.102.328
- [8] Garba, B: Effect of temperature and retention period on biogas production from lignocellulosic material, Elsevier science Ltd. 938 (1996).
- [9] Sathish, S., and S. Vivekanandan. "Experimental Investigation on Biogas Production Using Industrial Waste (Press Mud) To Generate Renewable Energy." *Int. J. Innov. Res. Sci. Eng. Technol.* 4 (2015): 388-392.
- [10] Santosh, Y., Sreekrishnan, T. R., Kohli, S., Rana, V.: Enhancement of biogas production from solid substrates using different techniques—a review. *Bioresource Technology*, 95, 1–10 (2004). Doi: 10.1016/j.biortech.2004.02.010.
- [11] AOAC (1980), *Official Methods of Analysis* (14th Edition), Association office analytical chemistry, Arlington,VA.
- [12] Mette Hedgard Thomson (2005), *Complex media from processing of agricultural Crops for microbial fermentation*, *Appl. Microbiol biotechnol* 68: pp 598-606.
- [13] Alriva P, Tomas – Pejo, Ballesteros M and Negro MJ (2010), Pretreatment Technologies for an efficient bioethanol production process based on enzymatic hydrolysis: A review, *Bio Resour Tehcnol.* 101: pp 4851-4861.
- [14] Ye, J., Li, D., Sun, Y., Wang, G., Yuan, Z., Zhen, F. and Wang, Y., Improved biogas production from rice straw by co-digestion with kitchen waste and pig manure, *Waste Management*, Vol. 33, No. 12, 1-6, 2013.
- [15] Suntikunaporn, Malee, et al. "Evaluation of Agricultural Wastes for Biogas Production." *Thammasat International Journal of Science and Technology* 19.1 (2014).
- [16] Onah D. U., et al. "Characterization of Biogas Produced from Rice Husks and Algae using a Metal Fixed-Dome Biodigester." *Global Journal of Science Frontier Research*, 14.1. (2014).
- [17] Pang, Y. Z., Liu, Y. P., Li, X. J., Wang, K. S., & Yuan, H. R. (2008). Improving Biodegradability and Biogas Production of Corn Stover through Sodium Hydroxide Solid State Pretreatment. *Energy & Fuels*, 22(4), 2761–2766. Doi: 10.1021/ef800001 .
- [18] Mona H, Zouheir F. Evaluation of microalgal alternative jet fuel using the AHP method with an emphasis on the environmental and economic criteria. *Environ. Prog.*2013; 32:721-733.
- [19] Montgomery, Lucy FR, and Günther Bochmann. "Pretreatment of feedstock for enhanced biogas production." *IEA Bioenergy. Ireland* (2014).
- [20] Sathish, S., and S. Vivekanandan. "Optimization of Different Parameters Affecting Biogas Production from Rice Straw: An Analytical Approach." (2015).
- [21] Vivekanandan s and G kamaraj Investigation on cow dung as co-substrate with pretreated sodium hydroxide on rice chaff for efficient biogas production. *Ijsat*, vol 1: no4, (2011).

## Effect of Gate Length on the DC and RF Performance of GaN HEMT Devices

Ahmet Toprak<sup>1</sup>, Ozlem A. Sen<sup>1</sup>, Ekmel Ozbay<sup>1,2,3</sup>

<sup>1</sup>Nanotechnology Research Center-NANOTAM, Bilkent University, 06800 Ankara, TURKEY

<sup>2</sup>Department of Electrical and Electronics Engineering, Bilkent University, 06800 Ankara, TURKEY

<sup>3</sup>Department of Physics, Bilkent University, 06800 Ankara, TURKEY

**ABSTRACT:** In this work, we report GaN high-electron-mobility-transistors (HEMTs) on SiC with gate lengths of various dimensions for optimum performance. 125  $\mu\text{m}$  gate width, 4  $\mu\text{m}$  drain source spacing AlGaIn/GaN HEMTs with gate lengths of 0.3, 0.6, 0.8, and 1.0  $\mu\text{m}$  were fabricated. For devices with the gate lengths in the range of 0.3-0.8  $\mu\text{m}$ , with an increase in gate length, the output power density ( $P_{out}$ ) at 4 GHz is increased from 1W/mm to 1.5W/mm, although the  $I_{ds,max}$ ,  $g_m$ ,  $f_t$  and  $f_{max}$  values are decreased in acceptable limits. The great enhancement in  $P_{out}$  with the increase in the gate length is due to fact that the increase in gate length affects the controllability of the electric field under the channel; hence the peak value of the electric field under gate contact decreases and the electric field variation under the gate contacts is smoother. For the device with the gate length of 1.0  $\mu\text{m}$   $I_{ds,max}$ ,  $g_m$  values are almost the same as the values with the gate length of 0.8  $\mu\text{m}$ , but  $P_{out}$  is decreased, since with this gate length the increase in parasitic capacitances is more effective and this limits the improvement due to the gate length increase.

**Keywords** -GaN HEMT, Gate length, RF power applications, coplanar waveguide, and power amplifiers.

### I. INTRODUCTION

AlGaIn/GaN high-electron-mobility-transistor (HEMT) devices are of great interest for high power, high frequency, high temperature and low noise radio frequency (RF) applications due to their high breakdown electric field, high breakdown voltage, high saturation velocity and high thermal conductivity<sup>[1-3]</sup>. In addition, AlGaIn/GaN HEMTs include high conduction band offset and high piezoelectricity resulting in high current density and high power density compared to GaAs and InP based HEMTs<sup>[4,5]</sup>.

In this work, a systematic study of the effect of the gate length on small signal gain, output power, efficiency and cut off frequency is presented. GaN-HEMTs are fabricated with different gate lengths. Increasing the gate length helps control the electric field under the channel that is caused by gate contact. Thus, it decreases the peak electric field value and the electric field distribution is smoothed under the gate contact, resulting in the improvement of the breakdown voltage and the output power performance of the HEMT. The benefit is due to the reduced high-field trapping effect resulting in the prevention of electron emission and electron trapping. As a result, the increase of the gate length helps the reduction of the current collapse effect of the HEMTs. In addition to output power performance, increasing the gate length also has an impact on the noise performance of HEMTs.

The schematic and layout of the designed HEMT is given in Fig. 1 and in Fig. 2. In Fig. 1,  $L_{gs}$  is 0.6  $\mu\text{m}$  and four different gate lengths are designed as 0.3, 0.6, 0.8 and 1.0  $\mu\text{m}$ . The thickness of the  $\text{Si}_3\text{N}_4$  dielectric passivation layer is 300 nm. The measured HEMT devices have six fingers and the average gate-to-gate distance is 60  $\mu\text{m}$  (Fig. 2).

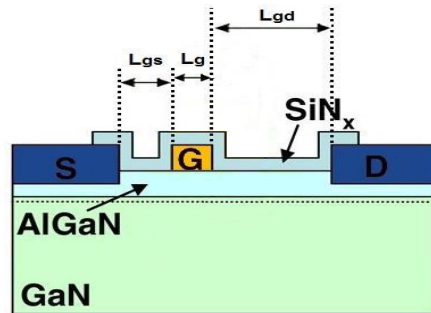


Fig.1. Schematic of an AlGaIn/GaN HEMT structure.

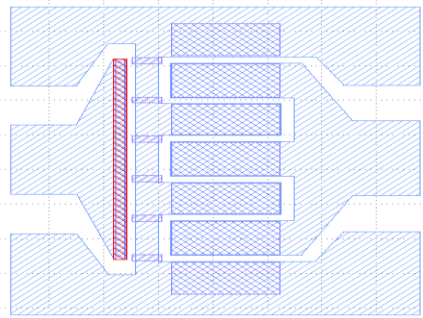


Fig. 2. Layout of an AlGaIn/GaN HEMT structure.

## II. DEVICE REALIZATION

An AlGaIn/GaN HEMT epitaxial structure was grown on a semi-insulating SiC substrate by metal organic chemical vapor deposition<sup>[6-8]</sup>. The epilayer consists of a 15 nm AlN nucleation layer, 2  $\mu\text{m}$  undoped GaN buffer layer, approximately 1.5 nm AlN interlayer, 20 nm undoped  $\text{Al}_{0.22}\text{Ga}_{0.78}\text{N}$  layer and a 2 nm GaN cap layer on the top of the structure. The Hall mobility was  $1384 \text{ cm}^2\text{V}^{-1}\text{s}^{-1}$  whereas the sheet carrier concentration was  $1.51 \times 10^{13} \text{ cm}^{-2}$ .

The fabrication process flow diagram of the HEMTs is shown in Fig. 3<sup>[9-12]</sup>.

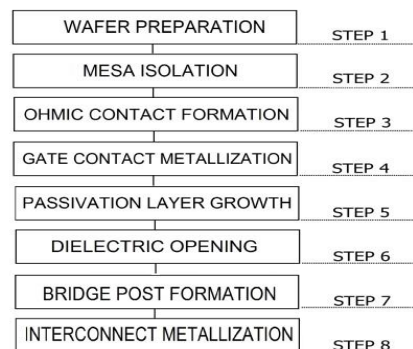


Fig. 3. Flow chart of the GaN HEMT fabrication process.

Mesa etching was performed with ICP-RIE with a  $\text{Cl}_2/\text{BCl}_3/\text{Ar}$  gas mixture. Ohmic contacts were formed by evaporated Ti/Al/Ni/Au (12 nm/120 nm/35 nm/65 nm) metals by the e-beam evaporation method and annealing them in nitrogen ambient at  $850 \text{ }^\circ\text{C}$  for 30 s. Ohmic contact resistance was  $0.12 \text{ } \Omega\text{-mm}$  and the sheet resistance was  $508 \text{ } \Omega\text{-}\square^{-1}$  measured by using the transfer length measurement (TLM) patterns. Ni/Au (50 nm/300 nm) was deposited for gate contacts. The devices were passivated with a 300 nm-thick  $\text{Si}_3\text{N}_4$  layer grown by plasma-enhanced chemical vapor deposition. After the passivation, the openings, where the interconnect metal will be deposited on, were formed by means of the dry etching of ICP-RIE with  $\text{CHF}_3$  gas. The airbridge post structures were constituted for preventing any case of the short circuit of the metals by functioning as a jumper. Finally, a relatively thick Ti/Au metal stack with e-beam evaporation was deposited as an interconnection on the sample, and then the fabrication process was completed with this last step. Figure 4 shows a  $6 \times 125 \text{ } \mu\text{m}$  wide device's optical microscope image and Figure 5 shows the SEM images of the gates with  $L_g = 0.3, 0.6, 0.8, \text{ and } 1.0 \text{ } \mu\text{m}$ .

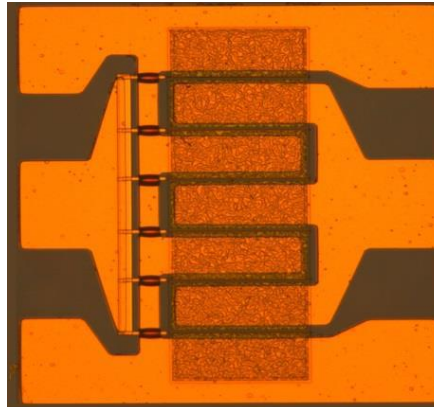


Fig. 4 Optical microscope image of fabricated 6×125μm HEMT.

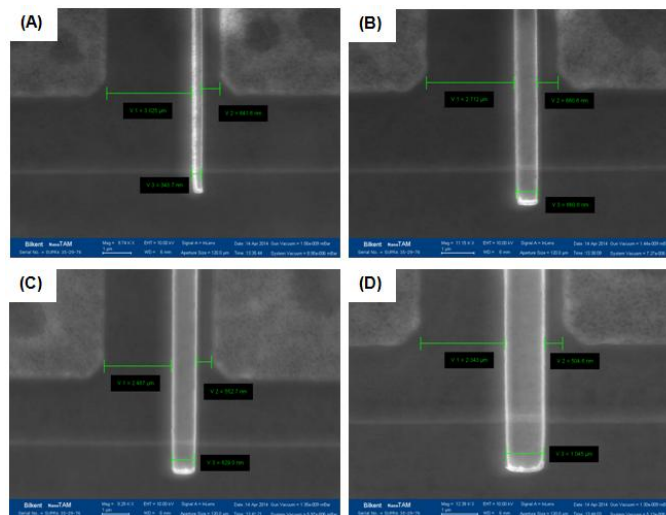


Fig. 5. SEM images of gates with an (A) 0.3 μm, (B) 0.6 μm, (C) 0.8 μm, (D) 1.0 μm gate length ( $L_g$ ).

### III. RESULTS AND DISCUSSIONS

DC on wafer measurements were performed using an Agilent B1500A semiconductor device parameter analyzer. For DC IV characterization, the gates were biased from -6V to 1V in a step of 1 V, and the drain current-voltage ( $I_{ds}$ - $V_{ds}$ ) characteristics were measured for a 6×125 μm AlGaIn/GaN HEMT with  $L_g = 0.3, 0.6, 0.8,$  and  $1.0 \mu\text{m}$  (Fig. 6). It can easily be seen that all of the devices have good pinch off characteristics and the devices completely pinch off at  $V_{gs} = -5\text{V}$ .

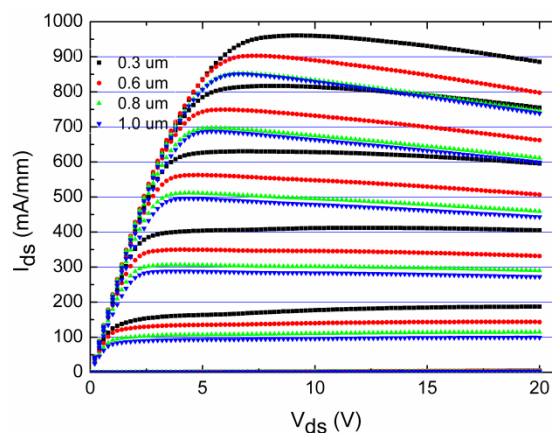


Fig. 6. Drain current-voltage ( $I_{ds}$ - $V_{ds}$ ) characteristics of a 6×125 μm AlGaIn/GaN HEMT with  $L_g = 0.3, 0.6, 0.8,$  and  $1.0 \mu\text{m}$ . The gate bias was swept from +1V to -6 V in a step of -1 V.

The extrinsic transconductance ( $g_m$ ) for all the devices was also measured. Fig. 7 shows the transconductance ( $g_m-V_{ds}$ ) characteristics of  $6 \times 125 \mu\text{m}$  AlGaIn/GaN HEMT with  $L_g = 0.3, 0.6, 0.8,$  and  $1.0 \mu\text{m}$ . It is seen that the maximum value of  $g_m$  is above  $250 \text{ mS/mm}$  for all the devices.

The change in the  $I_{ds, \text{max}}$  and  $g_m$  values as a function of the gate length is given in Figs. 8 and 9, respectively. As can be seen in Figs. 8 and 9,  $I_{ds, \text{max}}$  and  $g_m$  are decreased with the increase in  $L_g$  from  $0.3$  to  $0.8 \mu\text{m}$ . A maximum  $I_{ds, \text{max}}$  of  $960 \text{ mA/mm}$  was obtained for the shortest gate length, i.e.,  $L_g = 0.3 \mu\text{m}$ , and a minimum  $I_{ds, \text{max}}$  of  $852 \text{ mA/mm}$  was obtained for  $L_g = 0.8 \mu\text{m}$ . A maximum  $g_m$  of  $236 \text{ mS/mm}$  was obtained for the shortest gate length, i.e.,  $L_g = 0.3 \mu\text{m}$ , and a minimum  $g_m$  of  $203 \text{ mS/mm}$  was obtained for  $L_g = 0.8 \mu\text{m}$ .  $I_{ds, \text{max}}$  and  $g_m$  were not changed with the increase of  $L_g$  from  $0.8 \mu\text{m}$  to  $1.0 \mu\text{m}$ . The maximum current density of  $852 \text{ mA/mm}$  and the extrinsic transconductance of  $203 \text{ mS/mm}$  was obtained for both  $L_g = 0.8 \mu\text{m}$  and  $L_g = 1.0 \mu\text{m}$ .

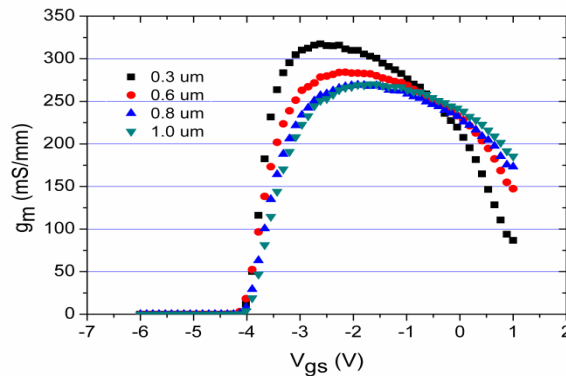


Fig. 7. Transconductance ( $g_m-V_{gs}$ ) characteristics of a  $6 \times 125 \mu\text{m}$  AlGaIn/GaN HEMT with  $L_g = 0.3, 0.6, 0.8,$  and  $1.0 \mu\text{m}$ . The gate bias was swept from  $-6$  to  $1 \text{ V}$  in a step of  $1 \text{ V}$ .

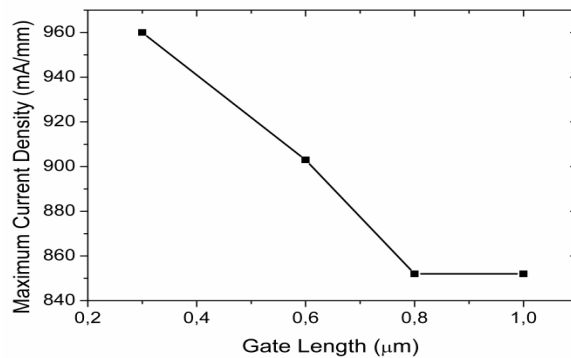


Fig. 8. The change of  $I_{ds, \text{max}}$  as a function of the gate length.

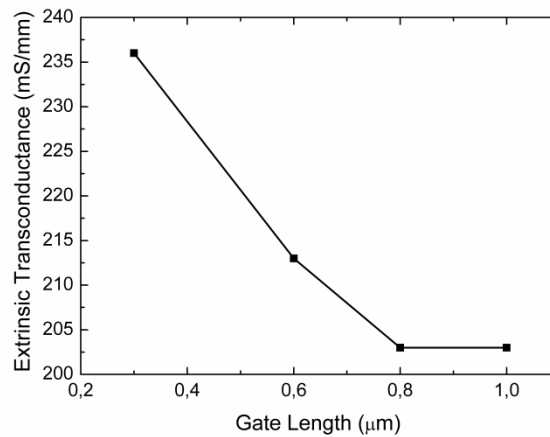


Fig. 9. The change in  $g_m$  as a function of the gate length.

According to these results, it can be said that when the gate length increases up to an optimum point, this increase helps the controllability of the electric field under the channel caused by the gate contact. Thus, it decreases the peak value of the electric field and improves the smoothness of the electric field under the gate contact. Due to this effect, the movement of electrons along the 2DEG channel is more difficult and this results in the decrease in maximum current density and the extrinsic transconductance. There is no change in the maximum current density and the extrinsic transconductance when the increase of the gate length is over the optimum point, because over the optimum gate length, the electric field under the channel caused by gate contact does not change any more.

On-wafer radio frequency (RF) measurements were carried out using a Cascade Microtech Probe and an Agilent E8361A PNA in the 1–20 GHz range. The change of the unity current gain cut off frequency,  $f_t$  and the maximum oscillation frequency,  $f_{max}$  as a function of  $L_g$  is shown in Figs. 10 and 11, respectively.

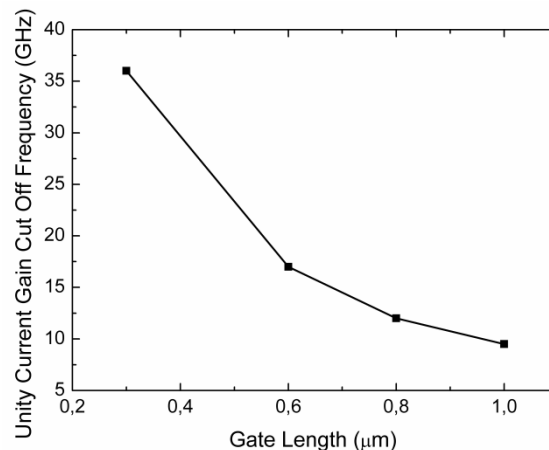


Fig. 10. The change of unity current gain cut off frequency ( $f_t$ ) as a function of the gate length.

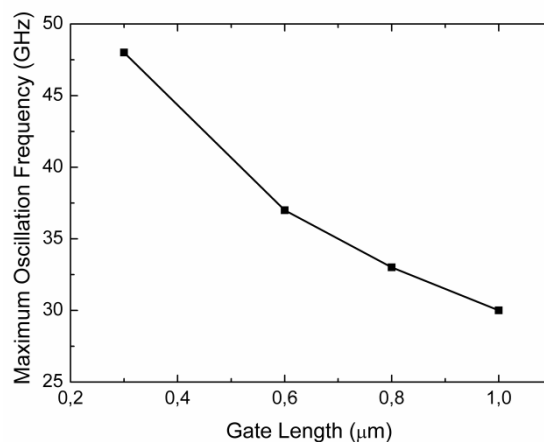


Fig. 11. The change of the maximum oscillation frequency ( $f_{max}$ ) as a function of the gate length.

The unity current gain cut off frequency ( $f_t$ ) and the maximum oscillation frequency ( $f_{max}$ ) were decreased with the increase in  $L_g$  due to the increasing capacitive effects as expected<sup>[13,14]</sup>. A unity current gain cut off frequency ( $f_t$ ) of 36 GHz and maximum oscillation frequency ( $f_{max}$ ) of 48 GHz were obtained for  $L_g = 0.3 \mu\text{m}$  and a minimum unity current gain cut off frequency ( $f_t$ ) of 9.5 GHz and maximum oscillation frequency ( $f_{max}$ ) of 30 GHz were obtained for the  $L_g = 1.0 \mu\text{m}$ .

A large signal load pull measurement was carried out using a Maury Microwave automated load pull system at 4 GHz to obtain output power performance. The data were taken on-wafer at room temperature without any thermal management. All the HEMTs were measured at a drain bias of 30 V, and the output powers were obtained at 2dB gain compression. A summary of the output power values obtained as a function of the gate length is shown in Fig. 12. The output power was increased when  $L_g$  was increased from 0.3 to 0.8  $\mu\text{m}$ . A maximum output power of 1461 mW/mm was obtained for  $L_g = 0.8 \mu\text{m}$  and a minimum output power density of 1012 mW/mm was obtained for  $L_g = 0.3 \mu\text{m}$ .



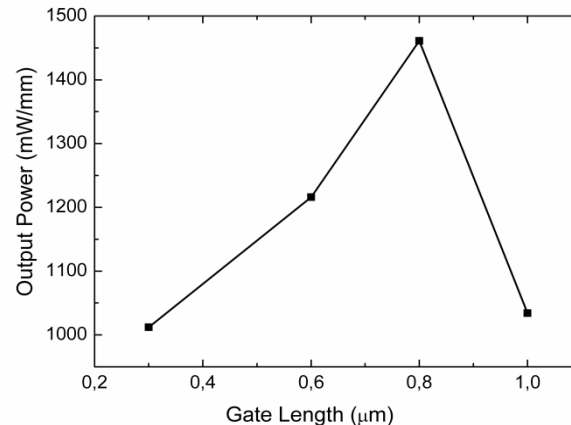


Fig. 7. Summary of output power as a function of the gate length. The devices were biased at  $V_{ds} = 30$  V,  $V_{gs} = -2.9$  V and 4 GHz.

The output power density of HEMTs was decreased when  $L_g$  is above  $0.8 \mu\text{m}$ . Up to the optimum value of the gate length, the increase in gate length smoothens the electric field under the gate contact and decreases the electron emission and electron trapping. As a result it helps the reduction of the current collapse and increases the output power density of the HEMTs.  $L_g$  of  $0.8 \mu\text{m}$  is optimum for the HEMTs with  $4 \mu\text{m}$  drain-source spacing. When the gate length exceeds the optimum length, the electric field under the channel caused by gate contact does not change, but due to the decrease of  $L_{gd}$  (gate drain spacing), the increase in parasitic capacitances especially in gate drain capacitance,  $C_{gd}$  becomes effective and this limits the gain and output power performance of the HEMTs.

The DC, small signal, and large signal results are summarized in TABLE 1.

TABLE I. Summary Of The Results Of The AlGaIn/GaN HEMTs with Varying Gate Length.

$L_g$ ( $\mu\text{m}$ )	0.3	0.6	0.8	1.0
$g_{m,max}$ (mS/mm)	236	213	203	203
$I_{ds,max}$ (mA/mm)	960	903	852	852
$f_t$ (GHz)	36	17	12	9.5
$f_{max}$ (GHz)	48	37	33	30
Output Power (mW/mm) @2dB comp.	1012	1216	1461	1034

#### IV. CONCLUSION

A systematic study has been performed to investigate the effect of a gate length on the DC characteristics, small signal gain and large signal performance of GaN-channel HEMTs. For HEMTs with six fingers,  $125 \mu\text{m}$  gate width,  $4 \mu\text{m}$  drain-source spacing,  $300 \text{ nm}$ -thick  $\text{Si}_3\text{N}_4$  as a dielectric passivation layer, an optimum gate length was found to be  $0.8 \mu\text{m}$  for maximum RF output power performance. It was observed that the increase in the gate length from  $0.3 \mu\text{m}$  to the optimum gate length,  $0.8 \mu\text{m}$ , results in increase of controllability of the electric field under the channel caused by gate contact and decreases the leakage current. Thus it decreases the maximum current density and the extrinsic transconductance, but increases the RF output power density of HEMTs. When the gate length is over the optimum value of  $0.8 \mu\text{m}$ , the length between drain and gate contacts decreases below  $2.2 \mu\text{m}$ , the capacitive effects between the gate and drain begin to dominate and the output power density of HEMTs are decreased. In order to improve the power density performance further the drain-source spacing should be improved as a future work and then it may be possible to obtain larger gate lengths without any degradation in output power density values of HEMTs.

#### V. ACKNOWLEDGEMENTS

This work is supported by the projects DPT-HAMIT, DPT-FOTON, and NATO-SET-193 as well as TUBITAK under Project Nos.113E331, 109A015, and 109E301. One of the authors (E.O.) also acknowledges partial support from the Turkish Academy of Sciences. The authors would like to acknowledge Gokhan Kurt, Yildirim Durmus, Huseyin Cakmak, Pakize Demirel, Omer Cengiz, Orkun Arican, Sinan Osmanoglu, Dogan Yilmaz, Burak Turhan, Ayca Emen and Semih Cakmakyapan for valuable support.

## REFERENCES

- [1] S. J. Pearton, J. C. Zolper, R. J. Shul, F. Ren, *Journal of Applied Physics* 86, (1999)
- [2] S. T. Sheppard, K. Doverspike, W. L. Pribble, S. T. Allen, J. W. Palmour, L. T. Kehias, T. J. Jenkins, *IEEE Electron Device Lett* 20, 161 (1999).
- [3] W. Lu, J. Yang, M. A. Khan, I. Adesida, *IEEE Trans Electron Devices* 48, 586 (2001).
- [4] J. W. Johnson, A. G. Baca, R. D. Briggs, R. J. Shul, J. R. Wendt, C. Monier, F. Ren, S. J. Pearton, A. M. Dabiran, A. M. Wowchack, C. J. Polley, P. P Chow, *Solid-State Electronics* 45, 1979 (2001).
- [5] V. Kumar, A. Kuliev, R. Schwindt, M. Muir, G. Simin, J. Yang, M. A. Khan, I. Adesida, *Solid-State Electronics* 47 1577 (2003).
- [6] R. Tulek , E. Arslan, A. Bayraklı, S. Turhan, S. Gökden, Ö. Duygulu, A. A. Kaya, T. Firat, A. Teke, and E. Ozbay, *Thin Solid Films* 551, 146 (2014).
- [7] E. Arslan, S. Turan, S. Gökden, A. Teke, E. Ozbay, *Thin Solid Films* 548, 411 (2013).
- [8] S. Çörekçi, M. K. Öztürk, Hongbo Yu, M. Çakmak, S. Özçelik, and E. Ozbay, *Semiconductors* 47, 820 (2013).
- [9] O. Kelekci, P. T. Tasli, S. S. Cetin, M. Kasap, S. Ozcelik, and E. Ozbay, *Current Applied Physics* 12, 1600 (2012).
- [10] Kelekci, P. T. Tasli, H. Yu, M. Kasap, S. Ozcelik, and E. Ozbay, *Physica Status Solidi A* 209, 434 (2012).
- [11] X. L. Wang, C. M. Wang, G. X. Hu, J. X. Wang, T. S. Chen, G. Jiao, J. P. Li, Y. P. Zeng, J. M. Li, *Solid-State Electronics* 49, 1387 (2005).
- [12] W. Luo, X. Wang, H. Xiao, C. Wang, J. Ran, L. Guo, J. Li, H. Liu, Y. Chen, F. Yang, J. Li, *Microelectronics Journal* 39, 1108 (2008).
- [13] W. Dongfang, Y. Tingting, W. Ke, C. Xiaojuan, L. Xinyu, *Journal of Semiconductors* 31, (2010).
- [14] D. Liu, M. Hudait, Y. Lin, H. Kim, S. A. Ringel, W. Lu, *Solid-State Electronics* 51, 838 (2007).

## Extraction of Soluble Sodium Silicate using Corn Cob Ash as a Silica Source

B.A. Ajayi<sup>1</sup>, S.S. Owoeye<sup>1</sup>

<sup>1</sup>Department of Glass and Ceramic Technology, Federal Polytechnic, P.M.B. 5351, Ado- Ekiti, Nigeria.

**ABSTRACT:** Extraction of soluble sodium silicate was carried out in this study using corn cob ash as silica source and alkali as soda source. Initially, received corn cob was burnt in open air to obtain the corn cob ash. The obtained corn cob ash was then placed inside refractory crucible and further heating was carried out inside muffle furnace at the temperature of 600<sup>0</sup>C for 5hrs. The thermally treated corn cob ash was mixed with 3M conc. NaOH and boiled with a constant stirring in a heating glass vessel placed inside a thermostatic water bath at 80<sup>0</sup>C for 4hrs and 90<sup>0</sup>C for 3hrs respectively. Various analyses such as PH value, specific gravity, electrical conductivity, viscosity were conducted on the produced sodium silicate and the results were compared with the reference sodium silicate sample.

**Keywords:** corn cob ash, sodium silicate, PH, viscosity

### I. INTRODUCTION

Corn has been identified as one of the most planted staple food crop in the world. For every 100kg corn grain 18kg of corn cob is approximately produced according to International Grain Council, 824million tons of corn was produced worldwide in the year 2011. Corn has been found to be one of the prominent staple foods in Nigeria with an estimated annual production of 9.4million tons, the cobs produced from corn are mainly used as manure for agriculture production [1]. Corn cobs as mostly practice all over are either thrown out as waste to landfill or burnt, a process with low added value, adding ash to soil; causing environmental impacts [2]. Most corn cobs generated in Nigeria are either sent as waste to landfill or as low grade fuels which poses a serious threat not only in storage but also for disposal, for example the combustion of corn cob is contributing to an increase in the amount of CO<sub>2</sub> in the atmosphere causing greenhouse effect. CO<sub>2</sub> being one of the green house gases and can result in global climate change. It has been estimated that corn cob contains a high amount of SiO<sub>2</sub> (>60%) which is being occupied by useful land or treated as waste [3]. Silica has been successfully extracted from different agricultural materials like rice husk [4-5]. [6] Also prepared and characterized nanoSiO<sub>2</sub> from corn cob ash by precipitation method.

The production of Na<sub>2</sub>SiO<sub>3</sub> basically comprises four main stages according to [7]: (i) calcinations of a mixture of Na<sub>2</sub>CO<sub>3</sub> and natural Quartz or sand (SiO<sub>2</sub>) in furnace at 1400<sup>0</sup>C -1500<sup>0</sup>C to produced a solid glass; (ii) Dissolution of the produced solid glass in a reaction vessel under high pressure and temperature to produced Na<sub>2</sub>SiO<sub>3</sub> solution and impurities (not reacted silica); (iii) Optimal filtration depending on the purity desired, (iv)Evaporation of H<sub>2</sub>O from the silicate solution for the production of solid sodium silicate.

Based on the energy consumption with burning fuel to reach high temperature of calcinations, this process is consider as being expensive besides production of air pollutants such as dust, Nitrogen and SiO<sub>2</sub> [7]. There is also a process different from the calcinations method used in industrial scale which is based on reaction of SiO<sub>2</sub> with concentrated sodium hydroxide (purity>99%) in autoclave, under high temperature and pressure as explained in some patents work [8-9].

This present work however extract soluble sodium silicate from corn cob ash (CCA) as silica source and concentrated NaOH as soda source using adapted method stated by [10]

### II. MATERIALS AND METHOD

#### 2.1. Combustion and heat treatment of corn cob into ash

The as-received corn cobs were first washed and dried, after drying it was placed inside a perforated cylinder pan for combustion into ash. 60g of the obtained ash was then placed inside an alumina crucible and put inside a muffle furnace and heated at a temperature of 600<sup>0</sup>c for 5hrs to reduce the carbonaceous matter and increase the percentage of active silica content.

## 2.2. Chemical analysis of the corn cob ash (CCA)

The chemical analysis was carried out using Atomic Absorption Spectrometry at the National Research Institute, Zaria, Nigeria. From the results of the AAS analysis it shows that the CCA contains 58.01% SiO<sub>2</sub>.

## 2.3. Weighing of the corn cob ash (CCA)

Two samples A and B measuring 15g each was weighed from the obtained corn cob ash which were later reacted with conc. NaOH and heated in a glass vessel at a temperature of 80°C and 90°C respectively.

## 2.4. Preparation of 3M NaOH

The preparation of 3M NaOH was carried out by firstly calculating the molarity of the sodium hydroxide pellet using the formula below.

Molarity = mass/molar mass x 1/ volume

Molar mass of NaOH = 32+16+1 = 40.

For example, to prepare one litre.

$3 = \text{mass}/40 \times 1/1$

Mass = 3 x40 = 120g.

This means 120g of NaOH Pellets will be dissolved in one litre of distilled water.

The solution was achieved by dissolving the NaOH pellets inside a 500ml conical flask containing distilled water using stirring rod to stir it until the pellets dissolve totally.

## 2.5. Reaction in the heating bath

From literature, for every 10g of CCA, you react with 60ml of NaOH [11]. 90ml portion of the 3M NaOH was poured inside 250ml Erlenmeyer flask containing 15g weighed sample of CCA placed inside a thermostatic heating bath and the temperature set to 80°C for 4hrs and 90°C for 3hrs for samples A and B respectively with continuous stirring. The solutions were then allowed to cool to room temperature after the experiment. The solutions obtained from samples A and B were filtered using a Whatman No. 41 filter paper into separate 250ml round bottom flask and the residue left on the filter paper was discarded.

## III. RESULTS

Table 1. Chemical Composition of the Corn Cob Ash at 600°C for 5hrs

Al <sub>2</sub> O <sub>3</sub>	SiO <sub>2</sub>	Fe <sub>2</sub> O <sub>3</sub>	K <sub>2</sub> O	Na <sub>2</sub> O	MgO	MnO <sub>2</sub>	CaO	LOI
9.2	58.01	3.05	4.1	4.94	4.1	3.2	10.4	3.0

Table 2. Analysis of the Produced Sodium Silicate and the Reference Sodium Silicate

	PH Value	Electrical conductivity µs/cm	Specific gravity g/cm <sup>3</sup>	Viscosity Centipoises	Characteristics
Sample A at 80°C for 4hrs	12.9- 13.0	1068	0.8231	280	Syrupy liquid, high alkalinity
Sample B at 90°C for 3hrs	12.7-12.8	1072	0.8509	400	Syrupy, alkaline liquid
Reference sample	8-13.0		1.39	830	Syrupy liquid

## IV DISCUSSION

### 4.1. Corn Cob Ash Characterization

Table 1 shows the chemical composition of the CCA sample obtained using Atomic Absorption Spectrometry. The analysis revealed that inorganic content of this ash contains a good percentage amount of SiO<sub>2</sub> (58.01%) which actually justify its use as a source of silica for this research.

### 4.2. Analyses of the produced Na<sub>2</sub>SiO<sub>3</sub>

Table 2 shows the results for the various analyses conducted on the produced Na<sub>2</sub>SiO<sub>3</sub> which were compared with the reference sample. The results showed that PH values for samples A and B ranges from 12.8-12.9 and 12.9-13.0 respectively; specific gravities are 0.8231 and 0.8509 respectively while the electrical conductivities are 1072 µs/cm and 1068 µs/cm for the two samples at 80°C and 90°C respectively. The samples A and B has viscosities of 280 and 400 centipoises respectively while they both exhibited characteristic syrupy, high alkalinity liquid.

### 4.3. Clay deflocculation test

From the clay deflocculation test, it was observed that sample A required more drops before the effect can be seen in a slip compare to sample B. Both samples however works in deflocculation but not as potent as the reference sample. This might however be attributed to the low temperature employed in this research compare to reference sodium silicate produced industrially.

## V. CONCLUSION

It can therefore be concluded from the various analyses conducted and in comparison with the reference  $\text{Na}_2\text{SiO}_3$  that the product is actually sodium silicate solution. However, the only shortcoming is the issue of low viscosity which has to do with parameters such as temperature, amount of silica extracted from the CCA.

## REFERENCES

- [1] F. Latif, B.I. Rajoka, Production of ethanol and xylitol from corn cobs by yeast. *Bio- resource Technology*, 77, 2001, 57-63.
- [2] G. Garrote, H. Dominguez, and J.C. Parajo, Hydrothermal processing of lignocellulosic materials. *Holz als Roh- und Werkstoff*, 57, 1999, 191-202.
- [3] W.J. Byung, C.H. Kim, G.H. Tae, and J.B. Park, Characteristics of cement mortar with nano-SiO<sub>2</sub> particles, *Const. Build. Mater.*, 21, 2007, 1351-1355.
- [4] S.R. Kamath, and A. Proctor, Silica gel from rice husk ash: preparation and characterization, *Cereal Chemistry*, 75, 1998, 484-487.
- [5] N. Yalcin, and V. Sevinc, Studies on Silica obtained from Rice Husk, *Ceramic International*, 27(2), 2001, 219-224.
- [6] K. Mohanraj, S. Kannan, S. Barathan, and G. Sivakumar, Preparation and characterization of nano-SiO<sub>2</sub> from corn cob ash by precipitation method. *Optoelectronics and Advanced Materials- Rapid Communication*, 6(3-4), 2012, 394-397.
- [7] R. Novotny, A. Hoff, and J. Schuertz, Process for hydrothermal production of sodium silicate solutions, United States Patent, 1991, 5,000, 933.
- [8] R. Haase, V. Hunger, and A. Lenz, Method of manufacturing aqueous solutions alkali Polysilicates, United States Patent, 1976, 3,984, 526.
- [9] J. Deabridges, Process for the manufacture of sodium Silicate. United States Patent, 1982, 4,336, 235.
- [10] N. Thuadaj, and A. Nuntiya, Synthesis and characterization of nanosilica from rice husk ash prepared by precipitation method. *Chiang Mai, J. Sci*, 35, 2008, 206.
- [11] U. Kalapathy, A. Proctor, and J. Shultz, A simple method for production of pure silica from rice hull ash. *Bioresource Technology*, 73, 2000, 257-262.

## Existence of Solution of Fractional Impulsive Delay Integrodifferential Equation in Banach Space

<sup>1</sup>R. P. Pathak, <sup>2</sup>Piyusha S. Somvanshi

<sup>1,2</sup>Department of Mathematics, National Institute of Mathematics, Raipur- 492001, Chhattisgarh, India

---

**Abstract.** This paper mainly concerned with existence of solution of fractional delay integrodifferential equation in Banach space. The results are obtained by the fixed point theorem.

---

### 1. INTRODUCTION

Fractional calculus deals with generalization of integrals and derivatives of noninteger order. Fractional calculus involves a wide area of applications by bringing into a broader paradigm concepts of physics, mathematics and engineering [12, 14]. In [3, 13] the authors have provided the existence of solutions of abstract fractional differential equations by using fixed point techniques. Several authors have been discussed different types of nonlinear fractional differential and integrodifferential equations in Banach spaces.

The theory of impulsive differential equations has undergone rapid developments over the years and played a very important role in modern applied mathematical modeling of real processes arising in phenomena studied in physics, population dynamics, chemical technology and economics. In [2, 8] Benchohra et al. established sufficient conditions for the existence of solutions for a class of initial value problems for impulsive fractional differential equations involving the Caputo fractional derivative of order  $0 < q \leq 1$  and  $1 < q \leq 2$ .

Anguraj and Karthikeyan [4] proved existence for impulsive neutral integrodifferential inclusions with nonlocal initial conditions via fractional operators. Benchohra and Seba [7] studied the existence of nonlocal Cauchy problem for semilinear fractional evolution equations. Balchandran and Trujillo [5] investigated the nonlocal Cauchy problem for nonlinear fractional integrodifferential equations in Banach spaces.

In the paper we consider the fractional impulsive delay integrodifferential equation of the form

$$(1.1) \quad \begin{cases} {}^c D_t^q(x(t)) = A(t, x)x(t) + f(t, x_t, \int_0^t h(t, s, x_s)ds), & t \in J = [0, T], \quad t \neq t_k \\ \Delta x|_{t=t_k} = I_k(x(t_k^-)), & t = t_k, \quad k = 1, 2, \dots, n. \\ x(0) = x_0 \end{cases}$$

where  $0 < q < 1$  and the state  $x(\cdot)$  belongs to Banach space  $X$  endowed with the  $\|\cdot\|$ ,  $A(t, x)$  is a bounded linear operator on a Banach space  $X$ .  $D_t^q$  is the Caputo fractional derivative.  $f$  is a continuous function.  $I_k : X \rightarrow X$ ,  $\Delta x(t_k) = x(t_k^+) - x(t_k^-)$  with  $x(t_k^+) = \lim_{h \rightarrow 0^+} x(t_k + h)$ ,  $x(t_k^-) = \lim_{h \rightarrow 0^-} (t_k + h)$ ,  $k = 1, 2, 3, \dots, n$ ,  $0 = t_0 < t_1 < t_2 < \dots < t_n < t_{n+1} = T$ .

The rest of this paper is organized as follows. In section 2, some preliminaries are presented. In section 3, we study the existence and uniqueness of solutions for the impulsive fractional system (1.1). In section 4, an example is given.

## 2. PRELIMINARIES

In this section we introduce some basic definitions, notations, lemmas and mathematical preliminaries which are used throughout this paper.

**Definition 2.1.** The Riemann-Liouville fractional integrable operator of order  $q \geq 0$  of function  $f \in L^1(R^+)$  is defined as

$$I_{0+}^q f(t) = \frac{1}{\Gamma(q)} \int_0^t (t-s)^{q-1} f(s) ds, \quad t > 0$$

where  $\Gamma(\cdot)$  is the Euler gamma function and  $L^\sigma$  is Banach space of Lebesgue measurable functions with  $\|l\|_{L^\sigma} < \infty$ .

Next we introduce the Caputo fractional derivative.

**Definition 2.2.** The Caputo fractional derivative of order  $q \geq 0$ ,  $n-1 < q < n$ , is defined as

$$D_{0+}^q f(t) = \frac{1}{\Gamma(n-q)} \int_0^t (t-s)^{(n-q-1)} f^{(n)}(s) ds, \quad t > 0$$

where the function  $f(t)$  has absolutely continuous derivative up to order

$(n - 1)$ .

If  $0 < q < 1$ , then

$$D_{0+}^q f(t) = \frac{1}{\Gamma(1 - q)} \int_0^t (t - s)^{(-q)} f^{(1)}(s) ds$$

where  $f^{(1)}(s) ds = Df(s) = \frac{df(s)}{ds}$  and  $f$  is an abstract function with values in  $X$ .

FRACTIONAL CALCULUS

3

**Lemma 2.3.** For  $q > 0$  the solution of fractional differential equation  ${}^c D_t^q x(t) = 0$  is given by

$$x(t) = c_0 + c_1 t + c_2 t^2 + \dots + c_{n-1} t^{n-1}.$$

where  $c_i \in R, i = 0, 1, 2, \dots, n - 1, (n = [q] + 1)$  where  $[q]$  denotes the integer part of  $q > 0$ .

**Lemma 2.4.** A function  $x : (-\infty, T] \rightarrow X$  is said to be a solution of system (1.1) if  $x(0) = x_0$ , the impulsive condition  $\Delta x|_{t=t_k} = I_k(x(t_k^-))$ ,  $k = 1, 2, 3, \dots, n$  is verified the restriction of  $x(\cdot)$ , to the interval  $J_k (k = 0, 1, 2, \dots, n)$  is continuous and following integral equation holds for  $t \in J$ . (See [1], Lemma 4.2)

(2.1)

$$x(t) = \begin{cases} x_0 + \frac{1}{\Gamma(q)} \sum_{0 < t_k < t} \int_{t_{k-1}}^{t_k} (t_k - s)^{q-1} A(s, x) x(s) ds + \frac{1}{\Gamma(q)} \int_{t_k}^t (t - s)^{q-1} A(s, x) x(s) ds \\ + \frac{1}{\Gamma(q)} \sum_{0 < t_k < t} \int_{t_{k-1}}^{t_k} (t_k - s)^{q-1} f(s, x_s, \int_0^s h(s, \tau, x_\tau) d\tau) ds \\ + \frac{1}{\Gamma(q)} \int_{t_k}^t (t - s)^{q-1} f(s, x_s, \int_0^s h(s, \tau, x_\tau) d\tau) ds + \sum_{0 < t_k < t} I_k(x(t_k^-)). \end{cases}$$

3. MAIN RESULT

We assume following conditions to prove existence of the solution of equation (1.1).

(H1)  $A : J \times X \rightarrow B(X)$  is a continuous bounded linear operator and there exists a constant  $M > 0$ , such that the function satisfies the Lipschitz condition

$$\|A(t, x) - A(t, y)\|_{B(X)} \leq M \|x - y\|, \quad \text{for all } x, y \in X.$$

(H2)  $f : J \times X \times X \rightarrow X$  is continuous and there exists a constant  $L > 0$ , such that



$$\|f(t, u, x) - f(t, v, y)\| \leq L\|u - v\| + \|x - y\|, \quad \text{for all } x, y, u, v \in X.$$

(H3)  $h : \Delta \times X \rightarrow X$  is continuous and there exists a constant  $L_1 > 0$ , such that

$$\|h(t, s, x) - h(t, s, y)\| \leq L_1\|x - y\|, \quad \text{for all } x, y \in X.$$

(H4) The functions  $I_k : X \rightarrow X$  are continuous and there exists a constant  $L_2 > 0$ , such that

$$\|I_k(x) - I_k(y)\| \leq L_2\|x - y\|, \quad \text{for each } x, y \in X \quad \text{and } k = 1, 2, \dots, m.$$

Let  $B_r = \{u \in X : \|u\| \leq r\}$  for some  $r > 0$ . For brevity let us take  $\gamma = \frac{T^q}{\Gamma(q+1)}$  and  $K = \sup_{t \in J} \|A(t, 0)\|$ ,  $N = \max_{t \in J} \|f(t, 0, 0)\|$ ,  $N_1 = \max_{(t,s) \in \Delta} \|h(t, s, 0)\|$ .

4

R. P. PATHAK AND PIYUSHA S. SOMVANSHI

From (H1) we observe that for any  $x \in B_r$ ,

$$\|A(t, x)\| \leq \|A(t, x) - A(t, 0)\| + \|A(t, 0)\| \leq M\|x\| + \|A(t, 0)\| \leq Mr + K$$

Further we assume that

(H5)  $\|x_0\| + \gamma(m + 1)((Mr + K)r + M_0) + mL_2r \leq r$  where  $M_0 = Lr + LL_1Tr + LN_1T + N$ .

(H6) Let  $p = \gamma(m+1)[(2Mr+K+L+LL_1T)+mL_2]$  be such that  $0 \leq p < 1$ .

**Theorem 3.1.** *If the hypothesis (H1)-(H6) are satisfied, then fractional delay integrodifferential equation (1.1) has a unique solution in  $J$ .*

*Proof.* Let  $\Omega = PC(J : B_r)$  as in [6]. Define the mapping  $\Phi : \Omega \rightarrow \Omega$  by

$$\begin{aligned} (3.1) \quad \Phi x(t) = & x_0 + \frac{1}{\Gamma(q)} \sum_{0 < t_k < t} \int_{t_{k-1}}^{t_k} (t_k - s)^{q-1} A(s, x)x(s)ds + \frac{1}{\Gamma(q)} \int_{t_k}^t (t - s)^{q-1} A(s, x)x(s)ds \\ & + \frac{1}{\Gamma(q)} \sum_{0 < t_k < t} \int_{t_{k-1}}^{t_k} (t_k - s)^{q-1} f(s, x_s, \int_0^s h(s, \tau, x_\tau)d\tau)ds \\ & + \frac{1}{\Gamma(q)} \int_{t_k}^t (t_k - s)^{q-1} f(s, x_s, \int_0^s h(s, \tau, x_\tau)d\tau)ds + \sum_{0 < t_k < t} I_k(x(t_k^-)). \end{aligned}$$

and we have to show that  $\Phi$  has a fixed point. This fixed point is then a solution of equation (1.1). We know from [6] that  $\Phi B_r \subset B_r$ . From the assumptions we have

$$\begin{aligned} \|\Phi x(t)\| &\leq \|x_0\| + \frac{1}{\Gamma(q)} \sum_{0 < t_k < t} \int_{t_{k-1}}^{t_k} (t_k - s)^{q-1} \|A(s, x)\| \|x(s)\| ds + \frac{1}{\Gamma(q)} \int_{t_k}^t (t - s)^{q-1} \|A(s, x)\| \|x(s)\| ds \\ &+ \frac{1}{\Gamma(q)} \sum_{0 < t_k < t} \int_{t_{k-1}}^{t_k} (t_k - s)^{q-1} \|f(s, x_s, \int_0^s h(s, \tau, x_\tau) d\tau)\| ds \\ &+ \frac{1}{\Gamma(q)} \int_{t_k}^t (t - s)^{q-1} \|f(s, x_s, \int_0^s h(s, \tau, x_\tau) d\tau)\| ds + \sum_{0 < t_k < t} \|I_k(x(t_k^-))\| \leq r. \end{aligned}$$

Thus  $\Phi$  maps  $B_r$  into itself. Now for  $x, x' \in \Omega$ , we have

FRACTIONAL CALCULUS

5

$$\begin{aligned} \|\Phi x(t) - \Phi x'(t)\| &\leq \frac{1}{\Gamma(q)} \sum_{0 < t_k < t} \int_{t_{k-1}}^{t_k} (t_k - s)^{q-1} \|A(s, x)x(s) - A(s, x')x'(s)\| ds \\ &+ \frac{1}{\Gamma(q)} \int_{t_k}^t (t - s)^{q-1} \|A(s, x)x(s) - A(s, x')x'(s)\| ds \\ &+ \frac{1}{\Gamma(q)} \sum_{0 < t_k < t} \int_{t_{k-1}}^{t_k} (t_k - s)^{q-1} \|f(s, x_s, \int_0^s h(s, \tau, x_\tau) d\tau) - f(s, x'_s, \int_0^s h(s, \tau, x'_\tau) d\tau)\| ds \\ &+ \frac{1}{\Gamma(q)} \int_{t_k}^t (t - s)^{q-1} \|f(s, x_s, \int_0^s h(s, \tau, x_\tau) d\tau) - f(s, x'_s, \int_0^s h(s, \tau, x'_\tau) d\tau)\| ds \\ &+ \sum_{0 < t_k < t} \|I_k(x(t_k^-)) - I_k(x'(t_k^-))\| \\ &\leq [\gamma(m + 1)(2Mr + K + L + LL_1T) + mL_2] \|x(t) - x'(t)\| \\ &\leq p \|x - x'\|. \end{aligned}$$

Since  $0 \leq p < 1$ , then  $\Phi$  is a contraction mapping and therefore there exists a unique fixed point  $x \in \Omega$  such that  $\Phi x(t) = x(t)$ . Any fixed point of  $\Phi$  is the solution of (1.1).  $\square$

#### 4. EXAMPLE

Consider the following fractional delay integrodifferential equation with impulsive condition of the form

(4.1)

$${}^c D^q x(t) = \frac{1}{24}(1 + \sin x(t))x(t) + \frac{1}{(x + 3)^2} \frac{x(\sin t)}{1 + x(\sin t)} + \frac{1}{9} \int_0^t e^{-\frac{1}{4}x(\sin s)} ds, \quad t \in J, \quad t \neq \frac{1}{2},$$

(4.2)

$$\Delta x|_{t=\frac{1}{2}} = \frac{|x(\frac{1}{2}^-)|}{3 + |x(\frac{1}{2}^-)|},$$

(4.3)

$$x(0) = x_0.$$

where  $0 < q \leq 1$ , take  $J = [0, 1]$ ,  $T = 1$

Let

$$A(t, x) = \frac{1}{24}(1 + \sin x(t)),$$

$$\text{let } H(x_t) = \int_0^t h(t, s, x_s) ds = \int_0^t e^{-\frac{1}{4}x(\sin s)} ds$$

$$f(t, x, H(x_t)) = \frac{1}{(t+3)^2} \frac{x(\sin t)}{1+x(\sin t)} + H(x_t), \quad t \in J, \quad x \in X.$$

6

R. P. PATHAK AND PIYUSHA S. SOMVANSHI

Let  $u, v \in X$  and  $t \in J$ . Then we have

$$\|H(x_t) - H(y_t)\| = \left\| \int_0^t e^{-\frac{1}{4}x(\sin s)} ds - \int_0^t e^{-\frac{1}{4}y(\sin s)} ds \right\| \leq \frac{1}{4} \|x(\sin t) - y(\sin t)\| \leq \frac{1}{4} \|x - y\|.$$

$$\begin{aligned} \|f(t, x, H(x_t)) - f(t, y, H(y_t))\| &= \left\| \frac{1}{(t+3)^2} \left( \frac{x(\sin t)}{1+x(\sin t)} - \frac{y(\sin t)}{1+y(\sin t)} \right) + \frac{1}{9} (H(x_t) - H(y_t)) \right\| \\ &\leq \left\| \frac{1}{(t+3)^2} \left( \frac{x(\sin t)}{1+x(\sin t)} - \frac{y(\sin t)}{1+y(\sin t)} \right) \right\| + \left\| \frac{1}{9} (H(x_t) - H(y_t)) \right\| \\ &\leq \frac{1}{(t+3)^2} \|x - y\| + \frac{1}{9} \|H(x_t) - H(y_t)\| \leq \frac{1}{9} (\|x - y\| + \|H(x_t) - H(y_t)\|). \end{aligned}$$

Hence the condition (H1)-(H3) hold with  $M = \frac{1}{24}$ ,  $L = \frac{1}{9}$ ,  $L_1 = \frac{1}{4}$ . Here  $K = \frac{1}{24}$ . Let  $x, y \in X$ , we have by (H4)

$$\|I_k(x) - I_k(y)\| = \left\| \frac{x}{3+x} - \frac{y}{3+y} \right\| = \frac{3\|x-y\|}{(3+x)(3+y)} \leq \frac{1}{3} \|x - y\|.$$

Note that  $L_2 = \frac{1}{3}$ . Choose  $r = 1$ ,  $m = 1$ . We shall check the condition

$$\gamma(m+1)(2Mr + K + L + LL_1T) + mL_2 < 1$$

It satisfies indeed

$$(4.4) \quad \gamma(m+1)(2Mr + K + L + LL_1T) + mL_2 < 1 \Leftrightarrow \Gamma(q+1) > \frac{19}{24}.$$

which is satisfied for some  $q \in (0, 1]$ . Further (H5) is satisfied by a suitable choice of  $x_0$ . Then by theorem 3.1 the problem (4.1)-(4.3) has a unique solution on  $[0, 1]$  for the values of  $q$  satisfying (4.4).

## 5. CONFLICT OF INTEREST

The authors declare that they have no conflict of interest.

## References

- [1] R. P. Agarwal, M. Benchohra, S. Hamani, A survey on the existence results for boundary value problems of nonlinear equations and inclusions, *Acta Applicandae Mathematicae*. 109, (2010),973-1033.
- [2] R. P. Agarwal, M. Benchohra, B. A. Slimani, Existence results for differential equations with fractional order and impulses, *Memoire on Differential Equations and Mathematical Physics*. 44, (2008),1-21.
- [3] A. Anguraj, P. Karthikeyan, G. M. N'Guereata, Nonlocal Cauchy problem for some fractional abstract integrodifferential equations in Banach spaces, *Communications in Mathematical Analysis*. 6(1), (2009),31-35.
- [4] A. Anguraj, P. Karthikeyan, Y. K. Chang, Existence for impulsive neutral integrodifferential inclusions with nonlocal initial conditions via fractional operators, *Nonlinear Analysis: Theory Methods and Applications*. 71, (2009),4377-4386.
- [5] K. Balchandran, JJ. Trujillo, The nonlocal Cauchy problem for nonlinear fractional integrodifferential equations in Banach spaces, *Nonlinear Analysis: Theory Methods and Applications*. 72, (2010),4587-4593.
- [6] K. Balchandran, S. Kiruthika, JJ. Trujillo, Existence results for fractional integrodifferential equations in Banach spaces, *Commun. Non-linear Sci Numer Simulat*. 16 (4), (2011),1970-1977.
- [7] M. Benchohra, D. Seba, Impulsive fractional differential equations in Banach spaces, *Electronic Journal of Qualitative Theory of Differential Equations Special Edition*. 8, (2009),1-14.
- [8] M. Benchohra, B. A. Slimani, Existence and uniqueness of solutions to impulsive fractional differential equations, *Electronic Journal of Differential Equations*. 10, (2009),1-11.
- [9] B. Bonilla, M. Rivero, L. Rodriguez-Germa, JJ. Trujillo, Fractional differential equations as alternative models to nonlinear differential equations, *Applied Mathematics and Computation*. 187, (2007),79-88.
- [10] Y. K. Chang, Controllability of impulsive fractional differential systems with infinite delay in Banach spaces, *Chaos, Solitons and Fractals*. 33, (2007),1601-1609.
- [11] Giesle M Mophou, Existence and uniqueness of solutions to impulsive fractional differential equations, *Nonlinear analysis*. 72, (2010),1604- 1615.
- [12] JH. He, Approximate analytical solution for seepage flow with fractional derivative in porous media, *Computer Methods in Applied Mechanics and Engineering*. 167, (1998),57-68.
- [13] E. Hernandez, D. O'Regan, K. Balchandran, On recent developments in the theory of abstract differential equations with fractional derivatives, *Nonlinear Analysis: Theory, Methods and Applications*. 73(10), (2010),3462-3471.
- [14] R. Hilfer, *Applications of fractional calculus in physics*, Singapore; World Scientific;2000.

## Evaluation and Critical Technical Study of Li-Fi Compared with Wi-Fi and WiMax Technology

Md. Biplob Hossain<sup>[1]</sup>, Md. Selim Hossain<sup>[2]</sup>, Md. Mahasin Ali<sup>[3]</sup>,  
Md. Toufikur Rahman<sup>[4]</sup>, Rupam Chandro<sup>[5]</sup>, Farhana Matin<sup>[6]</sup> and Md. Dulal Haque<sup>[7]</sup>  
*Department of Telecommunication and Electronic Engineering, Hajee Mohammad Danesh Science and  
Technology University Dinajpur-5200, Bangladesh*

**Abstract:** Modern life becomes easier and wireless communications play an important role to do so. In computer networking, wireless technology is a modern alternative to networks that use cables. Li-Fi is a wireless communication system in which light is used as a carrier signal instead of traditional radio frequency as in Wi-Fi. Li-Fi is a technology that uses light emitting diodes to transmit data wirelessly. Li-Fi is a form of Visible Light Communication (VLC). VLC uses rapid pulses of light to transmit information wirelessly that cannot be detected by the human eye. In modern age everyone wants to use wireless data but capacity is drying up. Wireless radio frequencies are getting higher, complexities are increasing and RF interferences continue to grow. In order to overcome this problem in future, light fidelity (Li-Fi) become a better technology. This new wireless technology can save a large amount of electricity by transmitting data through the light bulbs. Li-Fi is a better alternative to Wi-Fi and WiMAX in wireless communication. Li-Fi has thousand times greater speed than Wi-Fi and provides security as the visible light is unable to penetrate through the walls, which propose a new era of wireless communication. Such technology has brought not only greener but safer and cheaper future of communication. Despite of numerous advantages of Li-Fi technology, there exist some drawbacks also. Line of sight propagation problem is one of them. So we proposed a new method that not only reduces this problem but also increase the performance of this technology.

**Keywords:** Wi-Fi (Wireless Fidelity), WiMax, Li-Fi (Light Fidelity), VLC, LED, Photo detector, LoS

### I. Introduction

There are many factors which have been considered for the need to converge IEEE 802.x wireless network technologies. These factors range from device interoperability, cost effectiveness, manageability, service scalability and availability, and bandwidth usage. Due to their flexibility wireless networks, are becoming the preferred form of communicating data, voice and video, which were traditionally being transferred using separate networks [1], [5]. As number of user increases in wireless network, their requirement increases that leads to decreases in speed proportionally. It is still in shortage for accommodating huge requirements of users [3]. To rectify this limitation of Wi-Fi in small coverage area, WiMax has been introduced. WiMAX is a wireless communications standard designed to provide 30 to 40 megabit-per-second data rates, with the 2011 update providing up to 1 Gbit/s for fixed stations. Due to the technological development, A new era in wireless communication is soon going to hit the word, A German physicist, Herald Hass who evolve a method to transfer data through illumination which he called it as D-light (or LI-FI). LI-FI which is a very advanced version of WI-FI is basically light fidelity which uses visible light communication instead of radio wave communication as in WI-FI. As speed of light is way faster than radio waves hence it can be used with a speed of around 250 times more than any high speed broadband and its speed is above the 1 Gbps[4 ].

### II. Wi-Fi (Wireless Fidelity)

Wi-Fi is a local area wireless computer networking technology that allows electronic devices to network, mainly using the 2.5 gigahertz (12 cm) UHF and 5 gigahertz (6 cm) SHF bands and it is based on the Institute of Electrical and Electronics Engineers (IEEE) 802.11 standards [2]. The computers and handsets enabled with this technology use radio wave to send and receive data anywhere within the range of a base station. Wi-Fi typically provides local network access for around a few hundred feet which works up to 54 Mbps in 20 MHz channel. To

connect to a Wi-Fi LAN, a computer has to be equipped with a wireless network interface controller. All stations share a single radio frequency channel. Transmissions on this channel are received by all stations within range. A typical wireless access point using 802.11b or 802.11g with a stock antenna might have a range of 35 m (115 ft) indoors and 100 m (330 ft) outdoors. IEEE 802.11n, however, can more than double the range also varies with frequency band.

#### Advantages of Wi-Fi

- Wi-Fi allows cheaper deployment of local area networks
- Wi-Fi Protected Access encryption (WPA2) is considered secure, provided a strong passphrase
- Wi-Fi is a core technology in GPS Industries Applications.
- Wi-Fi technology available in hotels, airports, etc., will be more inclined to bring laptop with us
- Frees network devices from cables, allows for a more dynamic network to be grown.
- Changes the way people live, communicate, work and play

#### Disadvantages of Wi-Fi

- Spectrum assignments and operational limitations are not consistent worldwide
- The 802.11b and 802.11g use the 2.4 GHz spectrum which is crowded with other devices.
- Power consumption is high compared to other standards, making battery life and heat a concern.
- It is not always configured properly by users[2]

### III. WiMax

WiMAX (Worldwide Interoperability for Microwave Access) is a wireless communications standard designed to provide 30 to 40 Mbps data rates, with the 2011 update providing up to 1 Gbps for fixed stations.[wiki] WiMAX is a technology standard for long-range wireless networking. WiMAX equipment exists in two basic forms base stations, installed by service providers to deploy the technology in a coverage area, and receivers, installed in clients. It is also known as the IEEE 802.16 wireless metropolitan area network, along with the development of mobile communication and broadband technology and it has become a hot spot for global telecom operators and manufacturers [1],[5]. WiMAX is gaining popularity as a technology which delivers carrier-class, high speed wireless broadband at a much lower cost while covering large distance than Wi-Fi[7]

### IV. Li-Fi (Light Fidelity)

#### Advantages

- Single station can serve hundreds of users.
- Much faster deployment of new users comparing to wired netw
- Speed of 10 Mbps at 10 kilometers with line-of-site.
- It is standardized and same frequency equipment should work together.

#### Disadvantages

- Line of site is needed for longer connections
- Weather conditions like rain could interrupt the signal.
- Other wireless equipment could cause interference.
- WiMAX is very power intensive technology
- It requires strong electrical support
- Big installation and operational cost

Visible Light Communications Project in which several universities together has achieved 3.5GBps of the three primary colors from a small LED. Combined of this makes a total in excess of 10GBps of what is known as Li-Fi [4].

Li-Fi (Light Fidelity) as coined by Prof. Harald Haas during his TED Global talk is bidirectional, high speed and fully networked wireless communications, like Wi-Fi, using visible light [6]. As the speed of light is faster than radio waves hence it can be used with a speed of around 250 times more than any high speed broadband. Recently the use of internet is increasing and hence traffic is also increasing. Due to the disadvantage of Wi-Fi such as it covers Small distance, more traffic slower speed, costly. These limitations are overcome by Li-Fi which can be used for large coverage of area, traffic handling capacity, cheaper. It transmits data through LED which changes its intensity faster than human eye and that intensity is captured by a detector. Estimated transmission of data is around 10GBps. A recent project in foreign universities proved that, Ultra-Parallel Visible Light Communications Project in which several universities together has achieved 3.5GBps of the three primary colors from a small LED. Combined of this makes a total in excess of 10GBps of what is known as Li-Fi [4].

A. Working Principle of Li-Fi and Proposed Method

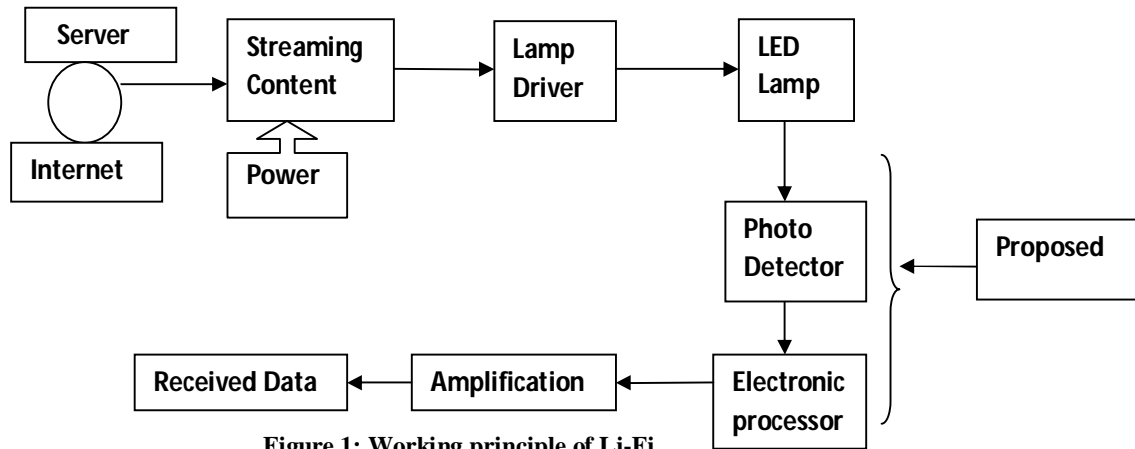


Figure 1: Working principle of Li-Fi

B. Working procedure[8]

The following factors are essential for the proper function of Li-Fi technology. These are:

1. Server

A server is a system (software and suitable computer hardware) that responds to requests across a computer network to provide, or help to provide, a network service. Internet and server run parallel. When we type a site for example-google.com, it sends request to various servers and finally sending request to the server of Google in USA. Finally after analyzing the request Google server sends us the required information in various packets. All this happens in a few seconds.

2. Lamp Driver

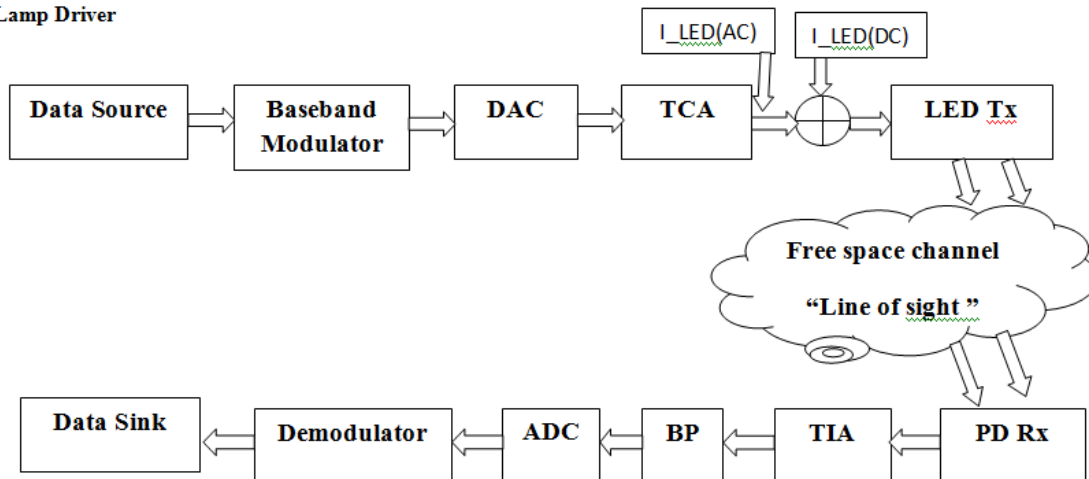


Figure 2: Working of lamp driver

Components of Light driver

i. Baseband modulator: Baseband modulation and demodulation techniques are fundamental to communication systems. Baseband is actual frequency band of signal (e.g. voice, video). If we consider the voice signal then voice signal band is approximately 4 kHz. That means voice signal contains frequencies ranging from 0-4kHz. Modulation is basically increasing signal frequency. This means voice base band of 4 kHz can be uplited to let's say, 1900 kHz.

ii. DAC: In electronics, a digital-to-analog converter (DAC, D/A, D2A or D-to-A) is a function that converts digital data (usually binary) into analog signal (current, voltage, or electric charge).

iii. TCA: A trans-conductance amplifier (gm amplifier) puts out a current proportional to its input voltage. In network analysis, the trans-conductance amplifier is defined as a voltage controlled current source (VCCS). It is common to see these amplifiers installed in a cascade configuration, which improves the frequency response.

iv. ADDER: It simply adds a dc current to the TCA output.

### 3. LED lamp

An overhead lamp fitted with an LED with signal processing technology streams data embedded in its beam at ultra-high speeds to the photo-detector.

### 4. Receiver

A receiver dongle then converts the tiny changes in amplitude into an electrical signal, which is then converted back into a data stream and transmitted to a computer or mobile device.

## C. Proposed method

Li-Fi technology has higher potential and it is highly possible to transmit data via light by changing the flicker rate that provides different strings of 1 and 0, and its intensity is modulated so quickly that the human eyes cannot notice its intensity. The functioning of Li-Fi is simple, we just need two things, first is LED (which acts as a light source) and other is photo detector (a light sensor for capturing light). When light source starts to emit light, light sensor on other end will detect it and gets a binary 1 otherwise binary 0. LED flashes certain time and builds up a message. Light sensor detects the light flashing of light and receives the message. But a major problem which has introduced for Li-Fi is the line of sight propagation. To solve the line of sight propagation problem of Li-Fi, we have proposed that the combination of photo detector and electronic processor by which we can get radio wave data at the receiver end. As a result we will find the data speed of Li-Fi at the receiver end and solve the problem of line of sight propagation that will increase the performance of Li-Fi technology.

### 1. Line of sight propagation

Line of sight (LoS) is a type of propagation that can transmit and receive data only where transmit and receive stations are in view of each other without any sort of an obstacle between them. FM radio, microwave and satellite transmission are examples of line-of-sight communication. Line-of-sight propagation is a characteristic of electromagnetic radiation or acoustic wave propagation. Electromagnetic transmission includes light emissions traveling in a straight line. The rays or waves may be diffracted, refracted, reflected, or absorbed by atmosphere and obstructions with material and generally cannot travel over the horizon or behind obstacles. At low frequency (below approximately 3 MHz) radio signals travel as ground waves. However, at higher frequencies any obstruction between the transmitting antenna (transmitter) and the receiving antenna (receiver) will block the signal, just like the light that the eye may sense. Therefore, since the ability to visually see a transmitting antenna (disregarding the limitations of the eye's resolution) roughly corresponds to the ability to receive a radio signal from it, the propagation characteristic of high-frequency radio is called "line-of-sight".

There are three mechanisms which may cause the path loss due to line of sight-

- Refraction in the earth's atmosphere, which alters the trajectory of radio waves, and which can change with time.
- Diffraction effects resulting from objects near the direct path.
- Reflections from objects, which may be either near or far from the direct path.

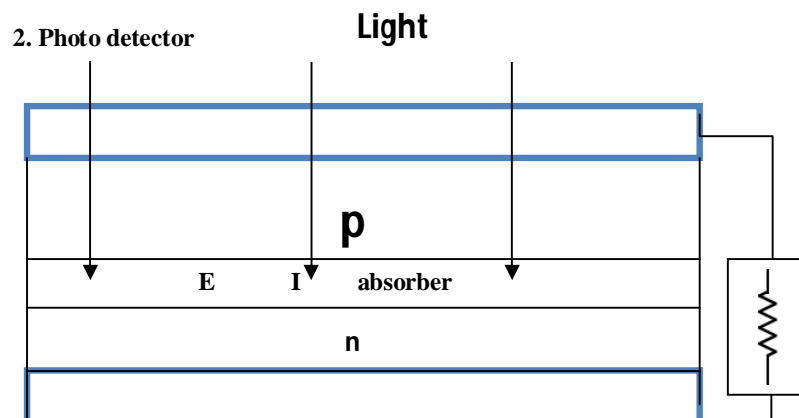


Figure 3: Photo detector

A photo detector operates by converting light signals that hit the junction. The junction uses an illumination window with an anti-reflect coating to absorb the light photons. The result of the absorption of photons is the creation of electron-hole pairs in the depletion region. PIN photodiode includes an intrinsic layer in between the P and N type materials. The PIN must be reverse bias due to the high resistivity of the intrinsic layer; the PIN has a larger depletion region which allows more electron-hole pairs to develop at a lower capacitance. The illumination window for a PIN is on the P-side of the diode because the mobility of electrons greater than holes which results in better frequency response. By another way, PIN junction diode has heavily doped p-type and n-type regions separated by an intrinsic region, which is a major absorption layer. When reverse biased, it acts like a constant capacitance and when forward biased it behaves as a resistor. Light is absorbed by intrinsic region. The result of the absorption of photons is the creation of electron-hole pairs in the depletion region which then produce electrical signal.

### 3. Converter/Transducer

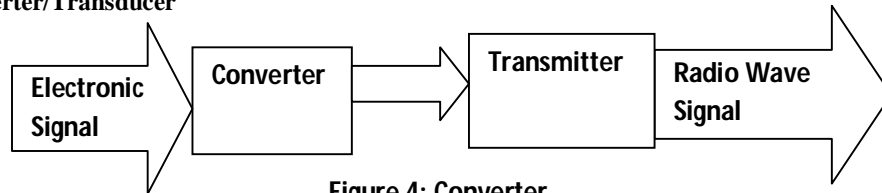


Figure 4: Converter

After taking the electrical signal from the photo detector, the electrical signal is converted by converter/transducer to get the radio wave signal. This signal is then transmitted by the transmitter and signal is thrown by means of radio wave.

#### D. Advantages of Li-Fi

- Capacity: Visible light spectrum is 10000 times bigger than RF spectrum.
- Security: Light cannot penetrate walls, but radio waves can, thus security is higher in using Li-Fi.
- Efficiency: The 1 million radio masts base stations consume a lot of energy, which indeed is used to cool the base stations and not to transmit radio waves.
- Transmission of data: Wi-Fi transmits data serially and Li-Fi transmits thousands of data streams parallel thus offering higher speed as high as above 1 Gbps.
- Li-Fi uses light rather than radio frequency signals
- Li-Fi may solve issues such as the shortage of radio frequency bandwidth
- Security is another benefit, since light does not penetrate through walls.

#### E. Disadvantages of Li-Fi

- The main problem is that light can't pass through objects
- Interference from external light sources like sun light, normal bulbs; and opaque materials in the path of transmission will cause interruption in the communication.
- High installation cost of the VLC systems can be complemented by large-scale implementation of VLC though Adopting VLC technology will reduce further operating costs like electricity charges, maintenance charges etc.
- We can't have a light bulb that provides data to a high-speed moving object or to provide data in a remote area where there are trees and walls and obstacles behind.[7],[9]

Still there are some backdrops like it can only transmit when in the line of sight. Due to this problem we propose the integrated circuit which helps to solve the propagation problem of Li-Fi

#### F. Applications of Li-Fi [18]

- Intelligent Transport System: LED equipped headlight and backlights where cars can talk to each other.
- Indoor Navigation: Li-Fi can be used to navigate through any hospital.
- Oil and gas wells: Testing and maintaining of gas wells can be performed with greater ease and efficiency. This can be obtained by placing the Li-Fi transmitter at the bottom of the well and the receiver at the surface, for real-time continuous monitoring.
- Intrinsically safe environments: This can be used in petroleum and chemical industries and other environments where the usage of radio waves or other transmission frequencies can be hazardous.
- Boon for Hospitals: Operating rooms in hospitals do not allow Wi-Fi over radiation concerns, and also there is lack of dedicated spectrum.
- Bulbs: There are around 19 billion bulbs worldwide, they just need to be replaced with LED ones that transmit data. We reckon VLC is at a factor of ten, cheaper than WI-FI.
- Traffic control: In streets for traffic control, Cars have LED based headlights, LED based backlights, and Car can communicate each other and prevent accidents in the way that they exchange Information.



Traffic light can communicate to the car and so on. Education systems: As with the advancement of science the latest technology is the LIFI which is the fastest speed internet access service.[111]

- Significantly Lower Power Consumption: Radio masts are very inefficient and require vast sums of power in order to broadcast and in some cases keep them cool enough to operate.
- Airlines: Airline Wi-Fi Nothing says captive audience like having to pay for the service of dial-up speed Wi-Fi on the plane. The best I have heard so far is that passengers will be offered a high-speed.

### G. Modulation techniques used in Li-Fi [15]

In order to actually send out data via LED, like any multimedia data, it is necessary to modulate these into a carrier signal. This carrier signal consists of light pulses sent out in short intervals. Li-Fi technology uses the following modulation techniques:

#### 1. Pulse-position modulation (PPM)

Sub-Carrier Inverse PPM (SCIPPM), method whose structure is divided into two parts (1) sub-carrier part and (2) DC part. The DC part is only for lighting or indicating. When there is no need of lighting or indicating SCPPM (Sub-Carrier PPM) is used for VLC to save energy.

#### 2. Frequency Shift Keying (FSK)

In frequency shift keying (FSK) data is represented by varying frequencies of the carrier wave. Before transmitting two distinct values (0 and 1), there need to be two distinct frequencies. This is also the normal form of frequency {shift keying, called binary frequency shift keying (BFSK).

#### 3. SIM-OFDM Technique (Sub-Carrier Index Modulation OFDM)

Traditional OFDM depicted in the SIM-OFDM technique splits the serial bit-stream B into two bit-sub streams of the same length. Unlike traditional OFDM depicted in the SIM-OFDM technique splits the serial bit-stream B into two bit-sub streams of the same length. . The next step is to select two different modulation alphabets MH and ML (i.e. 4-QAM and BPSK) to be assigned to the first and the second subsets of the first bit-sub stream.

## V. Comparison among Wi-Fi ,WiMax and Li-Fi

Although Wi-Fi, WiMAX and LiFi all are the wireless communication technology, there is a lot of difference among them.

### A. Comparison between Wi-Fi and WiMAX

Features	Wi-Fi	WiMAX
IEEE Standards	based on IEEE 802.11	based on IEEE 802.16
Range	a few hundred feet	up to 40 miles
Bit rate	Works at 2.7 bps/Hz and can peak up to 54 Mbps in 20 MHz channel.	Works at 5 bps/Hz and can peak up to 100 Mbps in a 20 MHz channel.
Primary Application	Wireless LAN	Broadband Wireless Access
Frequency Band	2.4 GHz ISM	Licensed/Unlicensed 2 G to 11 GHz
Channel Bandwidth	20-25 MHZ	Adjustable
Half/Full Duplex	Half	Full
Radio Technology	OFDM (64-channels)	OFDM (256-channels)
Bandwidth Efficiency	<=2.7 bps/Hz	<=5 bps/Hz
Modulation	BPSK, QPSK, 16-, 64-QAM	BPSK, QPSK, 16-, 64-, 256-QAM
Encryption	Optional-RC4 (AES in 802.11i)	Mandatory-3DES Optional- AES
Mobility	In development	Mobile-WiMax (802.16e)
Access Protocol	CSMA/CA	Request/Grant
Quality of service	does not guarantee any QoS	several level of QoS

Table 1: Comparison between Wi-Fi and WiMAX [11], [12], [13]

Features	Wi-Fi	Li-Fi
Speed	Uncontrolled speed	Controlled Speed due to intensity of light
Connection	Wireless- EMF	Wireless- Light
Security	Less secure due to transparency	More secure due to non penetration of light through walls
Reach	Excellent	Excellent
Impact	unknown	None
Cost	Expensive in comparison to Li-Fi Because its uses radio spectrum.	Cheaper than Wi-Fi because free band doesn't need license and it uses light.
Bandwidth Expansion	Limited	Exceptional
Operating frequency	2.4 GHz	Hundreds of Tera Hz
Data transfer medium	Used Radio spectrum	Used Light as a carrier
Spectrum Range	Radio frequency spectrum range is less than visible light spectrum.	Visible light spectrum has 10,000 time broad spectrum in comparison to radio frequency
Data Density	Transfer rate is less	transfer rate is more
Transmitter/Receiver power	Less	More

Table 2: Comparison between Wi-Fi and Li-Fi [14]. [15]. [16]  
Comparison among Wi-Fi, Li-Fi and WiMAX

Features	Wi-Fi	Li-Fi	Wi-Max
Speed	54 Mbps	>1 Gbps	70-100 Mbps
Connection	Wireless- EMF	Wireless- Light	Wireless- EMF
Security	Good	Excellent	Better
Reach	Excellent	Excellent	Excellent
Impact	unknown	None	unknown
Cost	Good	Low	Good
Bandwidth	Limited	Exceptional	Dynamic [ijtt]

IV. Simulation and result

Table 3: Comparison among Wi-Fi, Li-Fi and WiMAX [17]

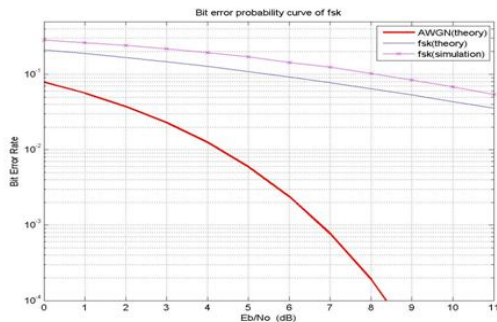


Figure 5: Bit Error Rate vs EB/No curve of FSK

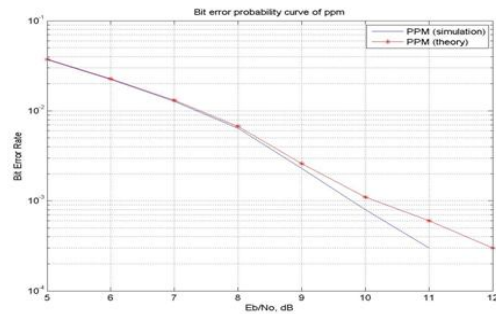


Figure 6: Bit Error Rate vs EB/No curve of PPM modulation

In figure 5: the red color for the Additive White Gaussian Noise (AWGN), the blue for theoretical BER and magenta for simulation BER of FSK modulation. If we observe we will see the AWGN is much smaller than BER. On the other hand the simulated magenta color signal is slightly higher than theoretical blue color signal, which is negligible. From the observation of figure 6; it is clear that the theoretical red color signal of PPM modulation is mostly overlapped by the simulated blue color signal and slightly change in the last portion which is negligible.

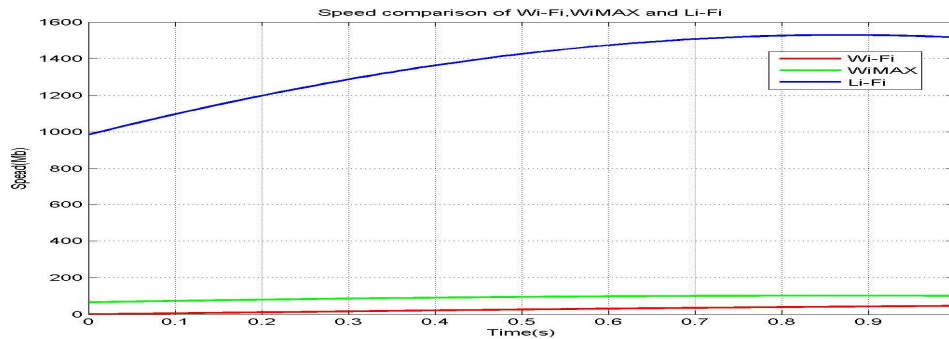


Figure 7: speed comparison curve of Wi-Fi, WiMAX and Li-Fi

From figure 8: we see, the Li-Fi technology has highest speed compare to Wi-Fi and WiMAX technologies. It also clear that Wi-Fi has a speed of 0-around 50 Mbps, WiMAX has 70-100 Mbps but Li-Fi started from greater than 1 Gbps(1024 Mbps) .

#### Future scope of Li-Fi

Existing spectrum becomes narrow and causes interference, so broad spectrum is required to accommodate wireless signals without any effect. In hospitals where radio waves can't be used due to harmful effect on body visible light can be used for wireless communication. In airplanes where radio waves can affect the equipments li-fi can be used without any distortion. In the depth of water where radio waves can't travel more visible light communication can be more beneficial. So li-fi has higher advantages than other wireless technologies and can be seen as a future technology [9].

#### V. Conclusion

As much as the wireless networks (Wi-Fi, WiMax and Li-Fi) have decreased the installation and deployment costs, increased productivity and better convenience through its flexibility compared to wired networks. WiMax has a superior and predominant technical position and influence in the history of wireless communication then Wi-Fi .The only solution to this is a high-speed bidirectional fully mobile wireless network is Li-Fi system. Currently, the LI-FI concept is attracting a great deal of interest, because it provides an authentic and very efficient alternative to wireless device which used radio spectrum. It is very advantageous and implementable in various fields that can't be done with the Wi-Fi and other technologies. Hence the future applications of the Li-Fi can be predicted and extended to different plat-forms like education fields, medical field, industrial areas and many others fields.

#### References

- [1] Swanson M , "Security Self-Assessment Guide for Information Technology Systems", The National Institute of Standard and Technology Special Publication 800-26, 2001.
- [2] <http://en.wikipedia.org/wiki/Wi-Fi>
- [3] Swati Singh, Prof. (Dr.) Y.P, "LI FI- A NEW PARADIGM", International Journal of Advanced Research in Computer Science and Software Engineering, Volume 4, Issue 2, February 2014.
- [4] Birender Singh Rawat, Brijesh Aggarwal, Dishant Passi, " LI-FI: A New Era Of Wireless Communication Data Sharing", International Journal Of Scientific & Technology Research Volume 3, Issue 10, October 2014.
- [5] <https://en.wikipedia.org/wiki/WiMAX>
- [6] <http://en.wikipedia.org/wiki/Li-Fi>
- [7] Sourangsu Banerji, Rahul Singha Chowdhury, " Wi-Fi & WiMAX: A Comparative Study", Indian Journal of Engineering, Vol.2, Issue. 5, 2013
- [8] Aman Sodhi, Jeslin Johnson, " Light Fidelity (LI-FI) - The Future of Visible Light Communication" International Journal of Engineering Research and General Science Volume 3, Issue 2, March-April, 2015 ISSN 2091-2730
- [9] , Ranjeet Kaur2, " Light Fidelity (LI-FI)-A Comprehensive Study" International Journal of Computer Science and Mobile Computing, Vol.3 Issue.4, April- 2014, pg. 475-481
- [10] Jitender Singh1, Vikash2, " A New Era in Wireless Technology using Light-Fidelity" International Journal of Recent Development in Engineering and Technology (ISSN 2347-6435(Online) Volume 2, Issue 6, June 2014

- [11] Fadeladib, "See Through Walls With Wi-Fi", Massachusetts Institute Of Technology, June 2013.
- [12] Tonderai Muchenje, "Investigation of Security Issues on a Converged WiFi and WiMAX Wireless Network", Telkom Centre of Excellence, University of Fort Hare, Alice 5700, South Africa, March 2008.
- [13] M Shakeel Baig, "Signal Processing Requirements for WiMAX (802.16e) Base Station", Chalmers University of Technology Göteborg, Sweden, 2005.
- [14] S.Vinay Kumar, K.Sudhakar, L.Sudha Rani, "Emerging Technology Li-Fi over Wi-Fi", International Journal of Inventive Engineering and Sciences (IJIES) ISSN: 2319-9598, Volume-2, Issue-3, February 2014.
- [15] Dhakane Vikas Nivrutti, Ravi Ramchandra Nimbalkar "Light-Fidelity: A Reconnaissance of Future Technology" International Journal of Advanced Research in Computer Science and Software Engineering, Volume 3, Issue 11, November 2013.
- [16] Megha Goyal<sup>1</sup>, Dimple Saproo<sup>2</sup>, Asha Bhagashra<sup>3</sup>, "New Epoch of Wireless Communication: Light Fidelity", International Journal of Innovative Research in Computer and Communication Engineering Vol. 1, Issue 2, April 2013.
- [17] Jitender Singh, Vikash, "A New Era in Wireless Technology using Light-Fidelity", International Journal of Recent Development in Engineering and Technology, Volume 2, Issue 6, June 2014.
- [18] Rahul R. Sharma, Raunak, Akshay Sanganal "Li-Fi Technology Transmission of data through light" Int.J.Computer Technology & Applications, Vol 5 (1), 150-154

### Author's Biography



[1] Md. Biplob Hossain is a final year student of B. Sc in Telecommunication and Electronic Engineering in Hajee Mohammad Danesh Science and Technology University, Dinajpur, Bangladesh. He has an interest to work on Networking, Telecommunication Engineering, Digital Communication, Optical Fiber Communication, Digital Signal Processing, Digital Electronic and Mobile Communication. He also completed a thesis on "Performance Analysis of Orthogonal Frequency Division Multiplexing (OFDM) System by using Peak to Average Power Ratio (PAPR) Algorithm".



[2] Md. Selim Hossain is studying B. Sc in Telecommunication and Electronic Engineering (Level-4 Semester-II) in Hajee Mohammad Danesh Science and Technology University, Dinajpur, Bangladesh. His main working interest is based on Software Engineering, Database Management system, Web development, Digital Signal Processing, Network Security and Optical fiber Communication. He also completed a thesis on "Performance Analysis of Orthogonal Frequency Division Multiplexing (OFDM) System by using Peak to Average Power Ratio (PAPR) Algorithm".



[3] Md. Mahasin Ali is studying (Level-4 Semester-II) in B. Sc in Telecommunication and Electronic Engineering in Hajee Mohammad Danesh Science and Technology University Dinajpur-5200, Bangladesh in 2015. His main interest is based on Teletraffic Engineering, Digital Signal Processing, Software Engineering and Networking security. He likes natural beauty. "Believe Is an Art."



[4] At the last stage of completion for the degree, Bachelor of Science in Telecommunication and Electronic Engineering, decided to make himself as a researcher. He has strong interest in wireless network specifically Ad Hoc network and wireless sensor network. But he has the capability to take challenge in new era of sciences and this thesis is the reflection of his youthful spirit.



[5] Rupam Chandro is studying B. Sc in Telecommunication and Electronic Engineering (Level-4 Semester-II) in Hajee Mohammad Danesh Science and Technology University, Dinajpur-5200 Bangladesh. His main working interest is based on Software Engineering, Database Management system, android developer, Web development, Digital Signal Processing and Networking.



[6] Farhana Matin is studying B. Sc in Telecommunication and Electronic Engineering in Hajee Mohammad Danesh Science and Technology University, Dinajpur-5200 Bangladesh. She is a final year student. Her main working interest is based on Wireless Communication, Bio- medical Signal processing, Digital Signal Processing and Networking.



[7] Md. Dulal Haque completed both B. Sc and M. Sc degree in Applied Physics and Electronic Engineering from Rajshahi University, Bangladesh. At present, He is serving as an assistant professor in the department of Telecommunication and Electronic Engineering in Hajee Mohammad Danesh Science and Technology University, Dinajpur, Bangladesh. His research interest is on electronic device fabrication and wireless communication.

## Broadening of Omnidirectional Photonic Band Gap in Graphene Based one Dimensional Photonic Crystals

<sup>1</sup>Neetika Arora, <sup>2</sup>Rakhi Agrawal

<sup>1</sup>Electronics & communication Department , Noida International University, Noida, India

<sup>2</sup>Electronics & communication Department , Dronacharya College of Engineering, Greater Noida, India

**Abstract**—A simple design of one dimensional gradual stacked photonic crystal has been proposed. This structure exhibits a periodic array of alternate layers of Graphene and Silica. These are the materials of low and high refractive indices respectively. Here the structure considered has three stacks .Each stack has five alternate layers of Graphene and silica. The transfer matrix method has been used for numerical computation. In this paper, such a structure has wider reflection bands in comparison to a conventional dielectric PC structure and structure with  $\text{SiO}_2$  and Si layers for a constant gradual constant  $Y$  at different incident angle.

**Keywords**—Photonic crystal; Graphene; transfer matrix; gradual costant.

### I. INTRODUCTION

Photonic crystals are periodic optical nanostructures that affect the motion of photons in much the same way that ionic lattices affect electrons in solids. Photonic crystals occur in nature in the form of structural coloration and promise to be useful in different forms in a range of applications.

Photonic crystals are composed of periodic dielectric, metallic-dielectric or even superconductor microstructures or nanostructures that affect the propagation of electromagnetic waves (EM) in the same way as the periodic potential in a semiconductor crystal affects the electron motion by defining allowed and forbidden electronic energy bands. Photonic crystals contain regularly repeating regions of high and low dielectric constant. Photons (behaving as waves) propagate through this structure – or not – depending on their wavelength. Wavelengths that are allowed to travel are known as modes; groups of allowed modes form bands. Disallowed bands of wavelengths are called photonic band gaps. This gives rise to distinct optical phenomena such as inhibition of spontaneous emission, high-reflecting Omni-directional mirrors and low-loss-wave guiding.

Here we are considering the graded material .the physical properties of the graded materials are different from both homogeneous and conventional materials .In general graded photonic crystal have a variation either in the refractive indices of the alternate layers or a variation in thickness.

This structure consist a periodic array of alternate layers of Graphene and Silica. These are the materials of low and high refractive indices respectively. Here the structure considered has three stacks .Each stack has five alternate layers of Graphene and silica.

Light absorption in thin films has always been a relevant topic in optics, especially from the application point of view. Graphene is in many ways the ultimate thin film, only one atomic layer thick, and has photonic properties of high interest for optoelectronic applications [1].besides this grapheme has a larger refractive index with excellent mechanical and thermal properties.

### II. THEORY

The one-dimensional GSPC structure has been considered along x axis. It consists of alternate layers of high and low refractive indices. The assembly is placed between semi-infinite media of refractive indices  $n_i$  (refractive index of the incident medium) and  $n_s$  (refractive index of the substrate), as shown in Figure 1.

By applying TMM, the characteristic matrices for the TE and TM waves is given by

$$M_j = \begin{bmatrix} \cos\beta_j & -\frac{i\sin\beta_j}{q_j} \\ -iq_j\sin\beta_j & \cos\beta_j \end{bmatrix} \quad (1)$$

Where  $q_j = n_j \cos \theta_j$ , ( $j = 1, 2$ ; for the first and the second layers of the unit cell respectively) for the TE polarization and  $q_j = \cos \theta_j / n_j$  for the TM polarization,  $\beta_j = (2\pi/\lambda)n_j d_j \cos \theta_j$ ,  $\theta_j$  is the ray angle inside the layer of refractive index  $n_j$  and  $\lambda$  is the wavelength in the medium of incidence. The total characteristic matrix for the  $N$  periods of the structure can be expressed as

$$M = (M_1 \times M_2)^N = \begin{bmatrix} M_{11} & M_{12} \\ M_{21} & M_{22} \end{bmatrix} \quad (2)$$

The reflection coefficient of the structure for TE and TM polarizations are given by

$$r = \frac{(M_{11} + q_s M_{12})q_i - (M_{21} + q_s M_{22})}{(M_{11} + q_s M_{12})q_i + (M_{21} + q_s M_{22})} \quad (3)$$

where  $q_{i,s} = n_{i,s} \cos \theta_{j,s}$  for TE wave and  $q_{i,s} = \cos \theta_{j,s} / n_{i,s}$  for TM wave, where the subscripts  $i$  and  $s$  belong to the quantities in the incident medium and substrate respectively. Whereas, the reflectivity of the structure can be expressed as

$$R = |r|^2 \quad (4)$$

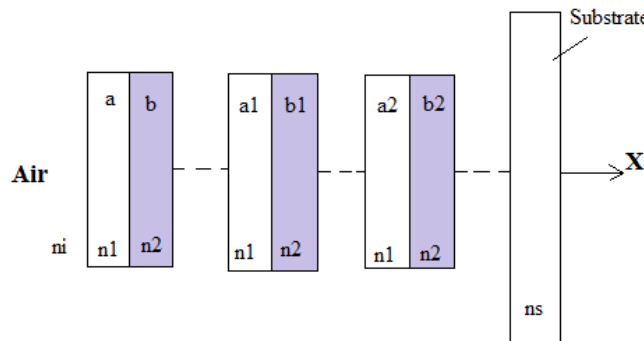


Fig 1. Schematic representation of GSPC structure

In one-dimensional PCs, there is no absolute photonic band gap (PBG) because of two factors. The first is as we increase the incident angle, the edges of PBG in certain direction will shift towards the higher frequency side. The second is that at the TM mode cannot be reflected at the Brewster angle. However, the absence of an absolute PBG does not mean that there is no Omni-directional reflection. There should be no propagating modes that can couple with the incident wave this is the criterion for the existence of total Omni-directional reflection. From Snell's law,

We know  $n_1 \sin \theta_1 = n_2 \sin \theta_2$  and  $n_1 \sin \theta_1 = n_2 \sin \theta_2$   
 i.e.,  $\theta_1 = \sin^{-1}(n_2 \sin \theta_2 / n_1)$  and  $\theta_2 = \sin^{-1}(n_1 \sin \theta_1 / n_2)$

Where  $n_1$  and  $n_2$  are the refractive indices of the low and high index media respectively and  $n_i$  is the refractive index of the incident medium. The maximum refracted angle is defined as  $\theta_{\max 2} = \sin^{-1}(n_1 / n_2)$  and Brewster angles  $\theta_B = \tan^{-1}(n_1 \sin \theta / n_2)$ . If the maximum refracted angle is smaller than the Brewster's angle then the incident wave from outside cannot couple to Brewster's window which results to total reflection for all incident angles. Thus, the condition for Omni-directional reflection without the influence of the Brewster's angle is  $\theta_B = \theta_{\max 2}$  [23]. This condition is satisfied by the selected parameters that we have taken for our numerical computations. Hence, in the present analysis there is no influence of Brewster's angle on the Omni-directional reflection bands.

### III. RESULT & DISCUSSION

From the computation of Equation (3), the reflection properties of one-dimensional GSPC can be represented graphically. For this purpose, we consider a GSPC structure having the following sequence — air/(AB)<sup>5</sup>/(A<sub>1</sub>B<sub>1</sub>)<sup>5</sup>/(A<sub>2</sub>B<sub>2</sub>)<sup>5</sup>/ Substrate(SiO<sub>2</sub>). For AB stack, we choose the material of layer A as Graphene and the material of layer B as Si having refractive indices 2.1 and 3.7 respectively. Here all the regions are assumed to be linear, homogeneous and non-absorbing. Also, the refractive indices of both the materials are considered to be constant. The thickness of the layers are taken as  $a = 283\text{nm}$  and  $b = 115\text{ nm}$  according to the quarter wave stack condition  $a = \lambda_c / 4n_1$  and  $b = \lambda_c / 4n_2$ , where  $\lambda_c (= 1700\text{ nm})$  is the critical wavelength which is the mid-wavelength of the wavelength range considered in our numerical computation. For A<sub>1</sub>B<sub>1</sub> stack, we choose the material of layer A<sub>1</sub> as Graphene and the material of layer B<sub>1</sub> as Si in which the thicknesses of the layers A<sub>1</sub> and B<sub>1</sub> are taken as  $a_1 = \gamma a$  and  $b_1 = \gamma b$  respectively, where  $\gamma$  is defined as gradual constant. In a similar way, we choose the material of layer A<sub>2</sub> as Graphene and the material of layer B<sub>2</sub> as Si in which the thicknesses of layers A<sub>2</sub> and B<sub>2</sub> are taken as  $a_2 = \gamma a_1$  and  $b_2 = \gamma b_1$  respectively. The reflectance spectra for conventional PC can be obtained by choosing  $\gamma = 1$  in this structure.

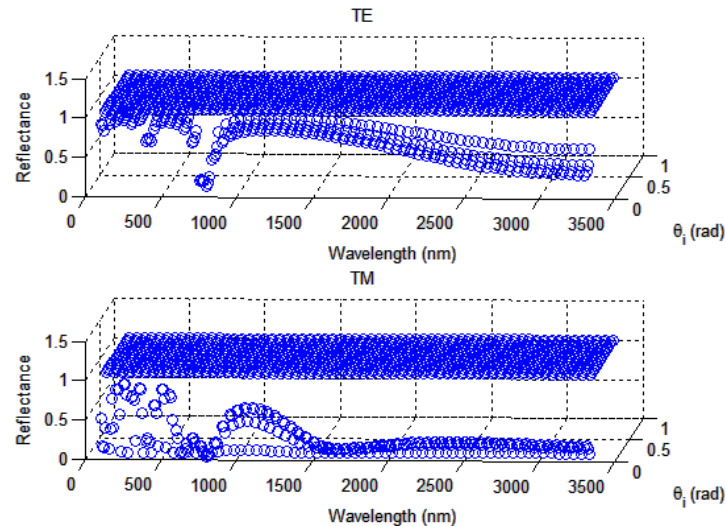


Fig 2. Reflectance spectra of SiO<sub>2</sub>/Si one-dimensional PC ( $\Upsilon = 1$ ) for TE and TM polarizations.

We observe from Table that the TE polarization has its Omni-directional reflection range from 1289 nm to 2210 nm and the Omni-directional reflection range for the TM polarization from 1289 nm to 1929 nm. Therefore, the total ODR for both TE and TM polarizations when  $\Upsilon = 1$ , i.e., for the case of conventional PC, has the bandwidth ( $\Delta\lambda = \lambda_H - \lambda_L$ ) of 640 nm. The upper wavelength edge of the ODR band is  $\lambda_H = 1929$  nm and the lower wavelength edge is  $\lambda_L = 1289$  nm. Hence, the normalized Omni-directional bandwidth is 37.65% of the total wavelength range considered around the critical wavelength  $\lambda_C = 1700$  nm.

TABLE 1. Total reflection region and gap width for SiO<sub>2</sub>/Si one-dimensional PC ( $\Upsilon = 1$ ).

Angle of incidence $\theta_i$ (degree)	TE polarization		TM polarization	
	Reflection range (nm)	Gap width (nm)	Reflection range (nm)	Gap width (nm)
0	1289–2342	1053	1289–2342	1053
30	1252–2379	1127	1298–2284	986
60	1210–2302	1092	1192–1971	779
85	1117–2210	1093	1197–1929	732

#### IV. CONCLUSION

To summarize, we have investigated theoretically the ODR range of one-dimensional GSPC structure. It is found that the ODR range of GSPC structure can be enhanced by changing the material Si by Graphene with constant the value of gradual constant and that the ODR range for one-dimensional GSPC structure is more than that of conventional PC and simple graded structure. Hence, a one-dimensional GSPC structure can be used as a broadband optical reflector, and the range of reflection can be tuned to a desired wavelength region by changing the material by Graphene and also by choosing proper thickness of the period ( $d$ ) of first stack and relative thicknesses of individual layers of the following stacks. These types of optical reflectors are compact in size and may have potential applications in the field of optical technology and optoelectronics.

#### REFERENCES

- [1] Yablonovitch, E., "Inhibited spontaneous emission in solid-state physics and electronics," *Phys. Rev. Lett.*, Vol. 58, 2059–2062, 1987.
- [2] John, S., "Strong localization of photons in certain disordered dielectric superlattices," *Phys. Rev. Lett.*, Vol. 58, 2486–2489, 1987.
- [3] Jannopoulos, J. D., P. Villeneuve, and S. Fan, "Photonic crystals: Putting a new twist on light," *Nature*, Vol. 386, 143–149, 1997.
- [4] Xu, K. Y., X. Zheng, C. L. Li, and W. L. She, "Design of omnidirectional and multiple channeled filters using one-dimensional photonic crystals containing a defect layer with a negative refractive index material," *Phys. Rev. E*, Vol. 71, 066604, 2005.

- [5] Singh, S. K., J. P. Pandey, K. B. Thapa, and S. P. Ojha, "Some new band gaps and defect modes of one dimensional photonic crystals composed of etamaterials," *Solid State Commun.*, Vol. 143, 217, 2007.
- [6] St. J. Russell, P., S. Treadwell, and P. J. Roberts, "Full photonic band gap and spontaneous emission control in 1D multilayer dielectric structures," *Opt. Commun.*, Vol. 160, 66–71, 1999.
- [7] Kumar, V., K. S. Singh, and S. P. Ojha, "Band structures, reflection properties and abnormal behaviour of one-dimensional plasma photonic crystals," *Progress In Electromagnetics Research M*, Vol. 9, 227–241, 2009.
- [8] Pandey, G. N., K. B. Thapa, S. K. Srivastava, and S. P. Ojha, "Band structures and abnormal behaviour of one dimensional photonic crystal containing negative index materials," *Progress In Electromagnetics Research M*, Vol. 2, 15–36, 2008.
- [9] Dowling, J. P., "Mirror on the wall: You're omnidirectional after all?," *Science*, Vol. 282, 1841–1842, 1998.
- [10] Yablonovitch, E., "Engineered omnidirectional external- reflectivity spectra from one-dimensional layered interference filters," *Opt. Lett.*, Vol. 23, 1648–1649, 1998.
- [11] Chigrin, D. N., A. V. Lavrinenko, D. A. Yarotsky, and S. V. Gaponenko, "Observation of total omnidirectional reflection from a one dimensional dielectric lattice," *Appl. Phys. A: Mater.Sci. Process.*, Vol. 68, 25–28, 1999.
- [12] Fink, Y., J. N. Winn, S. Fan, C. Chen, J. Michel, J. D. Joannopoulos, and E. L. Thomas, "A dielectric omni- directional reflector," *Science*, Vol. 282, 1679–1682, 1998.
- [13] Lusk, D., I. Abdulhalim, and F. Placido, "Omnidirectional reflection from Fibonacci quasi-periodic one-dimensional photonic crystal," *Opt. Commun.*, Vol. 198, 273–279, 2001.
- [14] Ibanescu, M., Y. Fink, S. Fan, E. L. Thomas, and J. D. Joannopoulos, "An all-dielectric coaxial waveguide," *Science*, Vol. 289, 415–419, 2000.
- [15] Srivastava, S. K. and S. P. Ojha, "Omnidirectional reflection bands in one-dimensional photonic crystal structure using fullerence films," *Progress In Electromagnetics Research*, Vol. 74, 181–194, 2007.
- [16] Srivastava, R., S. Pati, and S. P. Ojha, "Enhancement of omnidirectional reflection in photonic crystal heterostructures," *Progress In Electromagnetics Research B*, Vol. 1, 197–208, 2008.
- [17] Huang, J. P. and K. W. Yu, "Optical nonlinearity enhancement of graded metallic films," *Appl. Phys. Lett.*, Vol. 85, 94–96, 2004.
- [18] Sang, Z. F. and Z. Y. Li, "Effective negative refractive index of graded granular composites with metallic magnetic particles," *Phys. Lett. A*, Vol. 334, 422–428, 2005.
- [19] Huang, J. P. and K. W. Yu, "Second-harmonic generation in graded metallic films," *Opt. Lett.*, Vol. 30, 275–277, 2005.
- [20] Yeh, P., *Optical Waves in Layered Media*, John Wiley and Sons, New York, 1988.
- [21] Born, M. and E. Wolf, *Principle of Optics*, 4th edition, Pergamon, Oxford, 1970.
- [22] Winn, J. N., Y. Fink, S. Fan, and J. D. Joannopoulos, "Omni- directional reflection from a one-dimensional photonic crystal," *Optics Lett.*, Vol. 23, 1573–1575, 1998.
- [23] Lee, H. Y. and T. Yao, "Design and evaluation of omnidirectional one- dimensional photonic crystals," *J. Appl. Phys.*, Vol. 93, 819– 837, 2003.
- [24] Srivastava, S. K. and S. P. Ojha, "Broadband optical reflector based on Si/SiO<sub>2</sub> one dimensional graded photonic crystal structure," *J. Mod. Opt.*, Vol. 56, No. 1, 33–40, 2009.



## 3D Design & Simulation of Printed Dipole Antenna

Protap Mollick<sup>1</sup>, Amitabh Halder<sup>2</sup>, Mohammad Forhad Hossain<sup>3</sup>,  
Anup Kumar Sarker<sup>4</sup>

<sup>1</sup>(CSE, American International University-Bangladesh, Bangladesh)

<sup>2,3,4</sup>(EEE, American International University-Bangladesh, Bangladesh)

**ABSTRACT:** This paper represents design of a printed dipole antenna with both  $\lambda/2$  & half dipole. In this research paper the impedance increases with combined design on the FR-4 substrate and ground plane. The main feature of printed dipole antenna is there is a feeder between the radiant elements. Average impedance about 73 ohm, which is very large form other antenna. For vertical earth position impedance decreases about 36 ohm. Applied AC voltage forwarding bias dipole antenna gains are high but when reverse bias condition gains are low. Between ropes to station there is need extra insulator that abate high impedance current flow to dipole antenna. Feed lines are approximately 75 ohm and the main length between two poles are 143 meter. The radius of two pole line is very thin it's about 2.06 meter. Transmission lines are added in the last portion of feed lines, which situated apposite of two poles. Designs are simulated by hfss and solving equations are done my matlab.

**Keywords**—Rabbit ears, folded dipole, omnidirectional, azimuthal direction, 3db gain.

### I. INTRODUCTION

In radio and telecommunications a dipole antenna or doublet is the simplest and most widely used class of antenna. It consists of two identical conductive elements such as metal wires or rods, which are usually bilaterally symmetrical. The driving current from the transmitter is applied, or for receiving antennas the output signal to the receiver is taken, between the two halves of the antenna. Each side of the feed line to the transmitter or receiver is connected to one of the conductors. This contrasts with a monopole antenna, which consists of a single rod or conductor with one side of the feed line connected to it, and the other side connected to some type of ground. A common example of a dipole is the "rabbit ears" television antenna found on broadcast television sets [1].

The most common form of dipole is two straight rods or wires oriented end to end on the same axis, with the feed line connected to the two adjacent ends. This is the simplest type of antenna from a theoretical point of view. Dipoles are resonant antennas, meaning that the elements serve as resonators, with standing waves of radio current flowing back and forth between their ends [2]. So the length of the dipole elements is determined by the wavelength of the radio waves used. The most common form is the half-wave dipole, in which each of the two rod elements is approximately  $1/4$  wavelength long, so the whole antenna is a half-wavelength long. The radiation pattern of a vertical dipole is omnidirectional; it radiates equal power in all azimuthal directions perpendicular to the axis of the antenna [3]. For a half-wave dipole the radiation is maximum, 2.15 dBi perpendicular to the antenna axis, falling monotonically with elevation angle to zero on the axis, off the ends of the antenna. Several different variations of the dipole are also used, such as the folded dipole, short dipole, cage dipole, bow-tie, and batwing antenna. Dipoles may be used as standalone antennas themselves, but they are also employed as feed antennas (driven elements) in many more complex antenna types, such as the Yagi antenna, parabolic antenna, reflective array, turnstile antenna, log periodic antenna, and phased array. The dipole was the earliest type of antenna; it was invented by German physicist Heinrich Hertz around 1886 in his pioneering investigations of radio waves.

## II. DESIGN & EQUATIONS

The FR4 main ground plane substrate is closely related to the size and the impedance of the dipole antenna. Lower frequency constant of the substrate produces larger impedance. The cut-off frequency of dipole antenna and the size of the radiation patch can be similar to the following formulas while the high dielectric constant of the substrate results in smaller size of antenna.

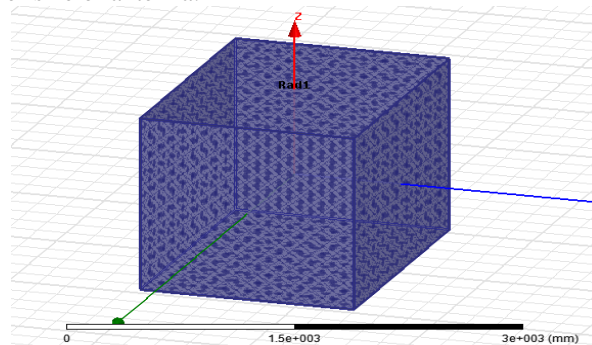


Figure 1: Dipole Antenna Body shape (Printed)

Figure 1 shows the geometry of the design of Dipole shape with a substrate line in which the Length of ground plane of Antenna is 38.4 mm and Width is 46.8 mm, L & W of the patch is 28.8 mm & 37.2 mm.

There are some necessary equations for Dipole antenna some of them are listed below:

$$E_{\theta} = \frac{-iI_0 \sin \theta L}{4\epsilon_0 cr \lambda} e^{i(\omega t - kr)}$$

$$E_{\theta} = \frac{j\eta I_0 e^{-jkr}}{2\pi r} \left[ \frac{\cos\left(\frac{kL}{2} \cos \theta\right) - \cos\left(\frac{kL}{2}\right)}{\sin \theta} \right]$$

$$H_{\phi} = \frac{E_{\theta}}{\eta}$$

$$R_{\text{radiation}} = \frac{\pi}{6} Z_0 \left(\frac{L}{\lambda}\right)^2 \approx \left(\frac{L}{\lambda}\right)^2 (197\Omega).$$

## III. TYPES OF DIPOLE ANTENNA

The dipole antenna consists of two conductive elements such as metal wires or rods which are fed by a signal source or feed energy that has been picked up to are cover. The energy may be transferred to and from the dipole antenna either directly straight into from the electronic instrument or it may be transferred some distance using a feeder. This leaves consider able room for a variety of different antenna formats.

Although the dipole antenna is often though in it's ha lf wave format, there are never the less many forms of the antenna that can be used.

- Half wave dipole antenna: The half wave dipole antenna is the one that is most widely used. Being half a wave length long it is a resonant antenna. A half-wave dipole antenna consist software-wavelength conductors placed end to end for a total length of approximately  $L = \lambda/2$ . The magnitude of current in a standing wave along the dipole. The current distribution is that of a standing wave, approximately sinusoidal along the length of the dipole, with an antinode (peak current) at the center [4].
- Multiple half wave's dipole antenna: It is possible to utilize dipole antenna or aerial that is an odd multiple of half wave lengths long.
- folded dipole antenna: As the name implies this form of the dipole aerial or dipole antenna is folded back on itself. While still retaining the length between the ends of half a wave conductor [5].

•Short dipole: A short dipole antenna is one where the length is much shorter than that of half a wave length. Where a dipole antenna is shorter than half a wave length, the feed impedance starts to rise and its response is less dependent upon frequency changes. Its length also becomes smaller and this has many advantages. It is found that the current profile of the antenna approximately a triangular distribution.

#### IV. SIMULATION RESULTS & TABLES

##### Radiation Pattern:

The antenna radiation pattern in same a sure of its power or radiation distribution with respect to a particular type of coordinates. We generally consider spherical coordinate in a spherically symmetrical pattern [6]. However antenna e in practice are not Omni directional but have a radiation maximum along one particular direction. Dipole antenna is a broad side antenna where in the maximum radiation occurs long the axis of the antenna. The radiation pattern of a typical dipole antenna is shown in figure2

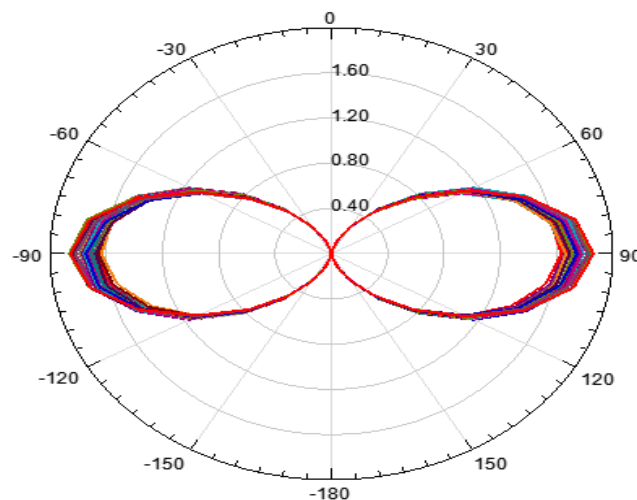


FIGURE 2: RADIATION PATTERN OF DIPOLE ANTENNA (FREQUENCY 0.3GHz)

In figure 2, it is clearly seen that average frequency is 0.3 GHz. highest level frequency is up to 0.50 GHz and lowest on is 0.01 GHz. So the frequency range for radiation pattern of Dipole antenna is (0.01-0.05) GHz. Highest gain for positive pole is 30 degree to 150 degree and for negative pole -30 degree to -150 degree.

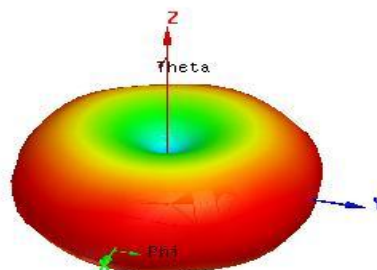


Figure 3: 3D pattern

In figure 3, Red colored side shown highest gain part of a radiation pattern. In 3D pattern both positive and negative shown in same axis. Yellow colored describe average gain pattern of Dipole antenna then the next phase is null radiation. In 3D XY, YZ, ZX three axis results are same for radiation pattern of a dipole antenna.

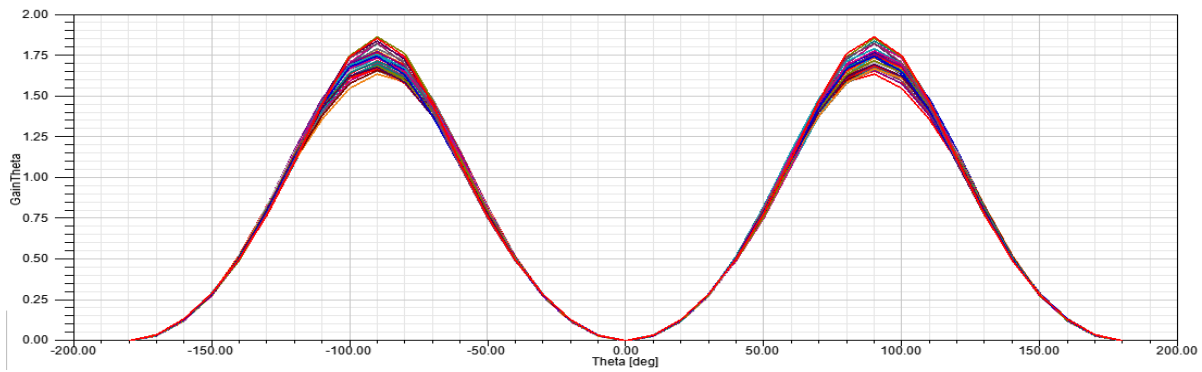


Figure 4: Gain analysis graph

Figure 4 describe graph of gain Vs Angle. Seen that obtain highest gain when the angle is -100 degree or +100 degree. In angle 0 degree gain touch the nadir point. Highest gain obtain from this is around 1.80. After obtained highest gain increasing angle gain will be decreasing.

#### IV. RESULTS & DISCUSSIONS

Data Table for Gain (-180 degree to -10 degree):

	Theta [deg]	GainTotal Setup1 : LastAdaptive Freq=0.3GHz Phi=0deg'	GainTotal Setup1 : LastAdaptive Freq=0.3GHz Phi=10deg'	GainTotal Setup1 : LastAdaptive Freq=0.3GHz Phi=20deg'	GainTotal Setup1 : LastAdaptive Freq=0.3GHz Phi=30deg'	GainTotal Setup1 : LastAdaptive Freq=0.3GHz Phi=40deg'	GainTotal Setup1 : LastAdaptive Freq=0.3GHz Phi=50deg'
1	-180.000000	0.000060	0.000060	0.000060	0.000060	0.000060	0.000060
2	-170.000000	0.035626	0.035790	0.035541	0.034960	0.034166	0.033281
3	-160.000000	0.134779	0.133941	0.131990	0.129470	0.126985	0.125025
4	-150.000000	0.288796	0.286416	0.283283	0.279688	0.276391	0.274602
5	-140.000000	0.499944	0.500072	0.502504	0.503668	0.502191	0.500235
6	-130.000000	0.767358	0.774812	0.788413	0.799573	0.804081	0.804063
7	-120.000000	1.092210	1.104690	1.116989	1.126786	1.136519	1.146247
8	-110.000000	1.448640	1.456419	1.441257	1.423697	1.430345	1.458110
9	-100.000000	1.740634	1.732001	1.677362	1.621753	1.620867	1.667864
10	-90.000000	1.853490	1.821980	1.744445	1.674943	1.675625	1.732527
11	-80.000000	1.741337	1.696103	1.628405	1.583232	1.598418	1.650505
12	-70.000000	1.450622	1.413632	1.380765	1.376000	1.405035	1.441767
13	-60.000000	1.089900	1.071716	1.070456	1.089597	1.118393	1.138739
14	-50.000000	0.760006	0.752338	0.759062	0.775703	0.792323	0.801341
15	-40.000000	0.495148	0.490455	0.491390	0.495602	0.499529	0.501714
16	-30.000000	0.285784	0.283644	0.281493	0.279421	0.277441	0.276035
17	-20.000000	0.129718	0.129254	0.127890	0.125957	0.123891	0.122165
18	-10.000000	0.033067	0.033103	0.032858	0.032412	0.031873	0.031356

This is the table for gain-180 degree to -10 degree. In starting gain is around 0 but increasing angle gain increasing this continue up to -90 degree. After -90 degree it decreases with the same ratio of increasing. This cycle run up to touch the next phase.

Data Table for Gain (10degree to 180degree):

Theta [deg]	GainTotal Setup1 : LastAdaptive Freq=0.3GHz' Phi=0deg'	GainTotal Setup1 : LastAdaptive Freq=0.3GHz' Phi=10deg'	GainTotal Setup1 : LastAdaptive Freq=0.3GHz' Phi=20deg'	GainTotal Setup1 : LastAdaptive Freq=0.3GHz' Phi=30deg'	GainTotal Setup1 : LastAdaptive Freq=0.3GHz' Phi=40deg'	GainTotal Setup1 : LastAdaptive Freq=0.3GHz' Phi=50deg'
20	10.000000	0.034091	0.033653	0.032969	0.032101	0.031138
21	20.000000	0.130450	0.129884	0.128470	0.126417	0.124169
22	30.000000	0.285126	0.285514	0.284892	0.282979	0.280589
23	40.000000	0.501976	0.503901	0.506792	0.508454	0.508985
24	50.000000	0.780361	0.782916	0.787657	0.793409	0.800731
25	60.000000	1.115131	1.115566	1.108959	1.107343	1.120273
26	70.000000	1.473772	1.465108	1.428858	1.403124	1.417168
27	80.000000	1.759985	1.734727	1.666431	1.616328	1.632675
28	90.000000	1.862702	1.823134	1.745515	1.693627	1.716465
29	100.000000	1.745917	1.705027	1.647719	1.618801	1.645693
30	110.000000	1.463267	1.435498	1.411752	1.410510	1.433510
31	120.000000	1.111075	1.101614	1.103110	1.115266	1.129079
32	130.000000	0.772962	0.773739	0.782182	0.792256	0.797495
33	140.000000	0.491395	0.491960	0.495458	0.498381	0.498734
34	150.000000	0.279198	0.277939	0.276857	0.275441	0.273710
35	160.000000	0.131147	0.130379	0.128861	0.126881	0.124718
36	170.000000	0.035947	0.035805	0.035277	0.034436	0.033388
37	180.000000	0.000060	0.000060	0.000060	0.000060	0.000060

This is the table for gain 10 degree to 180 degree it is clearly shown that Dipole Antenna gain maintain per 90 degree cycle. Start from nadir point after reach 60degree it will be in crest then its goes down to nadir point again. Consider -180 degree to +180 for simulation result.

## VI. CONCLUSION

The main aim our research paper that we have to design printed dipole for obtain highest gain. Another objective is introduction of antenna simulation software hfss. Basically hfss is used for electromagnetic analysis & calculation gain. Cut off frequency also calculated by hfss. We obtain 3db gain from dipole antenna. Obviously there are some drawbacks for dipole antenna like:

- Low bandwidth
- High Impedance
- Moving space problem
- Size

## REFERENCES

- [1] Balanis, Constantine A, John Wiley & Sons, "Modern Antenna Simulation and analysis", IEEE Research and Development, Vol23, pp. 76-84, 2014.
- [2] E. Rohde, W. Hanry, "Communications Receivers, discussion on active antennas", IEEE Antennas and Propagation, Vol 16, pp145-148, 2010. [3] James W, R. Healy., "Analysis of Dipole Antenna", International Journal of Scientific Research, Vol.2, pp-26-30, 2011.
- [4] Silver, Samuel. "Microwave Antenna Theory and Design", IEEE Communication and Network Security, Vol.4, pp. 98-99, 2014.
- [5] B. Yugi, s.Soren. "Dipole Antenna Baluns" IEEE Communication and Propagation, Vol.2, pp. 18-19, 2013.
- [6] R. Graglie, T. Sarkar., "Wireless Antennas", IEEE International symposium and Propagation, Vol.1, pp.8-10, 2013.

## Institutional and specialized Distance learning program accreditation

Mehzabul Hoque Nahid<sup>1</sup>

<sup>1</sup>(Lecturer, Management information System Department, American International University-Bangladesh)

**ABSTRACT:** *Teaching and learning are no longer confined to the classroom or the school day. There are many technologies that can offer a great deal of flexibility in when, where, and how education is distributed. The Teacher's Guide to Distance Learning is intended for K-12 educators who are interested in implementing distance learning technologies. It provides an overview of the advantages and characteristics of the various technologies now being used to reach remote learners. Distance learning provides "access to learning when the source of information and the learners are separated by time and distance, or both." Distance education courses that require a physical on-site presence for any reason (excluding taking examinations) may be referred to as hybrid or blended courses of study. Massive open online courses (MOOCs), aimed at large-scale interactive participation and open access via the web or other network technologies, are recent developments in distance education. A number of other terms are used roughly synonymously with distance education. However distance is the oldest and mostly commonly used term globally. It is also the broadest term and has the largest collection of related research articles. The main objective of this paper is develop an understanding of the characteristics and needs of distant students with little first-hand experience and limited, if any, face-to-face contact.*

**Keywords** – E-learning, Distance Learning, Human computer interactions

### I. WHAT IS DISTANCE LEARNING?

According to the definition by the United States Distance Learning Association (USDLA), distance learning is any mediated instruction that occurs at a distance – regardless of the technology involved. So although you probably imagine online degrees that involve using websites, email, and video casts, corresponding through regular mail or talking over the phone are methods that also technically qualify. Still, in practical terms, most of what constitutes distance learning today is done by using electronic means. Teaching programs utilize not only computers, but satellites, video phones, interactive graphics, response terminals, and more. It is also something that occurs in a wide variety of fields and locations, reaching well beyond K-12 and college campuses to include corporate, government, and military training, telemedicine, and anyone interested in lifelong learning. Distance learning is especially important for those who lived in rural or otherwise underserved communities, as well as individuals whose own physical and mental limitations impair their ability to attend traditional educational settings. Key players in distance education typically include students, faculty, facilitators, support staff, and administrators, each of whom have very different roles. Meeting the instructional needs of students is the main goal of every effective distance education program. Regardless of the educational context, the primary role of the student is to learn. But the success of any distance education effort depends primarily on its faculty. Special challenges confront those teaching at a distance. For example, the instructor must:

- Develop an understanding of the characteristics and needs of distant students with little first-hand experience and limited, if any, face-to-face contact.
- Adapt teaching styles taking into consideration the needs and expectations of multiple, often diverse, audiences.
- Develop a working understanding of delivery technology, while remaining focused on their teaching role.
- Function effectively as a skilled facilitator as well as content provider.

Because of these challenges, faculty often find it beneficial to rely on a site facilitator to bridge the gap between students and instructor. Where budget and logistics permit, the role of on-site facilitators has increased even in classes in which they have little, if any, content expertise. At a minimum, they set up equipment, collect assignments, proctor tests, and act as the instructor's on-site eyes and ears. In addition, most successful distance education programs hire support staff to manage student registration, materials duplication and distribution, textbook ordering, securing of copyright clearances, facilities scheduling, processing grade reports, managing technical resources, and other tasks. Finally, administrators work closely with technical and support service personnel, ensuring that technological resources are effectively deployed to further the institution's academic mission. Most importantly, they maintain an academic focus, realizing that meeting the instructional needs of distant students is their ultimate responsibility.

## II. HISTORY OF DISTANCE LEARNING SYSTEM

Though many people think about distance learning as a relatively recent phenomenon, it's actually been going on for well over a hundred years. The first such program to appear in the United States was a correspondence school created by Anna Ticknor in 1873 – the Society to Encourage Studies at Home. Her main goal was to provide a way for women to become educated, and the school lasted for 24 years by keeping a low profile and utilizing mostly volunteers to send print materials through the mail. Other universities made attempts at correspondence schools, but none really got off the ground – or received any kind of official recognition – until the Chautauqua College of Liberal Arts in New York in 1883. After that, more and more people became interested in the idea of distance learning, and professors soon started predicting that this new form of education would quickly overtake traditional models. The founding of the National University Extension Association (NUEA) in 1915 raised the profile of correspondence schools further by calling for standardized policies regulating distance learning courses, educators, and credit transfer to “real” universities. Instructional radio programs gained popularity throughout the 20s, 30s, and 40s as the federal government granted broadcasting licenses to more than 200 school boards, universities, and colleges; and they added television in the 1950s. Still, correspondence study wasn't readily accepted by most of the academic world, and many saw it as unprofessional. Established in 1969, Open University in Britain changed a lot of those attitudes. Foregoing the traditional university model, it decided to see distance education as something completely disconnected from traditional education, offering a number of its own degrees. The university focused on research and technology to further distance education, and quickly became so popular that other Open Universities began operating in countries like the U.S. and Japan.

Over the last 40 years, technological advancements and practical necessity have worked hand-in-hand to continue the evolution of distance learning. More and more, educators recognize that our busy modern lives don't allow everyone the luxury of matriculating at a traditional university or even engaging in traditional independent study programs. And perhaps most importantly, much of the research collected over decades of studies showed that students tend to learn just as well from technological methods as they do from in-person teaching.

## III. DISTANCE LEARNING PROCESS

**Video Technology:** The ability to see and hear an instructor offers opportunities for behavior modeling, demonstrations, and instruction of abstract concepts. Video techniques for distance learning are often characterized by the transmission media (videotapes, satellites, television cables, computers, and microwave). Each of the media can be described as it relates to the direction of the video and audio signals -- one-way video; two-way video; one-way audio; and two-way audio (see Figure 1).

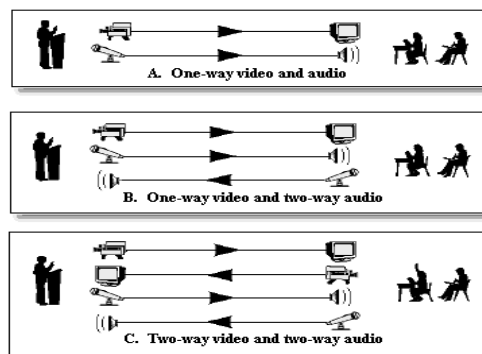


Figure 1: Three audio and video configurations.

Videotapes and DVDs offer popular, easy-to-use formats for instructional materials. Almost all students have access to a videotape or DVD player in the homes, and they are also common at school. Videotapes and DVDs have several advantages for the delivery of distance learning. In addition to easy access to the hardware, the tapes and discs are quite inexpensive. If a video camcorder is available, video is relatively easy to record (although professional staff and equipment provide in a much better product than will an amateur production team). Disadvantages of videotapes and DVDs include the fact that they are not interactive. In addition, they can be costly to send via the mail.

**Satellite Video conferencing:** Full-motion video teleconferencing offers the "next best thing to being there." "Satellite transmission is one of the oldest, most established techniques for videoconferencing. In most cases, satellite delivery offers one-way video and two-way audio. Two sets of equipment are needed for satellite systems. The uplink (a large satellite dish) transmits the video and audio signals to the satellite. The downlink (a small dish antenna) receives and displays the signals (see Figure 2).

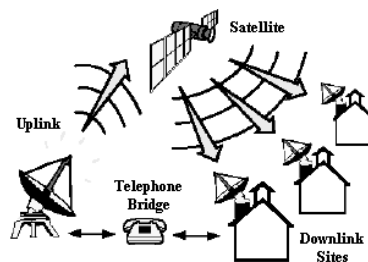


Figure 2: Configuration for satellite videoconferences.

When satellite videoconferences are used for distance learning, a studio classroom must be properly wired for the lighting, microphones, and cameras needed to produce an acceptable lesson. The cameras are usually connected to a control room, where one or more technicians control the signals. The resulting television signal is then sent to the uplink transmitter. Uplink transmitters are very expensive and are often shared with other schools or businesses. The receiving sites of satellite videoconferences (in most cases other schools) must have satellite downlinks. These dishes select, amplify, and feed the signals into the classrooms, where they can be displayed on standard television monitors. To provide two-way audio with interactions from the remote classrooms back to the teacher, a telephone bridge is usually employed. Satellite videoconferencing can be very expensive. It may not be cost-effective for most school systems to use uplinks to originate distance-education classes unless the school systems were in a position to market the classes over wide geographic areas. It is reasonable, however, for a school to use a downlink to receive commercial courses that are delivered through satellite channels.

**Microwave Television Conferencing:** Satellites are a popular method for enabling video communications over long distances. Microwave transmissions provide a cost-effective method for videoconferencing in more localized areas. Most microwave systems are designed to transmit video signals to areas that are not more than 20 miles apart (see Figure 3).

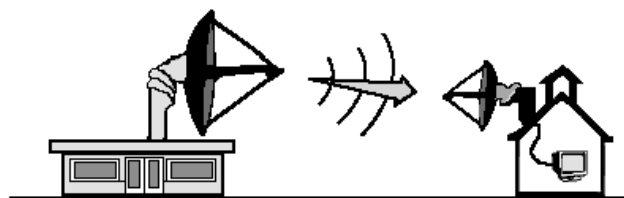


Figure 3: Configuration for microwave transmission.

The most common microwave systems use frequencies that have been designated by the Federal Communications Commission (FCC) as Instructional Television Fixed Service (ITFS) stations. When compared with satellite or commercial broadcast television, ITFS stations operate at a lower power, and the transmission equipment is relatively inexpensive. Reception equipment is also reasonably priced, as long as the receiving sites are located within 20 miles of the transmitter and there are no hills or tall buildings to block the line-of-sight signal.



**Cable and Broadcast Television:** Cable and public broadcast television have been used to distribute instruction for years. In addition to the educational networks, almost all public cable television systems allow schools to transmit television courses. This type of connection can be used to transmit one-way video and one-way audio to the community at large or between specific schools. For example, if two area high schools do not each have enough students to justify an advanced math course, they might team up to teach a single course delivered through cable television. In one school, the teacher would conduct a regular class; in the other school, the students would watch and listen through a standard cable television channel. Distance learning through cable television systems requires both a studio and channels through which to broadcast. The cost depends largely on the "partnership" offered by the cable or broadcast system. Even though the broadcast will take place at a scheduled time, research shows that the majority of the students will record the program and play it back at a convenient time.

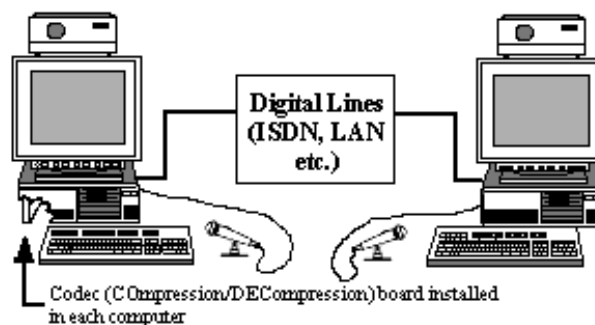


Figure 4: Broadcast from Television

#### IV. CONNECTIVITY ISSUE

Even with increased options for connectivity, the transmission speed is still an issue. The problem is that digital files are huge, and they require channels or cables with tremendous capacity to transmit quickly and effectively. The transmission capacity of a cable or a technology is referred to as the bandwidth. The greater the bandwidth, the greater the amount of digital information that can be transmitted per second. There are several options available that teachers and students can use to access the Internet, including telephone, DSL, cable, fiber, satellite, and wireless delivery. Note that although the table lists the maximum download speeds, these speeds will seldom be realized, due to hardware limitations, latency, simultaneous users, and many other reasons. In addition, the upload speeds are often considerably less than the download speeds.

**Cable Modems:** In most areas, cable companies are offering Internet access through the same cable that delivers television signals to our homes (see Figure 5). If your area has been configured for this service, you can connect a cable line to a network card on your computer. The main advantage of cable modems is the bandwidth. Cable modems can bring data to your computer between 10 and 30 Mbps. If you have a 10 Mbps network card in a computer, you may be able to receive information up to that speed. A disadvantage of cable modems is that the transfer rate may be slowed if too many people in your neighborhood all connect to the Internet at the same time.

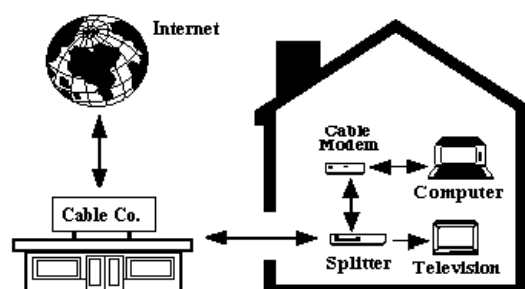


Figure 5: Cable modem in a home

**Satellite Delivery:**

It is also possible to receive information from the Internet via satellite. Satellite access is relatively fast, does not require the installation of telephone or data lines, and is not adversely affected by the number of simultaneous users. Satellite delivery, however, is usually one-way; you cannot send information back up to the satellite. In most cases, a telephone line is used to send information back to the Internet or service provider, and the satellite is used to receive information (see Figure 6). This configuration works well in most cases, because the information you send back is generally very small; whereas, the information you receive can be quite large.

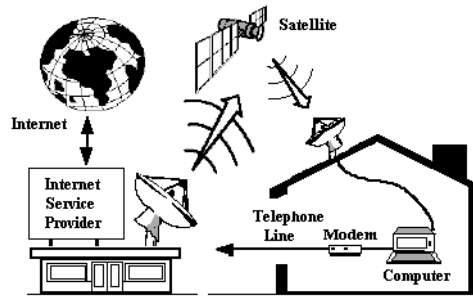


Figure 6: Connecting to the Internet via satellite.

## V. BENEFITS OF DISTANCE LEARNING

**Convenience**

Distance learning technologies can provide convenient locations for both students and instructors. Many of the technologies, such as the Internet and telephone, are easily accessed at home. Others, such as videoconferencing, can be distributed from a single point to multiple remote sites. Satellite transmissions can be viewed at specified sites, or the transmissions can be recorded for later viewing at home or school.

**Flexibility**

Many forms of distance learning provide students the option to participate whenever they wish, on an individualized basis. For example, some students may want to review a podcast in the middle of the night or read their e-mail during early morning hours. In addition, one student may wish to spend 30 minutes reviewing a website, while another spends an hour.

**Effectiveness**

Not only is distance learning convenient, it is also effective. Several research studies have found that distance learning is equally or more effective than traditional instruction when the method and technologies used are appropriate to the instructional tasks, when there is student-to-student interaction and when there is timely teacher-to-student feedback.

**Affordability**

Many forms of distance learning involve little or no cost. For example, almost all of the homes in the United States have televisions and many are connected to a cable-TV service. For these homes, it is relatively easy for the students to watch a public broadcast television show or educational documentary. In addition, almost all homes have access to a telephone and/or the Internet, enabling the use of voicemail and audio conferencing.

**Multi-sensory**

One of the benefits of distance learning is that there is a wide variety of materials that can meet everyone's learning preference -- at least part of the time. For example, some students learn from visual stimuli, such as video, and others learn best by listening or interacting with a computer program. If distance learning courses are well designed, they will likely offer learners a wide range of choices, thereby providing the optimal combinations of interaction and media.

**Equity**

Educational inequity is a major issue in this and other countries. Rural schools often have less contact with educational trends, fewer qualified teachers, and more need for technology. Distance learning offers great potential for alleviating these issues and has been employed very effectively in Canada and Australia -- two countries with geographically diverse student populations.

## VI. CONCLUSION

A well-structured distance learning course must place instructional objectives foremost. The technology should be as invisible as possible just another tool that teachers can use to effectively convey the content and interact with students. After the goals and objectives are outlined, the instructional materials can be designed and developed. It is important not to underestimate the commitment required for this step -- creating effective materials for distance learning is an extremely time-consuming and energy-consuming process. Regardless of whether the technology is audiotape or satellite video, ample time must be allocated to ensure that the materials are accurate, appropriate, and structured to maximize the benefits for distant students and to minimize the limitations. Many of the techniques and skills used in a classroom teaching situation do not translate directly into a distance education approach. Teacher training programs are important to acquaint the teachers with the use of technology as well as to help with the re-design of the instructional strategies. In particular, most teachers need assistance and practice with:

- Effective strategies for implementing small group activities and individual practice
- Techniques for maximizing teacher/student and student/student interactions
- Successful approaches for integrating technology into the teaching/learning process
- Tactics for motivating students at a distance

Facilitators and support personnel are also crucial to successful distance learning experiences. If students are located at remote sites, facilitators will likely be the on-the-spot contacts for the students. It is important that they are fully integrated into the course and communicate frequently with the instructor.

## VII. Acknowledgements

The author gratefully acknowledges his wife Adrita Sania Zaman for her assistance in drawing the figures with the help of Auto CAD application software in this paper.

## REFERENCES

- [1] Means, B., Toyama, Y., Murphy, R., Bakia, M., & Jones, K. (2009). *Evaluation of Evidence-Based Practices in Online Learning: A Meta-Analysis and Review of Online Learning Studies*. Available from the U.S. Department of Education.
- [2] Moore, M. G. & Thompson, M.M. (1990). *The effects of distance learning: A summary of the literature*. Research Monograph No. 2. University Park, the Pennsylvania State University, American Center for the Study of Distance Education (ED 330 321).
- [3] Parker, A. (1997). A Distance Education How-To Manual: Recommendations from the Field. *Educational Technology Review*, 8, 7-10. Picciano, A. G. & Seaman, J. (2009). *K-12 online learning: A 2008 follow-up of the survey of U.S. school district administrators*. Boston: Sloan Consortium.
- [4] Planty, M., Hussar, W., Snyder, T., Kena, G., KewalRamani, A., Kemp, J., Bianco, K., & Dinkes, R. (2009). *The Condition of Education 2009 (NCES 2009-081)*. National Center for Education Statistics, Institute of Education Sciences, U.S. Department of Education. Washington, DC.
- [5] Willis, B. (1995, October). *Distance Education at a Glance*. University of Idaho Engineering Outreach. Verduin, J. R. & Clark, T. A. (1991). *Distance education: The foundations of effective practice*. San Francisco, CA: Jossey-Bass Publishers.
- [6] Zandberg, I. & Lewis, L. (2008). *Technology-based distance education courses for public elementary and secondary school students: 2002-03 and 2004-05. (NCES 2008-08)*. Washington, D.C.: National Center for Educational Statistics.

## Effects, Evaluation and Corrosion of Heat Exchangers Performance in Seawater

Robert Poku<sup>1</sup>, Bebetaidoh O. Lucky<sup>1</sup>, Ezenwa A. Ogbonnaya<sup>1</sup>

<sup>1</sup>Department of Mechanical/Marine Engineering, Niger Delta University, Wilberforce Island, Bayelsa State, Nigeria

**ABSTRACT :** The durability of both aluminum and mild steel depends to a large extent on several factors prevailing in the operating environment. Among these factors are temperature and salinity. This paper therefore, investigates the impacts of temperatures and salt solutions on the corrosion rates of both aluminum and mild steel. The results obtained showed a significant effect of salt water and temperature as factors affecting the rate of corrosion. The results obtained as corrosion rates for aluminium at 35°C ranges from 0.1862mmph - 0.2065 mmph and when the temperature rises to 65°C, the range becomes 1.0567mmph – 1.994mmph. Mild steel tested at 35°C gives corrosion rates from 0.2145mmph – 0.5349 mmph while at 65°C it ranged from 0.386mmph - 1.1771mmph. The results also proved that corrosion rates of these metal rise with decrease in salt (salinity) content as 0.05M NaCl concentration of the solution results to 0.1862mmph for aluminum and 0.2145mmph for mild steel at 35°C and when the concentration of NaCl increases to 0.10M, the corrosion rates turned out to be 0.2065mmph for aluminum and 0.5349mmph for mild steel at same temperature. These results showed that temperature and salt content are two very significant properties needed to be paid attention to if corrosion is to be controlled.

**Key Words:** Heat Exchanger, Corrosion Rate, Seawater, Weight Loss.

### I. INTRODUCTION

Corrosion is a natural phenomenon, which can be considered either chemical or electrochemical in nature. It is defined as the deterioration or decay of metals by direct chemical attack or by reaction with its environment. [1] which may be referred to as rusting when iron is affected and tarnishing in the case of silver. Corrosion usually occurs when the environment's temperature goes above 0°C and the humidity is at 80% on a damp surface. The danger in corrosion is that it degrades the metallic properties of the affected metals [2]. Three essential elements necessary for corrosion to occur are: water, contaminants (e.g. salts) and oxygen [3]. Corrosion of metals is costly and is a major aspect of material science as well as industrial problems that have attracted much investigations and researches [4]. Besides, the consequences of corrosion could also constitute safety, economic and technological problems.

Corrosion can be due to either atmospheric or immersion [3]. However, since heat exchangers are generally pressure vessels that convey fluids under high pressure and temperature, they are vulnerable to corrosion and scale formation. Acid pickling is a descaling process used for removing undesired scale, rust or other corrosion products from the surface of equipment such as boilers, heat exchangers [5]. The acid pickling processes which involve the application of acidic bath may impart severe damages to the metallic substrate [2][6] and as a consequence, the metals become prone to corrosion.

Extensive works have been carried out in ensuring that the rate at which corrosion affects industrial materials are controlled. [7] studied the effect of thiourea and its derivatives as corrosion inhibitors in acid media as well as the influence of temperature, hydrochloric acid and inhibitor concentration on MS. The study showed that thiourea is an excellent anodic inhibitor for MS in hydrochloric acid medium. The result also demonstrated that temperature and acid concentration increase the rate of corrosion. An investigative research carried out by [8] used weight loss technique on the corrosion effect of orange fruit juice on carbon steel. Coupons with known weights were immersed in the test tubes containing natural juice, orange juice as media with preservative and water for a total exposure time of 10 days. From [9], the factors that influence the rate of corrosion in a shell and tube heat exchangers are: 1) the pH of the fluid; 2) the amount of oxygen in the fluid; 3) the chemical make-up of the fluid; 4) the temperature of the fluid; 5) the velocity/pressure of the fluid in the pipe and 6) humidity.

The methods of corrosion, control measure depend on the type of corrosion and the factors affecting the particular corrosion [10, 11, 12, 13 and 14]. Therefore, having known the various types of corrosion and there effects, this paper is aimed at investigating seawater on heat exchangers constructed with Al or MS material and are subjected to working temperatures of 35°C to 65°C.

## II. EXPERIMENTATION METHOD/TECHNIQUES

The method employed in this work to determine the effect of corrosion damages on metals is the weight loss method. The specimen also called coupon was weighed before it was exposed to the solvent. After exposing for a stipulated time, corrosion products on the metal were properly cleaned off and reweighed. The weight difference before and after exposure was the weight loss. From the weight loss the corrosion rate of the given specimen was calculated. The laboratory experimental procedure is outlined as follows:

### a. Apparatus Used

The apparatus used were venier caliper, weighing machine, beaker, iron brush, file, sand paper or emery cloth, supporting iron rod and string. Metals specimens used for the test were aluminum and MS. While the solvent was Sodium chloride (NaCl) solution. Table 1 shows the shapes, sizes and areas of the specimen used for the experimentation.

**TABLE 1: Shape, size and area of each specimen used.**

Specimen	Shape	Size (mm)			Area (mm <sup>2</sup> )
		Diameter	Width	Length	
Aluminium	Cylindrical	0.60	-	68	128.74
Mild steel	Cylindrical	3.00	-	68	655.02
Aluminium	Rectangular	-	1.60	68	108.80
Mild steel	Rectangular	-	3.80	68	258.40
Aluminium	Square	-	32	32	1024
Mild steel	Square	-	32	32	1024

### b. Method of exposing specimens to solvents:

The specimens were exposed to the solvents in such a way as to reveal a large surface area of the specimen to the corrodents. Each coupon was suspended in a known volume (250ml) of corrosion media through a supporting rod and a thread. This was with a view to ensure uniform contact of the specimen with the medium as shown in fig. 2.

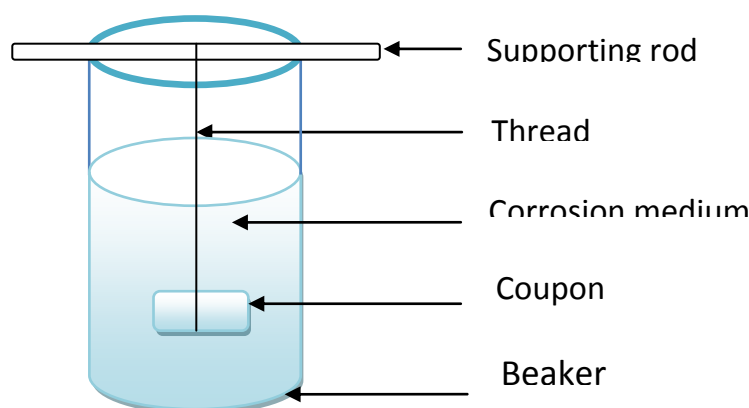


**Fig. 2: Beaker Used as Corrosion Medium**

Each Specimen was exposed first to the solvent at a concentration of 0.05M in a period of seven (7) days at temperature interval of 5°C with initial and final temperatures of 35°C and 65°C respectively. At the end of the seven days, the solvent concentration was increased to 0.10M and the same exposure method was repeated.

### 2.3 Preparation of Specimens for Reweighing:

This is another very important step in the laboratory procedures to determine the corrosion rate by weighing method. After exposing each metal for seven days (168 hours) at a particular temperature condition, the metal was brought out of the test solution.

### 2.4 Cleaning of corrosion products:

This method included scrubbing, scrapping and brushing. Surfaces of the metals were scrubbed with a very smooth emery cloth and brittle brush to remove the corrosion product.

### 2.5 Estimation of corrosion rates:

The test results can be referred to a unit of metal surface ( $\text{mm}^2$  or  $\text{cm}^2$ ) and sometimes (hour, day, year etc). Thus, corrosion rates are expressed in  $\text{g/cm}^2\cdot\text{hr}$  or  $\text{mg/mm}^2\cdot\text{day}$ . The corrosion resistance of a metal and the data obtained from the weight losses are converted into an index, which indicates the reduction in metal thickness. Such unit of corrosion resistance measurement is millimeter penetration per year (mmpy).

The corrosion rate expression using these units is given as follows:

$$\text{Corrosion Rate (CR)} = \frac{\text{Weight Loss}(W) \times K}{(D) \frac{\text{mg}}{\text{mm}^3} \times (A)\text{mm}^2 \times T} \quad 1$$

Where

$K$  = Rate constant (87.6)

$W$  = weight loss in gram

$D$  = density of metal in  $\text{mg/mm}^3$

$A$  = Surface Area of metal in ( $\text{mm}^2$ )

$T$  = Exposure time in hours

$$\text{Corrosion rate (mmph)} = \frac{87.6 \times W}{D \times A \times T} \quad 2$$

### 2.6 Exposure time

Metal specimens were tested in inorganic solvent for a period of seven days (168 hours or 0.0192 year). Thus, in this work 0.0192 year is substituted for Time (T) in the rate expression.

### 2.7 Density of Specimen

Since cylindrical materials of known lengths and weight were used the densities were easily calculated. The densities of the various specimen used are calculated and tabulated using the formula.

$$\text{Volume} = \pi r^2 L$$

Where,

$L$  = known length of specimen in cm.

(Taking  $\pi = \frac{22}{7}$ )

$$\text{Density} = \frac{\text{Mass}(m_g)}{\text{Volume}(\text{mm}^3)} \quad 3$$

$D$ : Aluminium (Al) =  $2.71\text{mg/mm}^3$

$D$ : Mild Steel (MS) =  $7.85\text{mg/mm}^3$

### 2.8 Area of Specimen

While the surface area of each coupon was calculated using:

$$\text{Surface Area } A = 2[(L \times B) + (B \times T) + (L \times T)] \quad 4 [8]$$

Where,

L = Length of the coupon

B = Width of the coupon.

T = Thickness of the coupon.

D = Diameter of hole in coupon

### III. RESULTS AND DISCUSSION

The original weights and the losses in weights as well as the corrosion rates data for aluminum and mild steel in sodium chloride solutions at different temperatures and concentrations are presented in tables 2 and 3 respectively as shown. Tables 2 and 3 clearly shows that the rates of corrosion rise with increase in temperature. A thorough examination and comparison of both tables also confirmed the fact that salt content (salinity) enhances the rate of corrosion as the higher corrosion rate for both specimen were recorded with 0.10M NaCl solution. A graphical demonstration of temperatures with the corrosion rates is as shown in fig. 3 illustrating the rise in temperatures with the corrosion rates for both specimen.

TABLE 2: Corrosion Rates Data for Specimen in 0.05 NaCl Solution

Weeks	T (°C)	Original Weight (mg)		Weight Loss (mg)		Al (Cylindrical) (mmpb)	MS (Cylindrical) (mmpb)	Al (Rectangular) (mmpb)	MS (Rectangular) (mmpb)	Al (Square) (mmpb)	MS (Square) (mmpb)
		Al	MS	Al	MS						
Day 1	35	78.37	156.3760	0.092	1.562	0.00066	9.836E-06	1.25E-08	1.337E-05	2.53E-10	0.00064
2	40	78.37	156.3760	0.172	1.812	0.0010797	1.141E-05	2.05E-08	8.299E-06	3.57E-10	0.000243
3	45	78.37	156.3760	0.244	2.022	0.0013614	1.273E-05	2.59E-08	6.528E-06	4.04E-10	0.000151
4	50	78.37	156.3760	0.332	2.202	0.0016572	1.387E-05	3.15E-08	5.256E-06	4.51E-10	0.0001
5	55	78.37	156.3760	0.398	2.402	0.0018169	1.513E-05	3.45E-08	4.754E-06	4.54E-10	8.26E-05
6	60	78.37	156.3760	0.489	2.652	0.0020463	1.67E-05	3.89E-08	4.272E-06	4.63E-10	6.59E-05
7	65	78.37	156.3760	0.522	2.812	0.0020164	1.771E-05	3.83E-08	4.243E-06	4.3E-10	6.64E-05
Second 1	35	78.37	156.3760	0.612	3.042	0.0043904	1.916E-05	8.34E-08	3.915E-06	8.66E-10	2.82E-05
2	40	78.37	156.3760	0.649	3.252	0.0040739	2.048E-05	7.74E-08	3.947E-06	7.51E-10	3.06E-05
3	45	78.37	156.3760	0.683	3.422	0.0038109	2.155E-05	7.24E-08	3.947E-06	6.68E-10	3.27E-05
4	50	78.37	156.3760	0.708	3.622	0.0035554	2.281E-05	6.75E-08	4.03E-06	5.89E-10	3.58E-05
5	55	78.37	156.3760	0.727	3.792	0.0033189	2.388E-05	6.31E-08	4.109E-06	5.25E-10	3.91E-05
6	60	78.37	156.3760	0.752	4.012	0.0031386	2.526E-05	5.96E-08	4.214E-06	4.69E-10	4.24E-05
7	65	78.37	156.3760	0.922	4.192	0.0035615	2.64E-05	6.77E-08	3.581E-06	5.1E-10	3.17E-05

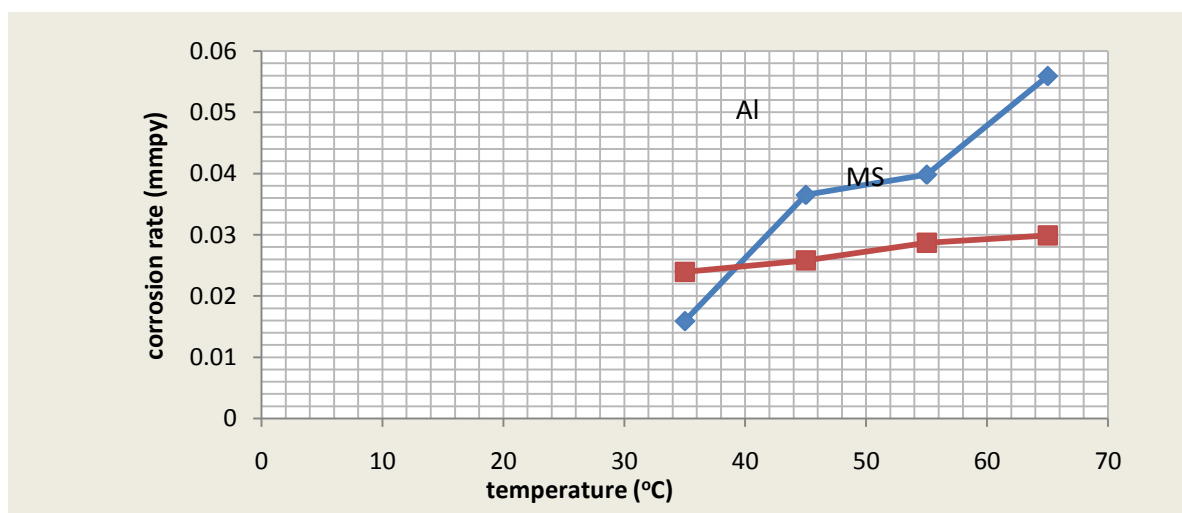
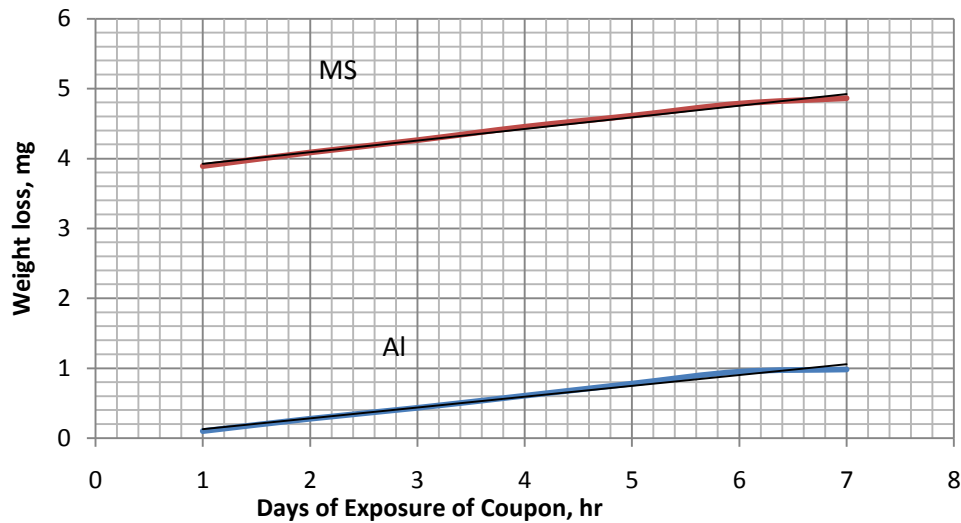


Fig. 3: Graphical illustration of Corrosion Rate Against Temperature Variations for Al and MS.

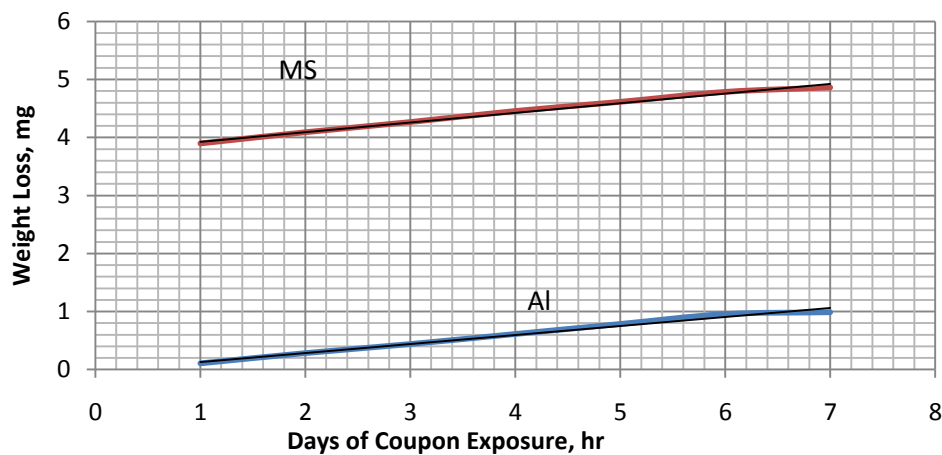


Fig. 3 showed the effect of temperature variations on corrosion rates for both aluminium and mild steel. The graph proved that as temperature changes from 35°C to 65°C, the corrosion rates of the metals increase as demonstrated in the case of both Al and MS that rose in from low to high. This affirms that corrosion rate is lower at room temperature than boiling temperature [15].



**Fig. 4: Effect of time on the weight loss of MS and Al for the first seven days of exposure to 0.05 NaCl Solution**

The effect of immersion time and the weight loss of both specimen in sea water was studied. From the gradual increases in loss in weight from 0.092mg to 0.522mg and 1.562mg to 2.812mg for Al and MS respectively, as clearly illustrated in fig 4, where it was shown that as the coupon was kept for a longer periods in the 0.05M NaCl solution, the extent of corrosion of the metals becomes deeper.



**Fig. 5: Effect of time on the weight loss of MS and Al for the second seven days of exposure to 0.05 NaCl Solution**

Fig. 5 is a repeat of the exposure time versus the weight loss method. However, this was done for another seven days at the end of the first seven days in which the first experiment was carried out. This, once again, confirms the interdependence of exposure time and weight loss. It was demonstrated to further affirm the effect of the exposure time on both specimen in 0.05M NaCl solution.

TABLE: Corrosion Rates Data for Specimen in 0.10 NaCl Solution

Weeks	Temp . (°C)	Original Weight (mg)		Weight Loss (mg)		Al (mmph )	MS (mmph )	Al (mmph )	MS (mmph )	Al (mmph )	MS (mmph )
		Al	MS	Al	MS						
Days 1	35	783 7	15637.60	0.1	3.894	0.00073	2.5E-05	1.4E-08	3E-05	1.1E-10	0.0013
2	40	783 7	15637.60	0.2 8	4.088	0.00175	2.6E-05	3.3E-08	1.2E-05	2.6E-10	0.00021
3	45	783 7	15637.60	0.4 4	4.264	0.00243	2.7E-05	4.6E-08	7.7E-06	3.4E-10	0.0001
4	50	783 7	15637.60	0.6 1	4.455	0.00306	2.8E-05	5.8E-08	5.8E-06	4.1E-10	5.9E-05
5	55	783 7	15637.60	0.7 8	4.613	0.00357	2.9E-05	6.8E-08	4.6E-06	4.6E-10	4.1E-05
6	60	783 7	15637.60	0.9 5	4.785	0.00399	3E-05	7.6E-08	4E-06	5E-10	3.1E-05
7	65	783 7	15637.60	0.9 9	4.862	0.0038	3.1E-05	7.2E-08	3.9E-06	4.7E-10	3.2E-05
Second 1	35	783 7	15637.60	1.1 6	4.97	0.00832	3.1E-05	1.6E-07	3.4E-06	1E-09	1.3E-05
2	40	783 7	15637.60	1.3 4	5.161	0.00838	3.2E-05	1.6E-07	3E-06	9.7E-10	1.1E-05
3	45	783 7	15637.60	1.4 8	5.298	0.00828	3.3E-05	1.6E-07	2.8E-06	9.4E-10	1.1E-05
4	50	783 7	15637.60	1.6 3	5.452	0.00818	3.4E-05	1.6E-07	2.6E-06	9E-10	1E-05
5	55	783 7	15637.60	1.7 8	5.634	0.00811	3.5E-05	1.5E-07	2.5E-06	8.6E-10	9.7E-06
6	60	783 7	15637.60	1.9 4	5.824	0.0081	3.7E-05	1.5E-07	2.4E-06	8.3E-10	9.2E-06
7	65	783 7	15637.60	2.0 6	5.95	0.00797	3.7E-05	1.5E-07	2.3E-06	8E-10	9E-06

The exposure time and weight loss procedure was again studied while the NaCl solution was increased to 0.10M. And as seen in fig. 6, the weight loss increases from 0.10mg and 3.894mg to 0.99mg and 4.862mg respectively for both Al and MS. This showed that Al as a common component ship superstructures and liquid cargo containers and heat exchangers are susceptible to corrosion due to their continual exposure to sea environment [16].

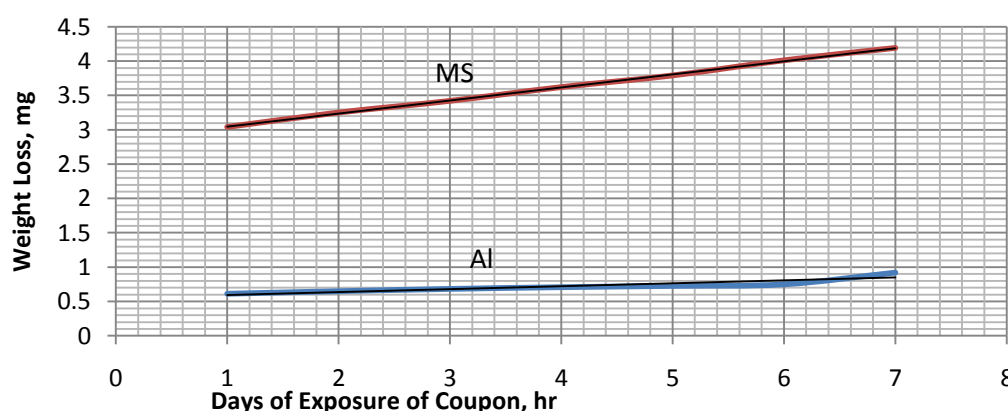


Fig. 6: Effect of time on the weight loss of MS and Al for the second seven days of exposure to 0.10 NaCl Solution.

Fig.7 is a demonstration of same procedure as in fig. 6, the difference being that the test specimen in the 0.10M NaCl solution was being observed for another seven days outside the seven days in which the initial procedure was subjected to. The results of this second experimentation as illustrated in fig. 7 shows that the weight loss against the exposure time clearly follows the pattern of fig. 6, 1.16mg and 4.97mg to 2.06mg and 5.95mg.

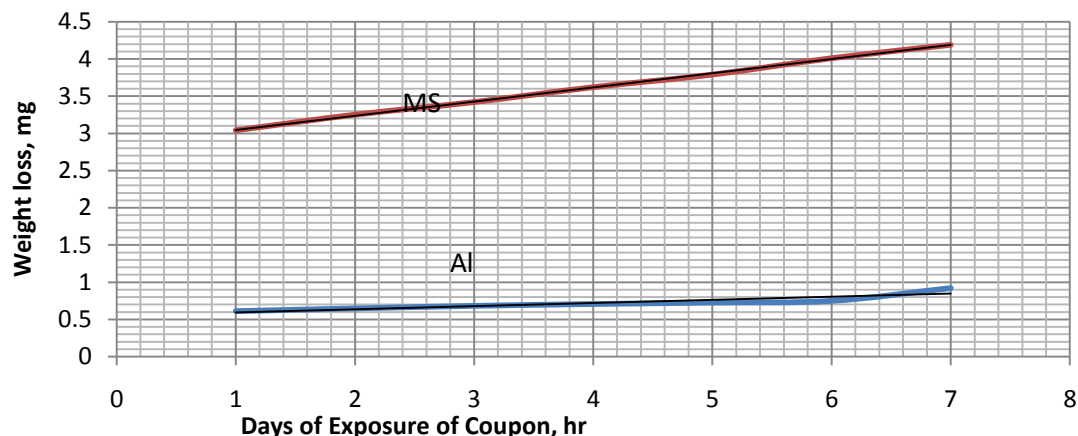


Fig. 7: Effect of time on the weight loss of MS and Al for the first seven days of exposure to 0.10 NaCl Solution.

The corrosion rate data obtained from the experimental work gave general information on the behavior of aluminium and MS in corrosive environment. For example, both the aluminium and MS tested showed a general high corrosion rate at increased temperatures with change in the salt content of the solution.

#### IV. CONCLUSION

In view of the usefulness and importance of both aluminum and MS and also the environmental conditions of the areas in which these very important metals will have useful applications, a study was carried out to determine the impacts of temperatures and salinity on the corrosion rates of these metals. The study affirmed that higher temperature and salt solution could result to corrosion rates of 1.1994mmph and 1.1771mmph for aluminium and MS respectively.

- For aluminium at 35°C, the corrosion rate ranged from 0.1862 - 0.2065 mmph while at 65°C, it ranged from 1.0567 – 1.994mmph
- MS tested at 35°C gave corrosion rates from 0.2145mmph – 0.5349mmph while at 65°C it ranged from 0.3862mmph – 1.1771mmph.

#### V. RECOMMENDATIONS

Based on the results obtained in this research work, the recommendations are as follows:

- 1) The coating system should be correctly used in conjunction with the anti-corrosion resins.
- 2) Consideration should be given to material selection for long time corrosion control.
- 3) All metals for marine application should be given a proper attention with proper periodic monitoring and cleaning.

**Acknowledgement :** The authors wish to heartily acknowledge Mr Calaba for his relentless effort in the running of the experiments. The enthusiasm displayed in collecting, verifying and authenticating the data is equally appreciated.

#### REFERENCES

- [1] Trethway, K.R. and Chamberlain J. (2000) Corrosion for Science and Engineering 2<sup>nd</sup> Edition, Houston Texas.
- [2] Rajendran, A. and Karthikeyan, C. (2012). The Inhibitive Effect of Extract of Flowers of Cassia Auriculata in 2 M HCl on the Corrosion of Aluminium and Mild Steel. *International Journal of Plant Research* 2012, 2(1): 9-14
- [3] Anderson, A. (2014). Protection of Ships. Retrieved 20 July, 2014 from the World Wide Web: [http://www.ncl.ac.uk/marine/assets/docs/NclUni\\_Lect1\\_1103.pdf](http://www.ncl.ac.uk/marine/assets/docs/NclUni_Lect1_1103.pdf)
- [4] Quartarone, G., Ronchin, L., Vavasori, A., Tortato, C. and Bonaldo, L. (2012). Inhibitive Action of Gramine Towards Corrosion of Mild Steel in Deaerated 1.0M Hydrochloric Acid Solutions. Retrieved 12 March, 2015 from the World Wide Web: <http://arca.unive.it/bitstream/10278/35426/1/ARTICOLO%20PUBBLICATO.pdf>
- [5] Bozorg, M., Shahrabi, T. F. Mohammadi, G. Z. Neshati, J. Chaghazardia, Z. Gholamzade, P. and Ektefa, F. (2014). Inhibitive Assessment of N-(8-Bromo-3H-Phenoxazin-3-Ylidene)-N, N'-Dimethylaminium, as A Novel Corrosion Inhibitor for Mild Steel In 1.0 M Hcl. *Journal of Advanced Materials and Processing*, Vol.2, No. 3, 27-38
- [6] The European Stainless Development Association. Retrieved 14 March, 2015 from the World Wide Web: [http://www.euro-inox.org/pdf/map/Passivating\\_Pickling\\_EN.pdf](http://www.euro-inox.org/pdf/map/Passivating_Pickling_EN.pdf)
- [7] Shetty, S. D., Shetty, P. and Nayak, H. V. S. (2005). Inhibition of Corrosion of Mild Steel in Hydrochloric Acid by N-cyclohexyl-N-phenyl Thiourea. *Indian Journal of Chemical Technology*. Vol. 12, pp: 462-465

- [8] Badmos, A. Y. and Ajimotokan, A. A. (2009). *The Corrosion of Mild Steel in Orange Juice Environment*. A technical report submitted to Department of Mechanical Engineering, University of Illorin, Nigeria.
- [9] Anyanwu1, I. S. and Agberegha, L. O. (2015). Characteristics Behaviour of Carbon Steel Exposed to Na<sub>2</sub>CO<sub>3</sub> and NaCl Solutions of Different Concentrations. *IOSR Journal of Engineering*. Vol. 5, Issues 02, pp: 42-52.
- [10] Tunbull, A. (2004). *Corrosion Chemistry in Pits, Crevices and Cracks*. HMSO London
- [11] Rashidi, N., Alavi-Soltani, S. and Asmatulu, R. (2007). *Crevice Corrosion Theory, Mechanisms and Prevention Methods*. Retrieved 25 March, 2015 from The World Wide Web: <http://soar.wichita.edu/bitstream/handle/10057/917/grasp%20216.pdf>.
- [12] Arikan, M. E. and Doruk, M. (2008). Determination of Susceptibility to Intergranular Corrosion of UNS 31803 Type Duplex Stainless Steel by Electrochemical Reactivation Method, Retrieved 28 March, 2015 from the World Wide Web: <http://journals.tubitak.gov.tr/engineering/issues/muh-08-32-6/muh-32-6-2-0807-5.pdf>.
- [13] Evans, U. R. (2011). *The Corrosion and Oxidation of Metals*. Arnold, London.
- [14] Corrosion Forms. Retrieved 29 March, 2015 from the World Wide Web: [http://www.uobabylon.edu.iq/eprints/paper\\_12\\_1893\\_228.pdf](http://www.uobabylon.edu.iq/eprints/paper_12_1893_228.pdf)
- [15] Al Zubaidy, E. H., Mohammed, F. S. and Bassioni, G. (2011). Effect of pH, Salinity and Temperature on Aluminum Cookware Leaching During Food Preparation. *International Journal of Electrochemical Science*. Vol. 6, pp: 6424 – 6441.
- [16] Wan Nik, W. B., Sulaiman, O., Fadhli, and Rosliza A. R. (2010). Corrosion Behaviour of Aluminum Alloy in Seawater. In *Proceedings of MARTEC 2010 The International Conference on Marine Technology*: Vol. 3 (pp: 175-180). BUET, Dhaka, Bangladesh.

## Design and Development of Sound Control Door Lock System

Elechi Promise

Department of Electrical Engineering, Rivers State University of Science and Technology, Port Harcourt, Nigeria.

**ABSTRACT:** Security is very important, especially the security of lives and properties. This work involves the use of sound in controlling the opening and closing of doors using electromechanical application. In this work, sound is used to activate the mechanisms which opens and closes the door without any external effort. The system is made up of two main features, the Security Access system and Control Mechanism. The security access system was designed using circuit wizard software and then constructed on a veroboard and other materials while the control mechanism was constructed using a simple DC motor for the opening and closing of the door. In its operation, a specific sound pattern in form of a positive voltage is sent to pin 14 of IC<sub>1</sub>, pin 14 of IC<sub>1</sub> is connected to a transistor(Q<sub>2</sub>) which causes the 555timer to oscillate sending pulses to pin 14 of IC<sub>2</sub>, during this, the output of IC<sub>2</sub> then operates in a sequential mode. The code switch then sets the number of beat that will set IC<sub>3</sub> into the desire sequential output set by the operator. The output signal energizes the relay which controls the DC motor to open the door and closes after a preset time. The testing showed quick and fast response in operation of the door lock system.

**KEYWORDS:** Sound, 555 Timer, Control, Door, Signal, Security

### I. INTRODUCTION

#### 1.1 Background of Study

Sound control doors are doors that employ the use of sound in opening and closing, this work is unique in every aspect of operation in terms of accessibility and control. It may be confused with sound control switch. A sound control switch is an electronic switch that employs the use of sound to ON and OFF a device. This work differs from sound switch even though sound is used to activate their mechanisms and operation. In this work, the system comprises of two systems; Security Access system and Control Mechanism. The security access system is the system that grants the user or operator an access into any system while the control mechanism controls the operation of the security device. The increasing rate of crime, attacks by thieves, intruders and vandals despite all forms of security gadgets and locks still need the attention of researchers in finding a permanent solution for the well-being of lives and properties of individuals [Adamu, 2009]. This work will employ the use of sound pattern of knock to grant access to only those who input the correct sound pattern (knock) on the door. It was designed to eliminate the problem of unwanted noise. One major problem of the sound control devices is environmental noise which triggers the devices. In this work, an obstacle sensor (infrared) was introduced into the device to avoid false triggering. Hence, the sound control system will only respond to whoever blocks the obstacle sensor to input the correct sound pattern set by the user or operator.

The control mechanism involves the use of a DC motor and gear system in opening and closing the door. Immediately the sound has been encoded by the user, the sound control system decodes it and sends a signal to the control mechanism which opens and closes the door depending on the signal sent by the sound control system. The major function of the DC motor is to provide the required turning torque when activated while the gear system is to increase or reduce the speed of the DC motor used.

The sound control door system was designed to serve well in different security applications, providing inexpensive inputting keys (sound) free from false triggering.

The design stages consist of the power supply unit, input sensor, sound decoding and oscillator. It also consists of special network components (infrared) to prevent false triggering and ensure desired performance objectives. A decade counter IC is used instead of flip-flop, special transistor and edge triggering network for low audio frequency.

The primary purpose of the switch is to provide means of connecting two or more terminals in order to permit the flow of current across them, to allow for an interaction between electrical components, and to isolate circuits so as to terminate communication flow when needed. The motivating force behind this design is based on the

desire to alleviate the problem faced by the aged, physically and insecurity challenges. It also takes into considerations the illiterates that may have problems operating some “complex” Hand-Held Sound Control Switch (VOX).

The device is activated by clapping or knocking twice within a set time period that is determined by an oscillator and sequential output of 4017 counter depending on the encoded preset signal.

### 1.2 Aim and Objective

The aim of this work is to design and develop a sound control door lock system, specifically this work will: Determine the signal needed to activate the door lock system and the mechanical system in opening and closing of door system.

### 1.3 Scope of Study

The scope of this work is to design a device which can be switched ON and OFF using voice signals. Specifically:

- i. The switching interface applied in this work is the general purpose type as it is not restricted to only one type of load.
- ii. The type of control this work employs is the simple ON/OFF control switch.

### 1.4 Limitations

This work was carried out within the design consideration; as a result of this very few limitations were observed. They are:

- It can only be used in a light weight door (<25kg).
- It can only be applied to swing doors.
- The degree of opening angle is ( $0 \leq \alpha \leq 95^\circ$ ).

### 1.5 Review of Related Work

Ogri, et al, 1996, designed a prototype security door that can be remotely controlled by a GSM phone acting as the transmitter and another GSM phone with dual tone multi-frequency (DTMF) connected to the door motor through a DTMF decoder interfaced with microcontroller unit and a stepper motor.

The design was composed of four main functional modules, namely; the GSM module, the decoding module, controlling module and the switching module. The GSM module acted as both transmitting and receiving unit, employing the use of a mobile phone serving as the communication device between the user at one end and the object of access (i.e. the door) at the other receiving end. The decoding module and the controlling module were made using modern integrated circuit chips ensuring proper conversion of signal to binary codes, enabling the microcontroller to communicate properly with the switching device responsible for opening and closing the door. The codes were written in assembly language with Visual basic software and compiled with M-IDE studio for MC-51 compiler which worked perfectly with Window XP environment, the program was ran without error before it was burned onto the microcontroller using a device called the programmer by placing the microcontroller on it socket equal to the pin number.

Adewale, et al, 1996, designed and developed a Microcontroller Based Wireless Security Door Access System. The system used a PIC 16F84 microcontroller for the transmitter design and PIC16F84 for the receiver module. The PIN for the person to be granted access was stored in selected general purpose registers in the controller. The microcontroller scans the data entry, and compares it with the stored PIN to grant or deny access to the person. The interfaces, equipment and also the components used in each stage of the prototype assembly and construction.

Input Type: Telephone Keypad, Pin: 3 Digits; Password: 464; Transmitter Frequency: 415MHZ; Supply Voltage: 5vdc, 12vdc (For Model Gate Dc Motors) Maximum Current: 500ma Access Mechanism: Model Sliding Door Microcontroller: PIC16F84 Sliding Door Interconnect: Small Computer System Interconnect (SCSI); DB-9 connector. The starting point of the project began with the remote control (transmitter). On this remote, is placed a keypad possessing a 12Key 3x4 matrix keypad connected to the PORTB of the microcontroller, which has been configured as the input.

The microcontroller scans the PORTB using a special subroutine program (SCAN), decodes any of the depressed keypads and sends the decoded binary number to the register where it is compared with the stored numbers. If all the entered numbers is the same as the saved numbers programmed in the special register, the microcontroller then sends a signal to modulate the transmitter. The signal modulates a 415MHz transmitter module capable of about 50meters. Supposing the numbers which are keyed on the keypad are not programmed in the special register or not keyed in the particular order as that saved in the special register, the access is denied. A LED is set off which has been configured on PORTA3. When the correct code has been keyed in the correct order; the access granted LED is set off which is configured on PORTA2 and in turn; an electric pulse is

sent to the Relay (RL1) via PORTA1. PORTA has been configured as an output port. After the pulse has been sent to the RELAY (RL1), the magnetic field created by the armature coil attracts the armature to connect the contact thereby connecting the circuit and the signal being sent to the receiver. On the receiver end, the signal is demodulated by the receiver module which sends the pulse to the PORTA1 of the microcontroller which has been configured as the input, and the output is now sent to the relays (RL1 AND RL2) via the transistors Q1 and Q2 that controls the opening and closing of the model door via PORTB6 and PORTB7. The system is also coded such that the output of PORTA2 on the transmitter module indicates ACCESS DENIED when the wrong code is sent, while the LCD indicates ACCESS GRANTED via PORTB0 to PORTB5.

### 1.6 Types of Security Access System

There are different types of electric security devices, they are; switch activated lock system, sound activated system, shadow access lock system, light detector security system, pressure pad, sensitive security system and smartcard security access system etc. these systems are designed to serve different purpose as their names implies, their operation are related because some of them give access while some deny access.

- **Physical Security Devices:** A physical device such as a key passes. Key chains by gas station are used to identify a person. Sometimes a password or personal identification number (pin) is also required to ensure that it is the right person.
- **Biometric Identification:** Biometrics is the science of identifying someone from physical characteristics. This includes technologies such as voice verification, a retinal scan, palm identification and thumbprint.
- **Sound Activated Lock System:** The principle behind the sound activated lock system is that, it uses sound. The system locks permanently when there is a noise in the environment. This system uses sequential IC's like 555 timer which is made to operate with high frequencies and microphones will trigger alarm if there is a change in its frequency. These systems are ideal in bank vaults.
- **Shadow Detector Access System:** Another security access system is the shadow detector access system. This is mainly designed to be used at doors and places that need to be secured, the system works with alarm, but this device is highly inefficient because at the change in the intensity of light in bad weather and its function is restricted to only day hours.
- **Pressure and Sensitive Security System:** Pad with sensitive layers are hidden under the floor, when the system is activated alarm is triggered as pressure is applied on the pads. These pads are made of slightly suspended switch which closes the circuit and triggers alarm only when pressure is applied on it [Wikipedia.org].
- **Smartcard Access System:** The card access control system secures an area using an electronic door locking mechanism that requires a card reader and valid card to access the area. Only persons who are permitted to access the area and who have been issued valid cards may gain entry. And the card is embedded with either a microprocessor or a memory chip, only a memory chip with non-programmable logic. The microprocessor can add, delete and manipulate information on the card, while a memory chip card (for example pre-paid phone cards) can only undertake a pre-defined operation [wikipedia.org].

### 1.7 Improved 555 Oscillator Duty Cycle

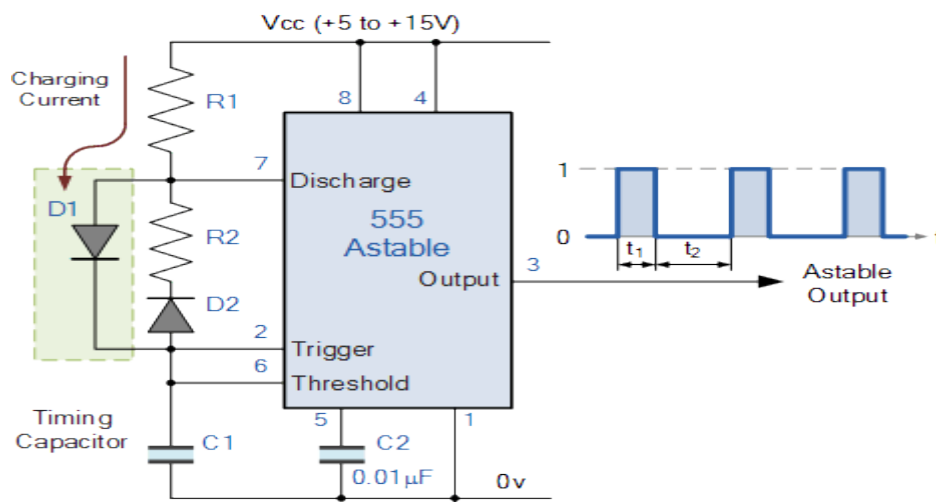


Figure 1: Astable Vibrator with 50 Percent Duty Cycle [www.google.com]

Figure 1 is an astablemultivibrator, by connecting this diode, D<sub>1</sub> between the trigger input and the discharge input, the timing capacitor will now charge up directly through resistor R<sub>1</sub> only, as resistor R<sub>2</sub> is effectively shorted out by the diode. The capacitor discharges as normal through resistor, R<sub>2</sub>. An additional diode, D<sub>2</sub> can be connected in series with the discharge resistor, R<sub>2</sub> if required to ensure that the capacitor will only charge up through D<sub>1</sub> and not through the parallel path of R<sub>2</sub> as during the charging process it is connected in reverse bias.

The charging time of  $t_1 = 0.693(R_1 + R_2)C$  is modified to take account of this new charging circuit and is given as:  $0.693(R_1 \times C)$ . The duty cycle is therefore given as  $D = R_1/(R_1 + R_2)$ . Then to generate a duty cycle of less than 50%, resistor R<sub>1</sub> needs to be less than resistor R<sub>2</sub>.

Although the previous circuit improves the duty cycle of the output waveform by charging the timing capacitor, C<sub>1</sub> through the bypass diode, D<sub>1</sub>, we can also produce a fixed square wave output waveform with an exact 50% duty cycle simply by moving the position of resistor, R<sub>2</sub> to the output pin as shown.

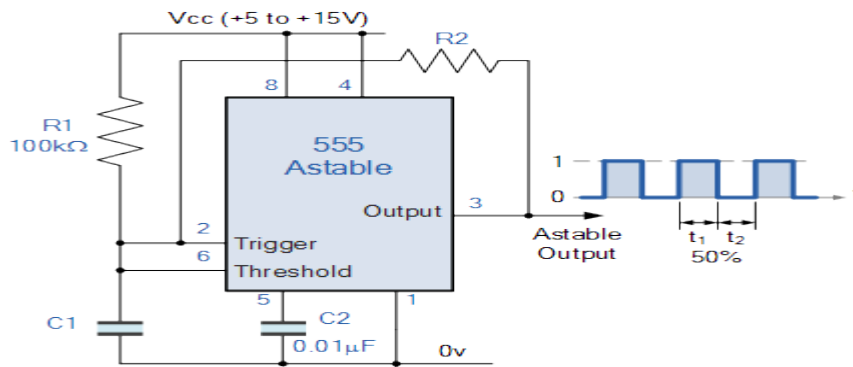


Figure 2: 50% Duty Cycle Astable Oscillator [www.google.com]

The reason for this 50% duty cycle is that capacitor; C<sub>1</sub> is now charging and discharging through the same resistor, R<sub>2</sub>. When the output from the 555 oscillator is HIGH, the capacitor charges up through R<sub>2</sub> and when the output is LOW, it discharges through R<sub>2</sub>. Resistor R<sub>1</sub> ensures that the capacitor charges up fully to the same value as the supply voltage.

However, as the capacitor charges and discharges through the same resistor, the above equation for the output frequency of oscillations has to be modified a little to reflect this circuit change. Then the new equation for the 50% Astable 555 Oscillator is given as [Boylestad, & Nashelsky]:

**50% Duty Cycle Frequency Equation**

$$f = \frac{1}{0.693 (2R_2) \cdot C} \text{ Hz} \quad (1)$$

Note that resistor R<sub>1</sub> needs to be sufficiently high enough to ensure it does not interfere with the charging of the capacitor to produce the required 50% duty cycle. Also changing the value of the timing capacitor, C<sub>1</sub> changes the oscillation frequency of the astable circuit.

**II. MATERIALS AND METHOD**

**2.1 Design of Power Supply Unit**

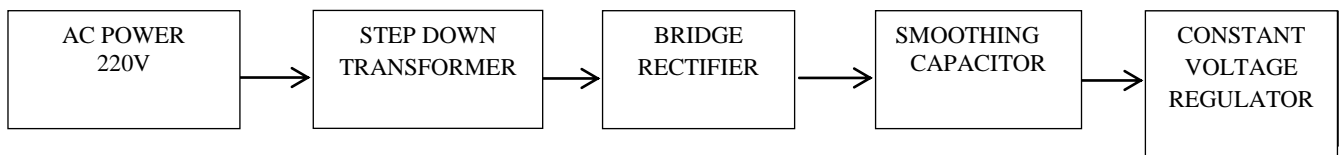


Figure 3: Block Diagram of the Power Supply Unit

The entire circuit is powered by a standard +5Volts DC power supply since most of the components are digital logic components. Before the power supply unity was designed, the total power requirement of the circuit was analyzed as follows:

- The CMOS IC for 555, CD4017 datasheet specified that the maximum voltage to be 15Volts and the minimum voltage to be 3Volts.
- The DC motor required 6 Volts.



Therefore, the circuit can adequately run on a 6Volts DC supply. However, in order to obtain the 6Volts DC supply from the public mains, the following circuit configuration was used. The transformer is a step down transformer rated 240V/9Vac at 500mA: since the expected output voltage is 5volts, any value above this is suitable. So a 9V transformer is chosen to step down the alternating current voltage from 240Vac to 9Vac at 500mA.

$$\text{And } D_{\text{Current}} = 1.5 \times 500\text{mA} = 0.75\text{A} \quad (2)$$

When  $D_{\text{current}}$  is the Diode forward current. Therefore the required device must have a:  $D_{\text{piv}} \geq 25\text{V}$  and  $D_{\text{current}} \geq 0.75\text{A}$ . From diode catalogue (datasheet), the IN4001 has the following characteristics;  $D_{\text{piv}} = 50\text{V}$  and  $D_{\text{current}} = 1\text{A}$ , this makes it more than suitable. Hence the four diodes of the bridge rectifier are IN4001.

#### ➤ **Filtering Stage:**

The filtering stage consists of two capacitors. The function of the capacitor is to remove the fluctuations or pulsation (called ripples) present in the output voltage supplied by the rectifier. Capacitor  $C_1$  and  $C_2$  are filter capacitor and improvement capacitor respectively [Rashi, 1986] and [Richard, 2001]. The voltage rating of the capacitors is chosen such that it is at least 1.5times the  $V_p$  from the rectifier output.

The  $V_p$  from the rectifier output is

$$V_{P(\text{in})} - V_d = V_{P(\text{out})} \quad (3)$$

Where  $V_{P(\text{in})}$  is the  $V_p$  from the transformer;  $V_d$  is the voltage drop across the rectifier diodes; and  $V_{P(\text{out})}$  is the  $V_p$  from the rectifier output.

Thus,  $V_{P(\text{in})} = 21.21$ ;  $V_d = 1.4\text{V}$  (voltage drop across each diode arm is 0.7V).

$$V_{P(\text{out})} = 21.21 - 1.4 = 19.81\text{V}, \quad (4)$$

The voltage of the capacitor should be

$$V_{P(\text{out})} \times 1.5 = 19.81 \times 1.5 = 29.715\text{V} \quad (5)$$

A capacitor that has a voltage of 35V was chosen. For effective filtering off of the ripple from the pulsating DC, the capacitance value chosen should be high enough to eliminate the ripple voltage ( $V_r$ ) to about 20% of the peak voltage ( $V_p$ ). The ripple voltage is given by;

$$V_r = I_o \div (2FC) \quad (6)$$

$$20\% \text{ of } V_p = 0.2 \times 21.21 = 4.242\text{V}$$

Where  $I_o$  is maximum current from supply = 500mA;  $F$  is frequency of supply = 50Hz;  $C$  is the expected capacitance of the capacitor, hence

$$C = I_o \div (2FV_r) \quad (7)$$

$$C = 500\text{mA} \div (2 \times 50 \times 4.242) = 1.178 \times 10^{-3}\text{F}.$$

However, the manufacturer specified that if the distance between the capacitor and the regulator is up to 6 inches, the inductance of the connecting cable may interfere with regulation [www.aldata sheet.com 2012], therefore a capacitor of capacitance value of 2200 $\mu\text{F}$  is recommended for  $C_1$ . Therefore  $C_1$  is rated 2200 $\mu\text{F}$  at 35V.  $C_2$  is mostly specified in rectifier circuits and its value is 0.01 $\mu\text{F}$ .

#### ➤ **Voltage Regulator Stage:**

The fixed voltage regulator is the 78xx series. 78 indicate that it is a positive voltage output regulator while xx signifies that value of the voltage; 09 for 9V, 12 for 12V. 7805 was used in this work to ensure that a 5V output voltage is obtained. To carry out effective voltage regulation, the minimum input voltage to the regulator is gotten from the manufacturer formula;

$$V_{\text{out}} = V_{\text{min}} - V_{\text{ref}} \quad (8)$$

Where  $V_{out}$  is the output voltage = 6volts;

$V_{ref}$  is the reference voltage given by the manufacturer = 2 or 3volts;

$$V_{in} = V_{out} + V_{ref} = 5 + 3 = 8V$$

The minimum required input voltage for effective regulation is 8 to 7V. Since we are getting a  $V_{rms}$  of:

$$V_{rms} = 0.707 V_p = 0.707 \times 21.21 = 14.995V$$

The power supply is adequate for proper regulation; hence the voltage regulator required is 7805.

➤ **Current Limiting Resistor and Power ON Light Emitting Diode:**

The series connected components are to indicate that there is power on to the circuit. The resistors protect the LED from damage and it value is given as:

$$R_1 = \frac{V_s - V_d}{I_d} \tag{9}$$

Where  $V_s$  is supply voltage = 5V;  $V_d$  is voltage of diode = 1.25V; and  $I_o$  is current of the diode = 10mA.

$$R_1 = \frac{5 - 1.25}{10} = 375\Omega$$

**2.2 Design of Sound Decoding Units**

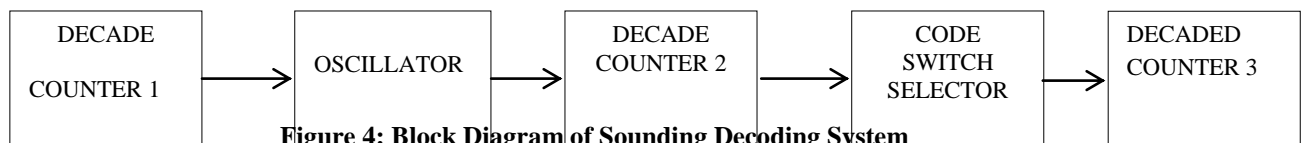


Figure 4: Block Diagram of Sounding Decoding System

This comprise of an oscillator (555) decade counter (hef 4017), diode(1n4001) and a transistor(bc547).

The figure below show the configuration of 555 Timer as a an Astable Vibrator, but in every design to achieve the desirable goal. They must be some assumption;

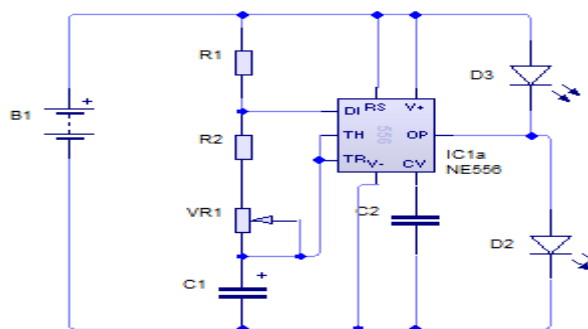


Figure 5: 555 Timer Configuration of the Circuit

❖ **Assumption**

- Assuming there must be a variation in frequency, in other words the frequency can be varied from low frequency to high frequency.
- Let  $C = 10\mu F$   
 $R_1 = 4.7k\Omega$ ,  $R_2 = 100k\Omega$

**Note:** The voltage range for 555 Timer IC is 3 – 15V.

∴ **Calculation**

Note that the 3 parameter mentioned earlier ( $R_1$ ,  $R_2$  and  $C$ ) will assist us in achieving two frequency if one parameters is being varied or alter.

$$f = \frac{1}{\ln 2 \times C \times (R_1 + 2R_2)} \quad (10)$$

$$f = \frac{1}{\ln 2 \times 10 \times 10^{-6} \times (4.7 + 200) \times 10^3}$$

$$f = \frac{1}{1.4186}$$

$$f = 0.7 \text{ Hz}$$

$$\therefore \text{Total Time} = \frac{1}{f} = \frac{1}{0.7} = 1.43 \text{ secs}$$

Time to on

$$\begin{aligned} T_{ON1} &= \ln 2 \times (R_1 + R_2) \times C & (11) \\ &= 0.693 \times 104.7 \times 10^3 \times 10 \times 10^{-6} \\ T_{ON1} &= 0.73 \text{ secs} \end{aligned}$$

Time to off

$$\begin{aligned} T_{OFF1} &= \ln 2 \times R_2 \times C & (12) \\ &= 0.693 \times 100 \times 10^3 \times 10 \times 10^{-6} \\ T_{OFF1} &= 0.693 \text{ secs} \end{aligned}$$

**Note:** I calculated the value for frequency when the parameter is at maximum capacity, and assuming that  $R_2$  is being varied at 50% interval the frequency and Time even the duty cycle will change. I choose to vary  $R_2$  because  $R_2$  take part in the on and off equation.

$$\begin{aligned} 1. \quad &\text{When } 100k \text{ is adjusted at } 50\% \\ \frac{50}{100} \times 100k\Omega &= 50k\Omega & (13) \end{aligned}$$

$$f = \frac{1}{\ln 2 \times C \times (R_1 + 2R_2)} \quad (14)$$

$$f = \frac{1}{\ln 2 \times 10 \times 10^{-6} \times (4.7 + 100) \times 10^3}$$

$$f_2 = 1.37 \text{ Hz}$$

$$f_2 \approx 1.4 \text{ Hz}$$

$$\text{Total Time} = \frac{1}{f_2} = \frac{1}{1.4} = 0.71 \text{ secs}$$

Time to ON

$$\begin{aligned} T_{ON2} &= \ln 2 \times (R_1 + R_2) \times C & (15) \\ &= 0.693 \times (54.7) \times 1000 \times 10 \times 10^{-6} \\ &= 0.38 \text{ secs} \end{aligned}$$

Time to off.

$$\begin{aligned} T_{OFF2} &= \ln 2 \times R_2 \times C & (16) \\ &= 0.693 \times 50 \times 1000 \times 10 \times 10^{-6} \\ &= 0.35 \text{ secs} \end{aligned}$$

$$\text{Duty Cycle} = \frac{T_{ON} \times 100}{T_{OFF} + T_{ON}} = \frac{0.38}{0.38 + 0.35} \times 100\% = 53\%$$

ii. Taking 0% of 100k,  $R_2 = 0$

$$f_3 = \frac{1}{\ln 2 \times C \times (R_1 + R_2)} \quad (17)$$

Note:  $R_2 = 0$

$$\text{Therefore; } f_3 = \frac{1}{\ln 2 \times C \times R_1} = \frac{1}{0.693 \times 4.7 \times 10^3 \times 10 \times 10^{-6}} = 30\text{Hz}$$

$$T_{Total} = \frac{1}{f} = \frac{1}{30} = 0.30 \text{ secs}$$

Time to on

$$T = \ln 2 \times C \times (R_1 + R_2) \quad (18)$$

When  $R_2 = 0$

$$T_{ON3} = 0.693 \times 4.7 \times 10^3 \times 10 \times 10^{-6} = 0.03\text{secs}$$

Time to off.

$$T_{OFF3} = \ln 2 \times C \times R_2 \quad (19)$$

When  $R_2 = 0$

$$T_{OFF3} = 0$$

$$\text{Duty Cycle} = \frac{T_{ON3} \times 100}{T_{ON3} + T_{OFF3}} \quad (20)$$

$$= \frac{0.03}{0.03 + 0} \times 100\% = 3\% \quad (21)$$

**Table 1: Values of Electronic Components Used**

C	R <sub>1</sub>	R <sub>2</sub>	T <sub>on</sub>	T <sub>off</sub>	Total	Frequency
10μF	4.7kΩ	100kΩ	0.73s	0.69s	1.43s	0.7Hz
10 μF	4.7kΩ	50kΩ	0.38s	0.35s	0.71s	1.4Hz
10μF	4.7kΩ	0kΩ	0.3s	0s	0.03s	30Hz

From the calculations, as  $R_2$  increases the frequency of the circuit decrease and vice versa. The figure below show the circuit of 555 in an Astable mode used for oscillation application. Note that every resistor as a tolerance limit that is why 1kΩ was added to  $R_2$  because when measured with an ohm meter the reading was closed:

$$R_2 = (100 \pm 1)$$

This circuit received signal from the input sensor twice to activate the astable oscillator which the output is fed into the decade counter for an output which depended on the number of oscillation received from the oscillator, at this point the code is set with the desired dip switch according to the number of chosen sound beat.

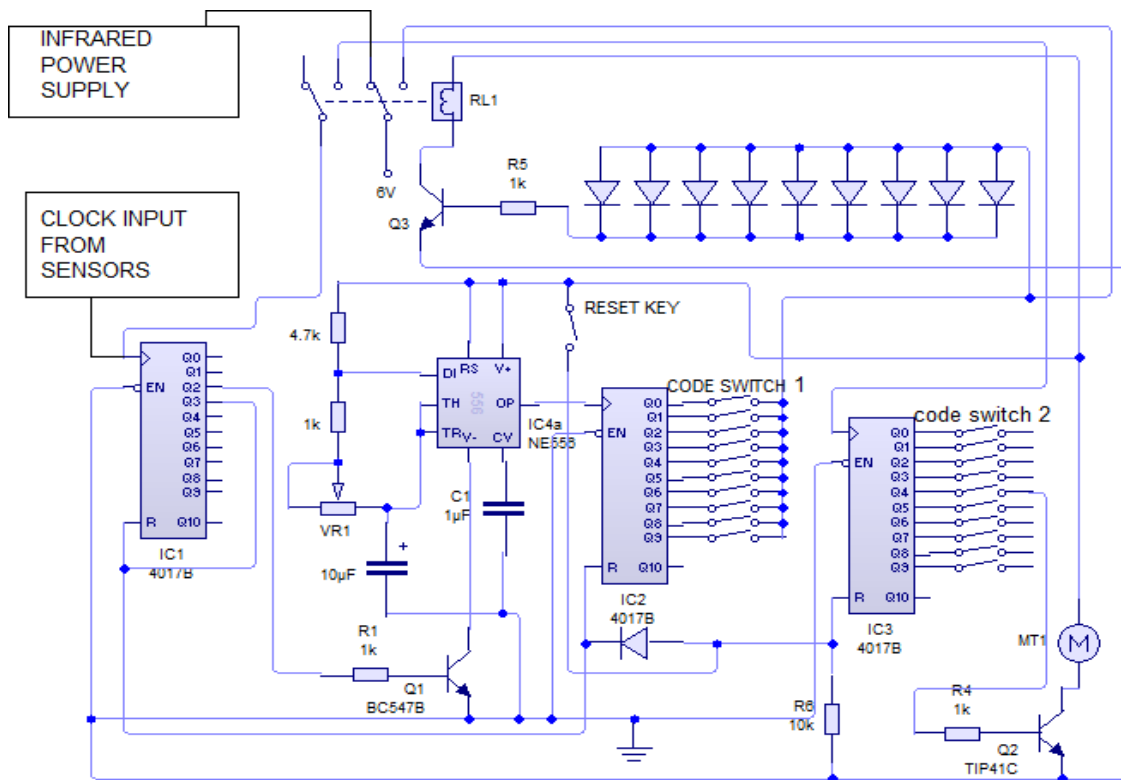


Figure 6: Sound decoder Circuit

from the circuit above the first decade counter receives the input from the sensor twice to make  $Q_2$  high and trigger the transistor which switches on the oscillator at the same time the oscillator output is fed in the second decade counter to get an output set by the help of the dip switch, this output must correspond to the set of the second sound beat received, please note that to input the second sound beat, the infrared sensor is inactive thereby the sound signal received at that time is only active at the third decade counter.

### 2.3 Construction

This work was constructed using electronic component and locally available materials, wire and plastic box for the casing of the electronic circuit. Before the construction was carry out, all the components were tested to confirm their proper working condition before proceeding into construction. Several steps were taken in the construction of the system which involved

1. To ensure that all the components to be used are functionally operating, they were first tested with a digital multi meter and ones that failed were replaced before finally soldering them on the veroboard.
2. To ensure that there was no breakage in the circuit path on the veroboard, immediately after soldering on the veroboard, the circuit path was tested using the Digital Multi-meter. This was done to also ensure continuity of circuit on the Veroboard.
3. Using Circuit WIZARD (Student Edition), National instrument simulator etc. to simulate the circuit. The results obtained from the simulation closely corresponds to the desired result, with some slight variations.
4. The period of time for the alarm remained high unless reset, the main reason for testing all the components before they were finally soldered on the Veroboard are to avoid the painstaking effort it will take to dis-solder faulty components at the end of the day. From the continuity test carried out on the Vero board to check the circuit path, it was discovered that the circuit was in a perfect working condition as continuity was ensured. Simulation of the circuit design was also done as mentioned. This section described the steps taken in the verification of calculated results through the real time implementation and measurements. The construction of the system is in 2 stages; the soldering of the components and the coupling of the entire system to the casing. The power supply stage was first soldered stage by stage. Each stage was tested using the multi-meter to make sure it is working properly before the next stage is done. This helps to detect mistakes and faults easily. The soldering of the circuit was done on a 10cm by 24cm Veroboard.

**2.4 The Door Construction**

The door was constructed from coated plywood with a maximum weight of 1.7kg, with a dimension of 150mm× 25mm ×325mm, the dc motor used on the door perform two vital functions which are;

To provide a pivoting point for the door and To provide the required turning torque

**2.5 Opening Mechanism**

The door uses a simple lever system in turning and closing of the door using a permanent magnet motor of 6v, 500mA. No complex control network was done on the dc motor. The direction of rotation depends on the polarity connection of the dc motor to power if reversed the direction reverses too

DC motor turning torque= force × distance

where

Force = mass × acceleration due to gravity

$$\tau = 25 \times 0.3 = 7Nm$$

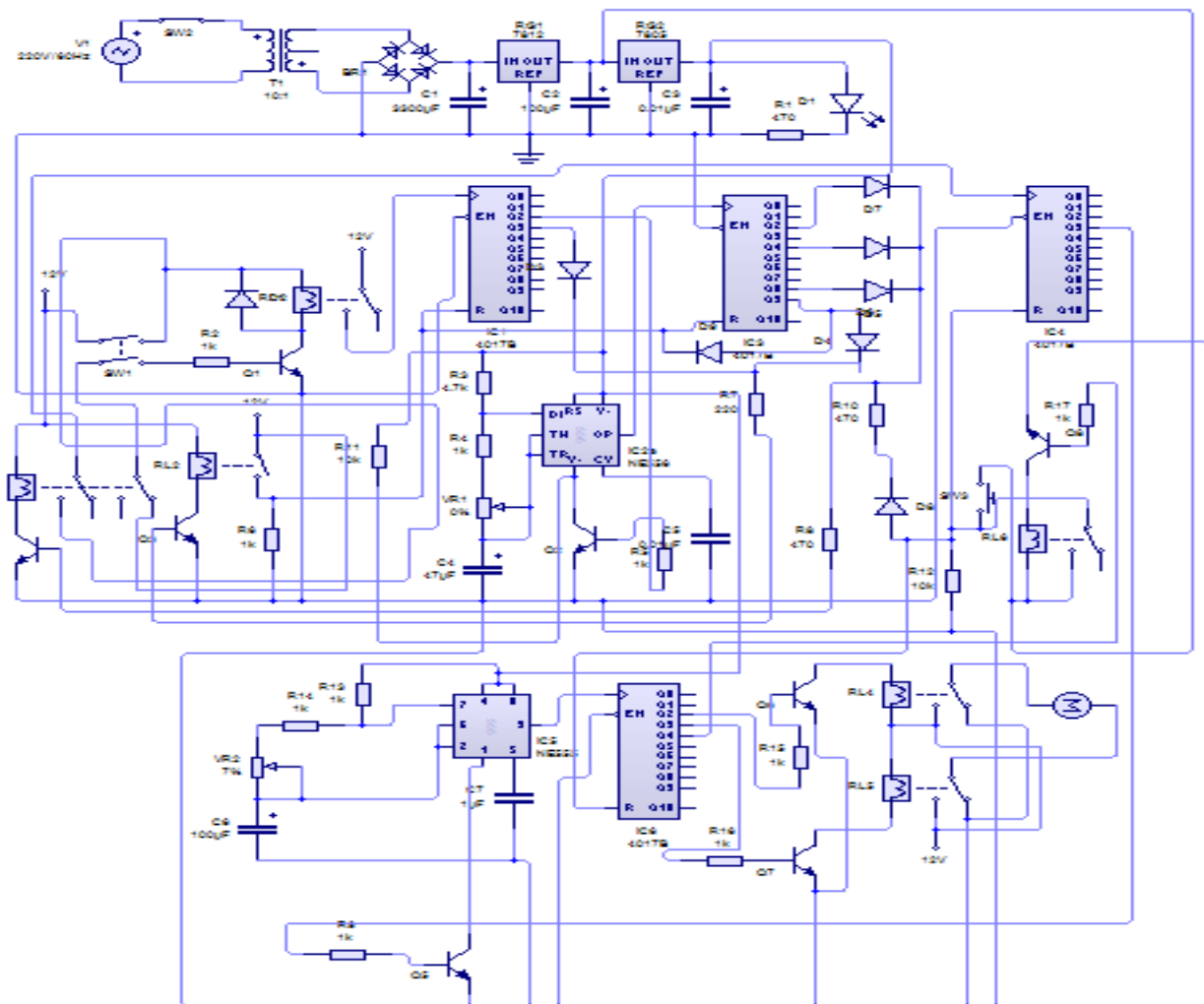


Figure 7: Circuit Diagram of the Sound Control Door Lock System

**III. RESULTS AND DISCUSSION**

**3.1 Results**

The testing was carry out with the mind of sensitivity of the circuit in relation to sound intensity and distance, the maximum distance the sound sensor can detect a sound is 7meters, it worked well both in ac and dc voltages, lastly it was not affected by weather or environmental noise .

### 3.2 General Circuit Operations

The mode of operation of this circuit is very simple, starting from the sensor, immediately the infrared sensor detects an obstacle within a length of 10cm it sends a signal (voltage) to the transistor which makes the transistor to conduct between the collector and emitter(negative voltage) to the relay, at this point, any positive voltage sent by the sound sensor will trigger the relay. Hence, a positive voltage is sent to pin 14 of IC<sub>1</sub>(4017) pin 4 of IC<sub>1</sub> is connected to a transistor(Q<sub>2</sub>) which causes the 555timer to oscillate sending pulses to pin 14 of IC<sub>2</sub>, during this, the output of IC<sub>2</sub>(4017) operate in a sequential mode from Q<sub>0</sub> to Q<sub>9</sub>, The main function of the code switch is to set the number of beat that will set IC<sub>3</sub> into the desire sequential output set by the operator. In figure 6, IC<sub>3</sub> was set at Q<sub>3</sub> this means that after the first two sound input, the second sound input must be four time for the door to open and lastly the knock must follow a pattern set by code switch lelse the code switch pattern will reset the circuit and when inputting the first sound signal must be twice, otherwise the circuit will reset. The figure 7 shows the circuit details of the work while figure is the simulation result of the DC motor response during the opening of the door.

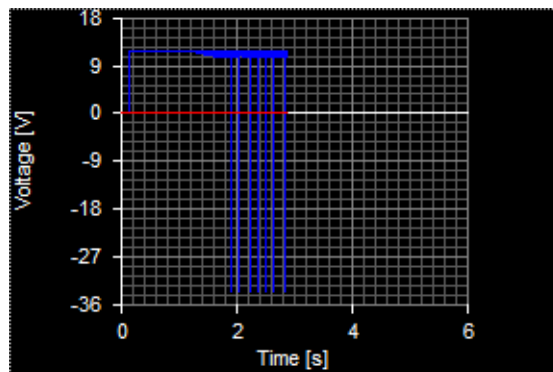


Figure 8: DC motor response voltage during operation

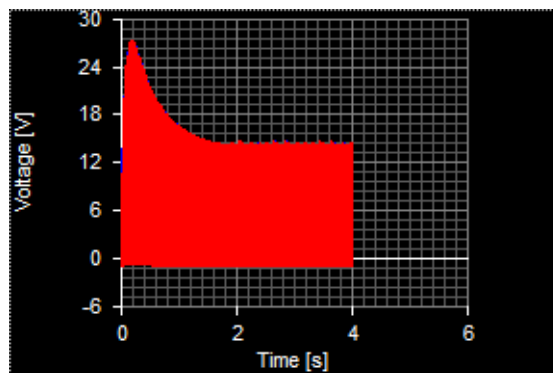


Figure 9: Circuit Response due to Sound

Figure 9 is the response of the simulation result of the sound decoder circuit. At the instance when the sound is produced, its raises the voltage at the decoder to 27V and thereafter, decays exponentially to 13V, this signal then sets the switch which then energizes the relay to operate the DC motor to open the door.

## IV CONCLUSION AND RECOMMEDATION

### 4.1 Conclusions

It can be concluded that the sole aim of carrying out the design of sound control door was achieved. The work when tested responded quick to the security of preventing intruders. One factor that accounts for the cheapness of the product was the proper choice of components used. The ones that were readily available were used, while a close substitute was found for those that were not readily available. The reliability of the entire work was considered in every aspect of design and construction. The system was tested and found to be working to specifications and predictions.

### REFERENCES

- [1] 555 Timer IC Datasheet
- [2] Adolphe, G. (1877): Elementary Treatise on Physics: Experimental and Applied, 8th ed. N.Y. Wm. Wood and Co., pp. 188-189.
- [3] Boylestad, L. & Nashelsky, L. (2004): Electronic Devices and Circuit Theory 8<sup>th</sup> ed. New Delhi. Pp.41-44

- [4] Frenzel, E. (2001): Introduction to Electronic Communication. In Communication Electronics<sup>3rd</sup> ed. Ohio: McGraw-Hill pp. 31-36.
- [5] Gupta, J. B. (2011). Modulation and Demodulation. In J. B. Gupta, Electronic Devices and Circuits (4<sup>th</sup> ed.) (pp. 451-452).
- [6] Huurdeman, A. (2003). The Worldwide History of Telecommunications. John Wiley & sons.
- [7] John, R. (1799). Encyclopedia Britannica, 3<sup>rd</sup> ed.
- [8] Kenedy, G., Davis, B. & Prasanna, S. (2011). Introduction to Communication Systems. In Electronic Communication Systems, 5<sup>th</sup> ed. Tata McGraw-Hill, New Delhi pp. 72:.
- [9] MacLeod, E. (1999). Alexander Graham Bell: An inventive life. Toronto: Kids Can Press.
- [10] Poynting, J.H. & Thomson, J.J. (1899). Sound (London: Charles Griffin and Co., pp. 37-41
- [11] Robert, T. Beyer, (1998): Sounds of Our Times: Two Hundred Years of Acoustics, New York: Springer Verlag, pp. 30-37.
- [12] Ronald, H. Chapman and Charles W. Stephens, (1967): Electronic siren including a shock excited resonant circuit. Pp.41-45.
- [13] [www.wikipedia.org/wiki](http://www.wikipedia.org/wiki). Accessed on 23<sup>rd</sup> June, 2015
- [14] Adamu, G. (2009): A Handbook on the Design of Electronic Devices, pp. 24-29.
- [15] Oгри, U.J., Okwong, B.D.E. and Etim, A. (2013): Design and Construction of Door Locking System using GSM, International Journal of Engineering and Computer Science, Vol.2, No. 7, Pp. 2235-2257
- [16] Adewale, A.A., Abdulkareem, A., Agbetuyi, A.F. and Dike, I. (2013): Design and Development of a Microcontroller Based Wireless Security Access System, International Journal of Computer Science Engineering, Vol. 2, No. 5, Pp.237-246.



**Elechi Promise** received his B.Eng and M.Eng degrees in Electrical/Electronic Engineering from University of Port Harcourt, Choba, Rivers State, Nigeria in 2006 and 2011 respectively and currently a Ph.D Student in Electronic and Telecommunication Engineering, University of Benin. He is a member of the Nigerian Society of Engineers (NSE) and Nigerian Institution of Electrical/Electronic Engineers (NIEEE) and also a registered practicing Engineer with the Council for Regulation of Engineering in Nigeria (COREN). His current research interest is on Radio Propagation for Mobile communications, GSM Technology, Microwave Propagation, Signal Analysis, NanoTechnology and ICT. He is currently a Lecturer in the Department of Electrical and Computer Engineering, Rivers State University of Science and Technology, Port Harcourt, Nigeria.



## Quali-quantitative evaluation for the definition of antiseismic recovery interventions in historical buildings.

D. Colapietro<sup>1</sup>, M. Pinto<sup>3</sup>, A. Fiore<sup>2</sup>, F. Fatiguso<sup>1</sup>, G.C. Marano<sup>2</sup>

<sup>1</sup>(Department of Civil Engineering, Environment and Territory, Construction and Chemistry, Politecnico di Bari, Via E. Orabona, 4 - BARI, Italy)

<sup>2</sup>(Department of Civil Engineering and Architecture, Politecnico di Bari, Via E. Orabona, 4 - BARI, Italy)

<sup>3</sup>(CFENG: Ingegneria Strutturale & Consulting, Via Ninna, 30 – CASAMASSIMA (BARI), Italy)

**ABSTRACT:** *The evaluation of the seismic vulnerability in historical buildings represents an area of recent interest in relation to the need to define appropriate interventions to improve the quality, compatibility with the historical-architectural characters, as well as with the static behaviour. The present work shows a completion of an operational methodology for the definition and evaluation of effectiveness of antiseismic recovery interventions in historical buildings defined qualitative-quantitative approach. The methodology allows you to define a coordinated system of structural interventions, appropriate in relation to the specific historical-architectural and technical-constructive characters of these structures giving a higher degree of security. The articulation operates as to take into account both the qualitative aspects, related to the technology of construction and to the rule of the art, and the quantitative aspects of the numerical analysis of the characteristics of resistance of the structural elements. The methodological approach has found a specific validation with reference to a masonry and concrete structure: a public housing complex called “Gruppo Piave – ex Gondar” in the city of Bari (Italy).*

**Keywords** -historic masonry building, qualitative-quantitative approach, linear and nonlinear analysis, seismic vulnerability, index of elastic-seismic improvement.

### I. INTRODUCTION

It is known that earthquakes have always represented the main cause of damage and losses to the architectural heritage [1]. Historical buildings are characterized by an inherent vulnerability to seismic action, because anyhow masonry is not very resistant to states of traction, especially on the horizontal planes of the courses, normally compressed [2, 3]. On these, in the case of an earthquake, the horizontal action causes the weak resistance of the material to exceed for the states of tangential stress and tension, causing damages because of the sliding or the detachment of the elements [4]. In addition, the history of these buildings, marked by different construction phases, accentuates that behavior which is already inherent in the material. The growths, the superfoetations, extensions that are planimetric, determine the presence of many facilities within the same building. In this way the behavior is strongly influenced by the action that strikes them. In the case of an earthquake, the horizontal inertial forces are capable of causing the loss of balance of these elements especially if slim or not properly connected to the rest of the building. This intrinsic vulnerability is extremely fed, in some cases, by the lack of assessment of effectiveness of some new construction techniques [5] that increase the propensity on the part of historical structures to be damaged; solutions such as the remake of a reinforced concrete roof, the inclusion of curbs that are too for walls, the use of seams armed as an alternative to traditional metal tie rods, have caused higher damage in most of the cases compared to those that the original structure would probably have presented. Therefore, there is a problem of seismic safety for the historical buildings, in other words we need to assure that the structure have a capacity of resistance comparable to that required of the new constructions, both for the protection of the public safety, and for the upkeep of the property; the intervention of earthquake recovery can certainly not be a compromise between conservation of architectural building and protection of the public safety, but neither should it be the optimal synthesis [6, 7]. All this requires a proper understanding of the structure in its whole, in order to identify elements of weakness with respect to the Rule of the Art. In other words it wants to permeate the concept of structural safety of the historic buildings with

all the aspects that are unlikely to be integrated within a mechanical model, even if it is refined. In this way the intervention, that comes from it, is certainly appropriate, because it poses as not a distortion of the "logic" (formal and spatial-material) of the pre-existent and in continuity with the "modal logic" (procedural) that it approves.

## II. OBJECTIVE OF THE STUDY AND METHOD

The following work presents a methodology for defining and assessing the effectiveness of interventions of earthquake recovery, defined quali-quantitative, through which improve the security level of an existing building, through a respect for its historicity. The approach selects quantitatively, as a result of dynamic analysis, combinations of interventions, adequately defined qualitatively related to conservative aspects of the product. In this way the need for conservation is not an obstacle but rather a guide to planning really effective antiseismic interventions. In other words, ways of knowledge and analysis are proposed in which the judgment on the suitability of an intervention emerges from the comparison between the ability of the structure, evaluated following a qualitative and quantitative knowledge of construction, and the seismic action. This comparison is not to be understood as binding occurs between strength of the structure and demand; on the contrary, it is attested, for each intervention, a quantitative parameter to bring into account, in conjunction with others, in a qualitative assessment that contemplates the desire to preserve the product from damage with seismic safety requirements about the enjoyment and the function [8]. The objective is to avoid unnecessary works, thus favoring the criterion of minimum intervention, but also by highlighting the cases in which it is appropriate to act more decisively. This study wants to highlight only which can be made in full compliance with the historical nature of the construction and excluding the rest.

## III. QUALI-QUANTITATIVE METHODOLOGICAL APPROACH

The methodological approach starts from the knowledge of the structure according to three levels of different deepening, necessary both for the purposes of a reliable evaluation of the seismic safety current, and for the choice of an effective intervention to improve seismic behaviour [9]. The purpose is certainly to put in place a model that allows a qualitative interpretation of the mechanism of structural operation, as many as the real structural analysis, for a quantitative assessment. Problems are those related to the recognition of geometric data, the changes occurred in the course of time, due to the phenomena of damage, resulting from anthropic transformations, aging of materials and by natural disasters. The first level unfolds therefore in an analysis of the building, showing the data collected in appropriate forms mostly cataloguing, suitably designed, in order of:

- 1.1 identification of building organism in its organic structure;
- 1.2 characterization of the spatial and functional relationships with respect to the bordering territories;
- 1.3 recognition of individual building block;
- 1.4 understanding of evolution of transformative structure in correlation to the successive uses in the course of time, through extensive historical-archival investigations;

Of course for the purposes of proper identification of the structural system, the reconstruction of the entire building history, the construction process and the subsequent transformations, play a decisive role. Historical analysis allows both to limit the number of investigations in historically homogeneous areas, and to focus on those parts that are less known or to possible solutions of continuity, identifying simultaneously previous consolidation interventions. However, the study of the historical evolution of the building cannot be separated from knowledge of the sequence of earthquakes [10] that have involved the same product in the past; it shows a real testing from which emerges awareness on the state of seismic stress which has been subjected. A second level of analysis is oriented towards complete spatial identification and diagnostics of the organism itself, through operations both of geometric survey, strain behavior, and of study of geomorphologic and structural plan. The knowledge and characterization of these latter aspects is of great importance in the prediction of seismic behavior due to the interaction ground - foundation - structure.

In this way, the approach facilitates the next step of input of the seismic model, completed by material constructive relief of the various elements that make up the structure. It represents a cognitive framework of third level, through which acquire a detailed morphology intrinsic in the same [11]. Performed a mechanical modeling of the structure, if the analysis-verification (linear or non-linear) shows an inability of the building in order to confront the seismic acceleration while waiting for the reference site, the approach requires the definition of one or more combinations of interventions of earthquake recovery. Modeled each combination of intervention, rather than perform for each a numerical evaluation of efficacy, such as to require a significant computational burden, the approach proposes a simplification of the problem, limiting the post tests of detail to the really effective combination. More precisely, after obtaining the modal forms of each combination of intervention and state of pre-consolidation, the approach requires the formulation of an index of elastic-seismic improvement, appropriately introduced therein in order to select the combinations in terms of effectiveness, calculating it and distinguishing between two cases that require two different formulations of this index. The two cases concern buildings regular in plan and elevation and buildings that instead have geometrical and / or construction material irregularities in plan and / or elevation.

For buildings regular in plan and elevation this operator, Eq. (1) is configured for each combination of intervention, such as normalized ratio between total pseudo- acceleration of consolidation and pre-consolidation. Both pseudo - accelerations derive from the elastic response spectrum, specific of the reference site, by a combination of partial values of accelerations, corresponding to periods relating to vibration modes with participating mass more than 1 %.

$$I_{mes} = \frac{A_{cons}}{A_{prec.}} = \frac{\left( \left( \sum_{i=1}^n (a_i \cdot m_i^*)^2 \right) \cdot (n_m) \right)_{cons.}}{\left( \left( \sum_{i=1}^n (a_i \cdot m_i^*)^2 \right) \cdot (n_m) \right)_{prec.}} \quad (1)$$

With:  $m_i^*$  = mass normalized modal,  $n_m$  = number of modes involved,  $a_i$  = modal pseudo-acceleration.

Instead in buildings with irregularities in plan and elevation, and wherein the second mode of vibration result of torsional type index of elastic-seismic improvement is defined as follows:

$$I_{mes} = \frac{A_{cons}}{A_{prec.}} = \frac{\left( \left( \sum_{i=1}^n (a_i \cdot m_i^*)^2 \right) \cdot (n_m) \cdot \beta_t^{0.65} \right)_{cons.}}{\left( \left( \sum_{i=1}^n (a_i \cdot m_i^*)^2 \right) \cdot (n_m) \cdot \beta_t^{0.65} \right)_{prec.}} \quad (2)$$

$$\text{With: } \beta_t = \frac{\max \{MPMx'; MPy'\}}{\min \{MPMx'; MPy'\}}$$

$MPx'(\%)$  = percentage of participating mass in the direction X 'of the torsional mode of vibration;  
 $MPy'(\%)$  = percentage of participating mass in the direction Y 'of the torsional mode of vibration.

In equation (2) is introduced the torsional factor  $\beta_t^{0.65}$ . This factor, obtained as a result of several experimental evaluations and interpolations of statistical data, refines the estimate of the index of elastic-seismic improvement evaluating the contribution due to the torsional motion.

In both equations, with the increase of the index of elastic-seismic improvement, induced by an increase in overall elasticity with respect to the pre-consolidated condition, building attenuates its vulnerability, in other words its propensity to suffer damage. The structure dissipates part of energy into the elastic phase and leaves the remaining contribution to plastic phase. Whether working on buildings of high historical and architectural interest or on solutions with lower value but still of undeniable interest, the approach provides an opportunity to recognize the combination of effective interventions quantitatively and qualitatively consistent with the history of artifact, promoting reduced invasiveness and reversibility of the same.

#### IV. REAL APPLICATION OF THE METHODOLOGICAL APPROACH

##### IV.I Case of study

The methodological approach has found a specific validation with reference to a public housing complex dating back to the late thirties of the twentieth century (built between 1937 and 1940) called “Gruppo Piave – ex Gondar” in the city of Bari (Italy)(Fig.1). It is formed by two C-shaped symmetrical bodies and is isolated from other adjacent buildings. The buildings are spread over four levels above ground and one basement and show irregularities in plan and elevation. The complex has a mixed construction type with presence of load-bearing masonry and vertical and horizontal elements in reinforced concrete (floor slabs, beams, pillars, curbs) and the building is of gallery type, unusual for the city of Bari, which was chosen for economic reasons. During the war, the complex has not been damaged or modified in any way; in subsequent years, until today, the building structure has not undergone substantial changes to anything, nor the structural parts; the few interventions concern a lacking and low end maintenance and numerous accretions. Concerning the seismic history the building has undergone during its existence a series of earthquakes including some quite significant to the local context in question, with peaks of intensity at the site of the 6th degree of the MCS scale, which suggests that it has been somehow stressed, though not seriously, from the seismic action over time.

##### IV.II Knowledge of the historical building

The cognitive framework of the building have been organized in three levels with increasing depth as expected from the approach and has been systematized in the drawings and schedule graphs forms. For the first level (Figs.2, 3) we proceeded with the location, general analysis and registry and relationship identification, using data from the maps, and in particular identifying the relationship and the distances to the surrounding buildings, important to assess the seismic behaviour. Extensive documentary researches were also carried out at the State Archive of Bari and at the home of the “Autonomous Institute of Public Housing of the province of Bari” and further literature searches from which have emerged a number of important documents and technical papers with which were reconstructed the story of the building and identified the structural macro - elements. In the second level (Fig.4) has been gained a complete geometric, spatial, and state of preservation identification through the historical technical drawings and the direct in situ survey. In the third level (Figs.5, 6, 7) have been

examined the material - structural and mechanical properties of each structural macro - element using both parameters provided by the legislation and data obtained from diagnostic tests performed on the artifact (cover meter and thermographic tests) and the archival documents. The mechanical values [7] have been appropriately scaled by applying the confidence factors related to the masonry and the reinforced concrete that are both equal to the level of knowledge and LC2 that is corresponding to a value of  $F_c$  equal to 1.20, based on the level of detail achieved, according to the Italian regulations [4].

#### IV.III Mechanical modeling and analysis

The modeling of the building under study was made according to the method SAM II (Simplified Analysis of Masonry buildings) based on a macro-elements modeling (pier elements, spandrel beam elements, joint elements) of the masonry structure, such as to enable analysis of entire buildings with a reduced computational analysis. The method idealizes a masonry wall by means of an equivalent frame constituted by pier elements (vertical axis), spandrel beam elements (horizontal axis), modeled with the introduction of rigid offsets at the ends. In order to avoid the processing of redundant data, modeling was made by considering one of the two buildings that constitute the complex "Gondar", in particular the one willing to south on Via Bruno Buozzi, this was possible given the symmetry and the complete correspondence of the geometric and material - constructive parameters of the two buildings (Fig.8). For more caution in the modeling were not considered masonry spandrel beam elements present above and below the openings, as deemed low resistance. For modeling and subsequent analysis the software CDMA Win (Computer Design of Masonries) of the STS s.r.l. which implements the method SAM II extending the three-dimensional case was used. The program is interfaced with the calculation engine Opensees (Open System for Earthquake Engineering Simulation), developed at the University of California at Berkeley, having high computing power and reliability. It follows a three-dimensional equivalent frame configuration of the various macroelements with elements, diversified according to the type of wall or element in reinforced concrete, but all linked together in joints, and solicited by the loads transmitted from the floor slabs, so as to obtain a complete and proper description of the structure together with a convenient method of modeling (for one-dimensional beam-column elements) and sufficiently suitable for the description of the behavior of masonry and reinforced concrete elements which make up the building object of study. The analysis, carried out in accordance with the regulations [1], were kind of dynamic modal and nonlinear static (pushover analysis). The verification of resistance of individual pier elements was carried out for the vertical loads and horizontal ones. For the static analysis was performed the calculation of slenderness and eccentricity of each wall. Were taken into account both the bending and the shear failure modes with the respective values of limit shifts laid down in the seismic regulations. For the seismic response analysis of the building have been used the response spectrum parameters of the area where the artifact is. The results of the analysis showed an inability of the structure to ensure the resistance to seismic action pending in the site at Limit State of Preservation of Life (SLV). In particular, the structural deficiencies are highlighted in the tabulation of data on the pushover curves generated by the software due to non-linear static analysis of the structure [12], in which are not verified at the SLV the curves corresponding to the numbers: 1, 2, 9, 10 as the demand structure displacement exceeds the capacity of the same determining the collapse. The curves in question (Figs.9, 10) correspond to a seismic action in the X direction according to the reference system established in the modeling with the software. Given the insufficient resistance to seismic action of the building a seismic recovery intervention was determined and then modeled and evaluated according to the qualitative - quantitative approach.

#### IV.IV Evaluation of the efficacy

The analysis performed showed that the inability of the building in facing an earthquake is due to insufficient strength of the masonry elements of the same, then the intervention should be aimed at strengthening the walls. In addition, given that the unmet SLV conditions refer to seismic actions agents in the X direction according to the reference system associated with the structural model (roughly coinciding with the direction north - south in the real building) it was decided to intervene solely on the load-bearing walls with this lying posture, in order to avoid unnecessary intervention with a further stiffening of the structure and a waste of economic resources, as well as a greater impact on the artifact. The intervention chosen (Fig.11) is the traditional consolidation through the application of reinforced plaster with the use of glass fiber reinforced plastic (GFRP) nets and connectors applied on both faces of the concerned walls, selected for its reliability and effectiveness widely proven, low cost, ease of execution even for unskilled labor, the relatively small impact because of the absence of decorative and valuable historical - artistic elements in this building. The dynamic modal analysis, performed on the consolidated model, has shown an increase in resistance of the elements affected by cracking mechanisms for bending or overturning in the plane of the wall. From the analysis data on total pseudo - accelerations in the X consolidated direction necessary for the calculation of the elastic - seismic improvement index and then the qualitative evaluation of effectiveness of the intervention (Table 1) have been

obtained. In addition was also made a pushover analysis in the adopted consolidated state that has further confirmed the fulfillment of the seismic demand in terms of moving for the site where the artifact is.

**IV.V Results**

For the effectiveness assessment of the proposed intervention the elastic - seismic improvement index has been calculated according to the formulation proposed in this paper. Firstly the data of the pre – consolidated state, obtained by modal analysis, have been defined as summarized in table 2. These were compared with the consolidated state data. The results of the modal analysis of the building showed that, despite irregularities in plan and elevation, the first two modes of vibration are of bending, singular condition due to the nearly coincidence between the center of mass and center of rigidity of the structure, therefore it was possible to use the equation 1 for the definition of the index. So it is derived the elasto - seismic improvement index. Afterwards the value of the index was compared with the values of the SDOF (single degree of freedom) elastic stiffness obtained from the bilinearization of the 8 pushover curves of the investigated direction (X) in the pre- and post-intervention (Table 3). The average values of the coefficients (K \*) in the two conditions were defined, then it is considered the ratio between the SDOF stiffness coefficient (K) pre and post consolidation for each pushover curve and it is compared with the ratio between the average values of the coefficients (K \*) and the value of the elasto - seismic improvement index (Table 4) (Fig.12). Finally, the standard deviation between these values that is equal to approximately 1.77% has been calculated.

**V. FIGURES AND TABLES**



Figure 1. Public housing complex “Gruppo Piave – ex Gondar” in Bari.



Figure 2. Example module I cognitive level.

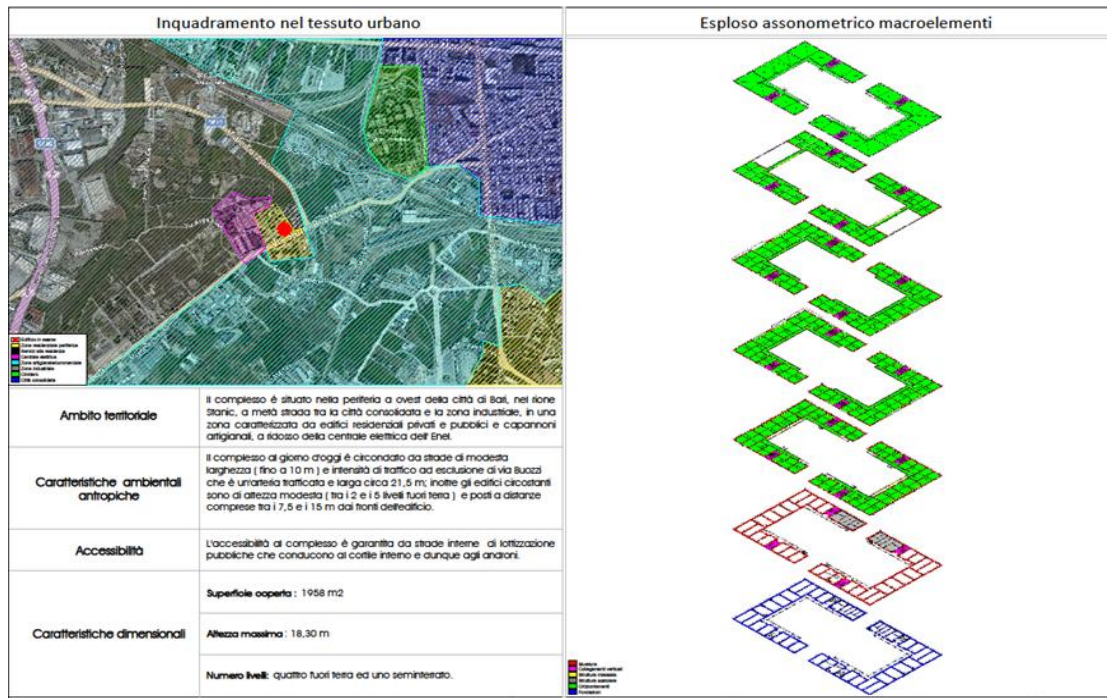


Figure 3. Example module I cognitive level.

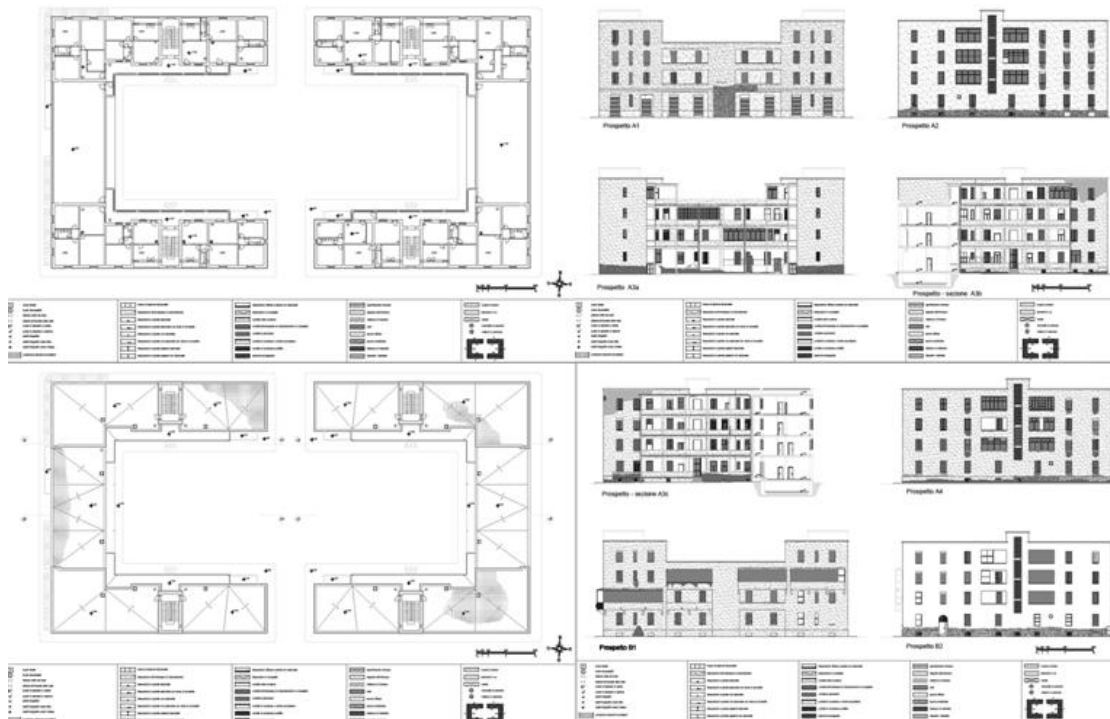


Figure 4. Example module II cognitive level.

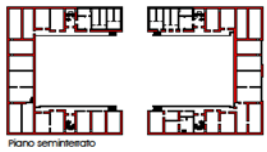
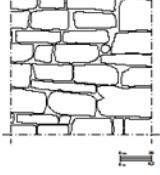
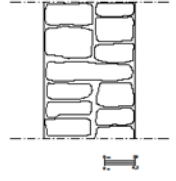
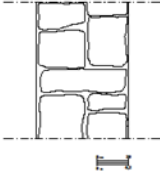
APPARECCHIATURA MURARIA		SCHEDA MACROELEMENTO : Muratura	
Tipo	<input type="checkbox"/> Arenata <input checked="" type="checkbox"/> Tufo <input type="checkbox"/> Mattoni Cudi <input type="checkbox"/> Calcare <input type="checkbox"/> Travertino <input type="checkbox"/> Mattoni Cotti	 <p>Localizzazione</p>	 <p>Prospetto</p>
Lavorazione	<input type="checkbox"/> Assente <input type="checkbox"/> Spigoli finiti e facce non lavorate <input checked="" type="checkbox"/> Accennata <input type="checkbox"/> Spigoli finiti e facce lavorate		
Forma	<input type="checkbox"/> Ciottoli <input type="checkbox"/> Bugnati <input type="checkbox"/> Blocchi Eratici <input type="checkbox"/> Conci <input type="checkbox"/> Lastre <input checked="" type="checkbox"/> Botze		
Dimensione	<input type="checkbox"/> Piccole (< 15 cm) <input checked="" type="checkbox"/> Medie (15 - 25 cm) <input type="checkbox"/> Grandi (> 25 cm)		
Stato di conservazione	<input type="checkbox"/> Buono <input type="checkbox"/> Cattivo <input checked="" type="checkbox"/> Medioce <input type="checkbox"/> Pessimo	 <p>Sezione trasversale</p>	 <p>Sezione longitudinale</p>
Listature	<input checked="" type="checkbox"/> Assenti <input type="checkbox"/> Presenti <small>Tipologia: _____ Dimensione media: _____</small>		
<b>MALTA</b>		<b>PARAMETRI MECCANICI MEDI</b>	
Funzione	<input checked="" type="checkbox"/> Allettamento <input type="checkbox"/> Stitatura <input type="checkbox"/> Riempimento	f <sub>m</sub> (resistenza media a compressione) : 210 N/cm <sup>2</sup> f <sub>tr</sub> (resistenza media a taglio) : 4.2 N/cm <sup>2</sup> E (modulo elastico normale) : 1080 N/mm <sup>2</sup> G (modulo elastico tangenziale) : 360 N/mm <sup>2</sup> w (peso specifico medio) : 16 kN/m <sup>3</sup>	
Tipologia	<input type="checkbox"/> Calce aerea <input checked="" type="checkbox"/> Calce idraulica <input type="checkbox"/> Cementizia	<b>NOTE</b>	
Aggregato	<input checked="" type="checkbox"/> Sabbia pozzolanica <input type="checkbox"/> Ghiaietto <input type="checkbox"/> Ghiaia	Formata da blocchi sbalzati di tufo bianco di tipo "scorza" posati a letto di cava intrecciati con malta di calce e pozzolana, formati da due paramenti, uno di tufo coesente e fatto di tufo a quadrelli, tali che 26+32+2= 60 cm, con collegamenti trasversali tra i paramenti con pezzi a tutto spessore collocati ogni due blocchi per ogni corso; malta formata da una parte di calce grassa in pasta e due di pozzolana (granulometria fino a 3mm), con resistenza a compressione di circa 25 kg/cm <sup>2</sup> .	
Forma aggregata	<input type="checkbox"/> Attondata <input checked="" type="checkbox"/> Spigolosa		
Stato di Conservazione e Consistenza	<input type="checkbox"/> Incoerente <input type="checkbox"/> Tenace <input checked="" type="checkbox"/> Firabile		
<b>FINITURE (intonaco)</b>			
Stato Attuale	<input type="checkbox"/> Assente <input checked="" type="checkbox"/> In parte assente <input type="checkbox"/> Presente		
Stato di Conservazione	<input checked="" type="checkbox"/> Degradato <input type="checkbox"/> Fessurato <input type="checkbox"/> Buono		

Figure 5. Example module III cognitive level.


SEZIONE TRASVERSALE		SCHEDA MACROELEMENTO : Muratura	
Tipologia	<input type="checkbox"/> Paramento Unico <input type="checkbox"/> Due Paramenti accostati <input checked="" type="checkbox"/> Due Paramenti ammassati <input type="checkbox"/> A sacco Incoerente <input type="checkbox"/> A sacco coesente <input type="checkbox"/> Paramento aggiunto		Scheda 1.2
Spessore	<input type="checkbox"/> < 30 cm <input type="checkbox"/> 80-100 cm <input type="checkbox"/> 40-50 cm <input type="checkbox"/> > 100 cm <input checked="" type="checkbox"/> 60-70 cm		
Presenza significativa vuoti	<input checked="" type="checkbox"/> Assente <input type="checkbox"/> Presente		
Presenza diatoni	<input type="checkbox"/> Assente <input checked="" type="checkbox"/> Presente		
<b>COLLEGAMENTI TRA LE PARETI MURARIE</b>		<b>IDENTIFICAZIONE NORMATIVA</b>	
Tipologia Angolate	<input type="checkbox"/> Paramento Unico <input type="checkbox"/> Due Paramenti accostati <input checked="" type="checkbox"/> Due Paramenti ammassati	<input type="checkbox"/> Muratura in pietra disordinata (ciottoli, pietre eretiche e irregolari) <input type="checkbox"/> Muratura in pietra disordinata (ciottoli, pietre eretiche e irregolari) e listature. <input type="checkbox"/> Muratura a conci sbalzati, con paramento diimitato spessore e nucleo interno. <input type="checkbox"/> Muratura a conci sbalzati, con paramento diimitato spessore con listature e nucleo interno. <input checked="" type="checkbox"/> Muratura a conci di pietre tenere (tufo, calcarenite, ecc.). <input type="checkbox"/> Muratura in pietra a spacco con buona tessitura. <input type="checkbox"/> Muratura a blocchi lapidei squadrati. <input type="checkbox"/> Muratura in mattoni pieni e malta di calce. <input type="checkbox"/> Muratura in mattoni pieni e malta di calce.	
Angolate elementi costitutivi	<input type="checkbox"/> Analoghi alla muratura <input type="checkbox"/> Di dimensioni maggiori <input checked="" type="checkbox"/> A conci squadrati		
Tipologia	<input type="checkbox"/> Analoghi alla muratura <input checked="" type="checkbox"/> Di altra natura: corcoli in c.a. <input type="checkbox"/> Ammassamento scadente <input checked="" type="checkbox"/> Collegamenti efficaci		
Qualità	<input type="checkbox"/> Analoghi alla muratura <input checked="" type="checkbox"/> Ammassamento scadente <input checked="" type="checkbox"/> Collegamenti efficaci		
<b>INTERVENTI DI CONSOLIDAMENTO</b>			
Tipologia	<input checked="" type="checkbox"/> Nessuno <input type="checkbox"/> Iniezioni malta <input type="checkbox"/> Scuci-cuci <input type="checkbox"/> Intonaco armato <input type="checkbox"/> Stitatura giunti <input type="checkbox"/> Altro tipologia: _____		
<b>ELEMENTI STRUTTURALMENTE EFFICACI (architravi)</b>			
NE:.....	<input type="checkbox"/> Assente <input checked="" type="checkbox"/> Presente, di natura: realizzati in c.a. gettato in opera		
<b>ELEMENTI DI PREGIO STORICO-ARTISTICO</b>			
NE:.....	<input checked="" type="checkbox"/> Assente <input type="checkbox"/> Presente, tipologia: _____		

Figure 6. Example module III cognitive level.

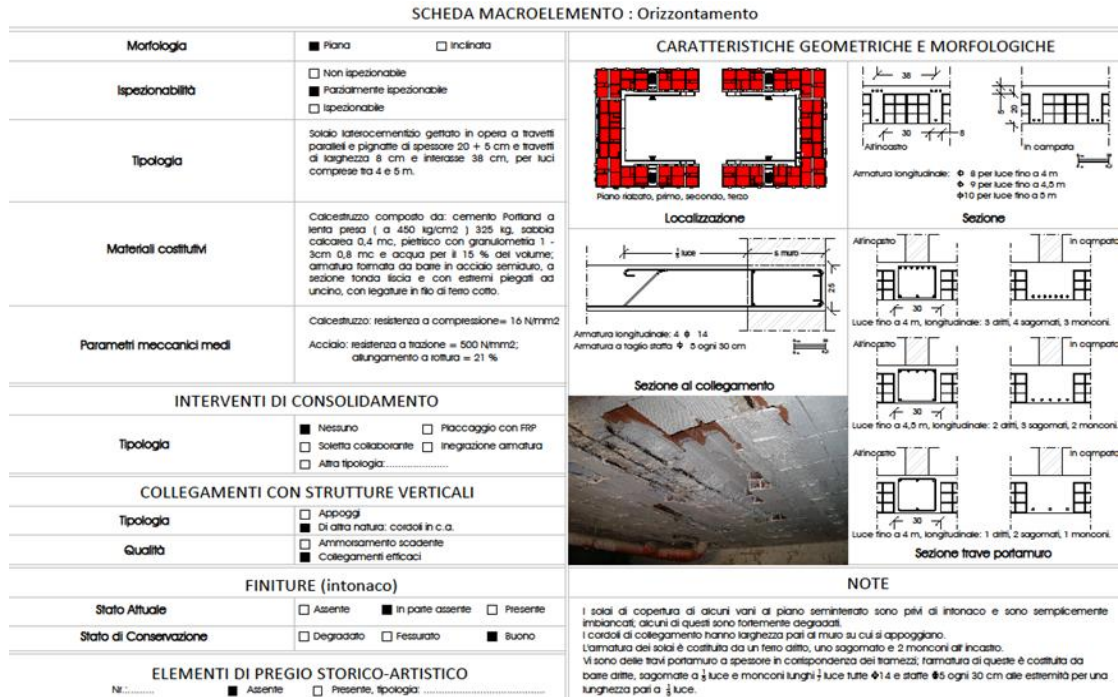


Figure 7. Example module III cognitive level.

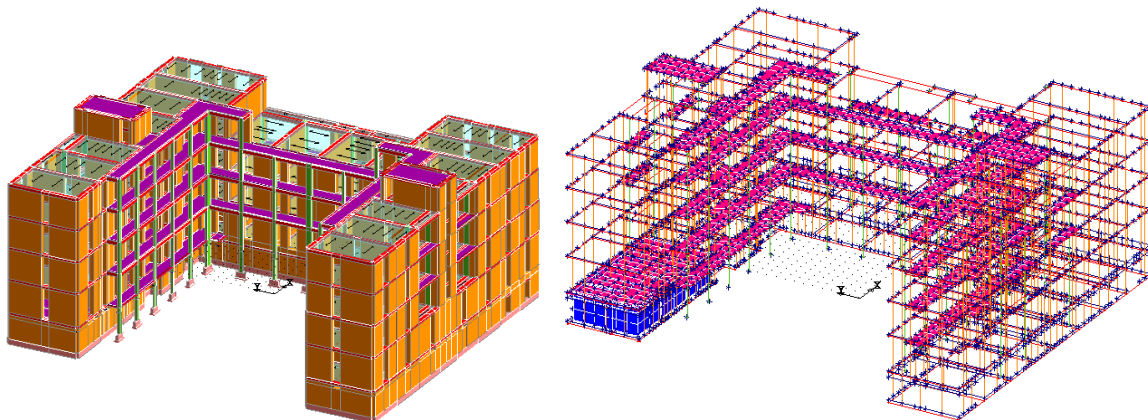


Figure 8. Three-dimensional mechanical modeling of the building.



Push-Over Nro: 1

Push-Over Nro: 2

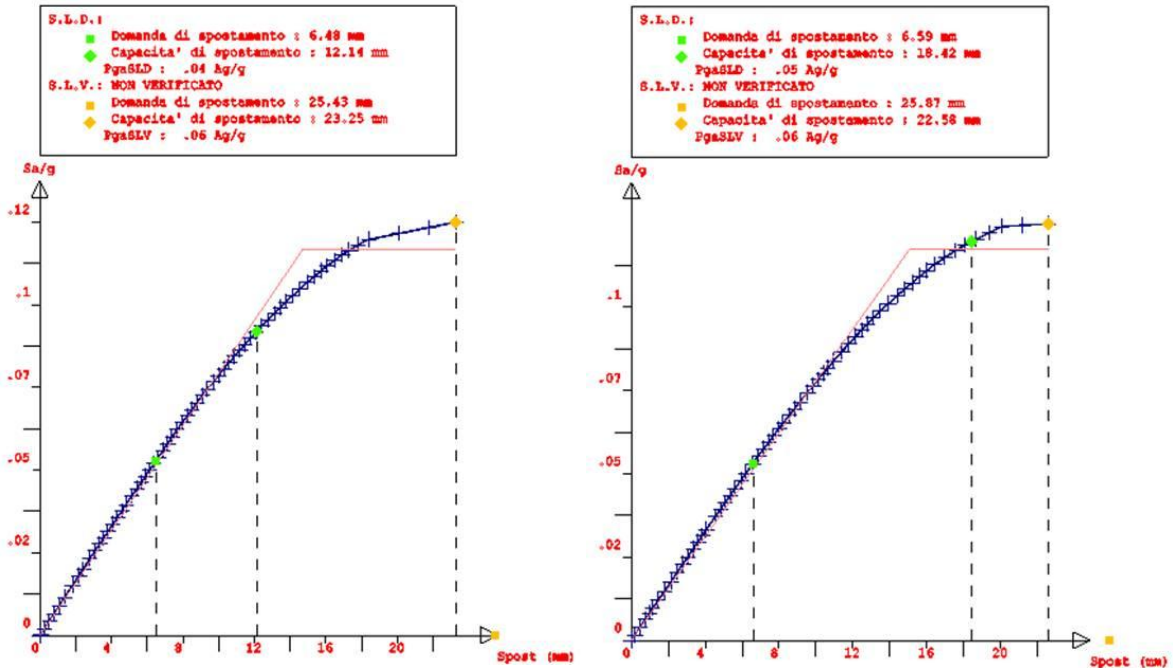


Figure 9. Unverified pushover curves, pre-consolidation state, X direction.

Push-Over Nro: 9

Push-Over Nro: 10

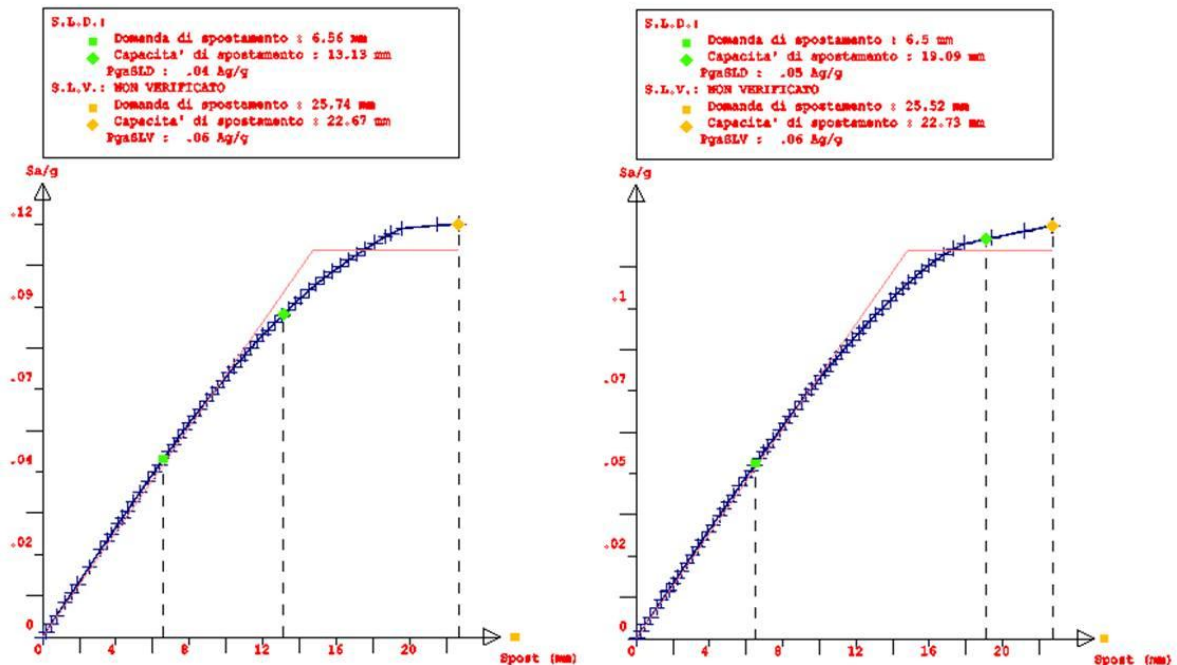


Figure 10. Unverified pushover curves, pre-consolidation state, X direction.

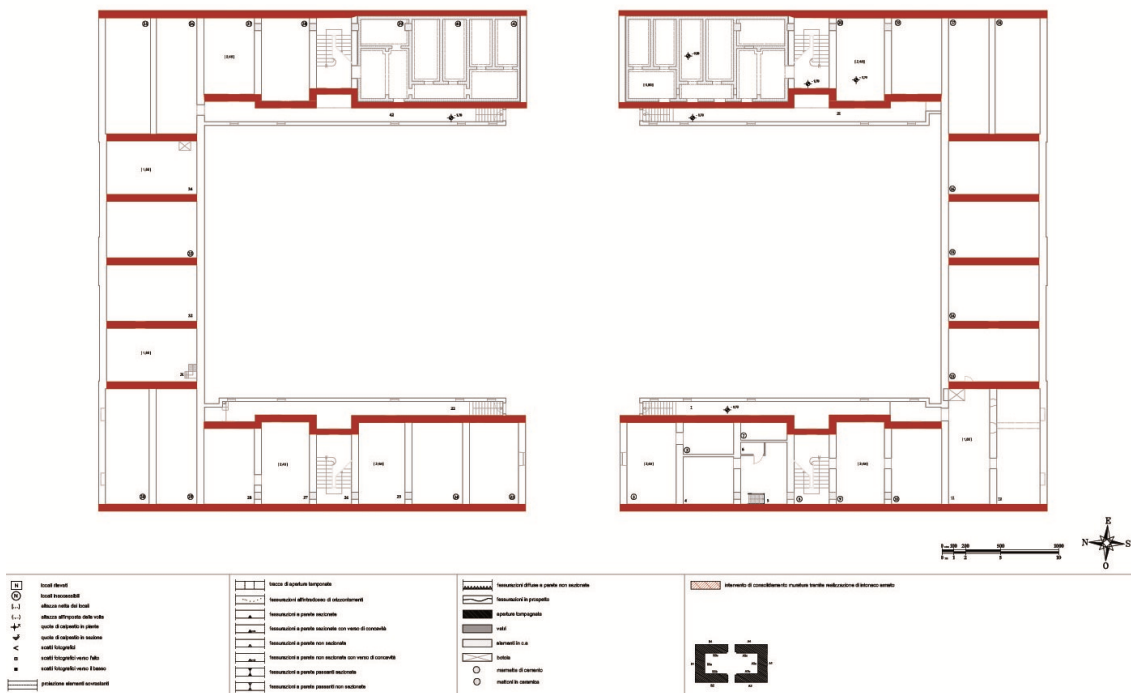


Figure 11. Localization of the seismic improvement intervention.

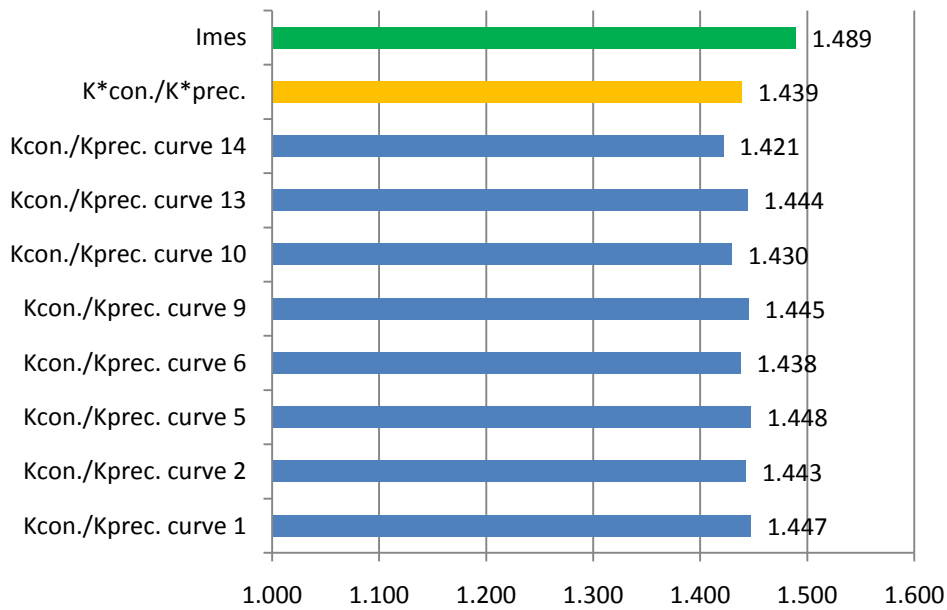


Figure 12. Graph comparing the values of the ratios between coefficients of elastic stiffness in pre and consolidated state for each pushover curve in the X direction and between their mean values and the elastic - seismic improvement index.

DIRECTION	MODE	MASS [%]	m*	PERIOD [s]	a [g]
x	1	1,54	0,025904	0,41616	0,187
x	2	59,45	1	0,38677	0,187
x	3	6,77	0,113877	0,36639	0,187
x	5	11,72	0,19714	0,13221	0,159
x	6	2,59	0,043566	0,1267	0,156
x	7	1,03	0,017325	0,08875	0,131
x	8	1,37	0,023045	0,08411	0,127
x	9	2,23	0,037511	0,08025	0,125
x	10	1,33	0,022372	0,07359	0,121
x	11	1,23	0,02069	0,06915	0,118
		nm		A	
		10		<b>0,709233</b>	

Table 1. Definition of total pseudo-acceleration of consolidation.

DIRECTION	MODE	MASS [%]	m*	PERIOD [s]	a [g]
x	1	62,59	1	0,47154	0,187
x	2	5,08	0,081163	0,43627	0,187
x	4	12,72	0,203227	0,16556	0,181
x	7	2,67	0,042659	0,10824	0,143
x	8	2,01	0,032114	0,1002	0,138
x	9	1,12	0,017894	0,09084	0,132
x	12	4,65	0,074293	0,07367	0,121
		nm		A	
		7		<b>0,476281</b>	

Table 2. Definition of total pseudo-acceleration of pre-consolidation.

SDOF STIFFNESS COEFFICIENTS			
DIRECTION	CURVE	K prec.[t/m]	K cons.[t/m]
x	1	49383,54	71477,76
x	2	48446,63	69890,31
x	5	75104,25	108719
x	6	75022,46	107862,7
x	9	49129,4	71011,02
x	10	49037,39	70109,79
x	13	74935,72	108234,3
x	14	75696,6	107601
		K* prec.	K* cons.
		<b>62094,5</b>	<b>89363,2</b>

Table 3. SDOF stiffness coefficients related to the pre-consolidated and consolidated state.

DIRECTION	CURVE	K cons./Kprec.
x	1	1,4474005
x	2	1,4426248
x	5	1,4475745
x	6	1,437739
x	9	1,4453875
x	10	1,4297211
x	13	1,4443615
x	14	1,4214778
		K*cons./K*prec.
		<b>1,439149</b>
		<b>Imes</b>
		<b>1,489106</b>

Table 4. Ratio between the stiffness coefficients SDOF relating to the consolidated and pre-consolidated state and comparison with the ratio between their average values and the elastic - seismic improvement index.

## VI. CONCLUSION

The study has helped to develop and perfect a practice for the selection of seismic recovery interventions in the historical buildings, assuring simultaneously safety and conservation of the structure. The complexity of the buildings, which have been chosen for the analysis, together with further tests carried out on other equivalent structures, has allowed us to test the applicability of the approach as a tool to address in overcoming of seismic risk at the territorial level. The elastic-seismic improvement index has been validated through the pushover analysis, which confirmed that the increase of the index, represents the increase of the

elastic stiffness and the decrease of the oscillation period of the structure, resulting in an attenuation of the request displacement expected for the site and therefore a reduction of the seismic vulnerability of the building. The study has also shown how the reliability of the evaluation approach is strongly influenced by the level of knowledge of the construction. The approach is therefore a tool able to grasp, with a reduced computational burden and an appropriate level of accuracy, the response in terms of improving the seismic vulnerability of the historical buildings, otherwise punishable by methodologies of much more complex analyses. For this way, it can be considered that the proposed approach, together with other practices for the assessment and mitigation of seismic risk, is capable to drive the design of interventions in existing buildings.

#### REFERENCES

- [1] L. Lagomarsino, On the vulnerability assessment of monumental buildings. *Bull. Earthq. Eng* , 4, 2006, 445–463.
- [2] *Italian Technical norms for the constructions*, D.M. 14 January 2008.
- [3] G. Magenes, A. Della Fontana, Simplified non-linear seismic analysis of masonry buildings, *Proceedings of the Fifth, International Masonry Conference*, British Masonry Society, No. 8, 1998, 190-195.
- [4] D. D’Ayala, E.Speranza, Definition of collapse mechanisms and seismic vulnerability of historic masonry buildings, *Earthq Spectra*, 19(3), 2003, 479–509.
- [5] D. D’Ayala, Seismic Vulnerability and Risk Assessment of Cultural Heritage Buildings in Istanbul, Turkey, *Proceedings of the 14th world conference on earthquake engineering*, Beijing, 2008.
- [6] G. Augusti, M. Ciampoli, P. Giovenale, Seismic vulnerability of monumental buildings, *Structural Safety*, 23, 2001, 253–274.
- [7] D. D’Ayala, E.Speranza, An integrated procedure for the assessment of seismic vulnerability of historic buildings, *Proceedings of 12th European conference of earthquake engineering*, Paper Reference 561, Elsevier Science Limited, London, 2002.
- [8] A. Borri, G. Castori, A. Grazini, A. Giannantoni, Performance of masonry elements strengthened with steel reinforced grout, *Fiber-reinforced polymer reinforcement for concrete structures (FRPRCS-8) international symposium proceedings*, Patras, Greece, 2007.
- [9] L. Binda, A. Saisi, C. Tiraboschi, Investigation procedures for the diagnosis of historic masonries, *Construction and Building Materials*, Elsevier, 14, 2000, 199-233.
- [10] M. Stucchi, et al, *DBMI11, the database of macroseismic survey of Italian earthquakes used for the seismic parametric catalogue CPT111*, (<http://emidius.mi.ingv.it/DBMI11/>), 2011.
- [11] A. Borri, M. Corradi, E. Speranzini, A. Giannantoni, Consolidation and reinforcement of stone walls using a reinforced repointing grid, *Structural analysis of historic constructions, VI Intern. Conference*, Bath, UK, 2008.
- [12] A. Fiore, P. Monaco, Earthquake-induced pounding between the main buildings of the “Quinto Orazio Flacco” school, *Earthquakes and Structures*, Techno-Press, Vol. 1, No. 4, 2010, 371-390.

## Numerical Integration and a Proposed Rule

Md.Amanat Ullah

(Mathematics, Uttara University, Bangladesh)

**ABSTRACT :** Numerical integration plays very important role in Mathematics. There are a large number of numerical integration methods in the literature and this paper overviews on the most common one, namely the Quadrature method including the Trapezoidal, Simpson's and Weddle's rule. Different procedures are compared and tried to evaluate the more accurate values of some definite integrals. Then it is sought whether a particular method is suitable for all cases. A combined approach of different integral rules has been proposed for a definite integral to get more accurate value for all cases.

**Keywords** -Integration, Quadrature formula, Trapezoidal rule, Simpson's  $\frac{1}{3}$  rule, Weddle's rule.

### I. INTRODUCTION

Numerical integration is the study of how the approximate numerical value of a definite integral can be found. It is helpful for the following cases:

- Many integrals can't be evaluated analytically or don't possess a closed form solution. For example:  

$$\int_0^t e^{-x^2} dx.$$
- Closed form solution exists, but numerical evaluation of the answer can be bothersome.
- The integrand  $f(x)$  is not known explicitly, but a set of data points is given for this integrand.
- The integrand  $f(x)$  may be known only at certain points, such as obtained by sampling.

Numerical integration of a function of a single variable is called Quadrature, which represents the area under the curve  $f(x)$  bounded by the ordinates  $x_0$ ,  $x_n$  and  $x$ -axis. The numerical integration of a multiple integral is sometimes described as Cubature.

Numerical integration problems go back at least to Greek antiquity when e.g. the area of a circle was obtained by successively increasing the number of sides of an inscribed polygon. In the seventeenth century, the invention of calculus originated a new development of the subject leading to the basic numerical integration rules. In the following centuries, the field became more sophisticated and, with the introduction of computers in the recent past, many classical and new algorithms had been implemented leading to very fast and accurate results.

An extensive research work has already been done by many researchers in the field of numerical integration. M. Concepcion Ausin<sup>[1]</sup> compared different numerical integration producers and discussed about more advanced numerical integration procedures. Gordon K. Smith<sup>[2]</sup> gave an analytic analysis on numerical integration and provided a reference list of 33 articles and books dealing with that topic. Rajesh Kumar Sinha<sup>[3]</sup> worked to evaluate an integrable polynomial discarding Taylor Series. Gerry Sozio<sup>[4]</sup> analyzed a detailed summary of various techniques of numerical integration. J. Oliver<sup>[5]</sup> discussed the various processes of evaluation of definite integrals using higher-order formulae. Otherwise, every numerical analysis book contains a chapter on numerical integration. The formulae of numerical integrations are described in the books of S.S. Sastry<sup>[6]</sup>, R.L. Burden<sup>[7]</sup>, J.H. Mathews<sup>[8]</sup> and many other authors. In this paper, a Quadrature formula has been used to get the different rules of numerical integrations.

For a given set of data points  $(x_0, y_0), (x_1, y_1), \dots, (x_n, y_n)$  of a function  $y = f(x)$ , which is not known explicitly, if is required to replace  $f(x)$  by an interpolating polynomial  $\varphi(x)$ . Different integration formula can be obtained depending upon the type of the interpolating formula used. The general formula for numerical integration using Newton's forward difference formula is

$$\int_{x_0}^{x_n} y \, dx = hn[y_0 + \frac{n}{2}\Delta y_0 + \frac{n(2n-3)}{12}\Delta^2 y_0 + \frac{n(n^2-4n+4)}{12}\Delta^3 y_0 + \dots + (n+1)^{th} \text{ term}] \dots \dots (i),$$

where  $h$  is the width of the subinterval and  $n$  is the number of subintervals.

For  $n = 1$ , the equation (i) reduces to  $\int_{x_0}^{x_1} y \, dx = \frac{h}{2}[y_0 + y_1]$

Repeating the process for the next intervals and combining all, we get

$$\int_{x_0}^{x_n} y \, dx = \frac{h}{2}[y_0 + 2(y_1 + y_2 + y_3 + \dots + y_{n-1}) + y_n] \dots \dots (ii),$$

which is known as composite Trapezoidal rule or simply Trapezoidal rule<sup>[6]</sup>.

When  $n = 2$ , the equation (i) yields to  $\int_{x_0}^{x_2} y \, dx = \frac{h}{3}[y_0 + 4y_1 + y_2]$

Continuing the process for the next intervals and combining them, we get

$$\int_{x_0}^{x_n} y \, dx = \frac{h}{3}[y_0 + 4(y_1 + y_3 + \dots + y_{n-1}) + 2(y_2 + y_4 + \dots + y_{n-2}) + y_n] \dots \dots (iii),$$

which is known as composite Simpson's  $\frac{1}{3}$  rule or simply Simpson's  $\frac{1}{3}$  rule<sup>[6]</sup>.

For  $n = 3$  and  $n = 4$ , Simpson's  $\frac{3}{8}$  and Boole's rules are obtained respectively but Simpson's  $\frac{3}{8}$  rule is not as accurate as Simpson's  $\frac{1}{3}$  rule<sup>[6]</sup>.

For  $n = 6$ , the equation (i) yields to

$$\int_{x_0}^{x_6} y \, dx = \frac{3h}{10}[y_0 + 5y_1 + y_2 + 6y_3 + y_4 + 5y_5 + y_6].$$

Repeating the process for the next intervals and combining all, we get

$$\int_{x_0}^{x_n} y \, dx = \frac{h}{10}[y_0 + 5(y_1 + y_5 + y_7 + \dots + y_{n-1}) + (y_2 + y_4 + y_8 + \dots + y_{n-2}) + 6(y_3 + y_9 + \dots + y_{n-3} + 2y_6 + y_{12} + \dots + y_{n-6})] \dots \dots (iv),$$

which is known as Weddle's rule.

Here a comparison among Trapezoidal, Simpson's  $\frac{1}{3}$  and Weddle's rule is shown in the following table to examine the better rule for accuracy.

Integral	Exact Value	Trapezoidal	Simpson's $\frac{1}{3}$	Weddle's
$\int_0^1 \sqrt{1-x^2} dx$	0.78539816	0.77834373	0.78262639	0.78311087
	Error	0.00705443	0.00277178	0.00228730
$\int_0^2 (e^{x^2} - 1) dx$	14.45262777	14.93311330	14.47143621	14.45523911
	Error	0.48048553	0.01880844	0.00261135
$\int_{0.1}^{2.5} (3 \log x + 2x^2) dx$	10.77895602	10.72289932	10.76522243	10.77098228
	Error	0.05605670	0.01373358	0.00797374
$\int_0^2 \sqrt{1+3\sin^2 x} dx$	3.26107456	3.25966472	3.26108019	3.26106689
	Error	0.00140984	0.00000563	0.00000768
$\int_0^1 (1 + e^{-x} \cos(4x)) dx$	1.00745963	1.00882686	1.00749796	1.00746025
	Error	0.00136722	0.00003833	0.00000062

Table-1: A comparison among Trapezoidal rule, Simpson's  $\frac{1}{3}$  rule and Weddle's rule for  $n = 12$

From the table-1, it is concluded that the Weddle’s rule is more accurate among them and then the Simpson’s  $\frac{1}{3}$  rule, but we know that for the Weddle’s rule and Simpson’s  $\frac{1}{3}$  rule, the number of subintervals must be divisible by 6 and 2 respectively. But in some real situation, it will may not be found the number of subintervals that is divisible by 6 or 2. For example, if the limits of an integral is 0 to 1, then to use Weddle’s rule, the length of subinterval will be taken approximately 0.166667, 0.083333, 0.0555556, ... etc. involving errors. If it is chosen an exact length of the subinterval like as 0.2, 0.1, 0.05, ..., then the number of subintervals will be 5, 10, 20,... respectively. In those cases, which rule will be used? Can it be used the Weddle’s or Simpson’s  $\frac{1}{3}$  rule?

Suppose the number of subintervals is an odd number and then the same examples are shown in table-2 and table-3 for Weddle’s rule and Simpson’s  $\frac{1}{3}$  rule respectively.

Integral	Exact value	For n = 11	For n = 13	For n = 15	For n = 17
$\int_0^1 \sqrt{1-x^2} dx$	0.78539816	0.76926180	0.77437914	0.77271621	0.77699034
	Error	0.01613636	0.01101902	0.01268195	0.00840782
$\int_0^2 (e^{x^2} - 1) dx$	14.45262777	11.06287216	12.11401731	11.29416797	11.9212543
	Error	3.38975562	2.33861046	3.15845980	2.53137347
$\int_{0.1}^{2.5} (3 \log x + 2x^2) dx$	10.77895602	9.21202478	9.72263745	9.39714488	9.74478881
	Error	1.56693124	1.05631857	1.38181114	1.03416721
$\int_0^2 \sqrt{1+3\sin^2 x} dx$	3.26107456	3.08729737	3.14344553	3.10857069	3.14961252
	Error	0.17377719	0.11762903	0.15250387	0.11146204
$\int_0^1 (1 + e^{-x} \cos(4x)) dx$	1.00745963	0.97520534	0.98568941	0.97889657	0.98606461
	Error	0.03225429	0.02177022	0.02856306	0.02139503

Table-2: Weddle’s rule for n = 11, n = 13, n = 15 and n = 17

Integral	Exact value	For n = 11	For n = 13	For n = 15	For n = 17
$\int_0^1 \sqrt{1-x^2} dx$	0.78539816	0.77879864	0.78029230	0.78127118	0.78198025
	Error	0.00659952	0.00510586	0.00412698	0.00341791
$\int_0^2 (e^{x^2} - 1) dx$	14.45262777	14.78689790	14.66206601	14.59780633	14.55619259
	Error	0.33427013	0.20943824	0.14517856	0.10356482
$\int_{0.1}^{2.5} (3 \log x + 2x^2) dx$	10.77895602	10.77157016	10.77456156	10.77621633	10.77718833
	Error	0.00738586	0.00439446	0.00273969	0.00176769
$\int_0^2 \sqrt{1+3\sin^2 x} dx$	3.26107456	3.26039821	3.26066659	3.26081369	3.26089730
	Error	0.00067635	0.00040797	0.00026087	0.00017726
$\int_0^1 (1 + e^{-x} \cos(4x)) dx$	1.00745963	1.00760821	1.00755069	1.00751499	1.00749533
	Error	0.00014858	0.00009106	0.00005536	0.00003570

Table-3: Simpson’s  $\frac{1}{3}$  rule for n = 11, n = 13, n = 15 and n = 17

Comparing the values of integral (from Table-1, Table-2 and Table-3) for different number of subintervals, It has been seen that the Weddle’s rule and the Simpson’s  $\frac{1}{3}$  rule can not be used when the number of subintervals is not divisible by 6 and 2 respectively. In this situation, a new method has been proposed.

## II. PROPOSED RULE

Let the number of subintervals is n in which first  $n_1$  is divisible by 6. So Weddle’s rule is applicable for the first  $n_1$  subintervals. From the remaining  $(n-n_1)$  subintervals, let next  $n_2$  subintervals are divisible by 2. Then Simpson’s  $\frac{1}{3}$  rule can be used for these subinterval (from  $n_1-n_2$ ). Trapezoidal rule can be used for the last subintervals if n is an odd number. For example: If n=13, then Weddle’s rule can be used for the first 12 subintervals and Trapezoidal rule can be used for the last subinterval. If n=14, then the Weddle’s rule can be used for the first 12 subintervals and Simpson’s  $\frac{1}{3}$  rule can be used for the last two subintervals. If n=15, then Weddle’s rule can be used for the first 12 subintervals, Simpson’s  $\frac{1}{3}$  rule can be used for the next 2 subintervals and Trapezoidal rule can be used for the last subinterval and so on. Finally it is added all the values obtained from these rules to get the values of an integral which are show in table-4.

Integral	Rules	For n=13	For n=14	For n=15	Exact Value
$\int_0^1 \sqrt{1-x^2} dx$	Combined	0.78029230	0.78320648	0.78127118	0.78539816
	Trapezoidal	0.779140612	0.77979801	0.78034785	
	Simpson's $\frac{1}{3}$	---	0.78319969	---	
$\int_0^2 (e^{x^2} - 1)dx$	Combined	14.66206360	14.46073778	14.59780633	14.45262777
	Trapezoidal	14.87970376	14.82130280	14.77408874	
	Simpson's $\frac{1}{3}$	---	14.46301848	---	
$\int_{0.1}^{2.5} (3 \log x + 2x^2)dx$	Combined	10.77456156	10.77403940	10.77621633	10.77895602
	Trapezoidal	10.73047512	10.73662659	10.74168779	
	Simpson's $\frac{1}{3}$	---	10.77003672	---	
$\int_0^2 \sqrt{1+3\sin^2 x} dx$	Combined	3.26066659	3.26107446	3.26081369	3.26107456
	Trapezoidal	3.25987344	3.26003901	3.26017256	
	Simpson's $\frac{1}{3}$	---	3.26107741	---	
$\int_0^1 (1 + e^{-x} \cos(4x)) dx$	Combined	1.00755069	1.00744598	1.00751499	1.00745963
	Trapezoidal	1.00862398	1.00846317	1.00833353	
	Simpson's $\frac{1}{3}$	----	1.00744897	---	

Table- 4: Comparison among Combined rule, Trapezoidal rule Simpson's  $\frac{1}{3}$  rule for n=13, n=14 and n=15

Table - 4 shows that combined rule gives more accurate result. Beside the above five example, so many examples have been tried and more accurate results are found.

### III. CONCLUSION

In this article, to find the a numerical approximate value of a definite integral  $\int_{x_0}^{x_n} f(x)dx$ , Trapezoidal rule, Simpson's  $\frac{1}{3}$  rule and Weddle's rule are used and it is seen that the Weddle's rule gives more accuracy than Simpson's rule. But these rules can't be used for all cases. In those cases it may be used theproposed rule to get the better result.

### REFERENCE

- [1] M. Concepcion Ausin, 2007, an introduction to quadrature and other numerical integration techniques, Encyclopedia of Statistics in Quality and reliability. Chichester, England.
- [2] Gordon K. Smith, 2004, Numerical Integration, Encyclopedia of Biostatistics.2<sup>nd</sup> edition, Vol-6
- [3] Rajesh Kumar Sinha, Rakesh Kumar ,2010, Numerical method for evaluating the integrable function on a finite interval, International Journal of Engineering Science and Technology. Vol-2(6)
- [4] Gerry Sozio, 2009, Numerical Integration, Australian Senior Mathematics Journal, Vol-23(1)
- [5] J. Oliver, 1971, The evaluation of definite integrals using high-order formulae, The Computer Journal, Vol-14(3)
- [6] S.S Sastry, 2007, Introductory Method of Numerical Analysis, Fourth Edition, Prentice-hall of India Private Limited.
- [7] Richard L. Burden, 2007, Numerical Analysis, Seven Edition, International Thomson Publishing Company.
- [8] Jonh H. Mathew, 2000, Numerical Method for Mathematics, Science and Engineering, Second Edition, Prentice Hall of India Private Limited.



## Adaptive Sliding Mode Control of Mobile Manipulator Welding System for Horizontal Fillet Joints

Tran Duy Cuong, Nguyen Thanh Phuong

HUTECH High Technology Research Institute, Viet nam.

**Abstract :** *In this paper, an adaptive sliding mode control of mobile manipulator welding system for horizontal fillet joints is presented. The requirements of welding task are that the end effector must track along a welding trajectory with a constant velocity and must be inclined to the welding trajectory with a constant angle in the whole welding process. The mobile manipulator is divided into two subsystems such as the tree linked manipulator and the wheeled mobile platform. Two controllers are designed based on the decentralized motion method. The effectiveness of the proposed control system is proven through the simulation results.*

**Keywords:** *mobile platform (MP), welding mobile manipulator (WMM), manipulator, trajectory tracking, Lyapunov function.*

### I. INTRODUCTION

Nowadays, the working condition in the industrial fields has been improved greatly. In the hazardous and harmful environments, the workers are substituted by the welding robots to perform the operations. Especially in welding field, the welders are substituted by the welding manipulators to perform the welding tasks. Traditionally, the manipulators are fixed on the floor. Their workspaces are limited by the reachable abilities of their structures. In order to overcome this disadvantage, the manipulators that are movable are used for enlarging their workspaces. These manipulators are called the mobile manipulators. In this study, the structure of the mobile manipulator includes a three-linked manipulator plus a two-wheeled mobile platform.

In recent years, there has been a great deal of interest in mobile robots and manipulators. The study about mobile robots is mostly concentrated on a question: how to move from here to there in a structured/unstructured environment. It includes three algorithms that are the point to point, tracking and path following algorithm. The manipulator is a subject of a holonomic system. The study on manipulators is mostly concentrated on a question: how to move the end effector from here to there and it also has three algorithms like the case of the mobile robot. Although there has been a vast amount of research effort on mobile robots and manipulators in the literature, the study on the mobile manipulators is very limited. It is hopeful that this thesis will make a little contribution for the mobile manipulator research.

The previous works are concentrated on the following topics

- Motion control of a wheeled mobile robot

The mobile platform is a subject of non-holonomic system. Assume that the wheels roll purely on a horizontal plane without slippage. The mobile platform robot used in this study has two independent driving wheels and one passive caster for balancing. Several researchers studied the wheeled mobile robot as a non-holonomic system. Kanayama et al.[8] (1991) proposed a stable tracking control method for a non-holonomic mobile robot. The stability is guaranteed by Lyapunov function. Fierro and Lewis[3] (1995) used the backstepping kinematic into dynamic method to control a non-holonomic mobile robot. Lee et al.[4] (1999) proposed an adaptive control for a non-holonomic mobile robots using the computed torque method. Fukao et al.[5] (2000) developed an adaptive tracking control method with the unknown parameters for the mobile robot. Bui et al.[6] (2003) proposed a tracking control method with the tracking point outside the mobile robot.

- Motion control of a manipulator

The control of a manipulator is an interesting area for research. In previous works, Craig et al.[1] (1986) proposed an algorithm for estimating parameters on-line using an adaptive control law with the computed torque method for the control of manipulators. Lloyd et al.[2] (1993) proposed a singularity control method for the manipulator using closed-form kinematic solutions. Tang et al.[9] (1998) proposed a decentralized robust control of a robot manipulator.

- Motion control of a mobile manipulator

A manipulator mounted on a mobile platform will get a large workspace, but it also has many challenges. With regard to the kinematic aspect, the movement of the end effector is a compound movement of several coordinate frames at the same time. With regard to the dynamic aspect, the interaction between the manipulator and the mobile platform must be considered. With regard to the control aspect, whether the mobile manipulator is considered as two subsystems is also a problem that must be studied.

In previous works, Dong, Xu, and Wang[7] (2000) studied a tracking control of a mobile manipulator with the effect of the interaction between two subsystems. Tung et al [10] (2004) proposed a control method for mobile manipulator using kinematic model.

Dung et al [11] (2007) proposed a “Two-Wheeled Welding Mobile Robot for Tracking a Smooth Curved Welding Path Using Adaptive Sliding-Mode Control Technique”

## 2. System modeling

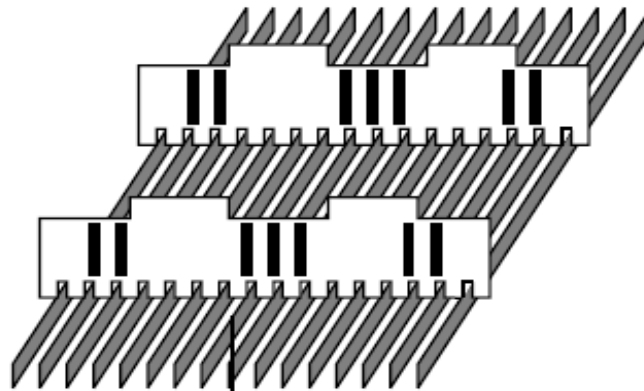


Fig 1. Grillage assembling method for flat hull block

The task is to track the horizontal fillet seam in the grillage assembling method, which is one of the conventional procedures for assembling the flat hull blocks in shipbuilding and consists of only the horizontal fillet seam.

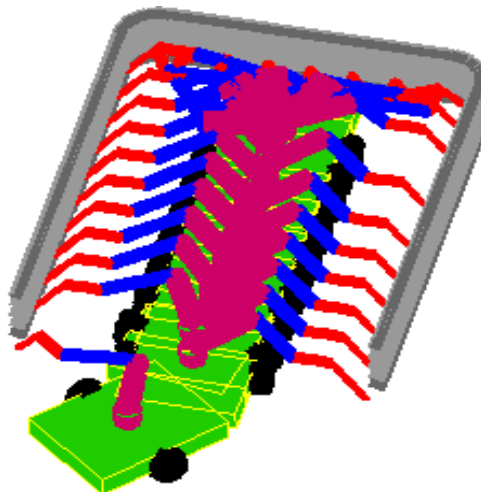


Fig 2. Three-link welding manipulator mounted on mobile platform

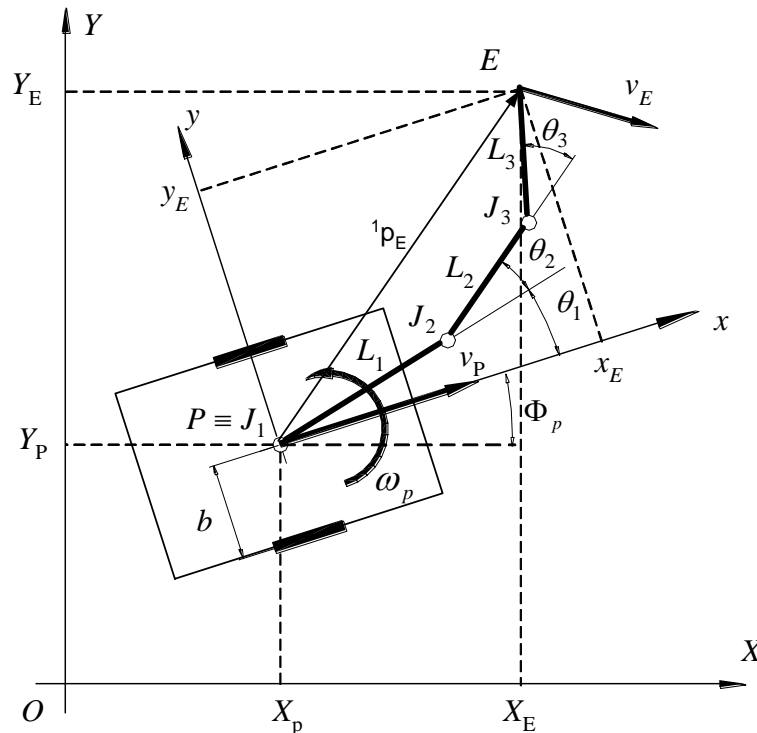


Fig 3. Schematic diagram of mobile platform-manipulator

The mobile manipulator is composed of a wheeled mobile platform and a manipulator. The manipulator has two independent driving wheels which are at the center of each side and two passive castor wheels which are at the center of the front and the rear of the platform.

Fig 3 shows the schematic of the mobile manipulator considered in this paper. The following notations will be used in the derivation of the dynamic equations and kinematic equations of motion.

**2.1 Kinematic equations**

Consider a three-linked manipulator as shown in Fig 3. The velocity vector of the end-effector with respect to the moving frame is given by (1).

$${}^1V_E = J\dot{\theta} \tag{1}$$

Where  ${}^1V_E = [\dot{x}_E \ \dot{y}_E \ \dot{\phi}_E]^T$  is the velocity vector of the end-effector with respect to the moving frame,  $\dot{\theta} = [\dot{\theta}_1 \ \dot{\theta}_2 \ \dot{\theta}_3]^T$  is the angular velocity vector of the revolution joints of the three-linked manipulator, and J is the Jacobian matrix.

$$J = \begin{bmatrix} -L_3S_{123} - L_2S_{12} - L_1S_1 & -L_3S_{123} - L_2S_{12} & -L_3S_{123} \\ L_3C_{123} + L_2C_{12} + L_1C_1 & L_3C_{123} + L_2C_{12} & L_3C_{123} \\ 1 & 1 & 1 \end{bmatrix} \tag{2}$$

where  $L_1, L_2, L_3$  are the length of links of the manipulator, and

$$C_1 = \cos(\theta_1); S_1 = \sin(\theta_1); C_{12} = \cos(\theta_1 + \theta_2)$$

$$C_{123} = \cos(\theta_1 + \theta_2 + \theta_3); S_{12} = \sin(\theta_1 + \theta_2);$$

$$S_{123} = \sin(\theta_1 + \theta_2 + \theta_3);$$

The dynamic equation of the end-effector of the manipulator with respect to the world frame is obtained as follows:

$$V_E = V_P + W_P \times {}^0Rot_1 {}^1p_E + {}^0Rot_1 {}^1v_E \tag{3}$$

Where

$$v_E = \begin{bmatrix} \dot{X}_E \\ \dot{Y}_E \\ \dot{\Phi}_E \end{bmatrix}; v_P = \begin{bmatrix} \dot{X}_P \\ \dot{Y}_P \\ \dot{\Phi}_P \end{bmatrix}; W_P = \begin{bmatrix} 0 \\ 0 \\ \dot{\Phi}_P \end{bmatrix}; {}^1p_E = \begin{bmatrix} x_E \\ y_E \\ \phi_E \end{bmatrix}; {}^1p_E = \begin{bmatrix} L_1C_1 + L_2C_{12} + L_3C_{123} \\ L_1S_1 + L_2S_{12} + L_3S_{123} \\ \phi_E \end{bmatrix}; {}^0Rot_1 = \begin{bmatrix} \cos \Phi_P & -\sin \Phi_P & 0 \\ \sin \Phi_P & \cos \Phi_P & 0 \\ 0 & 0 & 1 \end{bmatrix}$$

$$\Phi_E = \theta_1 + \theta_2 + \theta_3 + \Phi_p - \frac{\pi}{2}; \dot{\Phi}_E = \dot{\theta}_1 + \dot{\theta}_2 + \dot{\theta}_3 + \dot{\Phi}_p$$

The relationship between  $v$ ,  $\omega$  and the angular velocities of two driving wheels is given by

$$\begin{bmatrix} \omega_R \\ \omega_L \end{bmatrix} = \begin{bmatrix} 1/r & b/r \\ 1/r & -b/r \end{bmatrix} \begin{bmatrix} v_p \\ \omega_p \end{bmatrix} \tag{4}$$

Where  $b$  is the distance between the driving wheels and the axis of symmetry,  $r$  is the radius of each driving wheel.

The linear velocity and the angular velocity of the end-effector in the world coordinate (frame X-Y)

$$v_E = \dot{X}_E \cos \Phi_E + \dot{Y}_E \sin \Phi_E; \omega_E = \dot{\Phi}_E \tag{5}$$

**2.2 Dynamic equations**

In this application, the welding speed is very slow so that the manipulator motion during the transient time is assumed as a disturbance for MP. For this reason, the dynamic equation of the MP under nonholonomic constraints in  $A(q_v)\dot{q}_v = 0$  is described by Euler-Lagrange formulation as follows:

$$M_v(q_v)\ddot{q}_v + C_v(q_v, \dot{q}_v)\dot{q}_v = E(q_v)\tau_v - A^T(q_v)\lambda \tag{6}$$

where

$$A(q_v) = \begin{bmatrix} -\sin \Phi_p & \cos \Phi_p & 0 \end{bmatrix}; q_v = \begin{bmatrix} X_p & Y_p & \Phi_p \end{bmatrix}^T$$

$$M_v(q_v) = \begin{bmatrix} m + \frac{2I_w}{r^2} & 0 & -m_c d \sin \Phi_p \\ 0 & m + \frac{2I_w}{r^2} & m_c d \cos \Phi_p \\ -m_c d \sin \Phi_p & m_c d \cos \Phi_p & I + \frac{I_w}{2c^2} \end{bmatrix}$$

$$C_v(q_v, \dot{q}_v) = \begin{bmatrix} 0 & 0 & -m_c d \dot{\Phi}_p \cos \Phi_p \\ 0 & 0 & -m_c d \dot{\Phi}_p \sin \Phi_p \\ 0 & 0 & 0 \end{bmatrix}$$

$$E(q_v) = \frac{1}{r} \begin{bmatrix} \cos \Phi_p & \cos \Phi_p \\ \sin \Phi_p & \sin \Phi_p \\ b & -b \end{bmatrix}; \tau_v = \begin{bmatrix} \tau_R \\ \tau_L \end{bmatrix}$$

$$\lambda = \left( m + \frac{2I_w}{r^2} \right) (\dot{X}_p \cos \Phi_p + \dot{Y}_p \sin \Phi_p) \dot{\Phi}_p + m_c d \ddot{\Phi}_p$$

Consider a WMM as shown in Fig 3. It is model under the following assumptions:

- The MP has two driving wheels for body motion, and those are positioned on an axis passed through its geometric center.
- The three-linked manipulator is mounted on the geometric center of the MP.
- The distance between the mass center and the rotation center of the MP is  $d$ . Fig 3 doesn't show this distance. This value will be presented in the dynamic equation of MP.
- A magnet is set up at the bottom of the WMM to avoid slipping.

In Fig 3,  $(X_p, Y_p)$  is a center coordinate of the MP,  $\Phi_p$  is heading angle of the MP,  $\omega_R, \omega_L$  is angular velocities of the right and the left wheels,  $\tau_v = [\tau_R \quad \tau_L]^T$  is torques vector of the motors acting on the right and the left wheels,  $2b$  is distance between driving wheel,  $r$  is radius of driving wheel,  $m_c$  is mass of the WMM without the driving wheels,  $m$  is mass of each driving wheel with its motor,  $I_w$  is moment of inertia of wheel and its motor about the wheel axis,  $I$  is moment of inertia of wheel and its motor about the wheel diameter axis and  $I_c$  is moment of inertia of the body about the vertical axis through the mass center.

$$m = m_c + 2m_w; \quad I = I_c + 2m_w b^2 + 2I_m$$

III. CONTROLLERS DESIGN

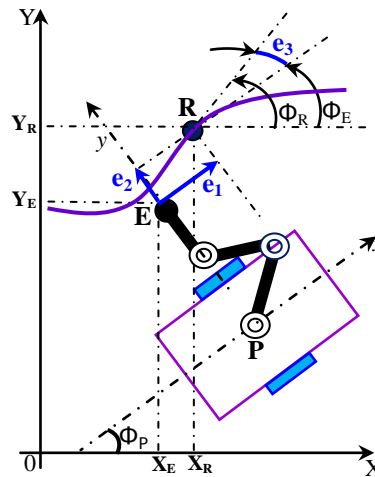


Fig 4. Scheme for deriving the tracking error vector  $E_E$  of manipulator

As the view point of control, this thesis addressed to an adaptive dynamic control algorithm. All of them are based on the Lyapunov function to guarantee the asymptotically stability of the system and based on the decentralized motion control method to establish the kinematic and dynamic models of system.

3.1 Defined the errors

From Fig 4, the tracking error vector  $E_E$  is defined as follows:

$$E_E = \begin{bmatrix} e_1 \\ e_2 \\ e_3 \end{bmatrix} = \begin{bmatrix} \cos \Phi_E & \sin \Phi_E & 0 \\ -\sin \Phi_E & \cos \Phi_E & 0 \\ 0 & 0 & 1 \end{bmatrix} \begin{bmatrix} X_R - X_E \\ Y_R - Y_E \\ \Phi_R - \Phi_E \end{bmatrix} \tag{7}$$

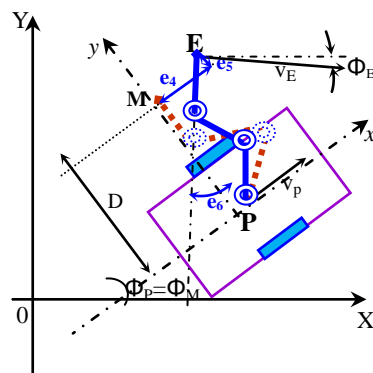


Fig 5. Scheme for deriving the MP tracking error vector

From Fig. 5, A new tracking error vector  $E_M$  for MP is defined as follows:

$$E_M = \begin{bmatrix} e_4 \\ e_5 \\ e_6 \end{bmatrix} = \begin{bmatrix} \cos \Phi_M & \sin \Phi_M & 0 \\ -\sin \Phi_M & \cos \Phi_M & 0 \\ 0 & 0 & 1 \end{bmatrix} \begin{bmatrix} X_E - X_M \\ Y_E - Y_M \\ \Phi_E - \Phi_M \end{bmatrix} \tag{8}$$

3.2 Kinematic controller design for manipulator

To obtain the kinematic controller a back stepping method is used. The Lyapunov function is proposed as follows:

$$V_0 = \frac{1}{2} E_E^T E_E \tag{9}$$

The first derivative of  $V_0$  yields

$$\dot{V}_0 = \dot{E}_E^T E_E \tag{10}$$

To achieve the negativeness of  $\dot{V}_0$ , the following equation must be satisfied

$$\dot{E}_E = -KE_E \tag{11}$$

where  $K = \text{diag}(k_1 \ k_2 \ k_3)$  with  $k_1, k_2$  and  $k_3$  are the positive constants. Substituting (1), (3) and (7) into (11) yields

$$\dot{\theta} = J^{-1} {}^0\text{Rot}_1^{-1} [A^{-1}(\dot{A}A^{-1} + K)E_E + V_R - V_P - W_p \times {}^0\text{Rot}_1^{-1} p_E] \tag{12}$$

### 3.3 Kinematic controller design for mobile platform

The Lyapunove function is proposed as follows:

$$V_1 = \frac{1}{2} E_M^T E_M \tag{13}$$

The first derivative of  $V_1$  yields

$$\dot{V}_1 = \dot{E}_M^T E_M \tag{14}$$

To achieve the negativeness of  $\dot{V}_0$ , the following equation must be satisfied

$$\begin{aligned} v_p &= v_E \cos e_6 + D\omega_p + k_4 e_4 \\ \omega_p &= \omega_E + v_E \sin e_6 + k_5 e_5 + k_6 e_6 \end{aligned} \tag{15}$$

with  $k_4, k_5$  and  $k_6$  are the positive constants.

### 3.4 Adaptive sliding mode controller design

To design a sliding mode controller, the sliding surfaces are defined as follows:

$$s = \begin{bmatrix} s_1 \\ s_2 \end{bmatrix} = \begin{bmatrix} \dot{e}_4 + k_4 e_4 \\ \dot{e}_6 + k_6 e_6 + k_5 \psi(e_6) e_5 \end{bmatrix} \tag{16}$$

where  $k_4, k_5$  and  $k_6$  are positive constant values.  $\psi(e_6)$  is a bounding function and is defined as follows:

$$\psi(e_6) = \begin{cases} 0 \rightarrow 1 & \text{if } |e_6| \leq \varepsilon \\ 1 \rightarrow 0 & \text{if } |e_6| \geq 2\varepsilon \\ \text{no change} & \varepsilon < |e_6| < 2\varepsilon \end{cases} \tag{17}$$

Where  $\varepsilon$  is a positive constant value.

The following procedure will design an adaptation law  $\hat{p}$  and a control law  $u$  which stabilize and converge the sliding surface  $s \rightarrow 0$  as  $t \rightarrow \infty$

Firstly, the adaptation law is proposed as the following:

$$\dot{\hat{p}} = -\xi^{-1} s^T(t) \tag{18}$$

Where  $\hat{p} = [\hat{p}_1 \ \hat{p}_2]^T$  is an estimate value of  $f = [f_1 \ f_2]^T$ ;  $\xi^{-1} = [\xi_1^{-1} \ \xi_2^{-1}]^T$  is positive definite vector which denotes as an adaptation gain and.

The estimation error is defined as follows:

$$\tilde{p} = f - \hat{p} \Rightarrow \hat{p} = f - \tilde{p} \tag{19}$$

Secondly, the control law  $u$  is chosen as follows:

To satisfy the Lyapunov's stability condition  $\dot{V} \leq 0$ , the following proposed controller  $u_{mb}$  can be calculated as follows:

$$u_{mb} = \begin{bmatrix} \dot{e}_5 \omega_r + (e_5 + D)\dot{\omega}_r - v_E \dot{e}_6 \sin e_6 \\ \dot{e}_3 \end{bmatrix} + \begin{bmatrix} k_4 \dot{e}_4 \\ k_6 \dot{e}_6 + k_5 \psi(e_6) \dot{e}_5 \end{bmatrix} + Qs^T + \hat{P} \tag{20}$$

where  $Q = \begin{bmatrix} q_{11} & 0 \\ 0 & q_{22} \end{bmatrix}$ ;  $\hat{P} = \begin{bmatrix} \hat{p}_1 & 0 \\ 0 & \hat{p}_2 \end{bmatrix}$

The above control laws  $u$  and adaptation law  $\hat{p}$  with the assumption (8) make the sliding surfaces in Eq. (16) be stabilized and converge to zero as  $t \rightarrow \infty$ .

### 3.5 Hardware design

#### Measurement of the errors

From Fig. 6, the tracking errors relations are given as

$$\begin{aligned}
 e_1 &= -r_s \sin e_3 \\
 e_2 &= d_e + r_s \cos e_3 \\
 e_3 &= \angle(O_1E, O_1O_3) - \frac{\pi}{2}
 \end{aligned}
 \tag{21}$$

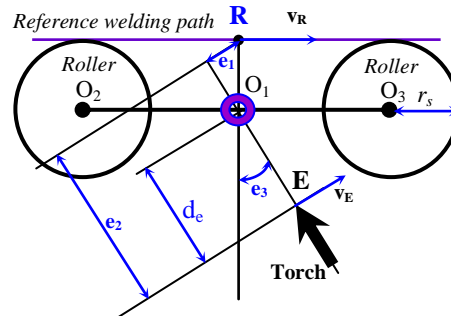


Fig 6. The scheme of measuring errors  $e_{1,2,3}$

From Fig. 5, the tracking errors  $e_4, e_5, e_6$  with respect to moving frame can be calculated as follows:

$$\begin{aligned}
 e_4 &= x_E - x_M = L_1 \cos \theta_1 + L_2 \cos(\theta_1 + \theta_2) + L_3 \cos(\theta_1 + \theta_2 + \theta_3) \\
 e_5 &= y_E - y_M = L_1 \sin \theta_1 + L_2 \sin(\theta_1 + \theta_2) + L_3 \sin(\theta_1 + \theta_2 + \theta_3) - D \\
 e_6 &= \phi_E - \frac{\pi}{2} = (\theta_1 + \theta_2 + \theta_3) - \frac{\pi}{2}
 \end{aligned}
 \tag{22}$$

3.6 Control algorithms

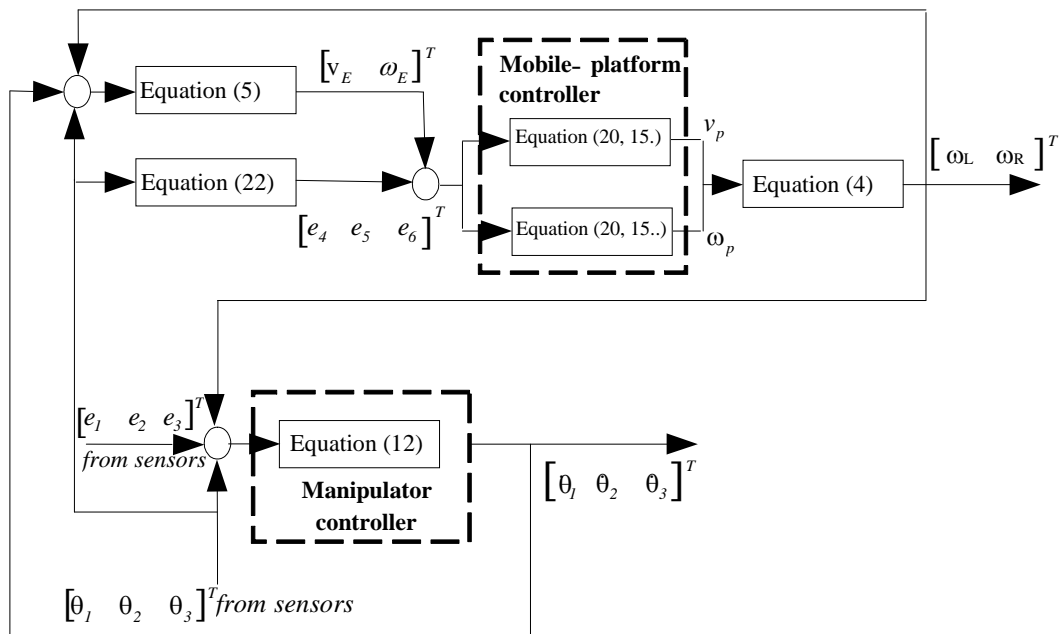


Fig 7. Block diagram of control system

The schematic diagram for a decentralized control method is shown in Fig 7. In this diagram, a relationship between controllers is illustrated by means of the output of this controller is one of the input of another controller and vice versa. The control task demands a real-time algorithm to guide the mobile manipulator in a given trajectory. Laser sensor, rotary potentiometer and linear potentiometer were adopted in the simulation to obtain the position and orientation of the mobile platform relative to the walls.

IV. SIMULATION RESULTS

In this section, some simulation results are presented to demonstrate the effectiveness of the control algorithm developed for Horizontal Fillet Joints welding.

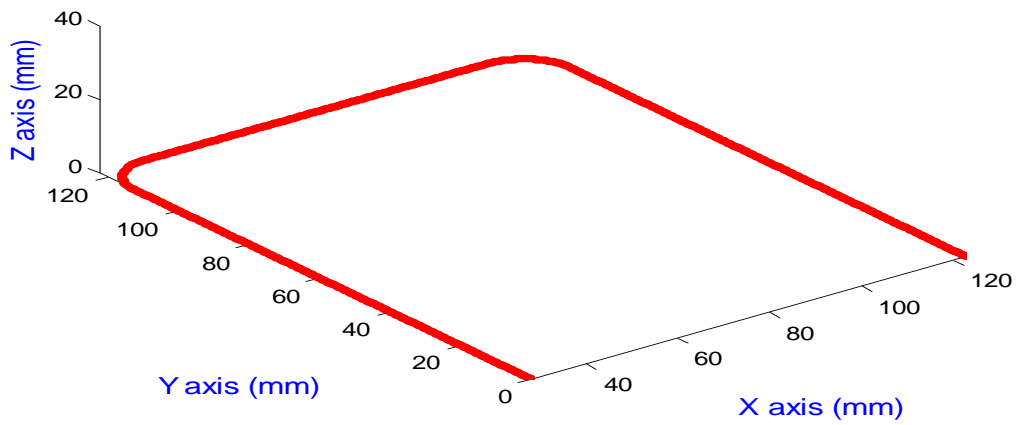


Fig 8. Welding reference trajectory

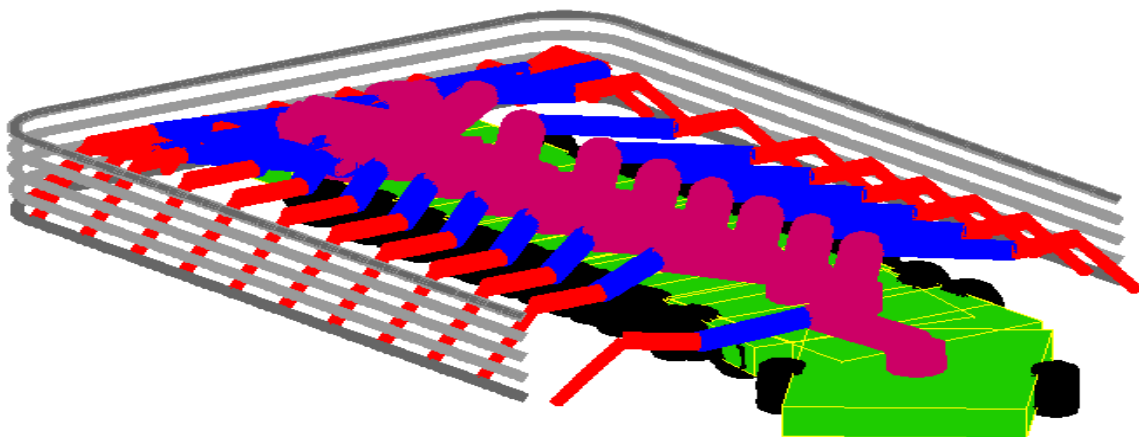


Fig 9. 3D model of the welding mobile manipulator

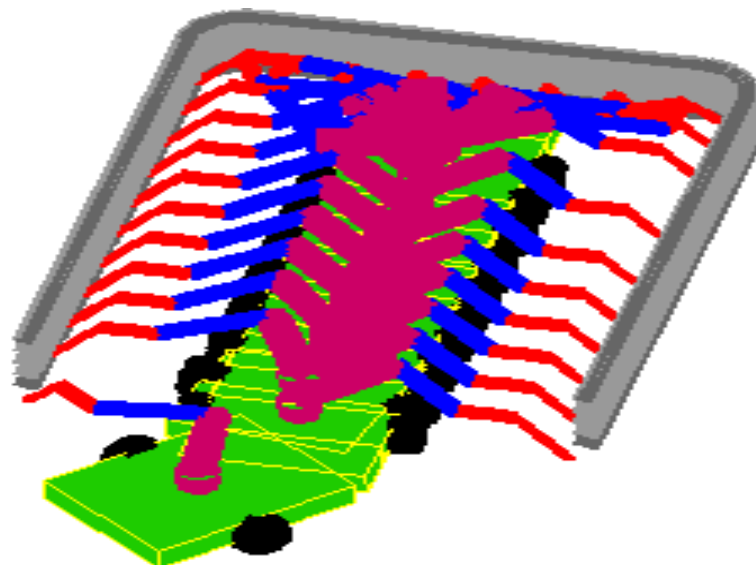


Fig 10. The WMM is tracking along the welding path



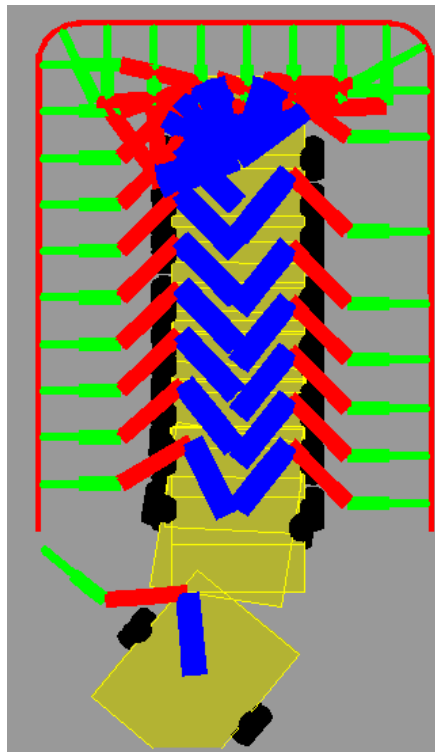


Fig 11. Different perspective about WMM.

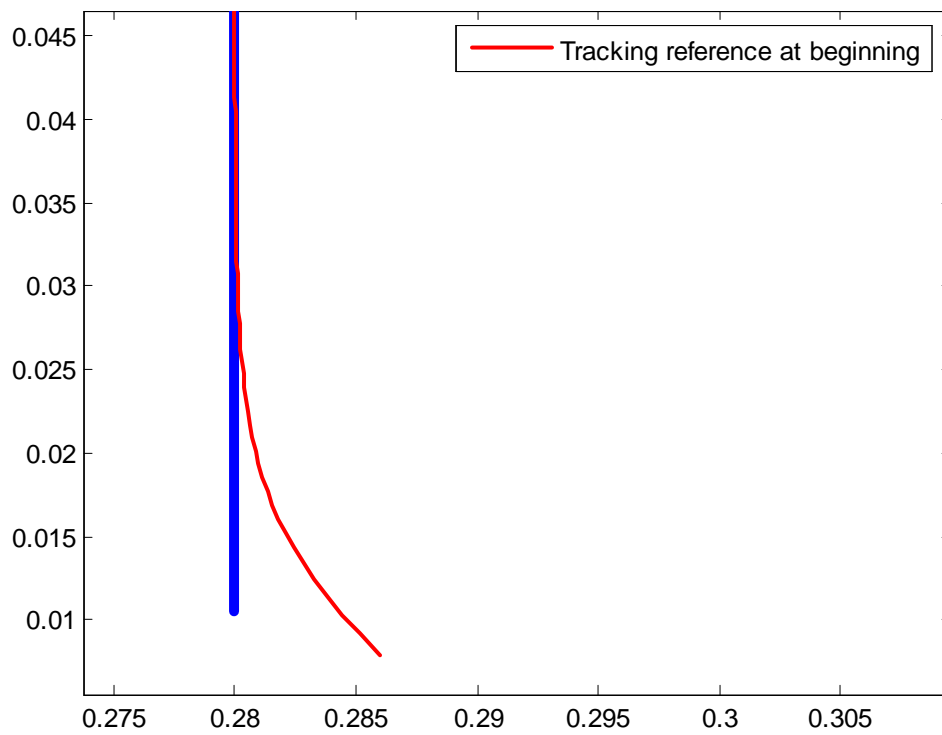


Fig 12. Trajectory of the end-effector and its reference at beginning

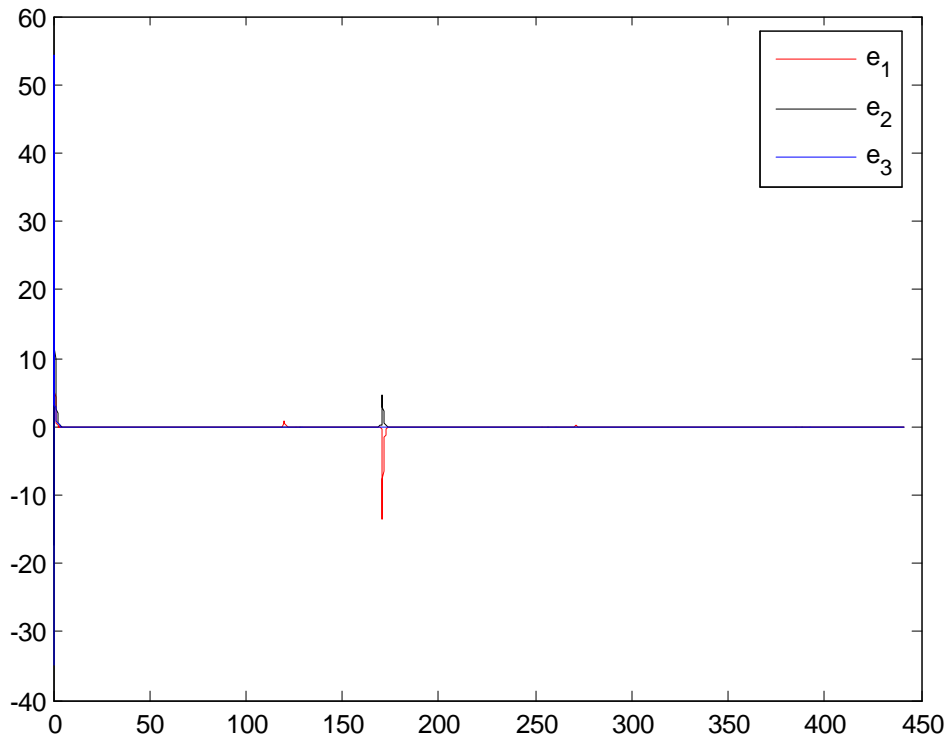


Fig 13. Tracking errors  $e_1$   $e_2$   $e_3$  at beginning

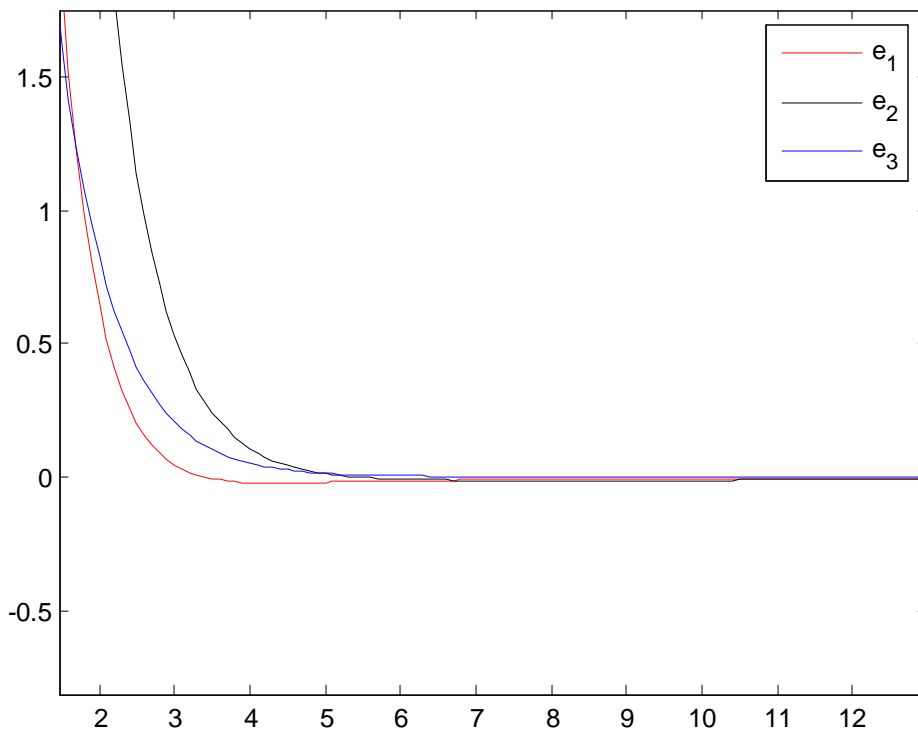


Fig 14. Tracking errors  $e_1$   $e_2$   $e_3$  at beginning (zoom in)

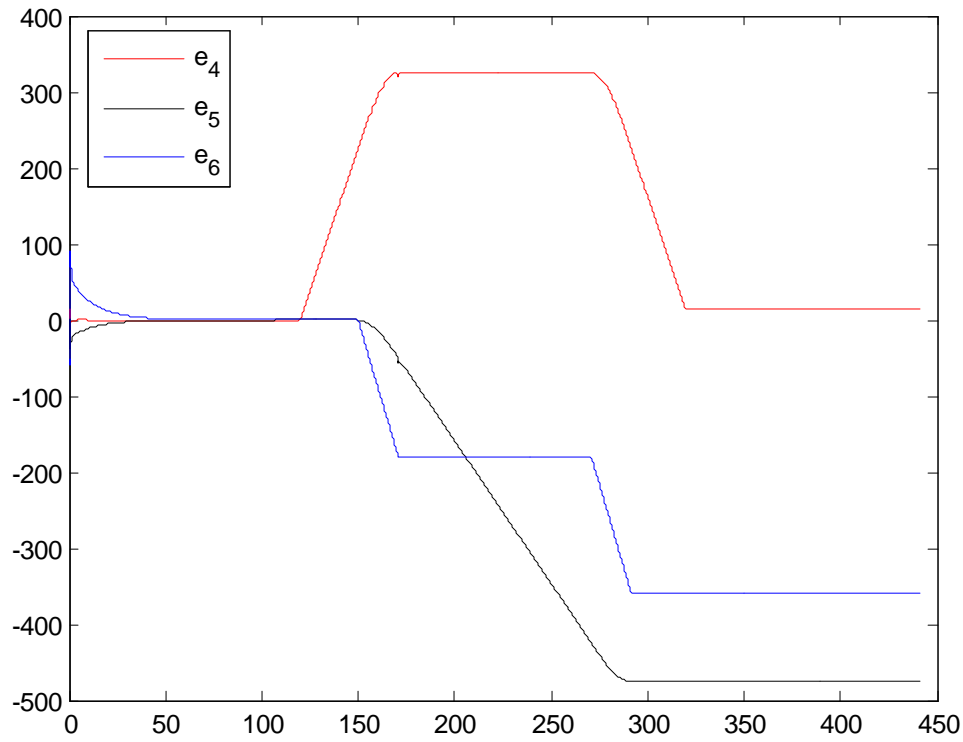


Fig 15. Tracking errors  $e_4$   $e_5$   $e_6$  at beginning

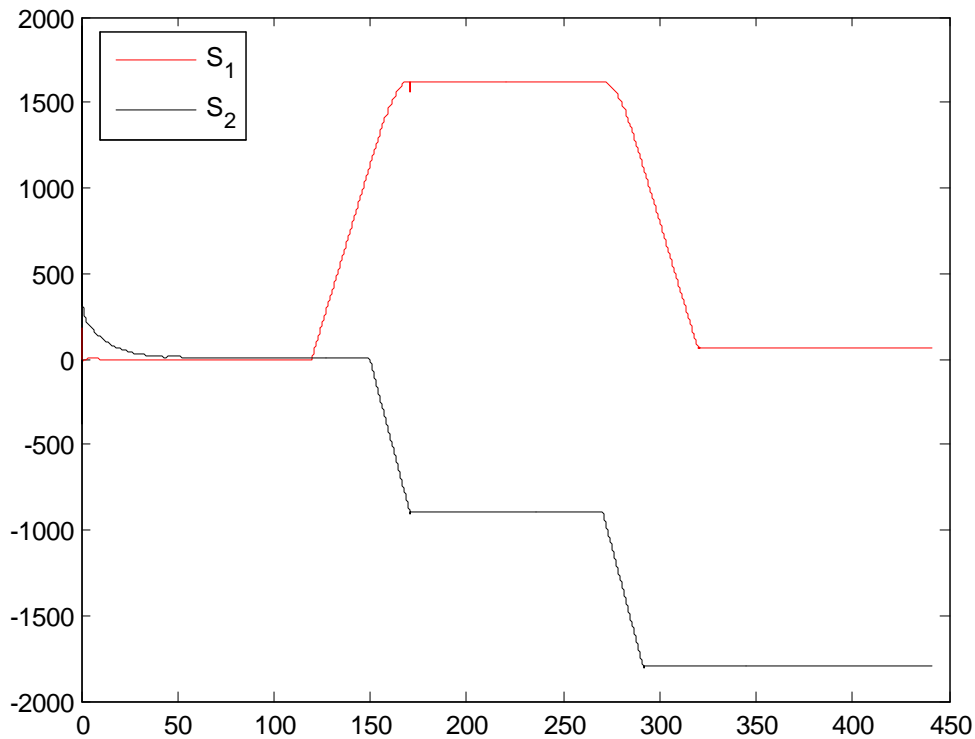


Fig 16. Sliding surfaces

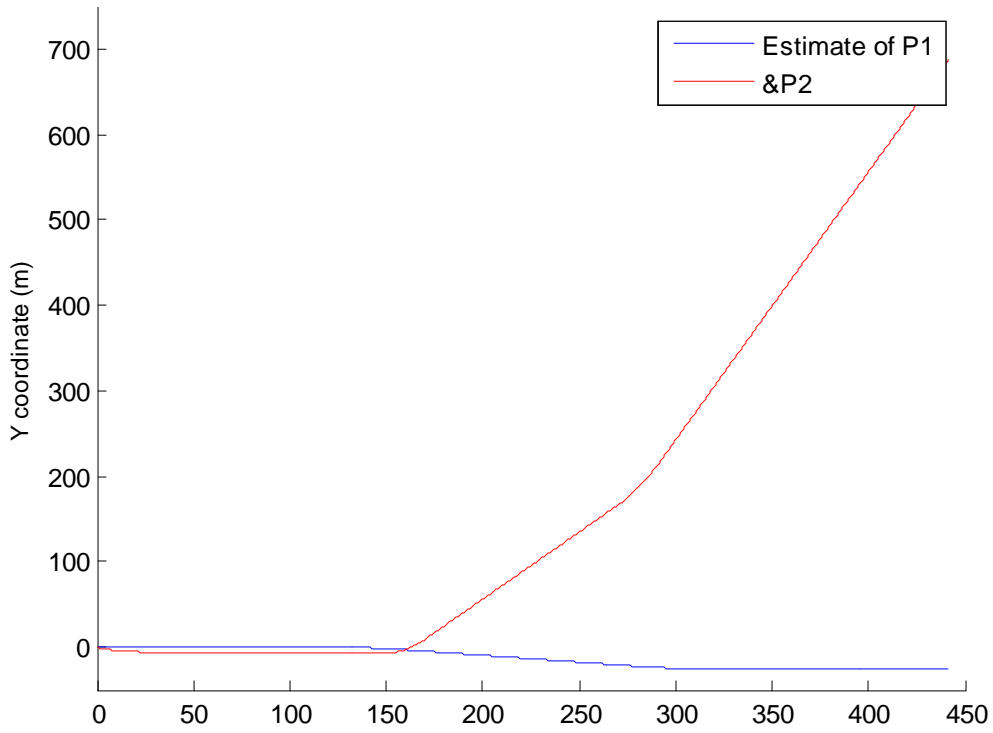


Fig 17. Estimated value of the P1 & P2

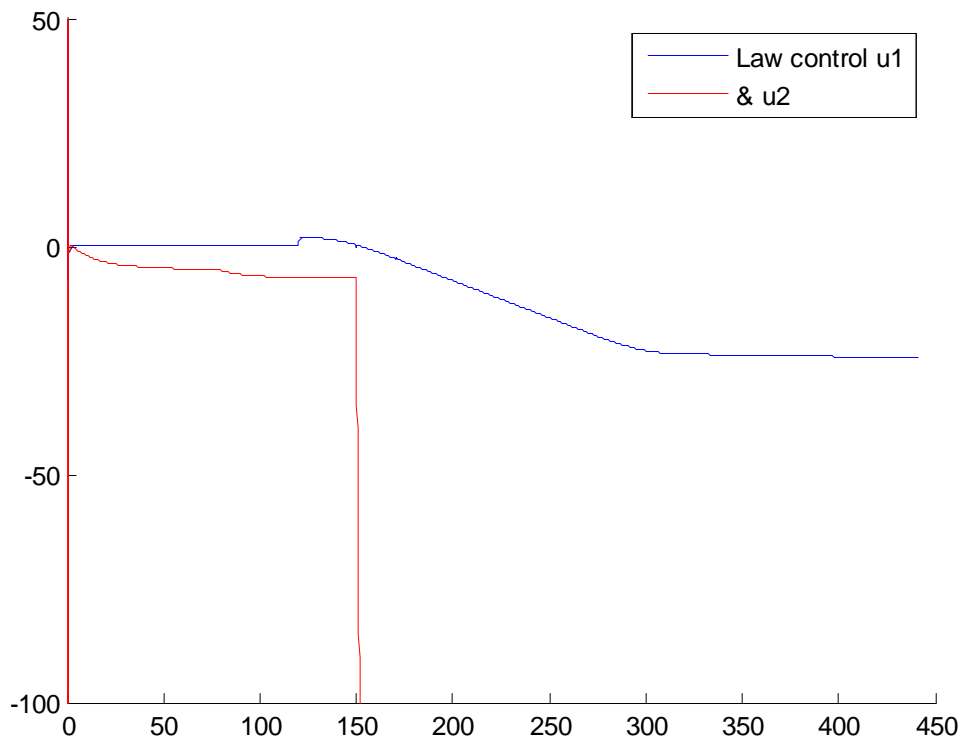


Fig 18. Law control

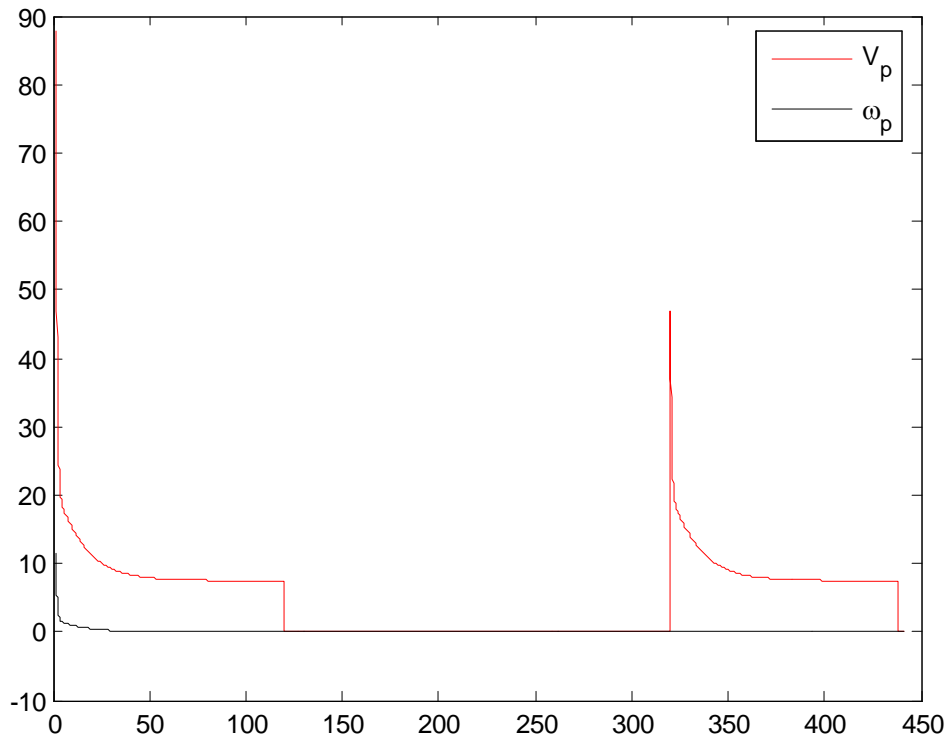


Fig 19. Angular velocity and velocity of the center point of platform

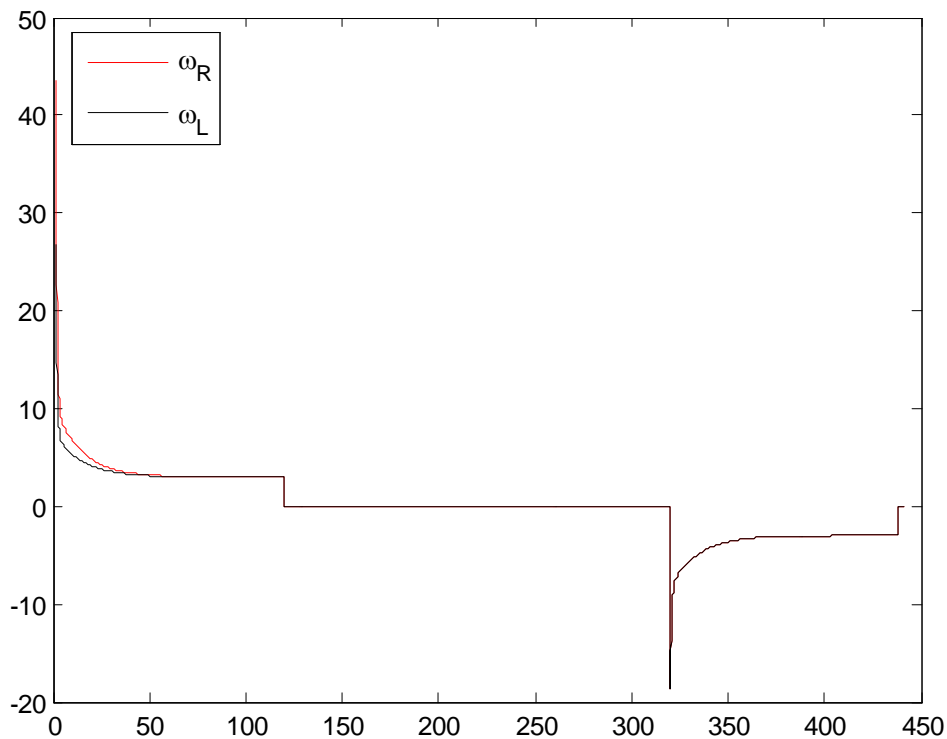


Fig 20. Angular velocities of the right and the left wheels

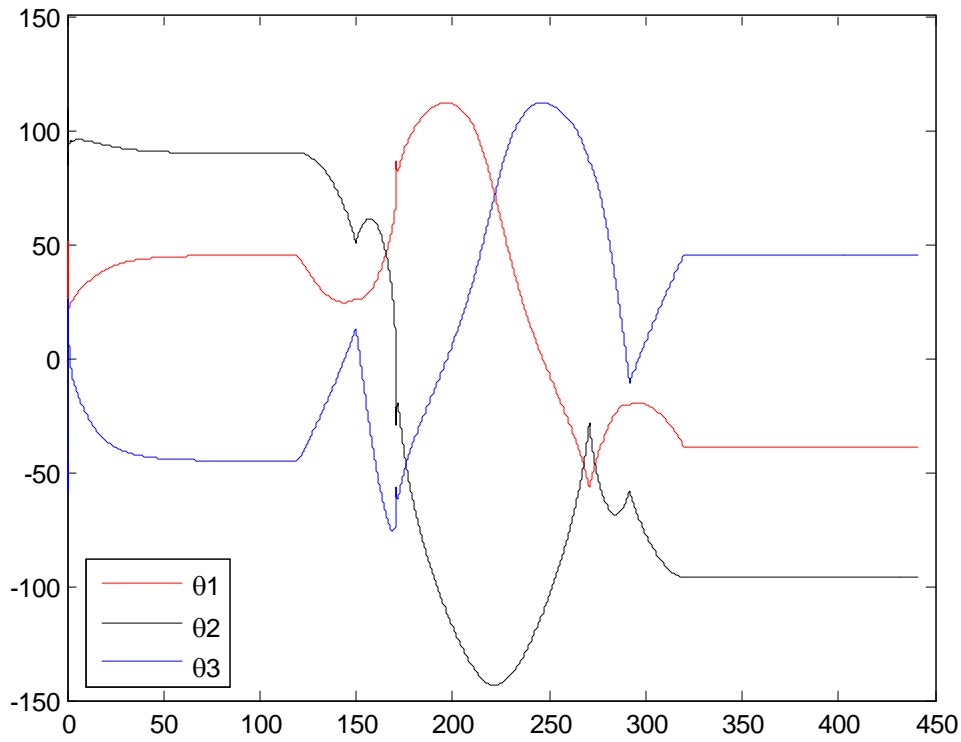


Fig 21. Angular of revolution joints

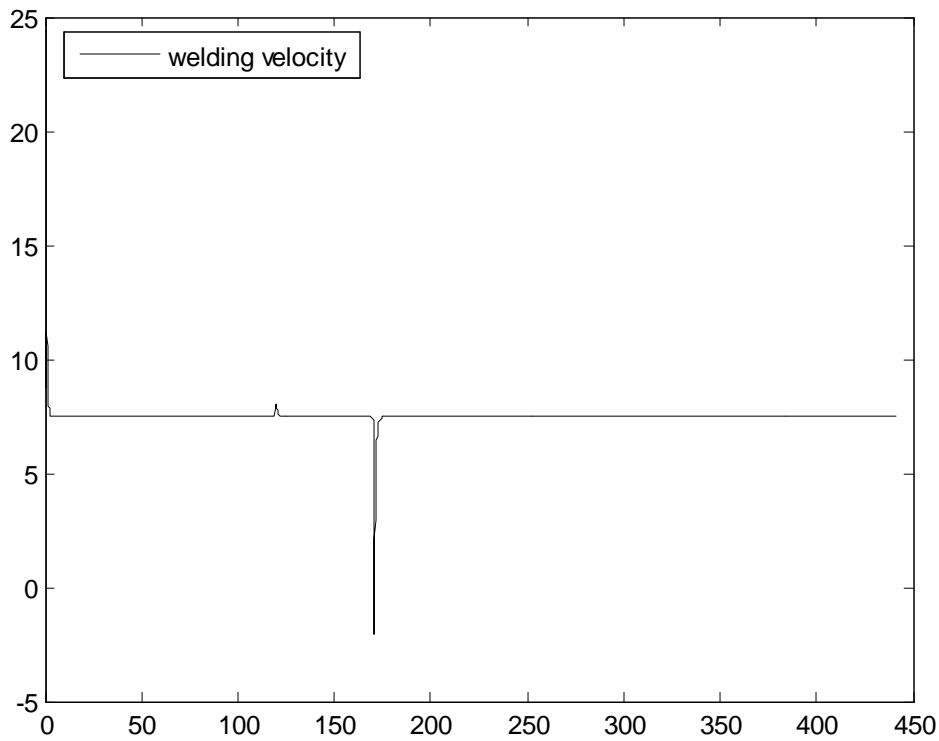


Fig 22. Linear and angular velocities of welding point

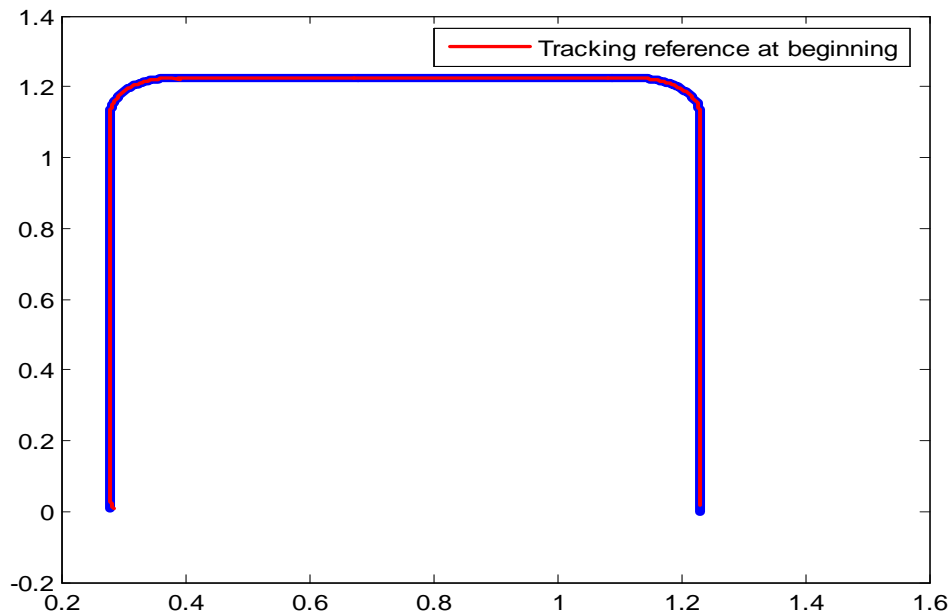


Fig 23. Results of trajectories of the end effector and its reference

## V. CONCLUSION

In this study, developed a WMM which can co-work between mobile platform and manipulator for tracking a long Horizontal Fillet Joints welding path. The main task of the control system is to control the end-effector or welding point of the WMM for tracking a welding point which is moved on the welding path with constant velocity. The angle of welding torch must be kept constant with respect to the welding curve. The WMM is divided into two subsystems and is controlled by decentralized controllers. The kinematic controller and adaptive sliding mode controller are designed to control the manipulator and the mobile-platform, respectively. These controllers are obtained based on the Lyapunov's function and its stability condition to ensure the error vectors to be asymptotically stable. From the simulation results are presented to illustrate the effectiveness of the proposed algorithm.

## REFERENCES

- [1] J. J. Craig, P. Hsu, and S. S. Sastry, "Adaptive Control of Mechanical Manipulators", *Proceedings of the IEEE International Conference on Robotics and Automation*, Vol. 2, pp. 190-195, 1986.
- [2] J. Lloyd, and V. Hayward, "Singularity Control of Robot Manipulator Using Closed Form Kinematic Solutions", *Proceedings of the Conference on Electrical and Computer Engineering*, Vol.2, pp. 1065-1068, 1993.
- [3] R. Fierro, and F. L. Lewis, "Control of a Nonholonomic Mobile Robot: Backstepping Kinematics into Dynamics", *Proceedings of the IEEE Conference on Decision and Control*, Vol. 4, pp. 3805-3810, 1995.
- [4] T. C. Lee, C. H. Lee, and C. C. Teng, "Adaptive Tracking Control of Nonholonomic Mobile Robots by Computed Torque", *Proceedings of the Conference on Decision and Control*, Vol. 2, pp. 1254-1259, 1999.
- [5] T. Fukao, H. Nakagawa, and N. Adachi, "Adaptive Tracking Control of a Nonholonomic Mobile Robot", *Transactions on Robotics and Automation*, Vol. 16, No. 5, pp. 609-615, 2000.
- [6] Tr. H. Bui, T. L. Chung, J. H. Suh, and S. B. Kim, "Adaptive Control for Tracking Trajectory of a Two Wheeled Welding Mobile Robot with Unknown Parameters", *Proceedings of the International Conference on Control, Automation and Systems*, pp. 191-196, 2003.
- [7] W. Dong, Y. Xu, and Q. Wang, "On Tracking Control of Mobile Manipulators", *Proceedings of the IEEE International Conference on Robotics and Automation*, Vol. 4, pp. 3455-3460, 2000.
- [8] Y. Kanayama, Y. Kimura, F. Miyazaki, and T. Noguchi, "A Stable Tracking Control Method for a Nonholonomic Mobile Robot", *Proceedings of the IEEE/RSJ International Workshop on Intelligent Robots and Systems*, Japan, Vol. 3, pp. 1236-1241, 1991.
- [9] Y. Tang, and G. Guerrero, "Decentralized Robust Control of Robot Manipulator", *Proceedings of the American Control Conference*, Pennsylvania, USA, pp. 922-926, June 1998.
- [10] Tan Tung Phan, Thien Phuc Tran, Trong Hieu Bui, and Sang Bong Kim, "Decentralized Control Method for Welding Mobile Manipulator", *Proceedings of the International Conference on Dynamics, Instrumentation, and Control*, Nanjin, China, pp. 171-180, August 18-20, 2004.
- [11] Ngo Manh Dung, Vo Hoang Duy, Nguyen Thanh Phuong, Sang Bong Kim\*, and Myung Suck Oh, "Two-Wheeled Welding Mobile Robot for Tracking a Smooth Curved Welding Path Using Adaptive Sliding-Mode Control Technique" *Proceedings of the International Journal of Control, Automation, and Systems*, vol. 5, no. 3, pp. 283-294, June 2007.
- [12] W.-S. Yoo, J.-D. Kim, S.-J. Na, "A study on a mobile platform-manipulator welding system for horizontal fillet joints" *Mechatronics* 11 (2001) 853-868

## OKUMURA-HATA: A PERFECT MODEL FOR DRIVING ROUTE UHF INVESTIGATION

Omohimire P. Omolaye<sup>#1</sup>, Gabriel A. Igwue<sup>#2</sup>, Godfrey A. Akpakwu<sup>#3</sup>

<sup>#1</sup>Dept. of Electrical and Electronics Engineering, University of Agriculture, Makurdi, Nigeria

<sup>#2</sup>Dept. of Electrical and Electronics Engineering, University of Agriculture, Makurdi, Nigeria

<sup>#3</sup>Dept. of Electrical and Electronics Engineering, University of Agriculture, Makurdi, Nigeria

**ABSTRACT:** *In today's competitive world, a successful utility must take maximum advantage of its resources, from people to equipment to information. Using GIS on RF to integrate geographic with other corporate data has become absolutely vital to this task. The truthfulness and understandability of information is dependent upon the way it is presented. Urban planner, biologist, geologist, hydrological engineer and RF engineer tend to discuss some common factor of interest by having a better understanding of their environment (the geographic space of their study area). All these professionals work with data that relates to space. Most precisely, they deal with questions related to geographic space, which might informally be characterized as having positioned data to the earth's surface. In this paper, we investigate and predict best model suitable for driving route of UHF wave propagation in Ondo state, Nigeria by comparing measured values using GIS equipment with the empirical results.*

**Keywords:** *GIS, Urban planner, Biologist, Geologist, Hydrological Engineer, RF engineer, UHF, Wave propagation*

### I. INTRODUCTION

The telecommunication industry is experiencing exponential growth, resulting in tough competition and an ever-increasing scope of services offered to subscribers. Solving the many business problems of a telecommunications company requires a good understanding of where your clients and facilities exist and information about those locations. GIS as a tool in partner with the field of remote sensing has become an important component for modelling radio wave prediction [1]. Urban planner, biologist, geologist, hydrological engineer and RF engineer tend to discuss some common factor of interest by having a better understanding of their environment (the geographic space of their study area). For instance, urban planner might like to find out about urban fringe growth in the city; a biologist might be interested in the impact of slash-and-burn practices on the population of an amphibian species in the forests; a geologist might identify the best localities for construction of building in an area with regular earthquakes occurrence by looking at rock formation characteristic; a geoinformatic engineer might be hired by a telecom giant to determine the best sites for the base stations, taking various accounts of cost factors such as land prices, undulation of the terrain, et cetera; an RF engineer might be interested in the signal strength evaluation and prediction of a particular sub-station. All these professionals work with data that relate to space. Most precisely, they deal with questions related to geographic space, which might informally be characterized as having positioned data to the earth's surface.

### II. LITERATURE REVIEW

Radio wave propagation is the study of the transfer of energy at radio frequencies from one point, a transmitter, to another, a receiver. Radio waves are part of the broad electromagnetic spectrum that extends from the very low frequencies which are produced by electric power facilities up to the extremely high frequencies of cosmic rays. All electromagnetic waves propagate at the same velocity, regardless of the frequency. A typical electromagnetic wave is light wave and the propagation velocity is often referred to as "the speed of light" ( $c$ ), which for a vacuum is approximately  $3 \times 10^8$  m/sec. The velocity of any wave is dependent upon the medium in



which it is travelling, but for simplicity is usually considered with respect to a vacuum. The frequency of a wave is defined in terms of the number of cycles per second or hertz (Hz) and is related to the wavelength ( $\lambda$ ) by the expression,  $f = \frac{c}{\lambda}$ . The Ultra High Frequency (UHF) band lies between 300 MHz and 3GHz which is the ideal choice for ground to air communication with wide band-width that propagate principally on line of sight (LOS) from the transmitter to the receiver. The effects of local area topography and conditions in the lower atmosphere mostly govern UHF propagation. For communication to take place, the transmitting and receiving antennas must have a fairly unobstructed path between them, hence the term line-of-sight [2]. Radio wave is a function of frequency of propagation, lower radio frequencies, such as AM/FM radio, have lower wavelengths which allow them to penetrate geographic features such as vegetation, building wall and others. As the wavelength decreases, the frequency increases which makes more influence by geographic feature in the environment [3] and thus [1] the quality of signal strength is extensively blocked or degraded by nature and man to the relatively short wavelength propagation.

In this vein, the prime importance of attenuation investigation and prediction for radio waves propagation can never be over emphasized by the communication researchers when dealing with planning, budgeting and design of high performance communication systems [4],[5],[6],[7]. From the transmitter, radio propagation takes different propagation path to the receiver which depends on the interaction with interfering objects along the path of propagation [8]. Therefore, the path that the radio wave will take depends on many factors such as frequency, antenna type and height, atmospheric conditions and terrain. So, it is important to discuss, understand and appreciate other propagation losses due to complex obstructions such as buildings, tunnels, forests, rainfall, ice, and other atmospheric conditions. Geographic features hinder the propagation of wave which can be easily modeled in visibility theory i.e line of sight theory [9].

The classification done by [10] grouped propagation models into three: deterministic, statistical and empirical models. Deterministic models accuracy is usually very high but at the expense of high computation complexity. This is because, it requires 3D data of the propagation environment and makes use of the physical laws which determine radio wave propagation mechanisms for a particular location. Stochastic models, on the other hand, require the least information about the environment, model the environment as a series of random variables but provide the least accuracy. Empirical models are based on extensive measurements and mainly give prediction of path loss which is more often used in practice than statistical and deterministic propagation models, because of low cost and model simplicity with acceptable accuracy. There are several radio frequency propagation models in which each is useful for specific environment and the accuracy of any of the model depends on the parameter required by the model and the environment. There is no universal model for all kinds of propagation situation. All propagation models are based on the terrain parameters (rural, urban and suburban area) and system parameters like antenna height, frequency [10]. Example of these models are Okumura-Hata model, Walfisch-Bertoni model, Eglic model, Erecg Model, COST 231-Hata model, 2D and 3D ray tracing, SUI model, COST -231-Walfisch-Ikegami, Cluster Factor, etc.

Until recently, empirical propagation prediction models seemed sufficient. However, more efficient prediction models are required in transmitting data (voice and non voice) from the antenna to the receiver. These propagation models are usually based on the computation of the physical interaction of radio waves and the environment. Thus, more detailed geo-databases of the environment are required, especially in urban environments where most users are located [17]. In broadcast frequency planning, GIS is relevant in base station programming, base station position selection, field strength prediction, coverage analysis, interference analysis, frequency distribution, and so on. For accurate prediction of radio wave, interference analysis and coverage calculation demand detailed location spatial database of the required area. As the wireless technology grows, the industry development trend uses geographic information system to strengthen TV broadcasting coverage network management and construction [12]. The inability of radio wave to penetrate or bend around geographic features which result in non line of sight can be easily modeled in geographical information system. GIS has ability to model the communication sheds (commshed) which is also known as the viewshed. Having the LOS properties of the wave length, the viewshed shows the zone where there will be signal [13].

In a study conducted in Eugene, Oregon, USA to investigate the impact of different groundcover data have on radio wave in a wireless network. The transmitting antenna was mounted at height 570 meters from the mean sea level and Eugene town was found to have 120m and 850m as the minimum and maximum elevation value respectively above the mean sea level. Signal strength measurement was carried out based on terrain and groundcover. The researchers calculated the signal strength at each location and developed a spatial signal pattern based on effect of

terrain [14]. [15] used GIS to predict radio wave coverage in Peru Mountain District using 16 Tx antenna locations with 100 meter height above the ground. The size of the study area was 343,820 square kilometers having a minimum elevation values of 136 meters above sea level and maximum values of 6,687 meters above sea level. Landuse in the mountains consists mostly of shrublands, 32%, grasslands, 32%, and tundra, 17%. Environmental Systems Research Institute’s (ESRI) ArcGIS 9.1 was used for prediction. The Okumura-Hata model path loss results were assessed based on the free space curve. The free space propagation formula was applied in a GIS environment to generate free-space path loss over distance for a Tx antenna. The Okumura-Hata model path loss curve was similar to the GIS generated free space model with the use of raster calculator. Values were tested at various locations and compared with values on the Okumura-Hata model curve which are similar.

**Features of The Study Area:** As shown below, the study area covers 25km from Ondo State Radiovision Corporation (OSRC) Antenna which lies within latitudes 6° 30’ 00” and 8° 00’ 00” and longitudes 4° 30’ 00” and 5° 30’ 00” with minimum elevation value of 204m above the mean sea level and maximum elevation value of 1065m above the mean sea level.

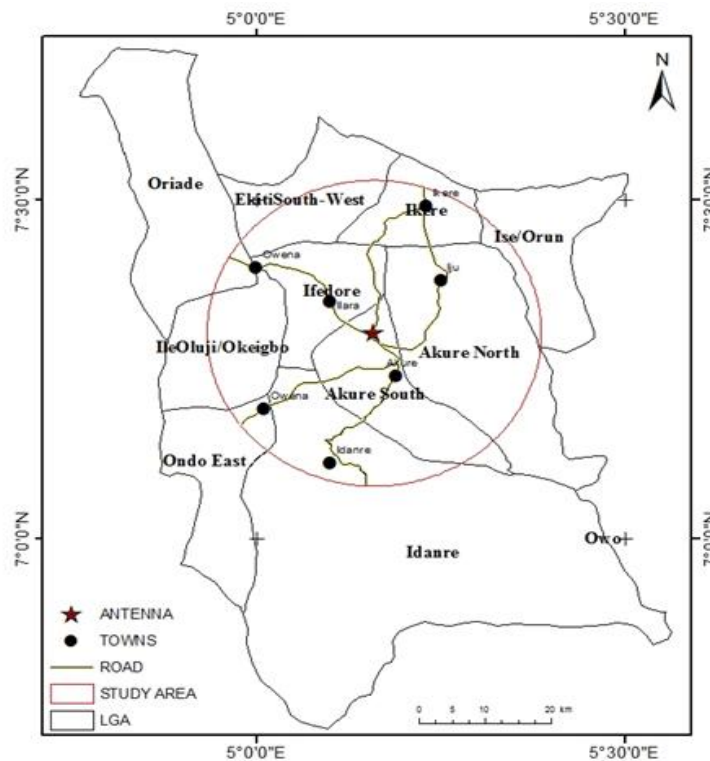


Fig 1: The map of the Study Area

### III. METHODOLOGY

Table 1: Data and their sources

Data	Year	Source	Relevance
Google image	2007	Google earth	For route design and navigation
ASTER	2011	USGS	For digital elevation model and spot height
Field measurement	2014	Self	For signal strength measurement
Antenna description	2013	OSRC	For path loss calculation
Landsat	2014	USGS	For landuse /cover classification

**A. Driving Route Test Design**

The GPS coordinate of the transmitting antenna was obtained. This was plotted in ArcGIS environment and 25km ring buffering around the transmitting antenna was carried out at 1km interval. Points where the buffer crosses the route were recorded. These coordinates were traced to the ground for signal observation. This was carried out based on terrain variation, land cover and distance from the antenna which served as a guide and to provide necessary navigation information. Five driving routes were followed which cut across the study area as shown below

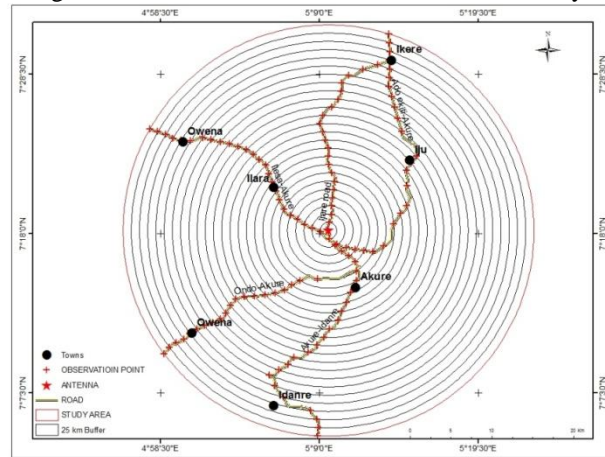


Fig 2: Driving route drive

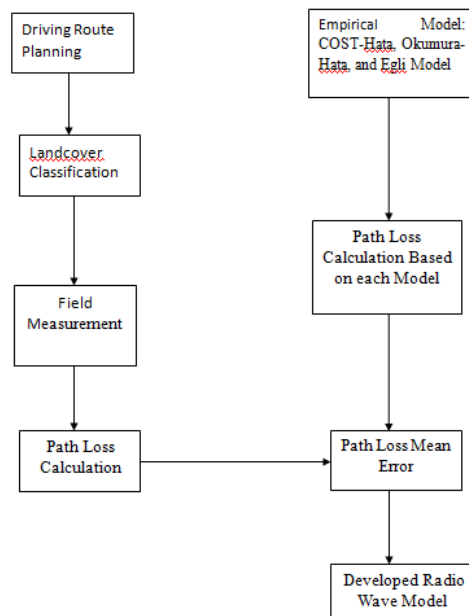


Fig 3: Work Flow Diagram

**B. Signal Strength Measurement**

The signal strength measurement was carried out at frequency 487.25MHz based on the coordinates obtained during driving route design. Coordinates information from ArcGIS software for every point of observation were used after carrying a ring buffer operation from the transmitting antenna at every 1km up to 25km. Signal strength across terrain variation was measured and recorded in every route

### C. Signal Strength Measurement with Expected Signal Strength Value:

The signal strength measurement was carried out based on the above route design. Measurements were carried out in different defined route land use type and terrain classification in order to predict signal strength. Distance and line of sight (LOS) from the transmitter to the receiver were considered. Field signal strength data were acquired within ten days. This was carried out in late January with little or no atmospheric interference. The measured signal was compared to theoretical value. Equation 1 was used to calculate theoretical values.

$$E \left( \frac{V}{m} \right) = \frac{\sqrt{30P_t G_t}}{d(LOS)} \quad (1)$$

where  $P_t$  is the transmitted power in (W),

$G_t$  is the gain of the transmitter,

$d$  is the LOS distance in (m).

### D. Signal Strength Measurement with Existing Models

The field measurements were carried out in the study area and compared with empirical models that were developed to predict signal strength. The empirical model used in this study are Okumura Hata, Egli and COST 123 model which were compared with field measurements in the study area in order to develop a base model for the study area. Equations 2, 3 and 4 were used to determine the corresponding path loss for each measurement taken.

$$E_h = \frac{88\sqrt{f}h_r h_t d_h^{N-2}}{\lambda d^2} \quad (2)$$

$$P_r = \frac{P_t G_t G_r}{PL} \quad (3)$$

$$P_r = \frac{P_t G_t G_r h_t^2 h_r^2}{d^4} \quad (4)$$

Where  $P_t$  is in watts,  $h_r$ ,  $h_t$  is in metre,  $d_h$ ,  $d$  are in Km and  $f$  is the frequency in MHz, [11].

## IV. RADIO WAVE PROPAGATION MODELS

All radio wave models are mathematical models to predict radio wave attenuation. Communication researchers make use of these models for planning, budgeting, design and managing of high performance communication systems. Measurements are mostly carried out for verification of the existing model and the measured observation [16]. There are several existing models for radio wave prediction reviewed in this research but the paper is limited to three models namely; Okumura-Hata, COST 123 and Egli model.

### A. Okumura-Hata Model

One of the most common propagation models for predicting signal attenuation in a macro cell environment. The model developed by Y. Okumura and M. Hata and is based on measurements in urban and suburban areas. Validity range of the model is frequency  $f_c$  between 150MHz and 1500 MHz, TX height  $h_b$  between 3 and 200 m, RX height  $h_m$  between 1 and 10m and TX-RX distance  $r$  between 1 and 10 km [9]. Okumura-Hata's equations are classified into three models. They are:

- Rural area: Open space, no tall trees or building in path.
- Suburban area: Village high-way scattered with trees and houses with some obstacles near the mobile station but not very congested.
- Urban area: Built up city or large town with large buildings and houses.

The Path loss for Okumura-Hata model is defined as below:

$$L(\text{dB}) = 69.55 + 26.16 \log_{10} f_c - 13.82 \log_{10} h_t e + (44.9 - 6.55 \log_{10} h_t e) \log_{10} R - E \quad (5)$$

- Suburban areas path loss (dB)

$$L(\text{dB})=69.55+26.16\log_{10} fc-13.82 \log_{10} hte+(44.9 -6.55 [(\log_{10} fc/28)^2+5.4]) \quad (6)$$

- Rural path loss (dB)

$$L(\text{dB})=69.55+26.16 \log_{10} fc -13.82\log_{10} hte +(44.9 - 6.55 \log_{10} hte) \log_{10} R - 4.78 (\log_{10} fc)^2+18.33\log_{10} fc + 40.94. \quad (7)$$

where

- $h_m$ : mobile station antenna height above local terrain height [m]
- $d_m$ : distance between the mobile and the building
- $h_0$ : typical height of a building above local terrain height [m]
- $h_{te}$ : base station antenna height above local terrain height [m]
- $r$ : great circle distance between base station and mobile [m]
- $R = r * 10^{-3}$  great circle distance between base station and mobile [km]
- $f$ : carrier frequency [Hz]
- $f_c : f * 10^{-6}$  carrier frequency [MHz]
- $\lambda$ : free space wavelength [m]

### B. Egli Model

The Egli model's ease of implementation and agreement with empirical data make it a popular choice, particularly for a first analysis. The Egli model for median path loss over irregular terrain is given as

$$L_{50} = G_b G_m \left[ \frac{h_b h_m}{d^2} \right]^2 \beta \quad (8)$$

where  $G_b$  is the gain of the base antenna,

$G_m$  is the gain of the mobile antenna,

$h_b$  is the height of the base antenna,

$h_m$  is the height of the mobile antenna,

$d$  is the propagation distance,

$\beta = (40/f)^2$ , where  $f$  is in MHz

### C. COST 231 (Walfisch and Ikegami) Model

This model is a combination of the models from J. Walfisch and F. Ikegami. It was further developed by the COST 231 project. The frequency ranges from 800 MHz to 2000 MHz. This model is used primarily in Europe for the GSM1900 system [9].

Path Loss,

$$L_{50} (\text{dB}) = L_f + L_{rts} + L_{ms} \quad (11)$$

where,  $L_f$  = free-space loss,

$L_{rts}$  = rooftop to street diffraction and scatter loss,

$L_{ms}$  = multiscreen loss

Free space loss is given as

$$L_f = 32.4 + 20 \log d + 20 \log f_c \text{ dB} \quad (12)$$

## V. RESULT AND DISCUSSION

With the disparity shown between the measured values along the five chosen routes, it could be deduced that the propagation here suffered attenuation caused by physical environment, atmospheric refraction, and the natural atmosphere induced propagation delays. In the natural atmosphere, delays are induced by refractivity of gases, hydrometers, and other particulates, depending on their permittivity and concentration, and forward scattering from hydrometers and other particulates. Changes in temperature, moisture, and pressure in the atmospheric column cause a change in atmospheric density, which in turn causes variations in the intensity of waves in both the vertical and horizontal. Reflection and diffraction caused by obstruction (buildings, mountains with different elevations among others) and the effect of tree density with foliage along the paths chosen.

The path loss calculated for the three models is a function of LOS (observation points). The reason behind the choice of these models for path loss prediction lies in the fact that they form part of existing models which have wide

acceptability and are currently in use for mobile radio propagation. Their specifications and conditions were met by the parameters of this research work. When compared with measured path loss, the mean deviation errors of the models used for the predictions were then generated. These prediction errors were calculated as the difference between the measurement and prediction.

**A. Signal strength of the study area**

It was noticed and fully observed that there are direct line of sight between the transmitter and the receiver but the signal strength reduces as receiver is moved away from the transmitter. The reduction in signal strength is not uniform which is as a result of attenuation caused by land cover/use, atmospheric refraction and other factors. The signal strength map was classified into five categories based on field strength observed. At 2km away from the transmitter, the signal strength is strong and stable but as the receiver moved further away from the transmitter, the signal reduce gradually because each route differed as elements within the propagation zone also differed.

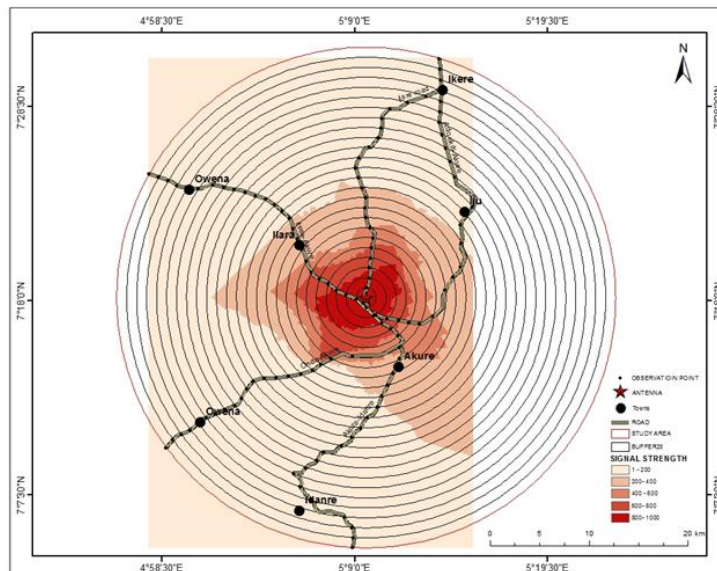


Fig 4: Signal strength map of the study area

**B. Various measured against the theoretical value**

After determining the field measurements for each route, the observations were made in order to make a comparison between the measured and theoretical values and the results clearly show that the measured value is less than the theoretical value due to geographical element and other factors along the path of propagation.

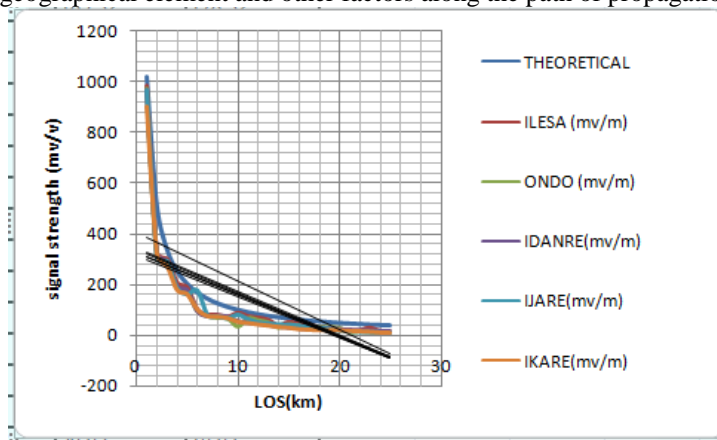


Fig 5: Various measurements against theoretical value

**C. Path Loss Prediction**

From the above diagram, Path loss for each model was calculated at each LOS. The result show that Egli model assumes that there is obstruction such as buildings and hilly area that is why the path loss is low which is not true while Okumura-Hata and COST 231 shows better prediction of signal strength. The overlap that occurs between the two models is that Okumura Hata model was modified to develop COST 231 model.

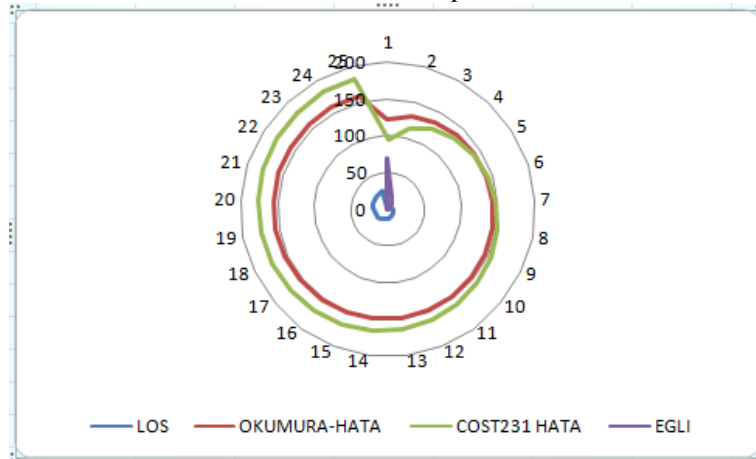


Fig 6: Path Loss Prediction radar graph

**D. Comparism of Empirical Models with Measurements**

The corresponding error statistics in terms of the mean prediction error is shown below. Note that PLME in the graph means Path loss mean error. It was observed from the analysis that out of the three models considered, Okumura-Hata model has minimum error of 52.08dB along Ilesha route, 50.02dB along Ondo route, 48.62dB along Idanre route, 50.05dB along Ijare route and 46.85dB along Ekiti route.

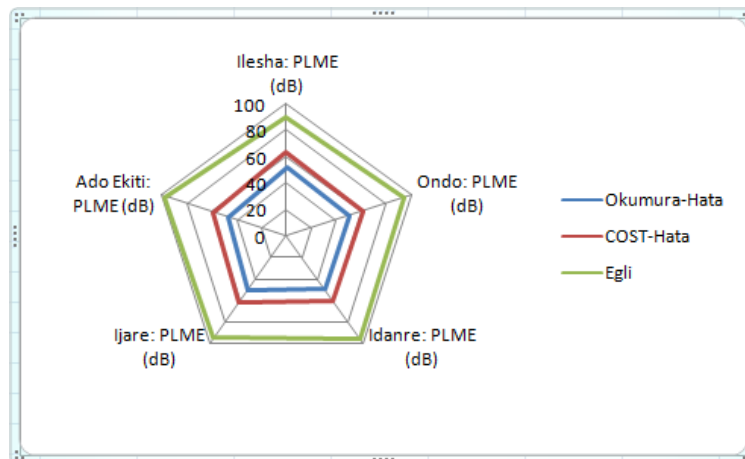


Fig 7: Comparism of Empirical Models with Measurements graph

**VI. CONCLUSIONS**

In this research work, field measurement and the corresponding elevation data was obtained. Signal strength map of the study area was developed by surface interpolation and the path loss for measured signal for each route was calculated and compared for the three empirical propagation models along the selected five routes. Field strength measurements taken were compared with the predictions made by the three propagation models used. The results of measurement were validated with theoretical models. Disparity shows that the presence of vegetation produces a constant loss independent of distance between communication terminals that are spaced 1 km or more apart.

The corresponding error statistics in terms of the mean prediction error and the prediction errors were calculated as the mean of the differences between the measurement and prediction. It could be observed clearly that all the three empirical models under-predicted the path loss with COST-Hata model and most especially Egli model grossly under predicted the path loss (i.e. Okumura-Hata model has minimum error in the prediction). Also shown is that all the three empirical models considered under-predicted the path loss with Okumura-Hata model and most especially Egli's model grossly under predicted the path loss (i.e. COST231-Hata model has minimum error in the prediction). Consequently, Okumura-Hata's model is best suitable for prediction along the five routes

## REFERENCES

- [1] Rose, S. (2001.). *The Effect of Digital Elevation Model Resolution on Wave Propagation Predictions at 24 GHz*. Virginia Tech.: MS thesis in Geography.
- [2] Harris. (2000). *Radio Communications in the Digital Age* (Vol. vol 2: VHF/UHF Technology). USA: Harris Corporation.
- [3] Weisman, C. J. (2000 ). *The Essential Guide to RF and Wireless*. New Jersey: Prentice Hall.
- [4] Lee (1998). *Mobile Communications Engineering: Theory and Applications*. McGraw-Hill, USA.
- [5] Rhodes (1999). *Antenna Handbook*. U.S. Marine Corps, Department of the navy Headquarters, Washington, D. C. 20380-1775, <http://www.doctrine.quantico.usmc.mil>.
- [6] Wesolowski. K (2002). *Mobile communication System*. ISBN: 0471 498378, John Wiley and Sons Ltd., New York.
- [7] Prasad M. V. S. N, Rama Rao T, Ahmad Iqbal and Paul K. M (2006). Investigation of VHF signals in bands I AND II in southern India and model comparisons. *Indian Journal of Radio and Space Physics*. Vol. 35, 198 - 205.
- [8] Fleury, B., and Lenthold, P. (1996). Radiowave Propagation in Mobile Communications. *An Overview of European Research, IEEE Communication Magazine* , 70-81.
- [9] Mardeni, R., and Kwan, K. F. (2010). Optimization of Hata propagation prediction model in suburban in Malaysia. *Progress In Electromagnetics Research C* , Vol. 13,
- [10] Abhayawardhana V. S, I.J.Wassell, D.Crosby, M.P.Sellars, and M.G.Brown. (2005). Comparison of empirical propagation path models for fixed wireless access system. *VTC 2005-Spring.IEEE 61st* , vol. 1, pp.73-77.
- [11] Omolaye, K.L., Omolaye P. O., and Akpakwu G. A (2014) A GIS Based UHF Radio Wave Propagation Model For Area Within 25km Radius From OSRC Transmitting Antenna. *IJERT Publication Vol. 3 Issue 5*, pp. 1784-1791, May – 2014.
- [12] Bing, L., Chang, X., and Ruoyi, w. (nd). *TV Broadcasting Frequency Programming based on GIS*. Liaoning.
- [13] Dodd, H. M. (2001). "The Validity of Using a Geographic Information System's Viewshed Function as a Predictor for the Reception of Line-of-Sight Radio Waves. Virginia Tech: MS thesis in Geography.
- [14] Kirtner, J L., and Anderson, H. R. (1999). *The Application of Land Use/Land Cover Data to Wireless Communication System Design*. eugene, Oregon, USA: EDX. Engineering,Inc.
- [15] ReMartinez, C. (2009). *A GIS Broadcast Coverage Prediction Model for Transmitted FM Radio Waves inPeru*: Santon.
- [16] Balanis, C. (2005). *Antenna Theory* (3rd Edition ed.). USA: John Wiley and Sons Ltd.,
- [17] Jean-Frederic, W., and Rizk, K. (2003). Radiowave propagation, building databases, and GIS: anything in common? A radio engineer's viewpoint. *Environment and Planning B* , 30, 767-787.

## Authors

**Engr. Philip Omohimire Omolaye** graduated from Electrical and Electronics Engineering Department at Federal University of Technology Akure, Ondo State of Nigeria and a Masters degree in Information Systems and Industrial Electronics. Presently, the author is pursuing PhD in Telecommunication System Engineering. He is a registered member of Council of registered Engineers of Nigeria (COREN), Nigeria Society of Engineers (NSE), Nigeria Institute of Electrical and Electronic Engineers (NIEEE) and the Technical Secretary of both NSE and NIEEE at branch level. The author has written several books and many journal articles.

**Engr. (Prof) Gabriel Agwu Igwue** holds a B.Sc of the University of Lagos, an SM of the Massachusetts Institute of Technology, and a PhD of North Carolina State University, all in Electrical Engineering. He has carried out research work in industrial fabrication of some solid-state devices. The author has written several books and many journal articles in his field. He is a registered member of Council of registered Engineers of Nigeria (COREN) and Nigeria Society of Engineers (NSE).

**Engr. Godfrey A. Akpakwu** graduated from Electrical and Electronic Engineering Department at University of Agriculture Makurdi, Benue State of Nigeria and a Master degree in Electronic Communication and Computer Engineering from the University of Nottingham, United Kingdom. He has carried out research work in areas of security, communication and antenna design with many journal articles to his credit. He is a registered member of Nigeria Society of Engineers (NSE).



## The Effect of Packaging Materials on the Quality Attributes of Crayfish During Cold Storage.

Ajala, A.S.,<sup>1</sup> Abiola, T.A.<sup>1</sup>

<sup>1</sup>Department of Food Science and Engineering, Ladoko Akintola University of Technology, P.M.B. 4000, Ogbomoso, Nigeria

**ABSTRACT:** This study evaluates the effects of packaging materials on the quality attributes of crayfish preserved in cold storage. This was done in order to ascertain the suitability of the different packaging materials on keeping the quality attributes of crayfish in cold storage. The “red claw” crayfish was harvested fresh, beheaded, washed, cleaned and packaged in different packaging materials of low-density polyethylene (LDPE), high-density polyethylene (HDPE), aluminum foil and plastic. The crayfish were stored for a period of eight weeks, and samples were taken for analysis every two weeks. The analyses carried out were proximate, mineral (calcium, iron and phosphorus) and microbial (yeast, mould, coliform and total viable counts). There were significant reduction changes in the proximate, minerals and microbiological analysis in respect to the packaging materials and storage period.

**Key-words:** crayfish, packaging material, quality, cold storage

### I. INTRODUCTION

Crayfish, crawfish or crawdad are freshwater crustaceans resembling small lobsters, to which they are probably closely related. (Hobbs, 1984). Crayfish are eaten in Europe, China, Africa, Australia, Canada, and the United States. Ninety-eight percent of the crayfish harvested in the United States come from Louisiana. Louisiana produces 90 percent of the crawfish in the world and consumes 70 percent locally. (Anderson, 2007). Food preservation is generally useful and important in ensuring food availability and stability supply all over the world, without these, there might be difficulties arising from food shortage, famine, and a huge downturn in the economy all over the world. To avoid these, food preservation processes must therefore be put in place to ensure adequate food supply, stability and availability. (Bentley and Amy, 2008). Preservation of crayfish is very paramount because of it is easily susceptible to deterioration immediately after harvest and to prevent economic losses (Okonta and Ekelemu, 2005). According to Akinyele *et al.*, (2007), the development of machinery that could be employed for effective handling, harvesting, processing and storage of sea foods such as fish and crayfish cannot be over-emphasized especially when aquaculture is growing fast in Nigeria. Good processing method is achievable by adapting basic parameters of unit operations necessary to achieve quality product which can satisfy the consumers and in turn yields good dividend for the processors. Packaging is an integral part of the crayfish processing as it facilitates handling during marketing and distribution. Song *et al.*, 2009 listed general features of a good packaging material for foods. One of the impediments to the growth of crayfish industries in Nigeria is the lack of adequate packaging technology that could effectively preserve the quality attribute during transportation which has resulted in wastages and poor quality of the available crayfish. Few researchers have worked on preservation and packaging of crayfish, Ajala and Oyategbe (2013) has also published work on the influence of packaging and storage on quality of white shrimp at room temperature. The latest report perhaps on crayfish was from Chen *et al.*, (2007) who worked on crayfish using 3 different packaging systems namely modified atmosphere packaging (MAP), vacuum packaging (VP) and aerobic packaging using polyvinylchloride (PVCP). However, report on effect of packaging materials (such as aluminum foil, low-density polyethylene and high-density polyethylene) on nutritional quality of crayfish at cold temperature has rarely been published. Hence there is a need to evaluating the effects of different packaging materials on the quality attributes and storage life of frozen crayfish. This forms the thrust of the study.

## II. MATERIALS AND METHOD

### (a) Preparation of the samples:

The fresh crayfish used in this project was obtained from Makoko River in Lagos state, Nigeria. After harvesting, it was immediately put into ice slurry and transported to Food Science and Engineering Department Laboratory, Ladoké Akintola University of Technology, Ogbomoso, Nigeria where it was processed. The process involved beheading and washing. 0.25kg of crayfish was then weighed into each packaging material of sizes (14.5x13.5cm), which included low-density polyethylene (LDPE) of  $90 \text{ cm}^3/\text{cm}^2\text{s}^{-1}$  water transmission rate, high-density polyethylene (HDPE) of  $41 \text{ cm}^3/\text{cm}^2\text{s}^{-1}$  water transmission rates, Polyvinyl Chloride of  $275 \text{ cm}^3/\text{cm}^2\text{s}^{-1}$  water transmission rate and aluminum foil. They were then packaged and frozen at  $-16^\circ\text{C}$  for 8 weeks at Bol-Raib Investment Nigeria Limited Mega fish cold room, Ogbomoso, Oyo state. At interval of 0, 2, 4, 6 and 8 week; sample pack of crayfish of each packaging materials was removed for mineral, microbial and proximate analyses.

### (b) Chemical analysis

Microbial, minerals and proximate analyses were carried out using the official methods of Association of Official Analytical Chemists (AOAC 2000).

### (c) Statistical analysis

Data were analyzed using SPSS (version 9.0) package. Analysis of variance was carried out to know the significant effect of the packaging material on the samples. Significant ( $P < 0.05$ ) difference between means were identified using the least significant difference procedure.

## III. RESULT AND DISCUSSIONS:

### (a) Proximate Analysis.

The results obtained from proximate analysis of crayfish stored with different packaging materials are presented in Table 1. All the samples generally gained moisture in the first two weeks to equilibrate with the surrounding humidity in the freezer, except sample C and D which decreased in moisture content. This could be attributed to the observation of Sing and Heldman 2009 on freezing diagram of food, in which the post cooling enthalpy (which is a function of specific heat and moisture content) decreased for some freezing time. At this time, the moisture content seems decreased due to slight reduction in post cooling enthalpy. However as the weeks increased, all the samples gained a significant amount of moisture, this might be due to their ability to allow moisture transfer across their boundaries. In other word it could be accrued to the nature of the packaging material in which transfer of water and oxygen is possible as reported by (Potter and Hotchkiss, 2006). It is observed from the table that sample at 8<sup>th</sup> week recorded highest value of moisture which implies that the higher the storage time, the higher the moisture content of the frozen crayfish samples. This observation has been earlier asserted by other authors such as Ajala and Oyategbe (2013), Akintola and Bakare (2012), Joseph *et al.*, (1998), Basavacumer *et al.*, 1998

The protein content decreased generally as the storage days increased. However, sample C had the highest protein content present at the end of 8<sup>th</sup> week meaning the packaging material retained the protein content better and was significantly different from the other packaging materials, however sample B had the lowest protein content and was also significantly different from other samples. The major loss of protein in sample B was as a result of leakages of protein content from the packaging material. This is a similar finding to the work of Gong *et al.*, (2010) in which there was reduction in protein content of red claw crayfish packaged with polyethylene stored at  $-20^\circ\text{C}$ .

The percentage range of the fat content is in agreement with work of Nahid and Fayza, (2009) with values of 2.45 %. However, the results showed that crayfish samples were generally low in fat contents as earlier reported by Chien *et al.*, (2007). As the storage days increased, there were reductions in fat contents in all the samples.

**Table 1: Results of proximate composition**

Samples	Fresh (0 Week)	2 Weeks	4 Weeks	6 Weeks	8 Weeks
Moisture contents (%)					
A	72.37 <sup>a</sup> ±0.69	74.17 <sup>a</sup> ±0.15	75.83 <sup>a</sup> ±0.15	77.70 <sup>a</sup> ±0.20	78.33 <sup>a</sup> ±0.15
B	72.37 <sup>a</sup> ±0.69	74.13 <sup>a</sup> ±0.06	75.86 <sup>a</sup> ±0.06	77.73 <sup>a</sup> ±0.15	78.93 <sup>a</sup> ±0.06
C	72.37 <sup>a</sup> ±0.69	67.83 <sup>c</sup> ±0.11	70.00 <sup>c</sup> ±0.10	71.73 <sup>c</sup> ±0.38	74.67 <sup>c</sup> ±0.15

D	72.37 <sup>a</sup> ±0.69	69.87 <sup>b</sup> ±0.06	72.57 <sup>b</sup> ±0.30	74.53 <sup>b</sup> ±0.21	75.43 <sup>b</sup> ±0.15
Protein contents (%)					
A	20.47 <sup>a</sup> ±0.39	17.90 <sup>c</sup> ±0.10	18.27 <sup>c</sup> ±0.15	18.43 <sup>c</sup> ±0.11	18.47 <sup>c</sup> ±0.06
B	20.47 <sup>a</sup> ±0.39	17.30 <sup>d</sup> ±0.17	17.53 <sup>d</sup> ±0.06	17.63 <sup>d</sup> ±0.06	17.77 <sup>d</sup> ±0.11
C	20.47 <sup>a</sup> ±0.39	18.47 <sup>a</sup> ±0.15	18.90 <sup>a</sup> ±0.10	18.97 <sup>a</sup> ±0.06	19.03 <sup>a</sup> ±0.15
D	20.47 <sup>a</sup> ±0.39	18.27 <sup>b</sup> ±0.06	18.50 <sup>b</sup> ±0.10	18.67 <sup>b</sup> ±0.06	18.77 <sup>b</sup> ±0.06
Fat contents (%)					
A	3.87 <sup>a</sup> ±0.14	1.27 <sup>c</sup> ±0.11	1.20 <sup>b</sup> ±0.10	1.27 <sup>b</sup> ±0.06	1.23 <sup>c</sup> ±0.05
B	3.87 <sup>a</sup> ±0.14	1.27 <sup>c</sup> ±0.06	1.23 <sup>b</sup> ±0.06	1.27 <sup>b</sup> ±0.06	1.27 <sup>c</sup> ±0.06
C	3.87 <sup>a</sup> ±0.14	1.53 <sup>b</sup> ±0.06	1.57 <sup>a</sup> ±0.06	1.60 <sup>a</sup> ±0.00	1.63 <sup>b</sup> ±0.06
D	3.87 <sup>a</sup> ±0.14	1.67 <sup>a</sup> ±0.06	1.60 <sup>a</sup> ±0.10	1.67 <sup>a</sup> ±0.06	1.73 <sup>a</sup> ±0.11
Ash contents (%)					
A	3.10 <sup>a</sup> ±0.14	1.93 <sup>c</sup> ±0.06	1.83 <sup>c</sup> ±0.11	1.83 <sup>c</sup> ±0.05	1.80 <sup>c</sup> ±0.10
B	3.10 <sup>a</sup> ±0.14	1.77 <sup>d</sup> ±0.12	1.70 <sup>d</sup> ±0.10	1.73 <sup>d</sup> ±0.06	1.83 <sup>c</sup> ±0.06
C	3.10 <sup>a</sup> ±0.14	2.10 <sup>a</sup> ±0.10	1.97 <sup>a</sup> ±0.12	2.00 <sup>a</sup> ±0.10	2.17 <sup>a</sup> ±0.06
D	3.10 <sup>a</sup> ±0.14	2.07 <sup>b</sup> ±0.06	1.87 <sup>b</sup> ±0.06	1.90 <sup>b</sup> ±0.00	1.97 <sup>b</sup> ±0.06
Fibre contents (%)					
A	0.10 <sup>a</sup> ±0.00	0.10 <sup>a</sup> ±0.00	0.10 <sup>a</sup> ±0.00	0.10 <sup>a</sup> ±0.00	0.10 <sup>a</sup> ±0.00
B	0.10 <sup>a</sup> ±0.00	0.07 <sup>b</sup> ±0.06	0.10 <sup>a</sup> ±0.00	0.10 <sup>a</sup> ±0.00	0.10 <sup>a</sup> ±0.00
C	0.10 <sup>a</sup> ±0.00	0.10 <sup>a</sup> ±0.00	0.10 <sup>a</sup> ±0.00	0.10 <sup>a</sup> ±0.00	0.10 <sup>a</sup> ±0.00
D	0.10 <sup>a</sup> ±0.00	0.07 <sup>b</sup> ±0.06	0.07 <sup>b</sup> ±0.06	0.07 <sup>b</sup> ±0.06	0.03 <sup>b</sup> ±0.06
Carbohydrate contents (%)					
A	0.10 <sup>a</sup> ±0.00	0.17 <sup>b</sup> ±0.01	0.90 <sup>d</sup> ±0.00	0.57 <sup>d</sup> ±0.15	0.23 <sup>a</sup> ±0.04
B	0.10 <sup>a</sup> ±0.00	0.13 <sup>a</sup> ±0.01	0.70 <sup>c</sup> ±0.20	0.40 <sup>c</sup> ±0.10	0.90 <sup>c</sup> ±0.10
C	0.10 <sup>a</sup> ±0.00	0.13 <sup>a</sup> ±0.02	0.73 <sup>b</sup> ±0.16	0.33 <sup>b</sup> ±0.12	0.23 <sup>a</sup> ±0.05
D	0.10 <sup>a</sup> ±0.00	0.17 <sup>b</sup> ±0.02	0.47 <sup>a</sup> ±0.11	0.13 <sup>a</sup> ±0.03	0.63 <sup>b</sup> ±0.15

Means with the same letter across the column are not significantly different,

**Codes:** A- Low-density polyethylene, B- High-density polyethylene, C- Aluminum foil, D- Plastic

However, samples C and D were able to retain fat content more than the other samples A and B, this is because perhaps sample A and B allowed oxidation to take place than sample C and D; this is similar to the work of Kong *et al.*, (2006). Samples C and D were able to form a good barrier against light and other factors which could cause oxidation.

The ash content decreased generally as storage time increased, this is an obvious reason of leakages of minerals as storage days increased. This observation is in line with the work of Ibrahim and El-Sherif (2008). The ash content was highest in sample C and least in sample A, and they were significantly different from each other. Sample C and D had higher ash contents than samples A and B; this might be because the packaging materials of A and B allowed more mineral loss sample C and D.

The results of fibre content show that crayfish is poor in fibre as its values range from 0.03- 0.1%. Virtually, the fibre content remained constant during the storage period which means the fibrous particles of the crayfish were greater than pore sizes of the packaging material hence the fibre were retained.

The carbohydrate results are as shown in Table 1. The least value of carbohydrate at the 8<sup>th</sup> week is found in sample A while the highest value is found in sample C. The samples are significant from each other. All the samples increased in values as storage days increased. The trend in increment in these values was as result of either increase or decrease in value of other parameters such as moisture, protein, fat, fibre and ash because carbohydrate is a percentage difference from addition of these parameters.

#### (b) Mineral analysis

The results obtained from the mineral analysis of the samples stored with different packaging materials are presented in Table 2. Sample D had the highest retention of calcium present followed by samples C while sample A has the lowest value. There was significant difference among all the samples at the second week of the storage but as storage days increased from 4<sup>th</sup> to 8<sup>th</sup>, Sample A and B were not significantly different but they were significantly different from sample C and D. The same trend was observed in iron and phosphorus content. There was a general minimal loss of mineral content of the samples through the packaging materials during storage. In a nut-shell, as the cold storage days increased, the values of minerals decreased. Similar observation has been earlier reported by other researchers such as Ajala and Oyategbe (2013); Nahid and Fayza (2009), Cemal Kaya (2011).

Table 2: Results of mineral content variation during the storage

Samples	Fresh (0 Week)	2 Weeks	4 Weeks	6 Weeks	8 Weeks
<b>Calcium (mg / 100 g wet sample)</b>					
A	215 ±2.45	211.00 <sup>c</sup> ±3.00	211.00 <sup>b</sup> ±3.00	210.33 <sup>b</sup> ±1.53	207.00 <sup>b</sup> ±1.73
B	215 ±2.45	213.67 <sup>b</sup> ±1.15	212.67 <sup>b</sup> ±1.15	211.87 <sup>b</sup> ±0.58	209.67 <sup>b</sup> ±0.58
C	215 ±2.45	214.00 <sup>a</sup> ±3.61	214.67 <sup>a</sup> ±3.51	213.67 <sup>a</sup> ±3.21	211.33 <sup>a</sup> ±3.79
D	215 ±2.45	215.33 <sup>b</sup> ±2.52	214.33 <sup>a</sup> ±2.52	213.33 <sup>a</sup> ±2.31	211.67 <sup>a</sup> ±3.06
<b>Iron (mg / 100 g wet sample)</b>					
A	1.70 ±0.00	1.70 <sup>b</sup> ±0.00	1.70 <sup>b</sup> ±0.00	1.70 <sup>b</sup> ±0.00	1.70 <sup>b</sup> ±0.00
B	1.70 ±0.00	1.73 <sup>b</sup> ±0.06	1.73 <sup>b</sup> ±0.06	1.73 <sup>b</sup> ±0.06	1.73 <sup>b</sup> ±0.06
C	1.70 ±0.00	1.77 <sup>a</sup> ±0.06	1.80 <sup>a</sup> ±0.00	1.80 <sup>a</sup> ±0.00	1.80 <sup>a</sup> ±0.00
D	1.70 ±0.00	1.87 <sup>a</sup> ±0.06	1.87 <sup>a</sup> ±0.06	1.87 <sup>a</sup> ±0.06	1.87 <sup>a</sup> ±0.06
<b>Phosphorus (mg / 100 g wet sample)</b>					
A	208.67 <sup>a</sup> ±2.31	208.33 <sup>a</sup> ±2.89	207.67 <sup>a</sup> ±1.69	207.67 <sup>a</sup> ±2.52	207.67 <sup>a</sup> ±2.52
B	209.33 <sup>a</sup> ±3.06	209.00 <sup>a</sup> ±3.61	209.00 <sup>a</sup> ±3.61	207.67 ±1.69	207.33 <sup>a</sup> ±5.03
C	208.67 <sup>a</sup> ±3.06	207.67 ±1.69	207.33 <sup>a</sup> ±3.06	205.67 <sup>a</sup> ±4.16	204.00 <sup>a</sup> ±3.61
D	207.67 ±1.69	199.67 <sup>b</sup> ±4.04	198.67 <sup>b</sup> ±7.57	197.33 <sup>b</sup> ±6.43	197.33 <sup>b</sup> ±6.43

Means with the same letter across the column are not significantly different,

**Codes:** A- Low-density polyethylene, B- High-density polyethylene, C- Aluminum foil, D- Plastic

The results of the microbial analysis of the samples stored with different packaging materials are presented in Table 3. The values of mould and yeast count in this work are greater than the values reported by Emad *et al.*, (2012) with value of  $3.12 \times 10^2$  and  $4.1 \times 10^2$  respectively. Also the values of both coliform and total viable count in this work are greater than the values reported by the same author. The difference in values may be as a result of species variety and primarily aquatic habitat factor. From the table total viable count was initially high in all the samples but later there was a general trend in reduction of yeast, mold, coliform and total viable count as storage days increased. The obvious reason for this could be because of low storage temperature effect on these microorganisms. Most of these microbes are mesophile which cannot withstand cold temperatures irrespective of the packaging materials. Therefore, lower temperature served as a critical factor in inhibiting the growth of these microbes as reported by Chien *et al.*, (2007), Potter and Hotchkiss, (2006).

#### IV. CONCLUSION

In summary, the fresh sample analyzed was quite better than the stored samples because finding shows a decrease in the quality attributes of the crayfish, these differences were however not pronounced to cause any devastating effect on the quality attributes of the crayfish. The results of the proximate, microbial and mineral analyses show that aluminum foil was better rated than other packaging material from microbiological standpoint. This implies that samples stored with aluminum foil formed effective barrier against chemical and biological changes on the crayfish than samples stored with the other packaging materials. However, aluminum foil is cost ineffective compare to others; hence the decision for packaging material for crayfish is left to individual crayfish processor

Table 3: Results of Microbial analysis during the storage

Samples	Fresh (0 Week)	2 Weeks	4 Weeks	6 Weeks	8 Weeks
<b>Yeast count (cfu/ml)</b>					
A	$5.17 \times 10^6 \pm 136$	780 <sup>d</sup> ±189	0.00 ±0.00	0.00 ±0.00	0.00 ±0.00
B	$5.17 \times 10^6 \pm 136$	105 <sup>a</sup> ±18	0.00 ±0.00	0.00 ±0.00	0.00 ±0.00
C	$5.17 \times 10^6 \pm 136$	401 <sup>c</sup> ±20	0.00 ±0.00	0.00 ±0.00	0.00 ±0.00
D	$5.17 \times 10^6 \pm 136$	143 <sup>b</sup> ±19	0.00 ±0.00	0.00 ±0.00	0.00 ±0.00
<b>Mould count (cfu/ml)</b>					
A	$6.05 \times 10^{4a} \pm 19$	0.00 ±0.00	0.00 <sup>a</sup> ±0.00	0.00 <sup>a</sup> ±0.00	0.00 ±0.00
B	$6.05 \times 10^{4a} \pm 19$	30 <sup>a</sup> ±18	20 <sup>b</sup> ±05	0.00 <sup>a</sup> ±0.00	0.00 ±0.00
C	$6.05 \times 10^{4a} \pm 19$	0.00 ±0.00	0.00 ±0.00	0.00 <sup>a</sup> ±0.00	0.00 ±0.00
D	$6.05 \times 10^{4a} \pm 19$	0.00 ±0.00	0.00 ±0.00	0.00 <sup>a</sup> ±0.00	0.00 ±0.00
<b>Coliform count (cfu/ml)</b>					
A	$3.02 \times 10^{4a} \pm 89$	102 <sup>c</sup> ±29	0.00 ±0.00	0.00 ±0.00	0.00 ±0.00
B	$3.02 \times 10^{4a} \pm 89$	0.00 ±0.00	0.00 ±0.00	0.00 ±0.00	0.00 ±0.00
C	$3.02 \times 10^{4a} \pm 89$	101 <sup>b</sup> ±24	0.00 ±0.00	0.00 ±0.00	0.00 ±0.00

D	$3.02 \times 10^{4a} \pm 89$	$202^a \pm 69$	$102^c \pm 59$	$0.00 \pm 0.00$	$0.00 \pm 0.00$
<b>Total viable count (cfu/ml)</b>					
A	$6.17 \times 10^6 \pm 147$	$890^a \pm 85$	$0.00 \pm 0.00$	$0.00 \pm 0.00$	$0.00 \pm 0.00$
B	$6.17 \times 10^6 \pm 147$	$150^c \pm 37$	$29 \pm 06$	$0.00 \pm 0.00$	$0.00 \pm 0.00$
C	$6.17 \times 10^6 \pm 147$	$120^d \pm 23$	$0.00 \pm 0.00$	$0.00 \pm 0.00$	$0.00 \pm 0.00$
D	$6.17 \times 10^6 \pm 147$	$350^b \pm 63$	$130 \pm 13$	$0.00 \pm 0.00$	$0.00 \pm 0.00$

Means with the same letter across the column are not significantly different,

**Codes:** A- Low-density polyethylene, B- High-density polyethylene, C- Aluminum foil, D- Plastic

## REFERENCES

- [1] Ajala and Oyategbe (2013). Influence of Packaging and Storage on Nutritional Quality of White Shrimp (*Penaeus vannamei*), International Journal of Advanced Scientific and Technical Research. Issue 3 volume 2, pp 232-235
- [2] Akintola, S.L. and Bakare, S.B. (2012). Effect of ice storage on the biochemical composition of *Macrobachium vollenhovenii*. Journal of Fishery and Aquatic Science, pp 1-5
- [3] Anderson, O.E (2007) Refrigeration in America. Port Washington, N.Y Kennikat Press. Pg 203-208.
- [4] AOAC (2000). "Official Methods of Analysis (16th edn). Association of Official Analytical Chemists". Virginia, USA, pp. 834 - 841.
- [5] Basavacumer, K.V., Bhaskar, N., Ramesh, A.M. and Reddy, G.S.V. (1998). Quality change in coloured tiger shrimps during ice storage. Journal of Food Science and Technology, 35:305-309
- [6] Bently O and Amy F (2008). Eating for victory: Food rationing and the politics of Domesticity. Page 14-21.
- [7] Cemal K.(2011). Effects of different phosphorus doses on the physico-chemical properties of strawberry during storage. Journal of Food, Agriculture & Environment Vol.9 (2): 106-109
- [8] Chen, G., Xiong, Y.L., Kong, B., Newman, M.C., Thomson, K.R., Metts, L.S. and Webster, C.D. (2007). Microbiological and physicochemical properties of red claw crayfish (*Cherax quadricarinatus*) stored in different package systems at 2°C. Journal of Food Science—Vol.72, No 8, pp 442-445
- [9] Emad M. E., Seham A. K. and Mohammed, A. T. A. (2012). Chemical, physical, microbiological and quality attributes studies on River Nile crayfish. African Journal of Biotechnology Vol. 11(51), pp. 11262-11270.
- [10] Gong YN, Li WW, Sun JL, Ren F, He L, Jiang H et al.(2010).Molecular cloning and tissue expression of the fatty acid-binding protein (Es-FABP) gene in female Chinese mitten crab (*Eriocheir sinensis*).BMC Molecular Biology 11: 71.
- [11] Ibrahim, S. M. and El-Sherif, S. A. (2008) Effect of some plant extracts on the quality aspect of frozen Tilapia (*Oreochromis niloticus* L.) filets. Global Vetrinaria 2:2:62-66
- [12] Joseph, J., Jerrygreen, P.A. and Gopalakrishna, T.S. (1998). Storage characteristics of cultured *Penaeus indicus* in ice and at ambient temperature. Fish Techn. 35: 84-89
- [13] Nahid F.Z. and Fayza, E. (2009). Study on chemical Quality and Nutrition Value of Fresh Water Cray Fish (*Procambarus clarkii*). Journal of the Arabian Aquaculture Society, vol. 4, No 1, pp1-6
- [14] Okonta, A. A. and Ekelemu, J. K. (2005), A preliminary study of micro-organisms associated with fish spoilage in Asaba, Southern Nigeria. Proceedings of the 20th Annual Conference of the Fisheries Society of Nigeria (FISON), Port Harcourt, Nigeria. pp557 – 560
- [15] Potter H, Hotchkiss I (2006). Food Science. (5th ed.). CBS Publishers and Distributors. New Delhi, India
- [16] Singh Paul R. and Heldman Dennis R.. (2009). Introduction of Food Engineering. 4th Edition: Academic Press, Incorporated. Chapter 7, Pp 503-507
- [17] Song, J. H., Murphy, R. J., Narayan, R. and G. B. H. Davies (2009). Biodegradable and compostable alternatives to conventional plastics. Phil. Trans. R. Soc. B. 364, 2127–2139

## ORGANIC LIGHT EMITTING DIODE (OLED)

Aririguzo Marvis Ijeaku<sup>1</sup>, Madu Hilary Chidubem<sup>2</sup>, Emerole Kelechi  
Chukwunonyerem<sup>3</sup>, Nwogu Uchenna Obioma<sup>4</sup>

<sup>1,2,3,4</sup> (Department of Electrical and Electronics Engineering, Federal Polytechnic Nekede, Owerri,  
Imo State, Nigeria)

**ABSTRACT :** An Organic Light Emitting Diode (OLED) is a device composed of an organic layer that emits lights in response to an electrical current. Organic light emitting diodes have advanced tremendously over the past decades. The different manufacturing processes of the OLED itself to several advantages over flat panel displays made with LCD technology which includes its light weight and flexible plastic substrates, wider viewing angles, improved brightness, better power efficiency and quicker response time. However, its drawbacks include shorter life span, poor color balance, poor outdoor performance, susceptibility to water damage etc. The application of OLEDs in electronics is on the increase on daily basics from cameras to cell phones to OLED televisions, etc. Although OLEDs provides prospects for thinner, smarter, lighter and ultra-flexible electronics displays, however, due to high cost of manufacturing, it is not yet widely used.

**Keywords -** Electronic, Display, Devices, Lifetime, Application

### I. INTRODUCTION

Do you remember old-style Television set powered by cathode-ray tubes (CRTs)? The biggest ones were about 30–60cm (1–2ft) deep and almost too heavy to lift by you. If you think that's bad, you should have seen what TVs were like in the 1940s. The CRTs inside were so long that they had to stand upright firing their picture toward the ceiling, with a little mirror at the top to bend it sideways into the room. Watching TV in those days was a bit like staring down the periscope of a submarine! Thank goodness for progress. Now most of us have computers and TVs with LCD screens, which are thin enough to mount on a wall, and displays light enough to build into portable gadgets like cell phones. If you think that's good, wait till you see the next generation of displays made using OLED (organic light-emitting diode) technology. They're super-light, almost paper-thin, theoretically flexible enough to print onto clothing, and they produce a brighter and more colorful picture. What are they and how do they work? Let's take a closer look!

The purpose of this research work is to explore the ground-breaking technology of the OLED. The following are the specific objectives:

- i. How an OLED works
- ii. Types of OLEDs
- iii. Advantages and disadvantages of OLEDs
- iv. Current and future OLED applications

This work discusses the Organic Light Emitting Diode (OLED) with interest on how it works its material properties, its prospects, limitations and application areas.

This work is intended to showcase the groundbreaking technological success in the electronics display world, in this masterpiece called the OLED. This research is also intended to supply sufficient information to students in their choice of electronic display for their electronics projects. Similarly, electronics engineers/technicians and mainstream display manufacturers, with the information in this research work could consider employing the use of OLEDs in their displays by taking advantage of all its jaw-sagging features.

## II. ORGANIC LIGHT EMITTING DIODE

The first observations of electroluminescence in organic materials were in the early 1950s by André Bernanose and co-workers at the Nancy-Université in France. They applied high alternating voltages in air to materials such as acridine orange, either deposited on or dissolved in cellulose or cellophane thin films. The proposed mechanism was either direct excitation of the dye molecules or excitation of electrons.

The first diode device was reported at Eastman Kodak by Ching W. Tang and Steven Van Slyke in 1987. This device used a novel two-layer structure with separate hole transporting and electron transporting layers such that recombination and light emission occurred in the middle of the organic layer; this resulted in a reduction in operating voltage and improvements in efficiency that led to the current era of OLED research and device production.

Research into polymer electroluminescence culminated in 1990 with J. H. Burroughes *et al.* at the Cavendish Laboratory in Cambridge reporting a high efficiency green light-emitting polymer based device using 100 nm thick films of poly(p-phenylene vinylene).

Before you can understand an OLED, it helps if you understand how a conventional LED works—so here's a quick recap. Take two slabs of semiconductor material (something like silicon or germanium), one slightly rich in electrons (called n-type) and one slightly poor in electrons (if you prefer, that's the same as saying it's rich in "holes" where electrons should be, which is called p-type). Join the n-type and p-type slabs together and, where they meet, you get a kind of neutral, no-man's land forming at the junction where surplus electrons and holes cross over and cancel one another out. Now connect electrical contacts to the two slabs and switch on the power. If you wire the contacts one way, electrons flow across the junction from the rich side to the poor, while holes flow the other way, and a current flows across the junction and through your circuit. Wire the contacts the other way and the electrons and holes won't cross over; no current flows at all. What you've made here is called a junction diode: an electronic one-way-street that allows current to flow in one direction only.

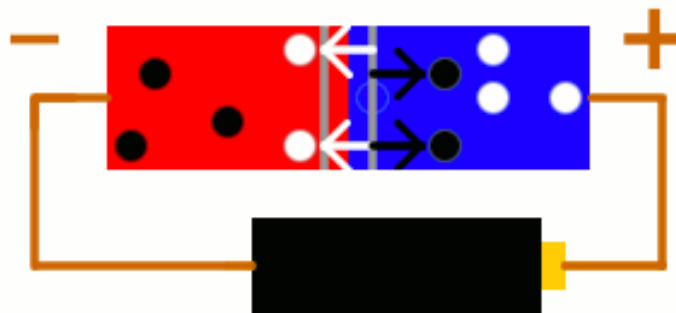


Fig.1. A junction diode in a forward biased condition

Fig.1 shows how a junction diode allows current to flow when electrons (black dots) and holes (white dots) move across the boundary between n-type (red) and p-type (blue) semiconductor material.

An LED is a junction diode with an added feature: it makes light. Every time electrons cross the junction, they nip into holes on the other side, release surplus energy, and give off a quick flash of light. All those flashes produce the dull, continuous glow for which LEDs are famous.

OLEDs work in a similar way to conventional diodes and LEDs, but instead of using layers of n-type and p-type semiconductors, they use organic molecules to produce their electrons and holes. A simple OLED is made up of six different layers. On the top and bottom there are layers of protective [glass](#) or [plastic](#). The top layer is called the seal and the bottom layer the substrate. In between those layers, there's a negative terminal (sometimes called the cathode) and a positive terminal (called the anode). Finally, in between the anode and cathode are two layers made from organic molecules called the emissive layer (where the light is produced, which is next to the cathode) and the conductive layer (next to the anode). Here's what it all looks like:

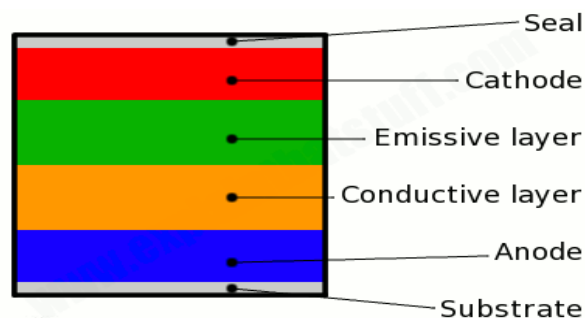


Fig. 2: The structure of an OLED

### How an OLED Emit Light

#### How does this sandwich of layers make light?

1. To make an OLED light up, we simply attach a voltage (potential difference) across the anode and cathode.
2. As the electricity starts to flow, the cathode receives electrons from the power source and the anode loses them (or it "receives holes," if you prefer to look at it that way).
3. Now we have a situation where the added electrons are making the emissive layer negatively charged (similar to the n-type layer in a junction diode), while the conductive layer is becoming positively charged (similar to p-type material).
4. Positive holes are much more mobile than negative electrons so they jump across the boundary from the conductive layer to the emissive layer. When a hole (a lack of electron) meets an electron, the two things cancel out and release a brief burst of energy in the form of a particle of light—a photon, in other words. This process is called recombination, and because it's happening many times a second the OLED produces continuous light for as long as the current keeps flowing.

We can make an OLED produce colored light by adding a colored filter into our plastic sandwich just beneath the glass or plastic top or bottom layer. If we put thousands of red, green, and blue OLEDs next to one another and switch them on and off independently, they work like the pixels in a conventional LCD screen, so we can produce complex, hi-resolution colored pictures.

## III. TYPES OF OLED

### 1. Passive-Matrix OLED (PMOLED)

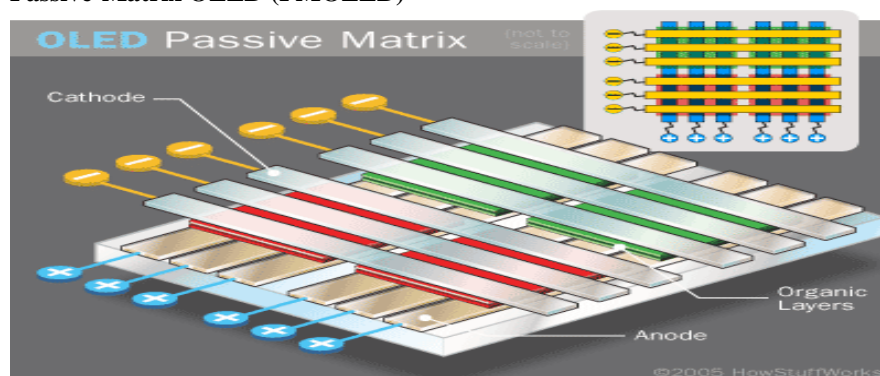


Fig.3: structure of a PMOLED.



Presumably this will be the first to hit the market since it was the passive LCD screens that came out first and more than likely OLEDs will follow in those footprints. PMOLEDs will be more expensive and will need more power than other OLEDs, though they will still use less power than LCDs out today. They are made up of a matrix of electrically conducting row and columns making pixels. Between these rows and columns are the organic layers and on the other side is the substrate. They are most efficient for smaller screens (2-3") such as PDAs and cell phones

## 2. Active-Matrix OLED (AMOLED)

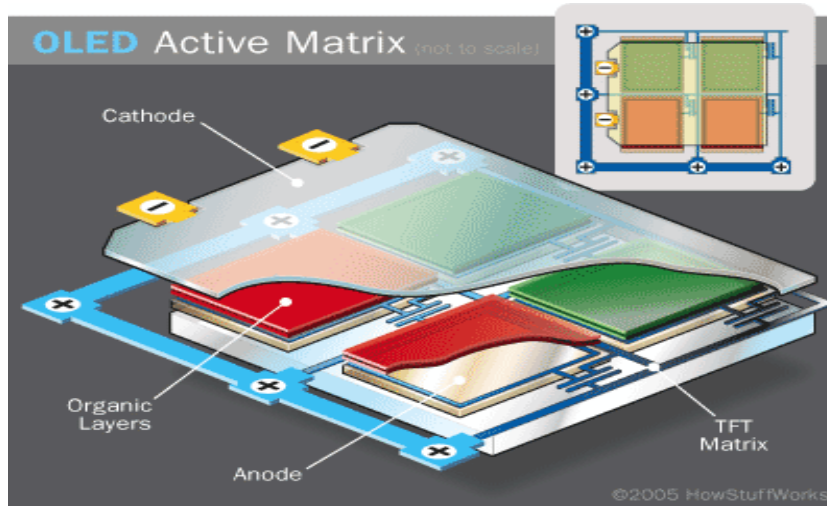


Fig.4: structure of an AMOLED.

AMOLEDs will be similar to passive but will have full layers of cathode, organic molecules, and anode; the anode layer will have a thin film transistor (TFT) back plate that forms a matrix. The TFT controls the brightness and which pixel gets turned on to form an image. In AMOLED there will be two TFT arrays per pixel, one starts and stops the charge and the other keeps a constant electrical current to the pixel. Since there is a TFT array there they will consume less power than the PMOLED since there is that constant current and they have faster refresh rates than the PMOLED. This allows the AMOLEDs to be used for computer monitors, large screen TVs, and even billboards. AMOLEDs have an opaque substrate which means it is only top emitting.

## IV. FOLDABLE OLED



Fig.5: A device made using foldable OLED.

Foldable OLEDs have substrates made of very flexible metallic foils or plastics. Foldable OLEDs are very lightweight and durable. Their use in devices such as cell phones and PDAs can reduce breakage, a major cause for return or repair. Potentially, foldable OLED displays can be attached to fabrics to create "smart" clothing, such as outdoor survival clothing with an integrated computer chip, cell phone, GPS receiver and OLED display sewn into it.

### 3. White OLED

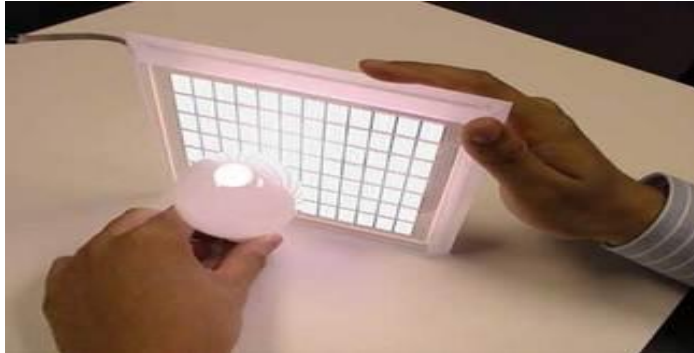


Fig. 6: White OLED used in lighting.

White OLEDs emit white light that is brighter, more uniform and more energy efficient than that emitted by fluorescent lights. White OLEDs also have the true-color qualities of incandescent lighting. Because OLEDs can be made in large sheets, they can replace fluorescent lights that are currently used in homes and buildings. Their use could potentially reduce energy costs for lighting.

## V. MERITS AND DEMERITS

The LCD is currently the display of choice in small devices and is also popular in large-screen TVs. Regular LEDs often form the digits on digital clocks and other electronic devices. OLEDs offer many advantages over both LCDs and LEDs:

- Because the light-emitting layers of an OLED are lighter, the substrate of an OLED can be flexible instead of rigid. OLED substrates can be plastic rather than the glass used for LEDs and LCDs.
- The plastic, organic layers of an OLED are thinner, lighter and more flexible than the crystalline layers in an LED or LCD.
- OLEDs are **brighter** than LEDs. Because the organic layers of an OLED are much thinner than the corresponding inorganic crystal layers of an LED, the conductive and emissive layers of an OLED can be multi-layered. Also, LEDs and LCDs require glass for support, and glass absorbs some light. OLEDs do not require glass.
- OLEDs do not require backlighting like LCDs. LCDs work by selectively blocking areas of the backlight to make the images that you see, while OLEDs generate light themselves. Because OLEDs do not require backlighting, they consume much less power than LCDs (most of the LCD power goes to the backlighting). This is especially important for battery-operated devices such as cell phones.
- OLEDs are easier to produce and can be made to larger sizes. Because OLEDs are essentially plastics, they can be made into large, thin sheets. It is much more difficult to grow and lay down so many liquid crystals.
- OLEDs have **large fields of view**, about 170 degrees. Because LCDs work by blocking light, they have an inherent viewing obstacle from certain angles. OLEDs produce their own light, so they have a much wider viewing range.

OLED seems to be the perfect technology for all types of displays, but it also has some problems:

- **Lifetime** - While red and green OLED films have longer lifetimes (46,000 to 230,000 hours), blue organics currently have much shorter lifetimes (up to around 14,000 hours (about 1.6 years).
- **Manufacturing** - Manufacturing processes are expensive right now.
- **Water** - Water can easily damage OLEDs.

## VI. CURRENT AND FUTURE OLED APPLICATIONS

Currently, OLEDs are used in small-screen devices such as cell phones, PDAs and digital cameras. In September 2004, Sony Corporation announced that it was beginning mass production of OLED screens for its CLIE PEG-VZ90 model of personal-entertainment handhelds.

Kodak was the first to release a digital camera with an OLED display in March 2003, the EasyShare LS633.



Fig. 7: Kodak LS633 EasyShare with OLED display.

Several companies have already built prototype computer monitors and large-screen TVs that use OLED technology. In May 2014, LG Electronics announced that it had developed a prototype super-thin-OLED-wallpaper-TV., the first of its size.



Fig. 8: LG super-thin-OLED-wallpaper-TV.

Research and development in the field of OLEDs is proceeding rapidly and may lead to future applications in heads-up displays, automotive dashboards, billboard-type displays, home and office lighting and flexible displays. Because OLEDs refresh faster than LCDs -- almost 1,000 times faster -- a device with an OLED display could change information almost in real time. Video images could be much more realistic and constantly updated. The newspaper of the future might be an OLED display that refreshes with breaking news -- and like a regular newspaper, you could fold it up when you're done reading it and stick it in your backpack or briefcase.

OLED technology is still relatively new and unused compared to similar, long-established technologies such as LCD. Broadly speaking, you can use OLED displays wherever you can use LCDs, in such things as TV and computer screens and MP3 and cell phone displays. Their thinness, greater brightness, and better color reproduction suggests they'll find many other exciting applications in future. They might be used to make inexpensive, animated billboards, for example or super-thin pages for electronic books and magazines. Or paintings on your wall you can update from your computer. Or even clothes with constantly changing colors and patterns wired to visualize software running from your iPhone.

## VII. CONCLUSION

OLED technology has advanced rapidly in recent years, with high-performing products now beginning to enter the marketplace for certain niche lighting applications. The thin, flexible structure of OLED panels provides new opportunities for innovative lighting products, and steady OLED efficiency improvements are expected to make OLEDs a viable, cost-competitive option for many lighting applications within the next five years. However, because of its high cost, it is advisable for students and non-blue-chip companies to the other alternatives such as LCD and LED which has comparative cost advantage.

Despite its numerous advantages, it's not advisable to be employed by students and non-blue-chip electronics companies because of its high cost of manufacture and implementation. However, I recommend that:

1. Nigerian technological institutions should partner with OLED manufacturing companies and related institutes in the training of Nigerian students in the field of electronics displays.
2. The NBTE and NUC should enrich their curriculum for electronics engineering students by including emerging technologies such as electronic displays.

## REFERENCES

- [1] Chris, W.(2014, August 20). OLEDs (Organic LEDs) and LEPs (light-emitting polymers). Retrieved from <http://www.explainthatstuff.com>
- [2] Freudenrich, Craig, Ph.D.(2008). "How OLEDs Work." Howstuffworks. Retrieved from <http://electronics.howstuffworks.com/oled.htm>.
- [3] Organic Lighting Technologies. "Technology." Organic Lighting Technologies LLC. 2006. Retrieved from <http://www.o-lite.com/technology.htm>.
- [4] OLED-info. "OLED Lights and Sony OLEDs." OLED displays and television resources, info and news. Retrieved from <http://www.oled-info.com>.

## Fluid Flow through Woven Fabrics by the Lattice-Boltzmann Method

<sup>1</sup>Mohammad Miyan, <sup>2</sup>Pramod Kumar Pant

<sup>1</sup>Department of Mathematics, Shia P. G. College, University of Lucknow, Lucknow, India

<sup>2</sup>Department of Mathematics, Bhagwant University, Ajmer, Rajasthan, India

**ABSTRACT:** The Lattice-Boltzmann method is used for investigating the dual scale problems of the fluid flow through three dimensional multifilament woven fabrics. These fabrics are generally characterized by two different length scales i.e., the thickness of a single filament and the thickness of a bundle of filaments, known as yarn. The thickness of yarn is of the two orders of magnitude greater than that of the single filament. The inter-yarn and intra-yarn spaces are also of the two different scales. The direct simulation of fluid flow in multifilament woven fabrics includes the resolution of the flow in the inter-yarn and intra-yarn pores of the media. In the present paper, there is an analysis of the fluid flow in woven fabrics with the Lattice-Boltzmann method. The tortuosities are given by the LB simulations and image analysis. The transverse and in plane tortuosities were determined by LB flow simulations and by image analysis that uses the chord length distribution algorithm [20]. The paper sheets formed as strictly layered structures in the laboratory sheet mold show little change in tortuosity with changing porosity as the fibres were refined the density of the sheet was increased. Hence, the transverse tortuosity has a significant change as a result of refining and densification. That indicates a more complex and less permeable structure. The chord length method tends to give higher values for tortuosity since the hydrodynamic tortuosity given by the LB method gives more weight to paths of least resistance, whereas this method does not prefer any particular fluid path or chord length. The graphs show that the tortuosity varies inversely with porosity of the media. The results are shown with the help of tables and figures.

**Keywords:** Flow, Woven Fabrics, Porous Media, Lattice-Boltzmann method.

### I. INTRODUCTION

The woven fibrous porous media can be found in various industrial applications including but unlimited to preforming in polymer liquid composite mouldings, filters for separation of solid particles and the gas diffusion layer of proton exchange membrane fuel cells. The application that is of main interest in the present paper is the flow in the woven fabrics preform of the resin transfer moulding (RTM) process. The RTM process is a popular method for manufacturing of both the small and large composite parts. The main challenge in the RTM process is the prediction of resin flow in the mould through preform. So the knowledge of the resin flow pattern inside the mould is necessary for the determination of optimum location of the air vents and injection gates on the mould for reducing the possibility of void formation in the manufactured parts. The preform is usually in the form of multifilament yarns bound together in the different forms and structures. In this work, we focus on preforms constructed from woven fabrics;

Hu [10] and Chou [5] have discussed the design and properties of the micro structure of woven preform. Woven fabrics are generally characterized by two different length scales:

- The length scale of a single filament, (e.g. its radius)
- The length scale of a bundle of filaments (a yarn), which is usually about two orders of magnitude greater than that of a single filament.

Nabovati A. *et al.*, [14] have analyzed in details about the three-dimensional multifilament of woven fabrics. The woven fabrics have a dual porosity characteristic. The first defined porosity is related with the internal structure of a yarn, and is termed here the *yarn porosity* or  $y$ . The yarn porosity gives the voids between the constituent filaments of a yarn and characterizes the intra-yarn flow. This is defined as the ratio of the void volume within a yarn to the total volume of the yarn. The second porosity is due to the void spaces between the yarns and is termed as the *weave porosity* or  $w$ . So, for calculating the weave porosity, the yarns are taken as a

solid *i.e.*, zero yarn porosity; so the weave porosity is taken as the ratio of the void volume between the yarns to the total volume of the minimal bounding box of the fabric sheet. The simulations of fluid flow through woven porous media capture the flow through both the yarn and weave porosities. The easiest structural form of fibrous media that has been studied in the analysis is a regular array of infinitely long solid cylinders. Sangani *et al.* [22], Gebart [6], and Brusckhe *et al.* [4] studied the flow around solid cylinders of infinite length with square and hexagonal arrangements and proposed correlations for the axial and transverse flow permeabilities. The flow in solid yarn woven fabrics was first characterized by using the orifice analogy [4], [19], in which the pores between the yarns were considered as a series of orifices and the discharge coefficient was given as a function of the pore structure. Later Lu *et al.* [12] investigated numerically the fluid flow in a monofilament filter cloth by using the commercial software, employing the finite volume method to simulate fluid flow in three basic, bi-axial, plain-weave models for the woven filters. Based on these three weave-models, four different pore structures were extracted to use in the fluid flow simulations. The corrected form for the discharge coefficient in the orifice model was proposed based on the simulation results. With the orifice analogy, Gooijer *et al.* [8] developed a geometrical model for the flow resistance

in monofilament woven fabrics by using the four unit pore structures of Lu *et al.* [12]. The proposed structure was in good agreement with the experimental data. With the methodology of Lu *et al.* [12] and Wang *et al.* [23] simulated fluid flow in a unit cell of monofilament woven fabric and given the values related to the discharge coefficient for fabrics with elliptical cross sections. By which, they found that the discharge coefficient decreases with the increasing aspect ratio of the cross-section of the fibres. Simulating fluid flow in multifilament woven samples is a hard and challenging task due to the dual scale nature of the weave and yarn structures. But the directly simulating flow at both scales is computationally expensive. So one popular approach is to simulate the fluid flow in two dimensions in the place of three dimensions. These simulations are less demanding and they are not able to predict the effects of the curvature of yarns and their relative structure on the overall permeability of the multifilament woven samples. Papathanasiou [15] solved numerically the Stokes equation in two dimensions by using the Boundary Element Method in square arrays of permeable multifilament yarns, in which every yarn was made up of circles representing the cross sections of the constituent filaments. So the effective permeability of the medium was found as a function of the weave and yarn porosities. In the same patterns the studies were performed for the square and hexagonal arrangement of filaments in yarns, where the yarns had the circular cross section [13] and for yarns with elliptical cross section [16]. Papathanasiou [17] had given a correlation for the effective permeability of two-dimensional hexagonal arrangements of filament clusters as a function of the weave and yarn permeabilities given by the formula:

$$K_p = K_w \left\{ 1 + \alpha \left( \frac{K_w}{K_y} \right)^{n-1} \right\} \quad (1)$$

Where  $K_p$  is the effective permeability of the multifilament fabric,  $K_w$  is the weave permeability,  $K_y$  is the permeability of the cross-sections of yarns and  $\alpha$  and  $n$  are constants related to the geometric structure of the fabric. The given relationship is based on dimensional arguments and from consideration of the behavior at high and low  $K_w/K_y$  ratio asymptotes. Papathanasiou [17] had given values for  $\alpha$  and  $n$  by fitting to the numerical simulation data and obtained the values as follows:

(1.1)  $\alpha = 2.3$  and  $n = 0.59$ ; when filaments are arranged in a square array,

(1.2)  $\alpha = 3.0$  and  $n = 0.625$ ; when filaments are arranged in a hexagonal array.

The author claims that values of  $\alpha = 2.67$  and  $n = 0.61$  give an acceptable fit for both square and hexagonal ordered

structures of filaments in the clusters and for high yarn and low weave porosities. For a two dimensional case, the  $K_w$  and  $K_y$  depend on the weave and yarn porosities, so the arrangement of the filaments inside the yarns and the arrangement of the yarns themselves. The flow in an ordered structures of cylinders has been studied in depth and

various correlations for the transverse permeability,  $K$ , of the media have been given, in which the taken relationship is given by Gebart [6] is one of the mostly used *i.e.*,

$$\frac{K}{R^2} = C \left\{ \sqrt{\frac{1 - \phi_c}{1 - \phi}} - 1 \right\}^{\frac{2}{n}} \quad (2)$$

Where  $R$  is the radius of the cylinder,  $\phi$  is the porosity of the medium,  $\phi_c$  is the critical value of porosity below which the fibres make contact and there is no permeating flow and  $C$  is a geometric factor which depends on the type of the packing;

Gebart calculates the values as follows:

(1.3)  $C = 16/9\pi\sqrt{2}$ ,  $\phi_c = 1 - \pi/4$  for the square array of cylinders,

(1.4)  $C=16/9\pi\sqrt{6}$ ,  $\phi_c=1-\pi/2$  for the hexagonal array.

The equation (2) will be used for predicting  $K_y$  by setting  $R$  equal to the filament radius and  $\phi$  equal to the yarn porosity and  $K_w$  can be predicted by setting  $R$  equal to the yarn radius and  $\phi$  equal to the weave porosity. The polymeric carrier fabrics are generally used in industrial processes mostly including manufacture of paper and board. The 3D structures of the fabrics play a critical role for deciding the energy and manufacturing efficiency of the process and end-use properties of the product. Now the analysis is based by using X-ray  $\mu$ CT to visualize the 3D structure of polymeric fabrics commonly used in paper manufacturing. The 3D structural characteristics and fluid transport properties for the tomographic images were measured with the image analysis techniques and the Lattice-Boltzmann method.

## II. TOMOGRAPHIC IMAGES

The X-ray tomographic images were taken by two different types of paper machine forming fabrics. The two samples of each wire type were imaged. The resolution of the images was  $4.41 \mu\text{m}$  and  $4.34 \mu\text{m}$  for the type I and type II samples respectively. A typical yarn diameter was thus of the order of 40 pixels, so the resolution of the images was very good, as for the level of discreteness effects. The lateral sizes of the rectangular images were about one unit cell of the wires that were about  $2.3 \times 2.2 \text{ mm}^2$  and  $3.0 \times 2.6 \text{ mm}^2$  for type- I and type-II wires respectively. The samples images of type-I and type-II of wires are given by figures-1 and figure-2 respectively.

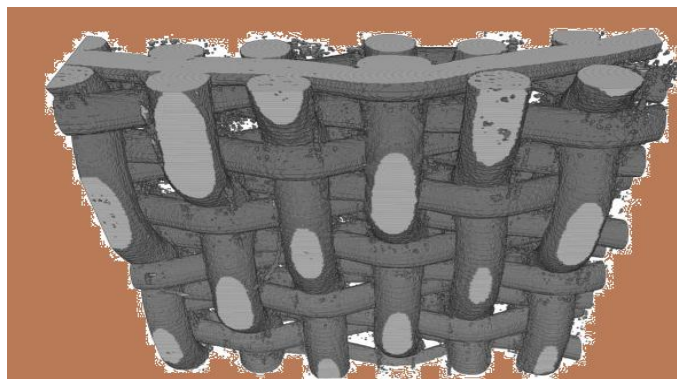


Figure-1 (Sample of the paper of type I)

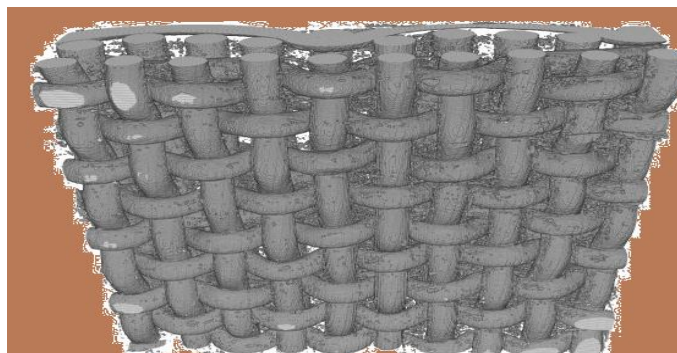


Figure-2 (Sample of the paper of type II)

The unlike disordered materials *i.e.*, paper, wires can be used to some extent to analyses the quality of the used tomographic images, as one can expect to obtain a regular interior structure. In this regard, one finds from the images that the surface of the wires seems rough and spurious tiny solid obstacles seem to be created by the imaging procedure within the pore space. In the similar manner, the solid phase seems to contain incidental small voids. So that the error created by the small irregularities can be analyzed to be very small *i.e.*, likely of the order of a few per cent.

Aaltosalmi U. analyzed in his thesis by taking the three different sample papers *i.e.*, filter paper, newsprint and hand sheets were taken to check the applicability of  $X - \mu$ CT techniques. The hand sheet was made of bleached softwood Kraft pulp of spruce. The newsprint was made of thermo-mechanical pulp of spruce in a paper machine and the paper was not calendared. The filter paper was a circular black ribbon filter paper made of cotton linters. The Table -1 shows the thickness, density and basis weight of the imaged sample papers. The accuracies of these quantities are typically of the order of a few per cent, so the taken samples have the distinct characteristics and properties, so are expected to give distinct results in the image analysis and fluid transport simulations [1].

Table -1 (Bulk properties of the imaged sample papers)

<i>Sample papers</i>	<i>Thickness (<math>\mu\text{m}</math>)</i>	<i>Density (<math>\text{kg}/\text{m}^3</math>)</i>	<i>Basis weight (<math>\text{g}/\text{m}^2</math>)</i>
Hand sheet paper	98	647	63.4
Newsprint	109	403	44.1
Filter paper	158	486	76.7

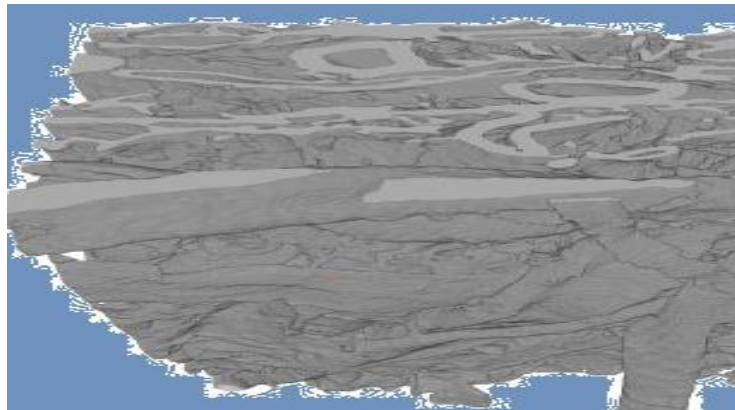


Figure-3(High resolution image of paper)

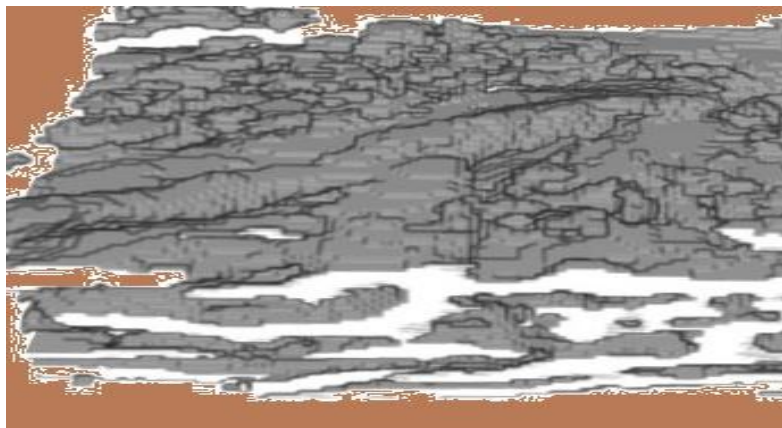


Figure-4(Low resolution image of paper)

So, to identify the necessary level of structural details for a reliable characterization of different paper grades, Aaltosalmi U. [1] used the samples imaged by using high and low resolution  $X - \mu\text{CT}$  techniques. The figure-3 and figure-4 show high and low resolution images of newsprint paper. The relatively small image sizes *i.e.*, below  $0.1 \text{ mm}^2$ , were used in the high resolution and several low resolution images. Also a set with a larger image size *i.e.*, about  $1 \text{ mm}^2$ , was taken for the low resolution technique. The low resolution images were obtained using polychromatic radiation [11] and the high resolution images were obtained using monochromatic synchrotron radiation in the phase-contrast mode [21]. The low and high resolution images were reconstructed and processed according to the routines [2], [11]. The small detached volumes of fibrous and porous phases were removed by the 3-D filtering technique and the surfaces of the samples were defined using the rolling ball algorithm [3], [22]. Due to this algorithm surface is defined by the route of a ball with a suitable radius that rolls along the surface. This method allows the detection of the main structures of uneven surfaces excluding the interior pores [1].

The image analysis techniques [11], [20] were used to determine 3-D structural characteristics such as porosity, specific surface area, hydraulic pore-radius distribution and diffusive tortuosity in the principal directions. The diffusive tortuosity measurements were based on various successful paths of a random walk simulation through the paper volume with a random starting point on an appropriate volume edge [1].



Table-2 (Some properties founded from the 3-D images of the samples)

Sample papers	Image size	Resolutions	Thickness $T$ ( $\mu\text{m}$ )	Density $\rho$ ( $\text{kg}/\text{m}^3$ )	Basis weight $B_w$ ( $\text{g}/\text{m}^2$ )	Porosity $\phi$ (%)	Specific surface area $SSA$ ( $\times 10^3/\text{m}$ )
Hand sheet paper	Small	High	90.1	829	74.9	46.4	303
	Small	Low	88.5	857	75.5	44.9	179
	Large	Low	101.5	796	79.6	49.0	176
News paper	Small	High	99.3	655	65.1	57.7	387
	Small	Low	119.2	651	76.1	58.2	179
	Large	Low	115.7	655	74.3	58.0	181
Filter paper	Small	High	190.9	550	105.5	64.3	234
	Small	Low	181.6	641	116.2	58.7	164
	Large	Low	179.4	570	101.8	63.4	157

The values were determined in the principal directions by Aaltosalmi U. [1]. So, such flow related objects parameters as the tortuosity of the flow paths and the permeability of flow in the transverse direction, were calculated by using direct numerical simulations with the Lattice-Boltzmann method. There is a use of a specific *LBGK* model with a uniform external body force and the bounce back boundary condition at the solid fluid interfaces. So, to ensure an unrestricted fluid flow at the inlet and outlet, a free fluid layer with the thickness of about 1/10 of the sample thickness was added on top of the sample and the boundary conditions were imposed in all outer boundaries of the rectangular computation volume. Then to compare the ability of the techniques of imaging to find out the correct amount of material in the imaged volumes, the quantities of table-1 *i.e.*, thickness, density and basis weight, were also computed by image analysis. The results shown in the table-2 are together with porosity and specific surface area. So, in the following, the values of low resolution samples are mean values obtained for available samples. The slight differences between the bulk properties and the image analysis results obtained in part from normal variation *i.e.*, are related to the formation of the samples used but also from the difference between the standard thickness and the rolling ball defined thickness and from a probable over estimation of the density of fibres *i.e.*, used in table-2 for all the papers. Hence the used techniques may over estimate the volume of the solid objects in the images. The specific surface area for the low resolution images is consistently less than that of the high resolution images. Now the observed differences are most probably occurs due to the differences in the level of detail. Then, it is clear from visual comparisons that the high resolution technique preserves the topology of the fibrous and porous structure objects better than the low resolution technique. But the large volume images are multiple times larger than the small volume images; there is no signified difference between the respective properties and characteristics. This indicates that even small volumes are sufficient and suitable for a good estimation of porosity and specific surface area.

### III. TORTUOSITY AND PERMEABILITY

For a better understanding and analysis of the transport resistance of the samples, their tortuosities and permeabilities were measured by Aaltosalmi U. [1], and the results are shown by the table-3.

Table-3 (Tortuosity and permeability determined for various paper samples and imaging techniques)

Sample papers	Image size	Resolutions	$\tau_1$	$\tau_2$	$\tau_3$	$\tau_4$	$\phi$
Hand sheet paper	Small	High	2.69	3.47	16.0	3.78	0.0363
	Small	Low	1.21	1.36	2.93	1.98	0.343
	Large	Low	1.25	1.36	3.25	2.11	0.325
News paper	Small	High	1.43	3.50	6.76	2.32	0.117
	Small	Low	1.12	1.56	3.57	2.04	0.524
	Large	Low	1.07	1.36	2.96	2.24	0.548
Filter paper	Small	High	1.23	1.33	4.69	1.58	1.95
	Small	Low	1.16	1.23	1.99	1.52	1.62
	Large	Low	1.10	1.17	1.61	1.55	2.78

In the table-3,  $\tau_1$ ,  $\tau_2$  and  $\tau_3$  are the diffusive tortuosity values in the machine direction, cross direction and transverse directions respectively obtained from the random walk simulations.  $\tau_4$  and  $\phi$  are the flow tortuosity and permeability in the transverse direction obtained by using direct numerical simulation by the Lattice-Boltzmann method.

The largest differences between the tortuosities, in different sample papers as well as in the different principal directions, were observed in the high resolution images, due to their higher level of detail. The smallest differences were found in the small, low resolution images. Increase in the resolution will though increase the differences in the measured tortuosity and will thus improve the possibility to measure the effects of paper structure on the tortuosity and other transport properties and characteristics. The low resolution images will mainly provide right trends in these properties, so are useful for comparative studies. Their applicability is limited by their lower ability to analyze small particles such as fines, fillers and fibrils, and fibre-orientation anisotropy. The flow tortuosity  $\tau_f$  was found to be systematically lower than the diffusive transverse tortuosity  $\tau_d$ . There are expectations since the streamlined hydrodynamic paths through the pore space are smoother than the winding random walk paths of diffusive particles. So that the dependence of the flow tortuosity on different structural properties of the samples is qualitatively similar to that of the diffusive tortuosity and the same qualitative analysis is suitable for both. About the results for permeability and flow tortuosity, there is no significant difference between the values calculated for small and large samples. Hence the permeabilities of the low resolution images are higher than those of the high resolution images. The difference is moderate at high porosities and becomes significant at lower porosities. Now, the poor resolution of the low resolution images makes dense, complex structures more open for transport, whereas already open and relatively simple structures are affected lesser. Particularly, the high resolution results seem to be in qualitative agreement with the known limiting behavior of flow tortuosity. This should approach unity as the porosity approaches unity and diverge at some small but non zero value of porosity. Generally, the results obtained for the high resolution samples by Aaltosalmi U. [1] will be taken more reliable and suitable. But the results discussed here, are qualitatively quite, they are subject to uncertainty arising from the limited available data and calculations. So to estimate the order of magnitude of purely numerical errors arising from the different used discretizations, there are a set of test samples by reducing the resolution of the original high resolution images to that of the low resolution images. The greatest difference between the tortuosities and permeabilities obtained for the original high resolution samples and the reduced resolution samples was about 1/5. The error due to the resolution could be compared with that due to sample size. The later was determined by dividing the original large images to several sub-images, the size of that coincided with that of the original smaller tomographic images. The greatest difference between the values calculated for the original large image and the mean value of the corresponding sub-images was about 1/20 for tortuosity and 1/5 for permeability and these values are very nearer with the values obtained by using *Kozeny's law*. The conclusion is that numerical uncertainties are not much suitable for the qualitative results obtained here. Instead, the natural variation intrinsic to paper material can be a much more important source of uncertainty for the results obtained on tomographic images. So, the uncertainties in the results are from the formation effect, to be of the order of a second factor in permeability and in the tortuosity.

#### IV. NUMERICAL SIMULATIONS

Aaltosalmi U. [1] analyses the numerical results of fluid flow through tomographic images of paper. The hand sheets of a basis weight of 300 g/m<sup>2</sup> were prepared from bleached softwood Kraft pulp, which was beaten to different refining levels between 220 and 670 CSF in a laboratory beater. The three dimensional  $X - \mu CT$  images of the samples were made by using the phase contrast method [7], [9]. The resolution and the size of the images were about 2  $\mu m$  and 1 mm<sup>2</sup> respectively. The paper surface layers were removed in the direction of the transverse axis, now the thicknesses of the final samples lie between 120  $\mu m$  and 200  $\mu m$ . The examples of structures observed by tomographic imaging of the paper samples are given by the figure-5. The images of these samples were observed for the transverse and inplane permeability, porosity, specific surface area, and tortuosity by using image analysis techniques [7], [20] and Lattice-Boltzmann flow simulations in the two orthogonal directions. So a reasonable comparison with conventional mercury intrusion porosimetry data from the same samples was obtained [20].

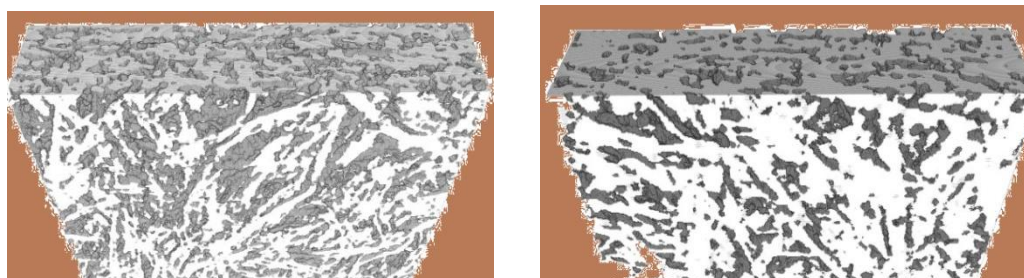


Figure-5 (Tomographic images of paper samples)

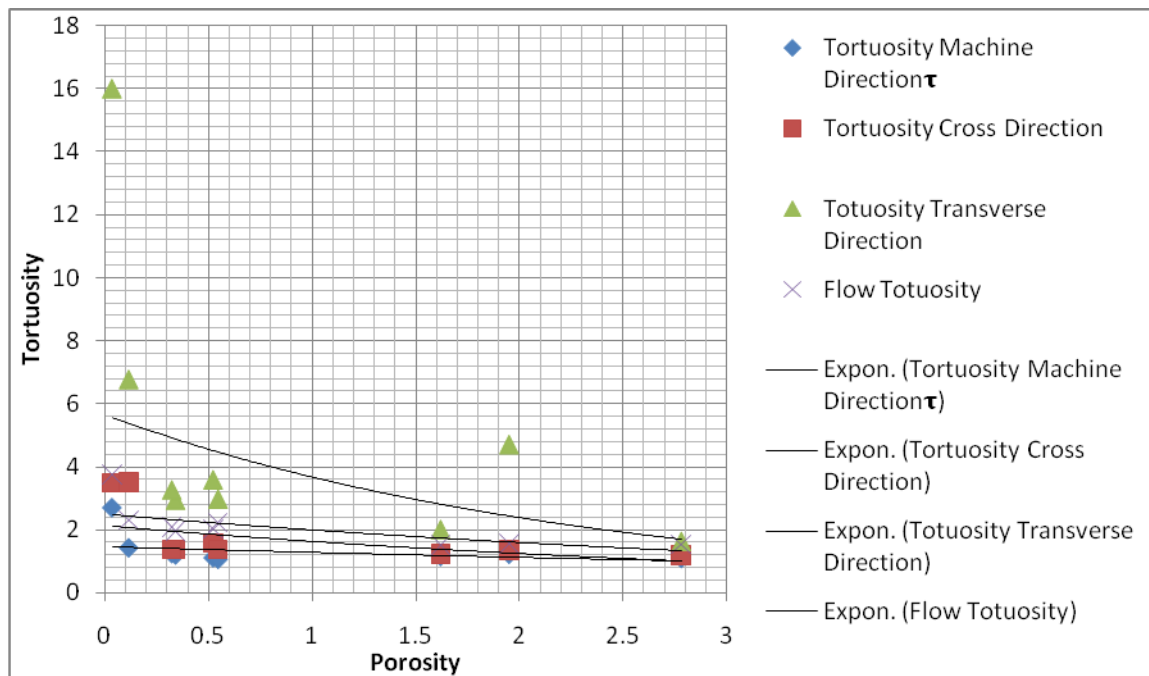


Figure-6

## V. DISCUSSION AND RESULTS

The graphical representations with the help of table-3 are shown by the figure-6. The figure-6 shows that the tortuosity varies inversely with porosity of the media. The tortuosities are given by the LB simulations and image analysis. The transverse and in plane tortuosities were determined by LB flow simulations and by image analysis that uses the chord length distribution algorithm [20]. The paper sheets formed as strictly layered structures in the laboratory sheet mold show little change in tortuosity with changing porosity as the fibres were refined the density of the sheet was increased. Hence, the transverse tortuosity has a significant change as a result of refining and densification. That indicates a more complex and less permeable structure. The chord length method tends to give higher values for tortuosity since the hydrodynamic tortuosity given by the LB method gives more weight to paths of least resistance, whereas this method does not prefer any particular fluid path or chord length.

## REFERENCES

- [1] Aaltosalmi U. Fluid flow in porous media with the Lattice-Boltzmann method, University of Jyväskylä, *Research report No. 3/2005*, Finland, pp.39-45.
- [2] Antoine C., Nygard P., Gregersen Q. W., Weitkamp T., Rau C. 3D images of paper obtained by phase-contrast X-ray microtomography: image quality and binarisation, *Nucl. Inst. Meth. Phys. Res. A* 490 (2002), pp. 392-410.
- [3] Aronsson M. On 3-D fibre measurements of digitized paper, Ph.D. thesis, *Swedish University of Agricultural Sciences* (2002).
- [4] Bruschke M.V., Advani SG. Flow of generalized Newtonian fluids across a periodic array of cylinders. *J Rheol* 1993; 37(3) pp. 479-98.
- [5] Chou T. Microstructural design of fiber composites. Cambridge: *Cambridge University Press*; 1992.
- [6] Gebart B.R. Permeability of unidirectional reinforcements for RTM. *J Compos Mater* 1992; 26(8) pp.1100-1133.
- [7] Goel A., Tzanakakis M., Huang S., Ramaswamy S., Choi D., Ramarao B. V. Characterization of the three-dimensional structure of paper using X-ray microtomography, *TAPPI J.* 84 (5) (2001), pp.1-8.
- [8] Gooijer H, Warmoeskerken M.M.C.G., Wassink J.G. Flow resistance of textile materials – Part I: monofilament fabrics. *Text Res J.* 2003;73(5), pp. 437-443.
- [9] Gureyev T. E., Evans R., Stevenson A. W., Gao D., Wilkins S. W. X-ray phasecontrast microscopy of paper, *TAPPI J.* 84 (2), (2001), pp. 52.
- [10] Hu J. Structure and mechanics of woven fabrics. Cambridge: *Woodhead Publishing*; 2004.
- [11] Huang S., Goel A., Ramaswamy S., Ramarao B. V., Choi D. Transverse and inplane pore structure characterisation of paper, *Appita J.* 55 (3) (2002), pp. 230-234.
- [12] Lu W.M., Tung K.L., Hwang K.J. Fluid flow through basic weaves of monofilament filter cloth, *Text Res J.* 1996; 66(5), pp. 311-23.
- [13] Markicevic B., Papathanasiou T.D. On the apparent permeability of regular arrays of non uniform fibers. *Phys. Fluids* 2002; 14(9), pp. 3347-3349.
- [14] Nabovati A., Llewellyn E.W., Sousa A. C. M. Through-thickness permeability prediction of three-dimensional multifilament woven fabrics, *Composites: Part A*, 41 (2010), pp. 453-463.
- [15] Papathanasiou T.D. On the effective permeability of square arrays of permeable fiber tows. *Int J Multiph. Flow* 1997; 23(1), pp. 81-92.
- [16] Papathanasiou T.D., Gravel E.M., Barwick S.C. Non-isotropic structured fibrous media: the permeability of arrays of fiber bundles of elliptical cross section, *Polym. Compos.* 2002; 23(4), pp. 520-529.

- [16] Papathanasiou T.D. Flow across structured fiber bundles: a dimensionless correlation, *Int J Multiph. Flow* 2001; 27(8), pp.1451–1461.
- [17] Pedersen G.C. Fluid flow through monofilament fabrics, *In: 64th national meeting of AIChE*, New Orleans; 1969.
- [18] Pedersen G.C. Fluid flow through mono filament fabrics, *Filtr Sep.* 1974; 11(6), pp. 586–589.
- [19] Ramaswamy S., Huang S., Goel A., Cooper A., Choi D., Bandyopadhyay A., Ramarao B. V. The 3D structure of paper and its relationship to moisture transport in liquid and vapor forms, in: *The Science of Papermaking - trans.12th Fundamental Research Symposium*, Vol. 2, The Pulp and Paper Fundamental Research Society, Bury, Lancashire, UK, 2001, pp. 1281–1311.
- [20] Samuelsen E. J., Gregersen Q. W., Houen P. J., Helle T., Raven C., Snigirev A. Three-dimensional imaging of paper by use of synchrotron X-ray microtomography, *J. Pulp Pap. Sci.* 27 (2) (2001), pp. 50–53.
- [21] Sangani A.S., Acrivos A. Slow flow past periodic arrays of cylinders with application to heat transfer, *Int. J. Multiph. Flow*, 1982; 8(3), pp.193–206.
- [22] Sternberg S. R. Biomedical image processing, *IEEE Comp.*, 16 (1), (1983), pp. 22–34.
- [23] Wang Q., Maze B., Tafreshi H.V. On the pressure drop modeling of monofilament-woven fabrics, *Chem. Eng. Sci.* 2007; 62(17), pp. 4817–4821.

## The Effect Of Chemical Treatment On Tensile Properties Of Soil Retted Entada Mannii Fibres.

O.P. Balogun<sup>1,2</sup>, J.A. Omotoyinbo<sup>1</sup>, K.K. Alaneme<sup>1</sup>, I.O. Oladele<sup>1</sup>, B.J. Babalola<sup>1,2</sup>

<sup>1</sup>(Department of Metallurgical and Materials Engineering, Federal University of Technology, Akure, Ondo State, Nigeria)

<sup>2</sup>(Prototype Engineering Development Institute (NASENI), Ilesha, Osun State, Nigeria)

**ABSTRACT :** This research work was carried out to investigate the influence of chemical treatment on tensile properties of soil extracted Entada mannii fibre. Entada mannii fibre was extracted by soil retting method and after which the fermented fibres were washed with distilled water and dried in an oven. The dried fibres obtained were treated with sodium hydroxide (NaOH) and potassium hydroxide (KOH) solutions and percentages of their constituents were determined. The fibre strands were characterized using the scanning electron microscope while the tensile properties were determined using instron universal tensile testing machine. The tensile results revealed that, fibres treated sequentially with (KOH) behaves superiorly than the NaOH treated and untreated fibres. The alkaline treatment also enhanced the removal of lignin and hemicellulose in treated fibres which may be detrimental to the interfacial bonding strength compared to untreated fibres. However, the results of SEM analysis revealed rough surfaces due to removal of impurities, waxes and the fibre constituents (lignin and hemicellulose) on treated while the untreated revealed smooth surface with the presence of the constituents.

**Keywords** - Chemical treatment; Soil retting; Extracted fibre; Constituents; Fermented

### I. INTRODUCTION

In recent years, natural fibres appear to be the outstanding materials which come as the viable and abundant substitute for the expensive and nonrenewable synthetic fibres [1]. The use of plant fibres as reinforcements of polymer is attracting the interest of industries and researchers because of the wonderful potentials and their unique properties [2]. Natural fibres like sisal, banana, jute, oil palm, kenaf and coir has been used as reinforcement in thermoplastic and thermoset composite for various engineering applications [3]. They are environmentally friendly, fully biodegradable, abundantly available, renewable, cheap, low density, specific strength and stiffness compared to glassfibres, carbon and aramid fibers [4]. Natural fibres properties are influenced by many factors, including plant type and variety, growth conditions, and the method used to extract the fibre bundles [5]. Among natural fibres for composites are the bast fibers, kenaf, flax, ramie and hemp extracted from the stems of plants due to their very good mechanical properties [6].

However, one of the bast plant with great potentials and that has not much received attention from researchers is *Entada mannii* bast fibre which belongs to the family (Oliv.) Tisser. leguminous mermosaesae, liana plant. The plant is 2 to 3m high semi-climber which grows in the tropical forest of Nigeria, Gabon and Madagascar [7]. They show extreme variations in mechanical properties which includes; the stiffness in the elastic range of bending, torsion, and tension as well as other properties in the nonelastic range up to failure, toughness, extensibility, and critical strain to mention a few make them suitable for use in composites reinforcements [8-9]. Extraction of the fibres from the bast by conventional method of retting is considered for this study. Retting is a microbial process that breaks the chemical bonds that hold the stem together and allows separation of the bast fibres from the woody core. The two traditional types of retting are soil retted and water retting [9]. To extract fibres for industrial uses, stems are retted to separate fibre from non-fibre stem issues. In this process, bast fibre bundles are separated from the core, epidermis, and cuticle and are also separated into smaller bundles [9-11]. Currently, soil retting is the primary process used for the industrial production of bast fibres nevertheless water retting is still carried out in some place [12]. In soil retting, stalks are laid on the

ground, and pectins are attacked by pectinolytic microorganisms, mainly aerobic fungi [13]. Soil retting is most popular in Europe although it is strongly dependent on the geographical location, produces coarser and lower quality fibres than those produced using water retting technique [14]

Hence, the use of natural fibre in composite reinforcement developed some drawback due to pertinent characteristics such as fibre incompatibility, fibre aggregations that occur during processing and compounding showing a poor fibre-matrix adhesion due to presence of the fibre constituents such as lignin, hemicellulose, wax and impurities [15]. The adoption of chemical treatment on natural fibres which removes these fibre constituents improves the compatibility of the fibre and the matrix and better surface adhesion [16]. Alkaline treatments such as potassium hydroxide and sodium hydroxides applied to fibre surface during treatment is called mercerization [17]. They promote the removal of the constituents, impurities and oil soluble in alkaline solutions thereby reduced the fibre diameter and level of aggregations of the fibres, improved the mechanical properties and exposed the fibre surface and becomes rougher [18].

Therefore this research work aimed at assessing the effect of soil retting extraction method on the mechanical properties of *Entada mannii* fibre.

## II. MATERIALS AND METHOD

### 2.1 Materials

The *Entada mannii* plant stem was obtained from Ikare Akoko, Ondo state, Nigeria. The *Entada mannii* plant was identified at the Federal College of Forestry Herbarium, Ibadan, Nigeria. NaOH and KOH were used to separate the fibre from their constituents.

### 2.2 Method

#### 2.2.1 Extraction of fibre (Soil retting)

The harvested *Entada mannii* stem plant was extracted by conventional soil retting method as shown in Figure 1. *Entada mannii* fibres were stripped from the stem bundles and buried in moist environment for 20 days during which the bark tissues undergo fermentation and the fibres were separated from the bark bundle as strands. However, the fibres obtained were washed with distilled water in order to separate fibre strands from undesirable foreign matters and dried in an oven at 50 °C for 48 h. The fibre were characterized by employing scanning electron microscope while the fibre constituents and mechanical properties were also evaluated.



Figure 1 (a) Hand stripped fiber from the *Entada mannii* stalk (b) Burying of the fibers in a moist environment (c) Soil retted fibers after 20 days.

### 2.2.2 Fibre surface treatment

*Entada mannii* fibres were treated with 5% NaOH and 5% KOH solutions differently in a shaker water bath at 50 °C for 4 h. The insoluble residue was delignified at pH 3, washed with distilled water in order to remove mineral traces and dried in an oven at 60 °C for 48 h in order to remove fibre moisture. The untreated fibres were left as control.

### 2.2.3 Determination of the fibre constituents

In general natural fibers are hydrophilic in nature and they absorb or release moisture depending on environmental conditions. Amorphous cellulose and hemicellulose that are present in the natural fiber are mostly responsible for the high moisture absorption, since they contain easily accessible hydroxyl groups which give a high level of hydrophilic character to fiber [19]. In order to determine the fiber constituents by gravimetric method [20]: Lignin, Hemicellulose and waxes contents on the *Entada mannii* fibres has to be removed in order to enhance proper bonding between the fibre and the matrix.

#### Lignin content

2.5 g of *Entada mannii* fibres was weighed mixed with 75% sulphuric acid concentration and the mixture was kept in an ice bath and stirred continuously for 12 h. The residue was filtered with purpling cloth and washed severally with hot water to remove the acid left and transferred to a crucible. The fibre residue was oven dried at 105 °C for 2 h and cooled in a desiccators.

#### Cellulose Content

2 g of the treated and untreated fibres were weighed and dried in an oven at 100 °C for 3 h and 25 ml of distilled water was added. 1 ml of concentrated nitric acid was added and the mixture was placed in a thermostat water bath and stirred continuously at 80 °C. The fibre residue obtained was placed inside a weighed crucible in an oven at 105 °C for 20 h. The final residue obtained was weighed and cooled in a desiccator. The percentage of cellulose was calculated by the measuring weight difference.

#### Hemicelluloses Content

*Entada mannii* sample of 0.5g was weighed into a beaker while 24% KOH and NaOH solution was added to the beaker and stirred continuously for 2 h. The sample mixture was filter with purpling cloth, washed with additional KOH and NaOH solution and the filtrate was collected into another separate beaker where alcohol was added to the sample precipitate formed. The precipitated hemicelluloses were isolated by centrifuging for 10 minutes. The samples were dried in oven for 2 h at 105 °C and later transferred into desiccators and allowed to cool for 30 minutes and weighed. The weight of the precipitate was recorded and the percentage was calculated.

### 2.2.4 Determination of the tensile properties of the fibre

The single fibre pull out test was performed on treated and untreated single fibre according to ASTM-638D [21] test standards. This was done by fixing the sample on the grips of the machine after which will operated automatically. Tensile testing machine equipped with a 5 KN load cell up to a strain of 8% at a cross-head speed of 50 mm/min. 6 specimens were tested and their average fibre tensile strengths and modulus were obtained.

### 2.2.5 Fibre Characterization

Scanning electron microscope of Model JEOL JSM-7600F was used for the morphological characterization of the *Entada mannii* fibre surface. The fibres were clean thoroughly, air-dried and coated with 100 Å thick irradium in JEOL sputter ion coater at 15kV.

## III. RESULTS AND DISCUSSION

### 3.1 Chemical Treatment

The effect of chemical treatment on soil retted treated and untreated *Entada mannii* fibres are presented in Fig. 2. It is observed that KOH and NaOH treatment removed fibre constituents that could be responsible for poor fibre –matrix interfacial adhesion from the fibre surface. The percentage of cellulose in the *Entada mannii* treated fibre increases from 62.76 % untreated fibre to 66.95 % NaOH and 69.06 % KOH which increases by 7% and 10% respectively. It is evident that, after treatment, the cellulose percentage increased with KOH treatment and which effectively removes adhesives in the fibre cell wall, such as lignin, pectins and hemicelluloses covering the cellulose. Hence this enhanced the fibre surface energy and interfacial adhesion with the matrix.

The fibre surface after treatment revealed pores and hole within the fibre which could be attributed to the removal of hemicellulose and lignin. This effect became more pronounce in the KOH treated than NaOH and untreated fibres. Generally alkali treatment influences all the constituents of natural fibres due to presence of hydroxyl group undergo surface modification by chemical treatment improve the properties of the fibres [22-23].

Hemicellulose was hydrolyzed by the action of KOH and NaOH solutions, whereas lignin was removed. Removal of hemicellulose and lignin increased the relative amount of cellulose contents on the treated fibres and thus NaOH and KOH treatments dissolved a portion of hemicellulose and lignin constituents from the fibres. NaOH play the critical role in removal of lignin by means of alkaline cleavage in the lignin, which may be accompanied by condensation reactions. Lignins can be completely attacked and removed without any residue left on the fibre after NaOH treatment, but the rate of lignin removal is dependent on the NaOH concentration [24, 25].

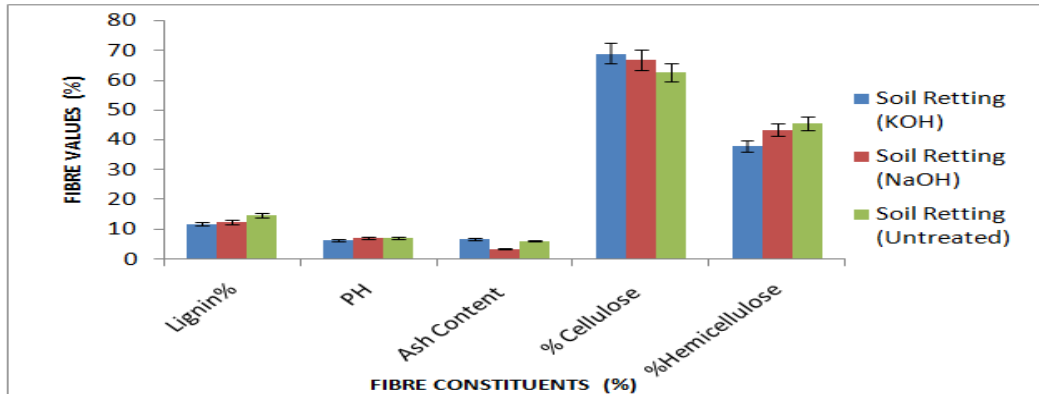


Figure 2 Plot of *Entada mannii* fibre Constituents and PH Values for both treated and untreated fibres.

### 3.2 Tensile Strength

Figure 3 show the response of the fibres to tensile strength of treated and untreated soil retted *Entada mannii* fibre. It is observed that KOH and NaOH treated fibre have the highest tensile strength of 1.6 5N/mm2, 1.33 N/mm2 and least with the untreated fibre of 0.8 N/mm2. The increase in tensile strength is attributed to removal of hemicellulose and lignin constituents covering the fibre surface which provided strength, stiffness and structural stability of the fibre as the cellulose content increase. Srinivasa et al. [26] also reported that, the areca fibres were treated in a solution of potassium hydroxide (KOH) and alkali treatment NaOH removed hemicellulose, waxes, impurities and lignin from the surface of natural fibers with increase in their tensile properties.

The agglomeration of fibre constituents occurs in the untreated fibre with the presence of these constituents and impurities thereby reduced surface energy and tensile properties of the untreated fibre. Hence, the untreated fibres exhibited lower tensile strength as compared to the treated fibers resulting in easy deformation of fibre micro fibrils during tensile loading and offer a likely poor fiber-matrix interface adhesion.

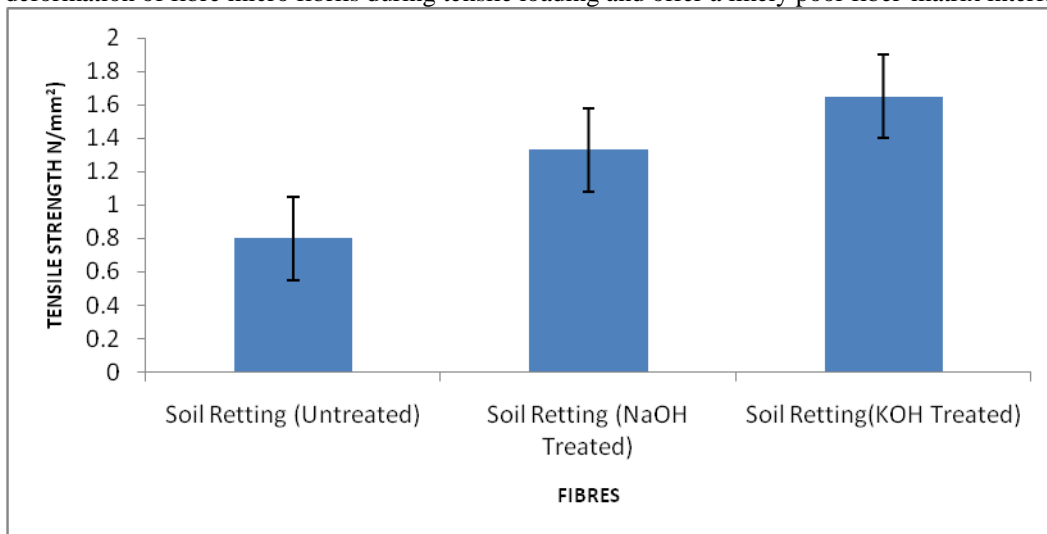


Figure 3 Tensile strength for both treated and untreated fibers



### 3.3 Young's Modulus of the Fibers

The results of the young's modulus of elasticity of the fibres are shown in Figure 4. Young's modulus is the slope of the stress-strain curve within the range of proportionality before yield. At the yield stress, a large amount of deformation takes place at constant stress [27-28]. The soil retted fibres treated with KOH gave the best young modulus of 59.8 N/mm<sup>2</sup> followed by fibres treated with NaOH of 55.53N/mm<sup>2</sup> and have the least value of 42.95 N/mm<sup>2</sup> of untreated fibre. Alkaline treatment influences surface modifications, stiffness and improved the porosity of the *Entada mannii* fiber due to the hydroxyl group within the fibre. However, untreated fibres shows a lower young modulus due to the presence of the moisture within the fibre. Natural fibres are hydrophilic in nature and have tendency to absorbed moisture than treated fibres. It is also evident that untreated fibre surface is found to be smooth due to the presence of lignin covering the fibre surfaces.

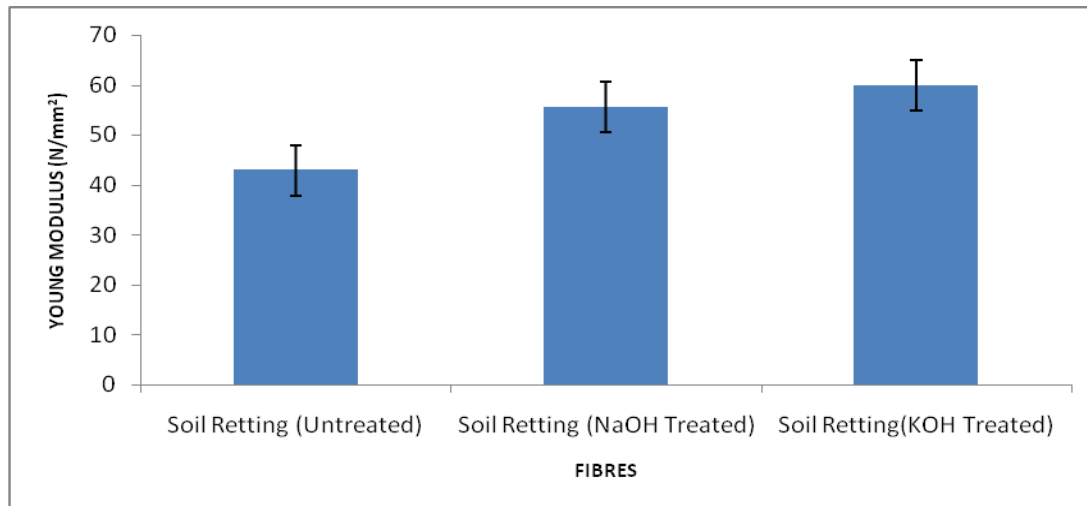


Fig.4 Young modulus against fibers for both treated and untreated fiber

### 3.4 Elongation at break

The elongation at break for the treated and untreated soil retted *Entada mannii* fibres are shown in Figure 5. The elongation at break or strain is expressed as the ratio of the total deformation to the initial dimension of the material body in which the force is applied [29]. An increase in elongation for the KOH treated was demonstrated compared to the NaOH and untreated fibres. This indicated that higher elongation of fibres indicated higher ductility and lower elongation indicates lower ductility of materials [30]. The elongation at break for the fibres experienced a significant drop with untreated fibres as a result of the impurities and waxes within the fibre as compared to the treated fibres. Hence the stiffness is interrupted and lead to the brittle nature of the untreated fibre.

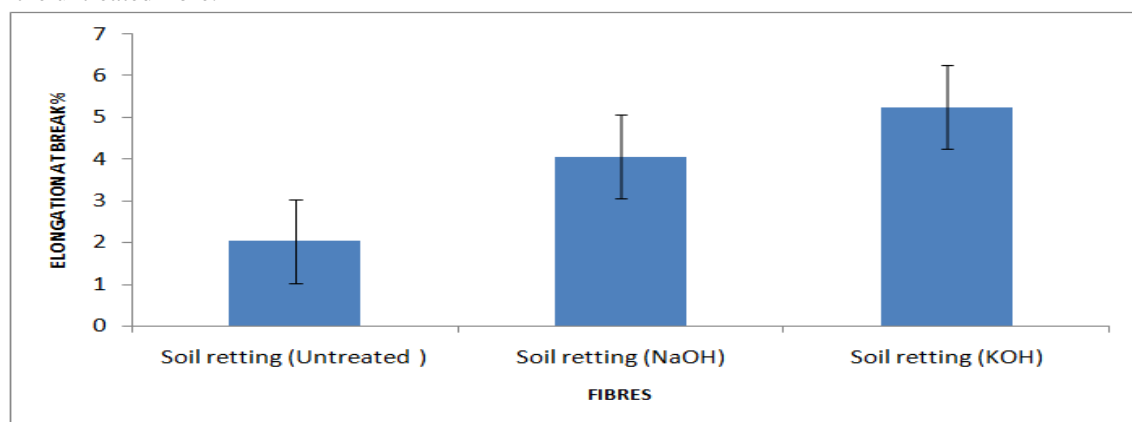


Fig.5 Elongation of fibers for both soil retted treated and untreated fibers

### 3.5 The scanning electron micrograph results

Fig.6a shows SEM micrographs of untreated *Entada mannii* fibres and constituent; cellulose, hemicellulose and lignin. The results show that untreated fibre were black in colour with smoother surface as a result of presence of the lignin, hemicellulose, wax, fatty and dirt than treated fibres. It is evident that external surface features of fibres such as contours, defects and damage and surface layer are deposited on the untreated fibre surfaces. Smooth surface of the untreated fibre connotes a lot of defects and fibre damages were observed on the surface due to presence of impurities.

Fig. 6b shows the soil retted NaOH treated fibre where surfaces appeared to be rough with increase in the cellulose. Alkaline treatment was found to be very effective in removal of lignin and hemicellulose and thereby increases the roughness of the surface which deposited pores to greater extent. Lignin acts as a cement between fibrils and when removes allows an increase in surface area thereby creating pore on the surface and improves the fibre/matrix adhesion [31]. The rough surface was observed as a result of removal of waxes and oil from the surface and thereby increases the overall roughness as shown in the Fig.6 b and 6 c. The chemical will breakdown the composite fibre bundles into smaller fibres and therefore a rough fiber surface topography is developed [32].

However, the removal of the extractives by KOH treatment in Figure 6c revealed the pore and pits. There is possibilities of Parenchyma cells that are naturally constituent of lignocelluloses fibres and presence of globular protrusion which are fatty deposit called Tylose. Exposing the rough surface with globular marks thereby increases the surface energy. The presence of the pits and globular marks affect the chemical treatment and important for the increase in the effectiveness of the surface area and higher increase in surface roughness of the fibre.

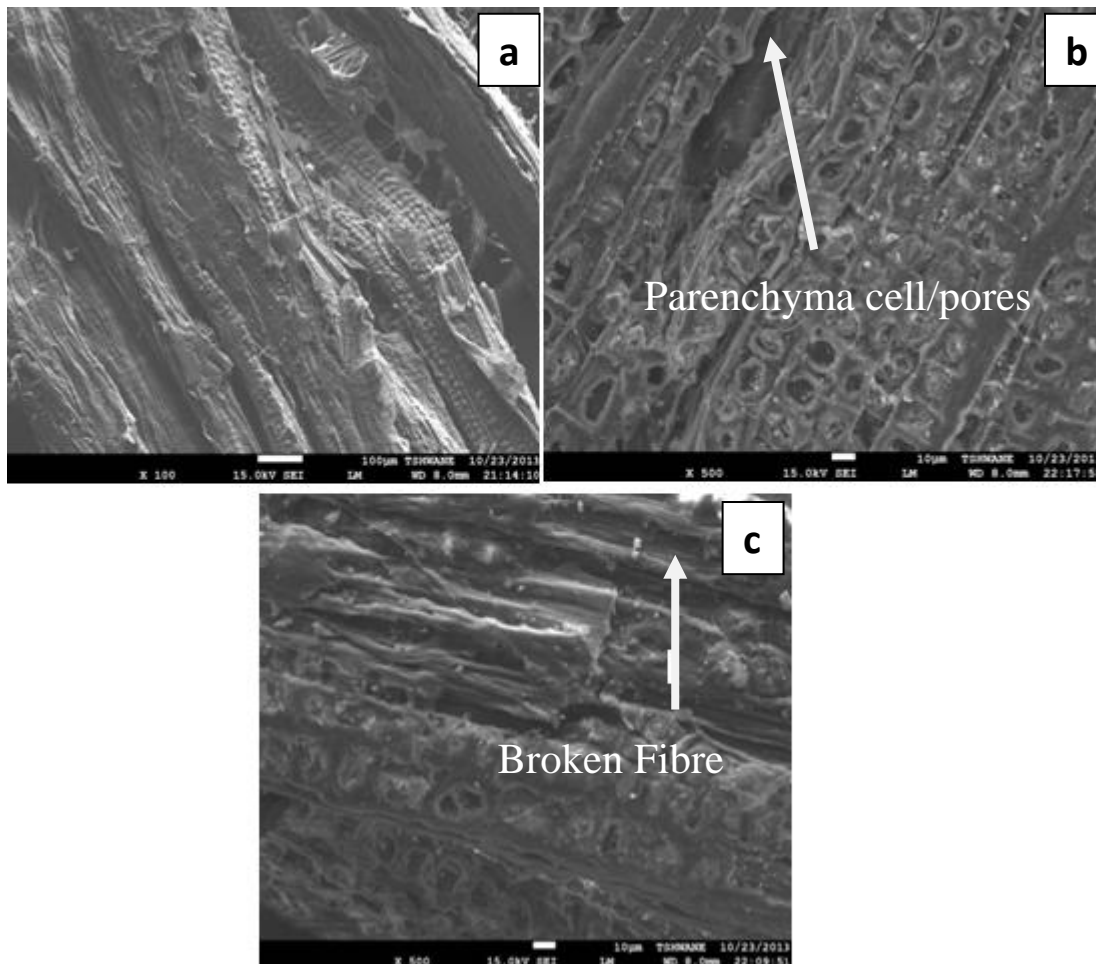


Figure 6 Scanning electron micrograph of both treated and untreated soil retted fibers

#### IV. CONCLUSION

The influence of soil retting extraction method and chemical treatment on tensile properties of *Entada mannii* (Olive Tisserant) plant stem fibres was investigated. The results show that:

1. The alkaline treatment plays a significant role in improving the mechanical properties (tensile strength, elastic modulus and elongation at break) of the *Entada mannii* fiber and decreasing the moisture absorption of the fibres.
2. KOH treated fibers gave the optimum tensile strength properties due to the removal of lignin and hemicelluloses from the fibre surface, as compared with untreated and NaOH treated fibers.
3. SEM analysis revealed that treated fiber surface differs after the removal of the lignin and hemicellulose which revealed the roughness of the fibre surface as compared than the smooth surface of the untreated fibers.
4. KOH and NaOH treated fibers show the removal of the lignin and the hemicellulose on the surface for proper adhesion but created pit and voids which could improve of bonding strength of the fibre.

#### ACKNOWLEDGEMENTS

I wish to acknowledge the following organizations for their support; Regional Initiative in Science Education (RISE), Science Initiative Group (SIG) and African Materials Science and Engineering Network (AMSEN). Prototype Engineering Development institute (PEDI-NASENI), Ilesha, Osun State Nigeria is gratefully appreciated for the time and support given to Oluwayomi Balogun.

#### REFERENCES

- [1] B.H.Amsted, F.O. Phillip and L.B.Myron, *Manufacturing Processes* (John Wiley & Sons 1987).
- [2] M.R.K. Murali, R.K. Mohana, and A.V.R. Prasad, Fabrication and testing of natural fibre composites, Vakka, sisal, bamboo and banana. *Materials and Design*, 31, 2010, 508–513.
- [3] A.I. Al-Mosawi, Mechanical Properties of plant-synthetic hybrid fiber composite, *Research Journal of engineering science*, 1(3), 2012, 22-23.
- [4] R.H. Daiane, O.J. Luiz, C.A. Sandro, and A.J. Ademir, Preparation and Characterization of Ramie-glass fiber reinforced polymer matrix hybrid composite. *Materials research Department, Engenharia de material*, 4, 2011, 445-452.
- [5] A.K. Bledzki, and J.Gasan, Composite reinforced with cellulose base fiber. *Journal Prog. Polymer Science*, 21, 1999, 74.
- [6] D.N. Saheb, and J.P. Jog, Natural fiber polymer composites: a review. *Advance Polymer Technology*, 18, 1999, 351–63.
- [7] R. Nick, I. Sandrine, and G. Friederick, and S.Thomas, Diversity of mechanical Architecture in climbing plants, *Anacological perspective*, 2005, 36-50.
- [8] K.J. Niklas, *Plant Biomechanics, an Engineering Approach to Plant Form and Function*, (The University of Chicago Press, Chicago.1992)
- [9] J. Zofija, and G. Elvyra, Physical parameters of dew retted and water retted hemp (*Cannabis sativa L.*) fibres. *Zemdirbyste-Agriculture*, 100, 2013, 71–8.
- [10] H.S. Sharma, Studies on chemical and enzyme retting of flax on a semi-industrial scale and analysis of the effluents for their physicochemical components. *International Biodeterioration*, 23, 1987, 329–342.
- [11] L. L. Zhang, R.Y. Zhu, J.Y.Chen, J.M Chen and X.X.Feng, Seawater-retting treatment of hemp and characterization of bacterial strains involved in the retting process. *Process Biochemistry*. 43, 2008, 1195–1201.
- [12] A. Daenekindt A. Flax, hemp and allied fibres in the world. *Euroflax Newsletter*, 21, 2004, 6–9, 2004.
- [13] G. Henriksson, D.E. Akin, R.T. Hanlin, C. Rodriguez, D.D. Archibald, L.L. Rigsby and K.L. Eriksson. Identification and retting efficiency of fungi isolated from dew retted flax in the United States and Europe. *Applied and Environmental Microbiology*, 63, 1997, 3950–3956.
- [14] C.Van Sumare, Retting of flax with special reference to enzyme-retting. The biology and processing of flax Belfast, Northern Ireland, 1992, 157–198.
- [15] A.Shaw, S. Sriramula, P.D. Gosling and M.K Chryssathopoulo, Introduction to polymer *Composite part B*. 2010, 41, 446-453.
- [16] N.Umar, K.O. Low and H. Jamil, *The effect of abrasiveness to process equipment using betelnut and glassfibres reinforced polyester composites*, master diss., Faculty of Engineering and Technology, Multimedia University, Malaysia, 2012, 33-36.
- [17] P. Ojaswi, *A Study on the Effect of Fibre Parameters on the Mechanical behavior of bamboo-glass fibre Reinforced epoxy based hybrid composites*, bachelor diss., Department of Mechanical Engineering National Institute of Technology Rourkela, 2012, 7 -12.
- [18] M.M. Kabir, H.Wang, K.T. Lau and F. Cardona, Effect of chemical treatment on hemp fibre structure, *Journal of Applied Surface Science*, 2013, 27, 15-21.
- [19] R.D. Chitta, *Preparation and Characterization of Polymer Matrix Composite Using Natural Fiber Lantana-Camara*, doctor diss., mechanical engineering submitted tonational institute of technology, Rourkela (deemed university) Rourkela, 2010, 2-30.
- [20] I.O. Oladele, J.A Omotoyinbo, and J.O.T. Adewara, Investigating the effect of chemical treatments on the constituents and tensile properties of Sisal Fibres. *Journal of Mineral. Materials. Char. Eng.*, 9, 2010, 569-568.
- [21] H.L. Habibi, M. Mahrouz, and Vignon, M.R...Morphological and Structural Study of Seed Pericarp of *Opuntia Ficus- Indica* prickly Pear Fruits. *Carbohydrate Polymers*, 72, 2008, 102-112.
- [22] A.L. Dotan, J.L.G. Da Silva, and H.A.L.Qureshi, Macro and Micro- Mechanical Behaviour of Natural Fiber Composites, Mechanics in Design Conf., University of Toronto, Canada, 2, 1996, 823-8319.
- [23] Y. Cao, S. Shibata, and I. Fukumoto, Mechanical properties of biodegradable composites reinforced with bagasse fiber before and after alkali treatments. *Compos Part A*, 2006, 37, 423–9.
- [24] N. Venkateshwaran, A.P. Elaya, D. Arunsundaranayagam, Fiber surface treatment and its effect on mechanical and visco-elastic behaviour of banana/epoxy composite, *Materials and Design*, 47, 2013, 979-988.
- [25] D. Roy, B.K. Sarkar, A.K. Rana, N.R. Bose, Effect of alkali treated Jute fibers on composite properties, *Bulletin of Material Science* 24, 2001, 129-135
- [26] C.V, Srinivasa, and K.N. Bharath, *Impact and Hardness Properties of Areca Fiber- Epoxy Reinforced Composites*, Master diss., Department of Mechanical Engineering, GM Institute of Technology, 2011. 4-10.

- [27] H. Nur, A.B.D. Khalid, and M.Y. Jamaludin, Tensile Behavior Of The Treated And Untreated Kenaf Fibers, National Postgraduate Seminar (NAPAS 10<sup>3</sup>), 1-9,2010
- [28] A.P. Sherey, B. Abderrahim, I. Laurent, C.Y.ves, J. Kuruvilla, and T. Sabu, Effect of fiber loading and chemical treatments on thermo physical properties of banana fiber/polypropylene commingled composite materials *Composites: Part A*. **39**, 2008, 1582–1588.
- [29] C.C Girisha and G.R Sanjeevamurthy and S. Manu, Tensile property of Natural fiber –reinforced epoxy –hybrid composite. *International Journal of Engineering Research and Applications (IJERA)*, **2** 471-478, (2012)
- [30] A. Pietak, S. Korte, E. Tan, A. Downard and M.P. Staiger, Atomic Microscopy of Characterization of the Surface wettability of Natural fiber, *Applied surface science*, *253*, 2001, 3627-3635.
- [31] C.C. Kelly, R.M. Daniella,J.C Herman, Voorwald and O.H Cioffi,, Chemical modification effect on the mechanical properties of HIPS/Coconut fiber composite, *Bioresources***5**, 2010 1143-1155.

## Determination of Traffic Delay at Selected Intersection within Ilorin Metropolis

Oladele Popoola<sup>1\*</sup>, John Wasiu<sup>2</sup>, Abimbola Owolabi<sup>3</sup>

Department of Civil Engineering, Afe Babalola University, Ado-Ekiti, Nigeria

**ABSTRACT** : Vehicle delay is one of the serious impacts of highway work zones on existing traffic operations. It is used to determine the overall level of service as well as the capacity of intersections. This work evaluated the overall delays at three various intersections in Ilorin metropolis which are tipper garage intersection, Oja Oba intersection and Judiciary-Offa road intersection. The three intersections were considered because of the commercial activities they serve such as linking up routes to important regions like the University, the post office, Government house and so on. Delay studies at each leg of intersection were carried out, the average delay was found out for each intersection and the corresponding level of service. Based on the results, the relocation of taxi/ bus terminals are proposed, on-street parking is discouraged, street hawking is discouraged at the intersections, potholes at the intersection approach should be mended, unpaved road should be overlaid with asphalt and the use of traffic signals should be encouraged so as to increase the present level of service and reduce traffic delay.

**Keywords:** traffic, intersection, delay, level of service

### I. INTRODUCTION

The increase in the number of road users always leads to increasing demand on the facilities. The proper way of determining the traffic should be adopted at intersected section and most especially the area where stopped-delay are more pronounced. According to highway engineering, intersection can be described as a highly complex component of many types of roadways. All the types of road involve numerous intersections with exception of freeways. In a simpler way, intersection is a place where two or more highways meet and provides an area for the cross movement of vehicular traffic. At intersections, a vehicle transfer from the route on which it is travelling to another route; crossing any other traffic streams, which flow between it and its destination. The performance of this maneuver involves a vehicle diverging from, merging with or crossing the paths of other vehicles. Intersections that do not carry a lot of traffic and where visibility is good from all approaches, control may not be needed. The driver uses simply the standing "rules of the road" to determine who gets right-of-way when two vehicles arrive at the same time. Level of service (LOS) of the intersection is measured with regards to stopped delay at intersection. For instance, on priority intersection, traffic volume on the major street may be so heavy that the traffic volume on the minor intersection street experiences excessive delays in entering or crossing the major street. Traffic volume is defined as the number of vehicles that pass a point along a roadway or traffic lane per unit of time. A measure of the quantity of traffic flow, volume is commonly given in units of vehicles per day, vehicles per minute and so forth. Daily on a road, the volume of traffic fluctuates widely with time. The nature of the pattern of variation depends on the type of highway facility. (Wright and Norman, 1978). Delay is the time lost by a vehicle due to causes beyond the control of the driver. It could also be described as the time consumed while traffic or a specific component of traffic is impeded in its free movement. (Garber & Hoel, 2014). Operational delay is that part of a delay cause by the impedance of other traffic. The impedance can occur either as side friction, where stream flow is interfered with other traffic (e.g parking or non-parking vehicles), or as internal friction where the interference is within the traffic stream (e.g reduction in capacity of the highway). Stopped time delay is that part of the delay for which the vehicle is at rest. (Garber & Hoel). Fixed delay is that of the delay caused by control devices such as traffic signals. This delay occurs regardless of traffic volume or the impedance that may exist.

Travel-time delay is the difference the actual travel and the time that will be obtained by assuming that a vehicle traverses the study section at an average speed equal to that for an uncongested traffic flow on the section being studied. (Garber & Hoel).

## II. METHODOLOGY

The intersection delay study was performed by the manual method due to the unavailability of delay meters. This involved the counting of 'vehicles stopped' and 'non-stopping' vehicles in the intersection approach at successive intervals. The duration for this interval was 15 seconds. Before the start of the field work, the identifying information is entered on the appropriate places on the field sheet and the first column is completed to indicate succession of sampling time intervals. When starting, the observer counts and records the number of vehicles stopped on the approach of each observation indicated. The stop watch is started at the beginning of the study and to advise the observers of the proper intervals for counting. A vehicle is counted more than once in the delay determination if it is stopped during more than one sampling time. This means that a particular vehicle will continue to be counted in all sample time periods during which it remains stopped on the intersection approach. A separate tabulation of the approach volume was obtained for each time period by classifying the vehicles as either stopping or non-stopping. The number of stopping vehicles is always equal or less than the total number of vehicles stopped on the approach for a specific time interval because vehicles can be delayed for more than one sampling period.

The results of the intersection delay study were summarized by calculating the following

1. Total stopped time delay in vehicles
2. Average delay per approach vehicle
3. Average delay per stopped vehicle
4. Percentage of vehicles stopped.

Other data collected were: number of vehicle waiting at intersection of each approach leg, the volume of traffic discharge at each leg of intersection per time period, physical features at intersection approach that may hinder free flow of traffic, the determination of total delay at intersection and evaluation of alternative intersection control measures.

## III. RESULTS AND DISCUSSION

Data collection was carried out at the three different intersections. This involves physical characteristics and delay studies.

**Table 3.1: Physical Characteristics of Judiciary/Offa Road Intersection**

Approach LEG	Number of lanes	Approach width(m)	Shoulder width(m)	Road surface
Nitel	1	6.90	0	G.C
Sabo-Oke	1	4.75	0	P.R
Post office	1	6.85	0	G.C
Judiciary	1	6.85	0	G.C

**3.2: Physical Characteristics of Tipper Garage Intersection**

Approach LEG	Number of lanes	Approach width (m)	Shoulder width (m)	Road surface
Tanke Junction	2	6.80	0	G.C
Pipeline	1	6.78	0	P.R
Unilorin	2	6.80	0	G.C
Opp.Pipeline	1	5.60	0	UPR

**3.3: Physical Characteristics of Oja-Oba Intersection**

Approach LEG	Number of lanes	Approach width (m)	Shoulder width (m)	Road surface condition
Surulere	2	7.20	0	P & G.C
Ita-Amodu	1	6.35	0	G.C
Emir's Road	2	6.83	0	G.C
Opp. Ita-Amodu	1	6.75	0	G.C

P...paved  
 P.R...paved road  
 G.C...good condition  
 UPR...unpaved Road

**3.4: Total Average at Judiciary/Offa Road Intersection**

Approach	Average delay per approach Vehicle (Sec)	Percent of stopped vehicle	Average delay per stopped vehicle (Sec)	Level of service
Nitel	10.56	36.85	26.46	B
Sabo-Oke	15.68	56.37	23.12	C
Post office	11.55	42.25	26.04	C
Judiciary	12.66	51.41	23.04	C
Total	50.61	188.53	98.66	
Av.average	12.61	47.13	24.67	

**3.5: Total Average at Tipper Garage Intersection**

Approach	Average delay per approach Vehicle (Sec)	Percent of stopped vehicle %	Average delay per stopped vehicle (Sec)	Level of service
TankeJunc	6.31	34.83	17.49	B
Pipeline	12.95	52.30	21.39	C
P.S	6.74	39.71	18.01	C
Opp pipeline	11.03	51.35	20.85	B
Total	37.03	178.19	77.74	
Av.average	9.26	44.55	19.44	

**3.6: Total Average at Oja-Oba Roundabout**

Approach	Average delay per approach Vehicle (Sec)	Percent of stopped vehicle %	Average delay per stopped vehicle (Sec)	Level of service
General	9.68	52.88	17.36	B
Ita- Amodu	9.91	54.14	17.05	B
Emir's Road	8.78	53.17	16.56	B
OppItaAmodu	8.45	53.78	15.76	B
Total	36.82	213.97	66.72	
Av. average	9.21	53.49	16.68	

**3.7: Summary of the Delay Parameters for the three Intersections**

Intersection location	Average delay per approach Vehicle (Sec)	Average delay per stopped vehicle (Sec)	Average Percent of stopped vehicle %	Level of service
Judiciary/Offa	12.61	24.69	47.13	C
Tipper Garage	9.26	19.44	44.55	B
Oja-Oba	9.21	16.68	53.49	B

**3.8: Average Traffic Volume Tables at Judiciary-Offa Intersection**

Approach	Lane of no	Traffic volume for 15 Mins duration	Rate of vehicle per hour (VPH)	Rate of flow of vehicles per lane (VPHL)
Nitel	1	123	492	492
Sabo-Oke	1	86	344	344
Post office	1	98	392	392
Judiciary	1	81	324	324
Total	4	388	1552	

**3.9: Tipper Garage Intersection**

Approach	Lane of no	Traffic volume for 15 Mins duration	Rate of vehicle per hour (VPH)	Rate of flow of vehicles per lane (VPHL)
Tanke junction	2	155	620	310
pipeline	1	89	356	356
P.S	2	158	632	316
Opp pipeline	1	70	280	280
Total	6	472	1888	

**3.10: Oja-Oba Intersection**

Approach	Lane of no	Traffic volume for 15 Mins duration	Rate of vehicle per hour (VPH)	Rate of flow of vehicles per lane (VPHL)
General	1	70	280	280
Ita- Amodu	1	163	652	652
Emir's Road	2	140	560	280
OppIta-Amodu	1	111	444	444
Total	5	484	1936	

From the field observation of traffic delay, it may be concluded that under saturated flow conditions, the interrelation of intersection traffic delay, in addition to intersection geometry and average vehicular delay is an important factor influencing the economic value of the people (i.e both commercial and private vehicle owner). This is evident from the fact that the delays observed are different when intersection delay are compared, even though the average vehicle delay is almost the same and there is only a marginal difference in the width of lanes available.

The amount of traffic, which can enter at a traffic signal controlled intersection, depends on the rate of flow of vehicles past the stop line during the green period and on the length of green time available.

From the summary of the delay parameters for the three intersections Table 3.3, it was observed that the average delay at approach varies from one another. It was also observed that the average value for each leg for each intersection varies. For instance the average value on leg of Judiciary/Offa road intersection (Sabo Oke) is more than post office (leg 3) due to more traffic delay at this intersection.

At tipper garage leg 2 (pipe line) has the highest delay due to part of the road section being used as parking space and as taxi terminus. Passengers from Gaa-Akanbi and Offa Grage alight and board taxi or private cab at this leg of the intersection. Passengers from Tanke junction also alight at this intersection thereby narrowing the road width for free flow of traffic.

From table 3.5, it was deduced that there is less delay on legs (P.S.) intersection and leg, (Tanke junction). The reason is because few cars make turning movement about the roundabout, which might cause little or no delay. The only periods delays were recorded was when motorist do not park appropriately or when a vehicle breaks down due to mechanical failure.

Table 3.6 shows a very close range in delay per approach vehicle but the percentage of vehicles stopped at the in intersection is more compared to Tipper Garage and Judiciary/Offa road intersection. It shows that more vehicles stop at the intersection but do not get delayed for a long time.

For the average traffic volume, table 3.8, 3.9 and 3.10 shows the result obtained.

It was observed that the Oja intersection has more traffic volume for 15mins duration of 484 vehicles, followed by Tipper Garage 472 vehicles and 388 vehicles for Judiciary/Offa road intersection.



Level of service A describes that level of operation at which the average delay per vehicle is 5 seconds or less. Level of service B describes that level of operation at which delay per vehicle is greater than 5 seconds but not greater than 10 seconds which shows a decline in freedom to maneuver within the traffic stream relative to level of service A. The vehicles stopped at the intersection is greater than A but progression is still good. Level of service C describes the level of operation at which delay per vehicle is greater than 10 seconds, and up to 20 seconds. This shows a significant vehicle stop and general decline in level of comfort of motorist although many vehicles go through the intersection without stopping. At Level of Service D, delay per vehicle is greater than 20 seconds and not greater than 30 seconds, unfavorable progression occurs and drivers experience reduction in physical and psychological comfort. Level of service E is between 30 and 45 seconds. Level of Service F describes the level of operation at which delay is greater than 45 secs. At LOS-F, over saturation occurs that is, arrival flow rates are greater than the capacity of the intersection.

#### IV CONCLUSION

At any intersection in an urban area with so much traffic, there is likely to be delays and congestion. It is then important to improve on the traffic performance at such intersection. Generally it was observed that the level of service was satisfactory but it could be enhanced. For this improvement, it is recommended that relocation of Cab/Bus-stops to at least 30 meters away from the intersection, on-street parking should be discouraged near intersection or at intersection approach, potholes right at the stop line of Sabo-Oke approach of judiciary/ Offa road intersection should be mended, road shoulders should be constructed to cater for emergencies, Ita-amodu approach of Oja intersection should be widened for easy maneuvering of vehicles, street hawking and partial placement of kiosk on the road pavement should be discouraged because it reduces the width of vehicle lane and proper planning and design of signalized intersections should be encouraged to maintain the level of service and for future traffic reduction.

#### REFERENCES

- [1] Box P.C (1968) Highway manual of traffic engineering studies. Institute of transportation Engineering pg 93
- [2] Department of Transportation (DoT) (1999) traffic capacities for urban roads. Advice Note TA 79/99, HSMO, UK
- [3] Gupter B, Gupter A (1986) Highway, Bridge and Tunnel Engineering
- [4] Harwood E., Douglas W. (1992) Traffic and operating characteristics. Institute of transportation Engineers
- [5] Thagesen B. (2005) Highway and Traffic Engineering in Developing Countries. Taylor & Francis, UK.
- [6] Kadiyali L.R. (2008) Traffic Engineering and Planning. Khanna Publishers 2-B Delhi-110006 India
- [7] Rodgers M. (2008) Highway Engineering. Blackwell publishing, UK.
- [8] Nicholas J.G Lester A.H (2014) Traffic and Highway Engineering. Cengage learning, Stamford, CT069 USA
- [9] Papacostas C.S (2005) Transportation Engineering and Planning, Pearson/Prentice Hall. USA

## Power Flow Analysis for Elastic Coupling Plates

Fei Han, Min-qing Wang

(School of Power and Energy, Northwestern Polytechnical University, China)

**ABSTRACT:** Based on mobility power flow method, the elastic connection between plates was simulated by torsion spring uniformly distributed along the coupling boundary, and the continuity equation of coupling boundary was modified. A theoretical analysis model of elastic coupling plates was obtained. The influence of connection stiffness on the vibration characteristic of coupling structure was analyzed. Simulation result show that with the increase of connection stiffness, modal of sub plate makes less contribution to the input power, but the situation is opposite to the modal of coupling structure. The transfer power increases significantly with the increase of connection stiffness, and the stiffness which makes the transfer power converging at natural frequencies of sub plate is less than that of natural frequencies of coupling structure.

**Keywords:** elastic connection; power flow; substructure; mechanical mobility

### I. INTRODUCTION

As a common periodic support structure, slicing plate is convenient to be manufactured, disassembled and examined. It is widely used in engineering community. Such as the cover plate of elevator, warship deck, bridge and so on. Structural vibration is excited by mechanical movement or human trample in their daily use, which has a great influence on the Device reliability and threatens the security of usage. Scholars have used many methods to analyze the vibration characteristics of coupling plates. P. J. Shorter [1] established the energy flow model of coupling plates by Finite Element Method (FEM) and calculated the average response and input energy of each substructure. When using FEM to analyze the vibration characteristics of complex structure in high frequency, the problem of huge calculation complexity can't be avoided, so it is usually used in the research on low frequency vibration characteristics. Statistical Energy Analysis (SEA) [2-4] has less calculation complexity when the structure has enough modal. Some parameters, such as coupling loss factor, are required in the calculation process. SEA is usually used in the research on high frequency vibration characteristic. Mobility power flow method [6,7] has clear physical concepts. It combines the idea of mechanical mobility and power flow. The characteristics of energy distribution and power flow in the coupling structure can be represented validly. And there is no frequency limit in this method. With continuous development, Mobility power flow method is widely used in engineering community [8-11].

In the manufacturing process of slicing plates, sub plate is usually obtained first and then assembled together. So the connection between sub plates is different from rigid connection, and the connection stiffness should be considered. Based on mobility power flow method, the elastic connection between plates will be simulated by torsion spring uniformly distributed. By modifying the continuity equation of coupling boundary, a theoretical calculation model of elastic coupling plates can be obtained. Based on this model, the influence of connection stiffness on the vibration characteristic of coupling structure will be analyzed.

### II. THEORITICAL MODEL

As shown in Fig.1, slicing plate is constituted by  $n$  sub plates. Four edges of each plate are all simply supported. The edge lengths of each plate are  $a_1, a_2, \dots, a_n$ . The width of the coupling boundary is  $b$ . Thickness, material density, Young modulus and Poisson's ratio of sub plate  $i$  are expressed as  $h_i, E_i, \rho_i$  and  $\sigma_i$ . The elastic connection between sub plates is simulated by torsion spring uniformly distributed. The stiffness value and amplitude of internal momenton boundary  $i$  are expressed as  $K_i$  and  $M_i$ .  $F_e$  represents the amplitude of external harmonic force which is applied on point  $(x_e, y_e)$ .

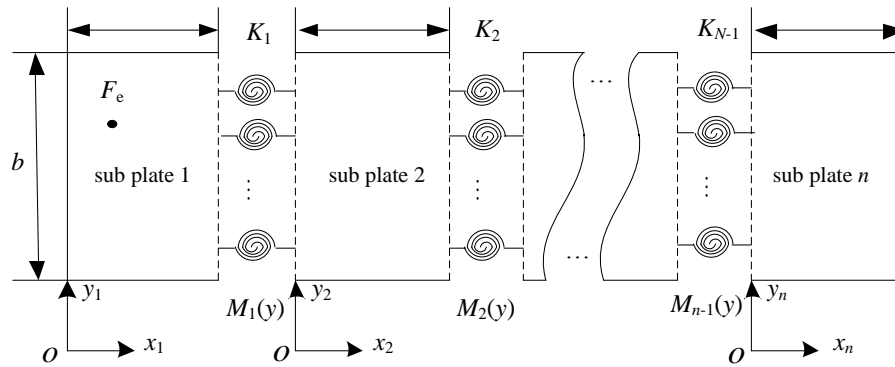


Fig.1 Schematic diagram of slicing plate

For the plate with all boundaries simply supported, its modal shape can be represented by trigonometric function. In the direction parallel to the coupling boundary, the point harmonic force and internal moment can be expanded in Fourier series. Based on the orthogonality of trigonometric function and the modal shape of the plate, terms containing  $y$  can be counteracted in the calculation progress so that the internal moment amplitude of each order can be obtained, concrete process can be referred to [12]. Subjected to  $p$  order sine distribution internal moment, the angular displacement of each sub plate on the coupling boundaries can be expressed as follows:

$$\begin{cases} \varphi_{1p}(1) = F_p Y_{Fp} + M_{1p} Y_1(1,1) \\ \varphi_{2p}(1) = -M_{1p} Y_2(1,1) + M_{2p} Y_2(2,1) \\ \varphi_{2p}(2) = -M_{1p} Y_2(1,2) + M_{2p} Y_2(2,2) \\ \varphi_{3p}(2) = -M_{2p} Y_3(2,2) + M_{3p} Y_2(3,2) \\ \vdots \\ \varphi_{(n-1)p}(n-1) = -M_{n-2}(x) Y_{n-1}(n-2, n-1) \\ \quad + M_{n-1}(x) Y_{n-1}(n-1, n-1) \\ \varphi_{np}(n-1) = -M_{n-1}(x) Y_n(n-1, n-1) \end{cases} \quad (1)$$

Where  $\varphi_{ip}(j)$  is the angular displacement of sub plate  $i$  on coupling boundary  $j$  subjected to  $p$  order coupling moment;  $F_p, M_{ip}$  are the amplitude of  $p$  order external force and internal moment;  $Y_{Fp}$  is the angular displacement mobility of sub plate subjected to  $p$  order external force, and it represents the mobility from emitting position to the points on coupling boundary;  $Y_i(j, k)$  expresses the angular displacement mobility of sub plate  $i$ , and it represents the mobility from coupling boundary  $j$  to boundary  $k$ .

There is only internal moment along the coupling boundary under simply-supported boundary condition, so only continuous condition of angular displacement is essential. With elastic connection introduced, the continuity equation can be written as:

$$\begin{cases} K_1 [\varphi_{1p}(1) - \varphi_2(1)] = M_{1p} \\ K_2 [\varphi_{2p}(2) - \varphi_{3p}(2)] = M_{2p} \\ \vdots \\ K_{n-1} [\varphi_{(n-1)p}(n-1) - \varphi_{np}(n-1)] = M_{(n-1)p} \end{cases} \quad (2)$$

It can be written in matrix form as:

$$(KY_p - E)M_p = K\Omega_p \quad (3)$$

Where  $K = \text{diag}\{K_1 \ K_2 \ \dots \ K_{n-1}\}$ ;  $M_p = [M_{1p} \ M_{2p} \ \dots \ M_{(n-1)p}]^T$ ;  $\Omega_p = [-F_p Y_{Fp} \ 0 \ \dots \ 0]$ ;  $E$  is  $n-1$  order unit matrix;  $Y_p$  expresses the mobility matrix of sub plates subjected to  $p$  order internal moment, it can be

written as:

$$Y_p = \begin{bmatrix} Y_1(1,1) + Y_2(1,1) & -Y_2(2,1) & \dots & 0 \\ -Y_2(1,2) & Y_2(2,2) + Y_3(2,2) & \ddots & \vdots \\ \vdots & \ddots & \ddots & -Y_{n-1}(n-1, n-2) \\ 0 & \dots & -Y_{n-1}(n-2, n-1) & Y_{n-1}(n-1, n-1) + Y_n(n-1, n-1) \end{bmatrix} \quad (4)$$

$M_p$  can be obtained according to equation (3). By substitution of  $M_p$  into equation (5), the amplitude and spatial distribution feature of each coupling moment can be obtained.

$$M_i(y) = \sum_{p=1}^{\infty} M_{ip} \sin \frac{p\pi y}{b} \quad (i = 1, 2, \dots, n-1) \quad (5)$$

The power flow from sub plate  $i$  to sub plate  $i+1$  can be written as:

$$Q_i = \frac{1}{2} \sum_{y=0}^b \text{Re} [M_i(y) \omega_i^*(y)] dy \quad (i = 1, 2, \dots, n-1) \quad (6)$$

Where Re expresses taking real part,  $^{*}$  expresses taking conjugate complex;  $\omega_i(y)$  is the angular velocity of sub plate  $i+1$  on boundary  $i$ , it can be written as:

$$\omega_i(y) \begin{cases} \int_0^b [-M_i(y) Y_{i+1}(0, y | 0, y_{i+1}) + M_{i+1}(y) Y_{i+1}(a_{i+1}, y | 0, y_i)] dy & i = (1, 2, \dots, n-2) \\ -\int_0^b M_{n-1}(y) Y_n(0, y | x_n, y_n) dy & i = n-1 \end{cases} \quad (7)$$

Where  $Y_{i+1}(0, y | 0, y_{i+1})$  is the angular velocity mobility of sub plate  $i+1$  from point  $(0, y)$  to point  $(0, y_{i+1})$ .

Input power of coupling plates can be obtained by:

$$Q_{\text{input}} = \frac{1}{2} \text{Re} [F_e v_e^*(x_e, y_e)] \quad (8)$$

### III. NUMERICAL STUDIES

#### 3.1. Validation of the theoretical model.

The simulation example contains two sub plates which share the same parameters  $a=2\text{m}$ ,  $b=1\text{m}$ ,  $h=0.005\text{m}$ ,  $E=2.16 \times 10^{10}\text{Pa}$ ,  $\rho=7900\text{kg/m}^3$ ,  $\eta=0.01$ , Poisson's ratio  $\sigma=0.27$ ; unit harmonic force is imposed on point of  $(0.6\text{m}, 0.2\text{m})$  in sub plate 1. The calculation frequency domain ranges from 10Hz to 10k Hz.

As the mobility of sub plate is obtained by modal superposition method, the truncation order number is determined by upper frequency limit. In the simulation example,  $M$  and  $N$  share the same value. The Input power of slicing plate at 10 kHz with different truncation order number is shown in Fig.2. It shows that the input power converges when  $M, N=60$ , the maximum nature frequency of sub plate is 75.4 kHz which is much greater than 10k Hz.

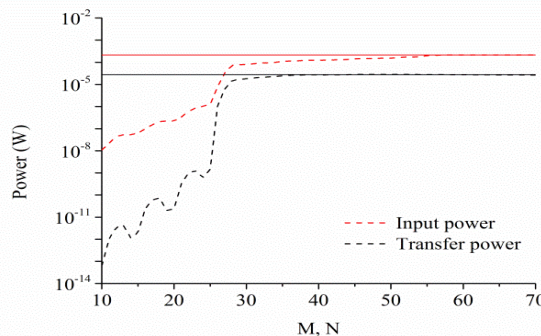


Fig.2 Convergence of input power

According to (2), when the connection stiffness tends to infinity, the angular displacements of nearby sub plates should tend to a same value as the amplitude of internal moment is a nonzero value. That is to say, the connection between sub plates tends to rigid connection. When  $K_{max}=10^{10}N/rad$ , the input power and transfer power is compared with that of rigid coupling plates which is obtained by reference [1], the results are shown in Fig.3 and Fig.4. It is seen from Fig.3 and Fig.4 that the rigid connection is a special case of elastic connection.

With the connection stiffness decreasing, the coupling degree between sub plates tends to be lower. When the connection stiffness tends to zero, the difference between angular displacements of nearby sub plates and the original structure will become two single plates with no connection. When  $K_{min}=10^{-2}N/rad$ , the input power is compared with that of single plate. Result is shown in Fig.5. It is seen from Fig.5 that except for small discrepancies in some peak value at natural frequencies, only small differences exist between the result of coupled plates and those of single plate. The reason for errors of some peak value lies in the fact that the difference between angular displacements of nearby sub plates is a finite value, so that the amplitude of internal moment can't tend to zero.

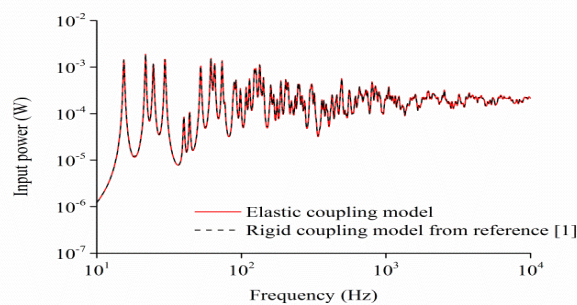


Fig.3 Curves of input power

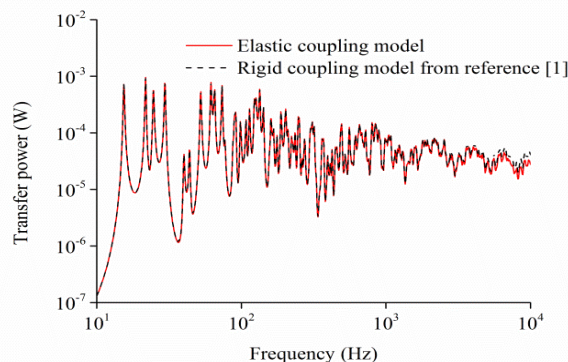


Fig.4 Curves of transfer power

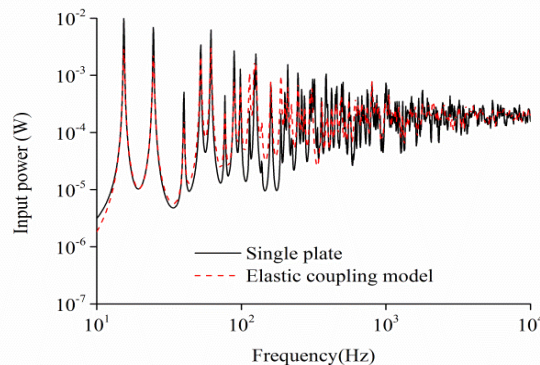


Fig.5 Input power of different model

**3.2. Effect of connection stiffness.**

In all calculations, the plates are assumed to be made up of steel, whose material property has been described above. Connection stiffness is changed as shown in Fig.6,  $K_1=1 \times 10^2 \text{N/rad}$ ,  $K_2=1 \times 10^4 \text{N/rad}$ ,  $K_3=1 \times 10^6 \text{N/rad}$ ,  $K_4=1 \times 10^8 \text{N/rad}$ .

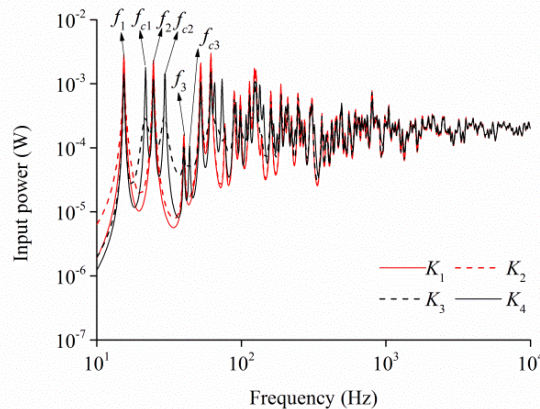


Fig.6 Curves of input power with different connection stiffness

It is seen from Fig.6 that with connection stiffness increasing, the trend of input power changes slightly but the peak value at  $f_1, f_2, f_3$ , which are the first three order nature frequencies of sub plate, decrease a little. At the same time, some new peaks appear at  $f_{c1}, f_{c2}, f_{c3}$ , which are the first three order nature frequencies of coupling structure.

Fig.7 shows the influence of stiffness on input power at those frequencies. It is seen from Fig.7 that with connection stiffness increasing, the trend of input power at natural frequencies of sub plate is totally different from those at natural frequencies of coupling structure. At the initial stage of stiffness increase, the modal of sub plate makes the main contribution to input power, but the degree becomes lower with the stiffness increasing, which makes the coupling degree sub plates stronger and the modal of coupling structure plays more important role in structure vibration. The input power at those frequencies converges when the value of stiffness increases to about  $10^8 \text{N/rad}$ , and then connection can be seen as rigid connection.

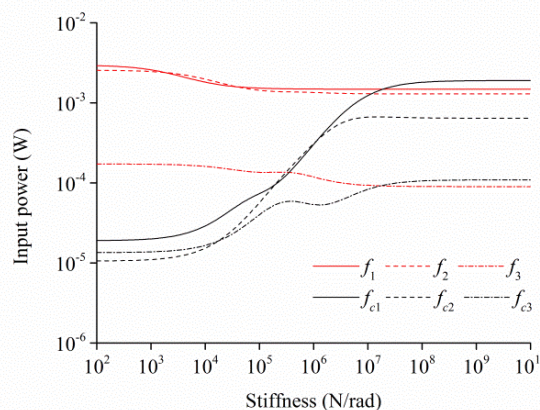


Fig.7 Curves of input power at different frequencies

The influence of stiffness on transfer power is shown in Fig.8. It can be seen from Fig.8 that transfer power increases significantly with stiffness increasing at frequency band of 10Hz to 10k Hz. And lower stiffness can restrain the vibration more effectively at high frequency. Some peaks also appear with the increase of stiffness. Transfer power at those frequencies is shown in Fig.9. Result shows that transfer power at natural frequencies of sub plate converges when stiffness increases to about  $10^6 \text{N/rad}$ , and transfer power at natural frequencies of coupling structure converges when stiffness increases to about  $10^8 \text{N/rad}$ .

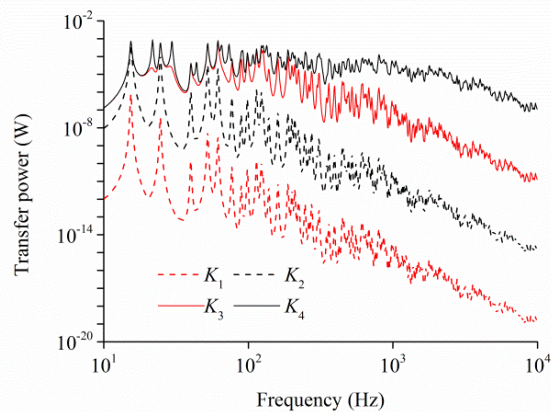


Fig.8 Curves of transfer power with different connection stiffness

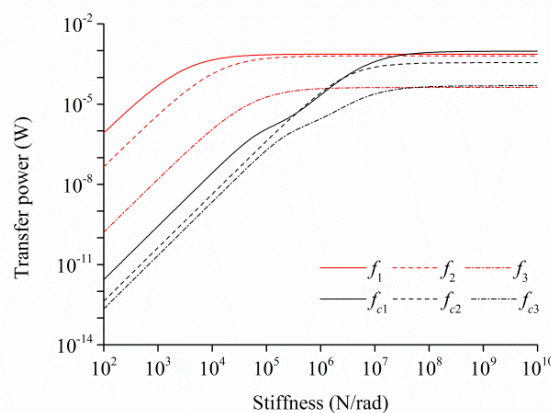


Fig.9 Curves of transfer power at different frequencies

#### IV. CONCLUSIONS

Based on mobility power flow method, the elastic connection between plates was simulated by torsion spring uniformly distributed, and the continuity equation of coupling boundary was modified. By introducing uniformly-distributed torsion spring and then modifying the continuity equation of coupling boundary, the elastic connection between plates can be well simulated. Based on the theoretical calculation model of elastic coupling plates, the influence of connection stiffness on the vibration characteristic of coupling structure is analyzed. Conclusions are shown as follows:

1. With the increase of connection stiffness, modal of sub plate makes less contribution to the input power but the situation is opposite to the modal of coupling structure.

2. The transfer power increases significantly with the increase of connection stiffness, and the stiffness which makes the transfer power converging at natural frequencies of sub plate is less than that of natural frequencies of coupling structure.

#### REFERENCES

- [1] B. R. Mace, P. J. Shorter. Energy flow models from finite element analysis [J]. *Journal of Sound and Vibration*, 233 (3), 2000, 369-389.
- [2] Fahy F. J. Statistical energy analysis: a critical overview [J]. *Philosophical Transactions of the Royal Society of London. Series A: Physical and Engineering Sciences*, 346(1681), 1994, 431-447.
- [3] Maxit L., Guyader J. L. Extension of SEA model to subsystems with non-uniform modal energy distribution [J]. *Journal of Sound and Vibration*, 265(2), 2003, 337-358.
- [4] Totaro N., Guyader J. L. SEA substructuring using cluster analysis: the MIR index [J]. *Journal of Sound and Vibration*, 290(1), 2006, 264-289.
- [5] Seçgin A. Numerical determination of statistical energy analysis parameters of directly coupled composite plates using a modal-based approach [J]. *Journal of Sound and Vibration*, 332(2), 2012, 361-377.

- [6] J M Cuschieri. Structural power-flow analysis using a mobility approach of an L-shaped plate [J]. *Journal of the Acoustical Society of America*, 87(3), 1990, 1159-1165.
- [7] M Cuschieri, M D McCollum. In-plane and out-of-plane waves' power transmission through an L-plate junction using the mobility power flow approach [J]. *Journal of the Acoustical Society of America*, 100(2), 1996, 857-870.
- [8] Kessissoglou N. J. Power transmission in L-shaped plates including flexural and in-plane vibration [J]. *The Journal of the Acoustical Society of America*, 115(3), 2004, 1157-1169.
- [9] Skelton E. A. Line force receptance of an elastic cylindrical shell with heavy exterior fluid loading [J]. *Journal of Sound and Vibration*, 256(1), 2002, 131-153.
- [10] Orefice G., Cacciolati C., Guyader J. L. The energy mobility [J]. *Journal of Sound and Vibration*, 254(2), 2002, 269-295.
- [11] Bonhoff H. A., Eslami A. Interface mobilities for characterization of structure-borne sound sources with multi-point coupling [J]. *Acta Acustica united with Acustica*, 98(3), 2012, 384-391.
- [12] ZHANG An-fu, SHENG Mei-ping, ZHAO Zhi-mei, et al. Power Flow Analysis of Multi-span Coupled Plates Using Fourier Expansion [J]. *Journal of vibration and shock*, 32(14), 2013, 103-108.



## Security and Architectural Patterns for Securing the Cloud Architecture

Golajapu Venu Madhava Rao<sup>1</sup>, Venu Madhav Kuthadi<sup>2</sup>, Rajalakshmi Selvaraj<sup>3</sup>

<sup>1</sup>Department of Network and Infrastructure, Faculty of Computing, Botho University, Botswana

<sup>2</sup>Department of Applied Information Systems, University of Johannesburg, South Africa

<sup>3</sup>Department of Information Systems, BIUST, Botswana

**ABSTRACT:** Operating a cloud securely and efficiently entails a great deal of advance planning. A data center and redundant internet connection is required at the beginning to connect to cloud. This can constitute the technology portion of an information security and some network devices that safely and securely serve the communication. National Institute of Standards and Technology states that the process of uniquely assigning the information resources to an information system will define the security boundary for that system. A massive amount of gear that is racked and cabled following defined patterns is enabled inside this boundary. Need for the infrastructure that is used to manage the cloud and its resources as it operates the cloud. Each component like server, network and storage requires some degree of configuration. While designing or planning a complex system it is important to look ahead the process and procedures required for operation of the system. Small cloud systems can be build without much of planning. But any Cloud system substantially bigger size needs significant planning and design. If we fail to plan it leads to higher cost due to inefficiency in design and process. In this paper we study on the architectural components that can be used to build a cloud with security as a priority. This can be achieved by identifying requirements for secured cloud architecture along with key patterns and architectural elements. This paper first discusses on security patterns and an architectural element required and also focuses on several different cloud architectures and secure cloud operation strategies.

**KEYWORDS:** Cloud, Security, Architecture, network, process.

### I. INTRODUCTION

Implementing a cloud computing architecture ultimately is the next generation in cost management -- a shifting of traditional IT platforms to a resource-efficient, dynamic, hosted framework. Although this cost-based view of the cloud dominates the dialogue on cloud adoption, it falls short of the complete picture [1]. Beyond cost organizations are looking to implement a cloud computing architecture to enhance worker productivity. To these organizations, the biggest benefit of implementing a cloud computing model is the model's ability to apply IT tools faster and more flexibly. Organizations want flexibility in presenting application services to users and in assigning applications to resources based on cost and other metrics. This means looking at the overall IT architecture specifically the network in a whole new way.

All cloud computing models have three key components: access, resource pools and address mapping [2]. The access component lets users connect with the applications they need. Resource pools support the servers and storage that users can draw on to run those applications. The address mapping component links elastic resource locations with such references as URLs; these allow users to access applications no matter where they run. Access networks typically are built on routing and VPNs. Resource pools typically are supported on data center networks built on the Ethernet and virtual local area networks, or VLANs. The technologies of these two areas will expand as the private cloud is built, but the real change will be in address mapping. This is what will connect users to the applications that now are running in a dynamic resource pool. Address mapping demands a level of network flexibility that's beyond the typical needs of static internal IT hosting or even Internet hosting. Without network flexibility, a cloud computing model's dynamism is lost.

In fact, it's the network that builds the cloud. Enterprise networks include data center LANs; storage area networks; Internet tunnels; and WANs built on switching, routing and a VPN or Virtual Private LAN Service. These network components are more costly than cloud software stacks, and making a mistake in the network part of cloud-building could be absolutely fatal to security and availability. What we call the private cloud

computing model is the one that will guide all future IT investment. It's the first model that recognizes the fusion of business and IT, public and private resources, networks and software. It's a model that's very different from the Internet or from the current enterprise data center, but it's also a model that can be built from current infrastructure components and can provide both immediate and sustainable benefits in IT return on investment and worker productivity.

## II. SECURITY REQUIREMENTS FOR CLOUD ARCHITECTURE

This section focus on the key architectural requirements for a cloud implementation [3]. The main aim of the cloud architecture is shown in fig.1 and should be appropriate to meet the needs of the cloud.

(1) Costs and Resources: The investment on technology and security controls will depend on cloud providers financial resources towards its implementation. The motivation factor for the customer towards the cloud services is cost. This constraint in the development and operation of the services will not be ideal to all the customers.

(2) Reliability: The underlying technology which provide delivery of services to a certain degree.

(3) Performance: This refers to usefulness of the system that includes responsiveness to the input and throughput the system can handle[4]

(4) Security: Confidentially, Integrity and Availability security principles are applicable to most of the systems and the responsibility is to match with the security requirements which must be derived from reliability performance and cost.

(5) Legal and regulatory constraints: Legal and regulatory constraints can lead to need for many additional requirements having to do with technical security controls, access polices, and retention of data among many others.

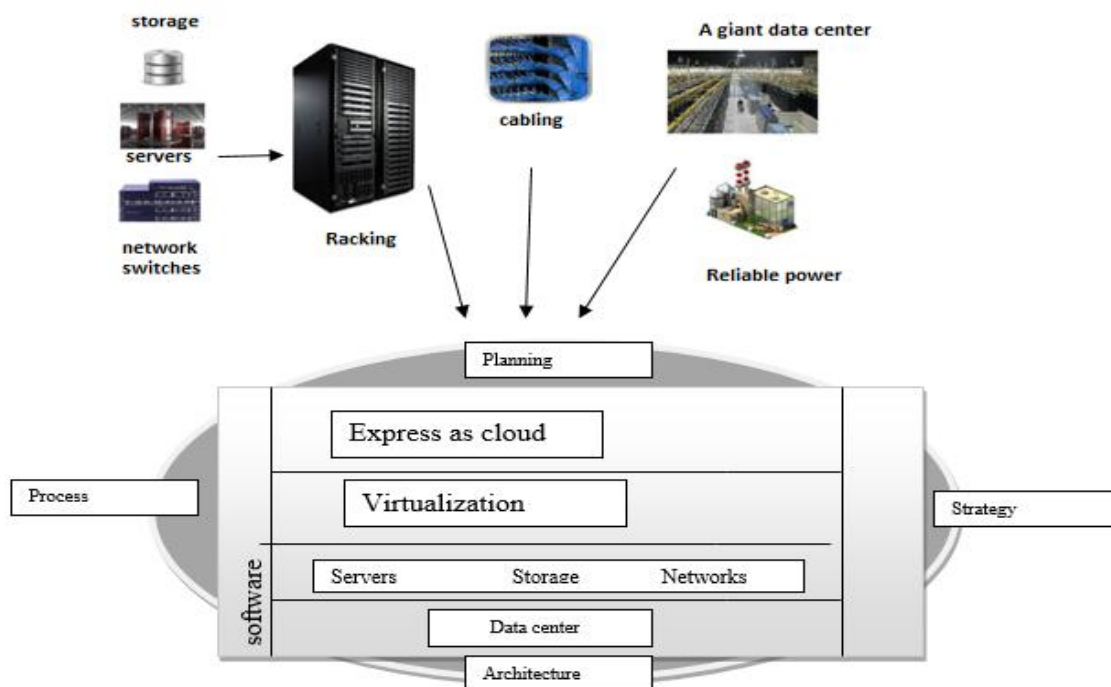


Fig 1: Cloud architecture and implementation

### 2.1 Cloud Security Standards and Policies

Requirements for cloud security should be consistent with appropriate standards such as International Organization for Standardization (ISO). All security requirements should derive from standard security policies. The policy should explain the need for the standard encryption methods should be used. The security policy should also have several supporting documents like guidelines for enabling security in development of infrastructure software, management processes and operational procedures. It should also contain an acceptable use policy for each category of user. A set of security standards for cloud should includes : Access controls, Incident Response and management, System and network configuration backups, security testing, data and communication encryption, password standards and continuous monitoring.

## 2.2 Requirements of Cloud Security

Security architecture of the cloud should be consistent as per the security policies mentioned in above section. A security policy for the cloud is one of the security requirements. A separate set of activities will revolve around identifying granular requirements that are preliminary in developing the cloud security architecture. On cloud architecture there are certain representative security requirements which are likely to apply are given below.

## 2.3 Cloud-Wide Time service

All systems must be synchronized to the same time source by using Network Time Protocol (NTP). When communicating computers reside in different locations correct and synchronized time is very important. The records and event time-stamps synchronized to a single source. A cloud infrastructure is subjected to all manner of errors and made difficult to diagnose failures if the clock drift between network devices or computers. Correct time information comes from authoritative national time standards through various paths which will include radio, satellite, cellular and hard-wired transmission to primary time servers. It is distributed through NTP subnets to millions of secondary servers and from there to end-clients. NTP provides coordinates Universal Time (UTC) all time zones or daylight saving time information must be provided separately. Some of the best practices to be followed for managing NTP are configure clients to reference at least two time servers to provide redundant time. Accurate time synchronization depends on how frequently clients update their time from time servers. Limit input network or radio broadcast signals to authoritative and legal ones.

## 2.4 Identity Management

Identity is key element in the security of operating the cloud. The information must be correct and available to cloud components that have a validated need for access. Requirements include controls to protect confidentiality, integrity and availability of identity information. Implement an identity management system that will support needs for authenticating cloud personal, support the larger scale needs for authenticating cloud tenants and users.

## 2.5 Access Management

Access controls use identity information to enable and constrain access to an operating cloud and its supporting infrastructure. Cloud personnel shall have restricted access to customer data in general. Cloud personnel may require access to a hypervisor on a customer allocated machine or to storage devices that host customer VMs or customer data but such access shall be tightly constrained and limited to specific operations that are well defined by security policy and SLAs. We can implement multifactor authentication for highly privileged operations with additional security controls. Authorization mechanism for cloud management are constrained and do not allow for cloud wide access.

## 2.6 Requirements of Key Managements

In a cloud encryption is a primary means to protect at rest and between storage and processing phases. Ensure that appropriate controls are in place to limit access to keying material that the cloud provider maintains control over. Ensure that root level and signing keys are managed appropriately.

## 2.7 System and Network Auditing

To manage the ongoing security of any system in cloud audit events will be generated at different trust zones like infrastructure system and network components. All security relevant events must be recorded and generated audit events must be logged in a near-real-time manner. All audit events logs shall be continually and centrally collected to make sure the integrity and to support timely altering and monitoring.

### III. SECURITY MONITORING

Security monitoring [5] shall include the generation of alerts based on automated reorganization that critical security event or situation has taken place or is detected. Delivery of critical alerts in timely manner. Implement a cloud wide intrusion and anomaly detection capability and consider this as a service for tenants or users. The fig. 2 shows the overview of security event management and relativity to security monitoring.

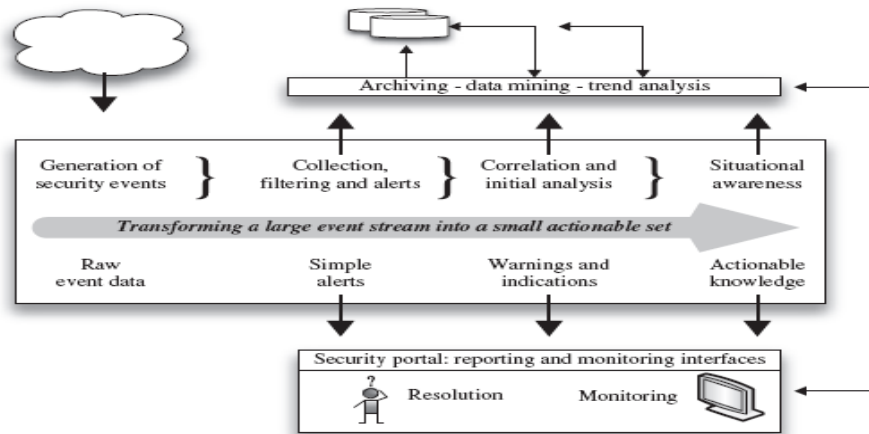


Fig2: Security event management and monitoring

The requirements for system and network controls are to ensure proper isolation, configuration and security for security components. Implementation of network isolation between functional areas in the cloud computing infrastructure. Implement completely separate networks which include use of physical separation and network virtualization for public accessible components. Use other network controls and also software firewalls on machines.

#### IV CLOUD OPERATION STRATEGIES

The technique for honeypot[6][7][8] can be applied for cloud computing. A honeypots virtual machine can be deployed and then used to monitor and report on any attempt to access it. Sandboxes is used at the software layer. It is a form of virtualization or abstraction between the software and code executed between the operating system. As per the cloud architecture [3] it is wise to design for mutually reinforcing controls to increase assurance. For defense in-depth for access control mechanisms it might require to use VPN for remote administrative access. A VPN connection attempt may be shunned by the ingress router for source IP. The use open system access control for remote administrative users could require use of a dynamically changing code that is owned by remote administrator.

The various types of private, public, SaaS, PaaS, IaaS, providers and technologies associated with all these types of architectures are Amazon Web Services, Amazon virtual private cloud, RackSpace cloud Hosting, GoGrid, Salesforce.com, Google Apps engine. VMware, Microsoft Hyper-V. The key strategies for cloud secure operations can be achieved by classifying data and systems and defining the valid roles for cloud personal and customers[9].

#### V CONCLUSION

The key architectural requirements for cloud implementation are discussed in the initial sections. Cloud security standards and policies should meet the ISO standards. All policies should derive from ISO. Security policy itself is one of the key security requirements in cloud. Security techniques like honeypots and sandboxes can be implemented in cloud computing architecture to monitoring and reporting. The key strategy for secure cloud operation can be achieved by classifying data and systems and defining the valid roles for cloud personal and customers.

#### REFERENCES

- [1] R. Schwarzkopf, M. Schmidt, Ch. Strack, S. Martin and B. Freisleben . Increasing virtual machine security in cloud environments. *Journal of Cloud Computing: Advances, Systems and Applications*, Springer, 2012, 1–12.
- [2] K. Hashizume, Nobukazu Yoshioka, and E. B. Fernandez . Three Misuse Patterns for Cloud Computing. *Security Engineering for Cloud Computing: Approaches and Tools*, IGI Global, 2013, 36–53.
- [3] Vic (J.R) Winkler, *Securing the cloud, cloud computer security techniques and tactics*, (Elsevier, 2011).
- [4] Dieter Gollmann, *Computer security*(Wiley, 2006).
- [5] E. B. Fernandez, *Security Patterns in Practice, Designing secure architectures using software patterns*. (Wiley Series on Software Design Patterns, 2013)
- [6] Selvaraj, R., Kuthadi, V.M. & Marwala, T. An Effective ODAIDS-HPs approach for Preventing, Detecting and Responding to DDoS Attacks. *British Journal of Applied Science & Technology*, Vol.5 (5), 2015, 500-509.
- [7] J. Wei, X. Zhang, G. Ammons, V. Bala, and P. Ning. Managing security of virtual machine images in a cloud environment. *In Proceedings of the 2009 ACM Workshop on Cloud Computing Security (CCSW09)*, Chicago Illinois, USA, ACM 2009, 91–96.
- [8] Selvaraj, R., Kuthadi, V.M. & Marwala, T. Enhancing Intrusion Detection system Performance using Firecol Protection Services based honeypot system. *Proceedings of the International conference on Communication, Computing and Information Technology*. India, 2014.
- [9] M. Okuhara, T. Shiozaki, and T. Suzuki. Security architectures for cloud computing. *Fujitsu Sci. Tech. Journal*, 46(4), 2010, 397–402.

## Influence of microwave pre-treatment on the flotation of low-grade sulphide ore

Omoyemi Ola-Omole (\*)<sup>1,2</sup>, B.O Adewuyi<sup>1,2</sup>, J.O. Borode<sup>1,2</sup>, P.A. Olubambi<sup>3</sup>

<sup>1</sup> The Federal University of Technology Akure, Nigeria.

<sup>2</sup> African Materials Science and Engineering Network (AMSEN)-a Carnegie-LAS Rise Network.

<sup>3</sup> Tshwane University of Technology, South Africa.

**ABSTRACT :** Sulphide ores are always difficult to process because of the complication in their mineralogical associations and the intergrown nature of their constituent minerals. These complexities usually result in a poor liberation of the associated minerals. Hence, full determination of comminution parameters relevant to the crushing and milling of these minerals will enhance higher recovery of the concentrate minerals as well as enable proper plant design to take place. Meanwhile, most high-grade deposits of the world have been depleted which give rise to the need to process low-grade ores. The conventional methods of mineral processing are also no longer effective for the processing of these low-grade ores. This work centres on understanding the effects of microwave pre-treatment on the flotation characteristics of the low grade-sulphide ores. The ore was characterized using JEOL JSM. 7600 SEM-EDX, Qurum150TE XRD-Ultima IV and XRF- ZSX Primus II. Microwave treatment was also carried out using 2.45 GHZ intellowave microwave oven at a power output of 750W. Comminution and particle size analysis of the ore shows that  $P_{80}$  for microwave treated sample is equal to  $-212\mu\text{m} +150\mu\text{m}$  while for the untreated sample  $P_{80}$  corresponds to  $-250\mu\text{m} +212\mu\text{m}$ . Sodium Ethyl Xanthate, SEX was used as the collector, Methyl Isobutyl Carbinol, MIBC as the frother and three different depressants (Starch, sodium silicate and potassium dichromate). Particle sizes  $150\mu\text{m}$ ,  $106\mu\text{m}$ ,  $75\mu\text{m}$  and  $53\mu\text{m}$  were used for flotation experiment. The trend of the recoveries of both microwave treated and untreated samples shows that recoveries are higher for the microwave treated samples.

**Keywords:** Microwave treatment, flotation, sulphide ore, collectors, depressants

### I. INTRODUCTION

Regardless of the form in which the different minerals occur and are associated in sulphide ores, in which galena-sphalerite are found, they are usually very difficult to process. These complex mineralogy present formidable challenges during processing and thus require that suitable techniques be adopted for optimal recovery of the constituent metals. When valuable minerals are not freed, due to poor liberation, they become very difficult to process in the sense that much more energy will be expended and efficient recovery becomes more difficult to attain. Determination of comminution parameters relevant to the crushing and milling of these minerals will enhance higher recovery of the concentrate minerals. Due to complicated mineralogical characteristics of these ores, it is necessary to properly grind and liberate all the mineral phases, to enable them to be exposed to processing. Meanwhile, most high-grade deposits of the world have been depleted, which gives rise to the need to process low-grade ores, The conventional methods of mineral processing are also no longer effective for the processing of these low-grade ores, as different concentrates obtained are of poor quality.

This work centres on understanding the effects of microwave pre-treatment on flotation characteristics of the low grade-sulphide ores from and Ishiagu  $6^{\circ} 20'00''$  N  $8^{\circ} 6'00''$ E in Nigeria. Microwave technology in mineral processing has been investigated over few decades. Some of its benefits are reported to be low cost, energy and time and also be environmental friendly. The method has been explored for mineral ores processing for which interaction between microwave and minerals, differential heating and reduction in comminution energy following comminution has been reported (Amankwah *et al.*, 2005, Kingman 2006, Kingman and Rowson,

1998, Haque, 1999, Xia and Pickles, 2000). Specifically for sulphide ores, Kingman *et al.*, 2000 reported on the influence of mineralogy on the response of ores to microwave radiation and the reduction in their grinding energy, concluding that microwave radiation may cause surface oxidation of sulphide minerals. Microwave treatment on copper flotation was also investigated and higher recovery for treated samples was reported (Sayhoun *et al.*, 2005). However, no specific work centred on evaluating the capacity of microwave technology in enhancing galena-sphalerite recovery from Ishiagu low grade sulphide deposit in Nigeria was found. The thrust for this work is that the little work available in the literature centres on the influence of microwave irradiation on heating characteristics, breakage response, mineralogy and mechanism of dissolution in sulphuric acid and hydrochloric acid (Olubambi *et. el.*, 2007). Studies reported so far on the influence of microwaves on ore dressing could not provide sufficient information from which industrial systems could be understood, and thus provide basis for its industrial acceptability. Therefore, the aim of this work is to investigate the effectiveness of microwave irradiation for enhancing the processing of low-grade sulphide ore, the interplay of mineralogy and microwave irradiation, and their dual effects on flotation characteristics of the sulphide ore.

## II. METHODOLOGY

### Ore sample

The Sample for this study is a low-grade complex consisting of Sphalerite, Galena, Anglesite, Pyrite, Hematite and Silica. The sample was taken from Abakaliki south of Ebonyi Nigeria on a coordinate's 12°6'30"N 5° 58'00"E and 6° 20'00" N 8 ° 6'00"E). The sample was divided into three portions, for mineralogical studies, pre-microwave treatment and microwave treatment respectively. The portion for characterization was crushed ground screened to sizes and were prepared for the analyses while the other two portions were taken for treatment and processing without treatment respectively.

### Microwave treatment

The 3500g of the bulk sample was placed on a glass revolving tray inside a 2.45GHz microwave oven with multi-modal cavity. The Exterior dimension of the microwave was 455x281x325mm and the interior was 310x196x294mm, it was ensure that the samples were placed on a central position of the microwave in other to minimize effect of field pattern variations as the glass rotates within the oven. The heating was carried out for 5mins at 750W power rating even though there were arcing within the ores.

### Particle size analysis and ore characterization

Both microwave treated and untreated samples were subjected to crushing and milling and particle size analysis. 1500g of each portion was crushed in a Chipmunk VD67 jaw crusher and milled in a rod Mill using 17 steel rods of 1.5cm by 30cm dimension. Pulverized sample were screened separately on a King Test VB 200/300 Model 51V520125 with Endecott's set of sieves 2000µm, 1700 µm, 1180 µm, 850 µm, 600 µm, 425 µm, 300 µm, 212 µm, 150 µm, 106 µm, 75 µm and 53 µm. Thereafter, the samples were characterized using JEOL JSM. 7600 SEM-EDX, Qurum150TE XRD-Ultima IV and XRF- ZSX Primus II.

### Froth Flotation

Selective froth flotation experiments were conducted in a standard Denver D-12 laboratory flotation cell to obtain concentrates of Lead and Zinc from both microwave treated and untreated samples. Particle sizes 53µm sizes 75µm, 106µm and 150µm were used for the flotation experiment. The pulp was prepared to 40% solid with initial pH of 6.53. Quick lime was added to raise the pH to 10.00, 400g/t of sodium ethyl xanthate, SEX was used as collector three times for each of the particle sizes, 125g/t of ZnSnO<sub>4</sub> was employed as depressant for zinc in the lead-zinc circuit as lead was floated without activation and three different depressants (10% starch solution, potassium heptaoxodichromate (VI) and sodium silicate) were also used to depress lead.in each of the experiments Other parameters; pH, concentration, speed, etc. were kept constant. 80g/t of CuSO<sub>4</sub> was used to reactivate zinc in zinc-lead circuit

## III. RESULTS AND DISCUSSION

### Ore characterization

Figures 1a indicates the mineral phases revealed by XRD prior to microwave treatment. Identified phases were galena, and quartz. It was difficult to identify sphalerite phase or that of other compounds due to low concentrations or overlapping peaks. The quantitative analysis results show about 77% of quartz and 23% of lead while an unidentified phase is suggested to be zinc (Figure 1b). Hence, further mineralogical examinations via SEM confirmed the presence of the identified minerals.

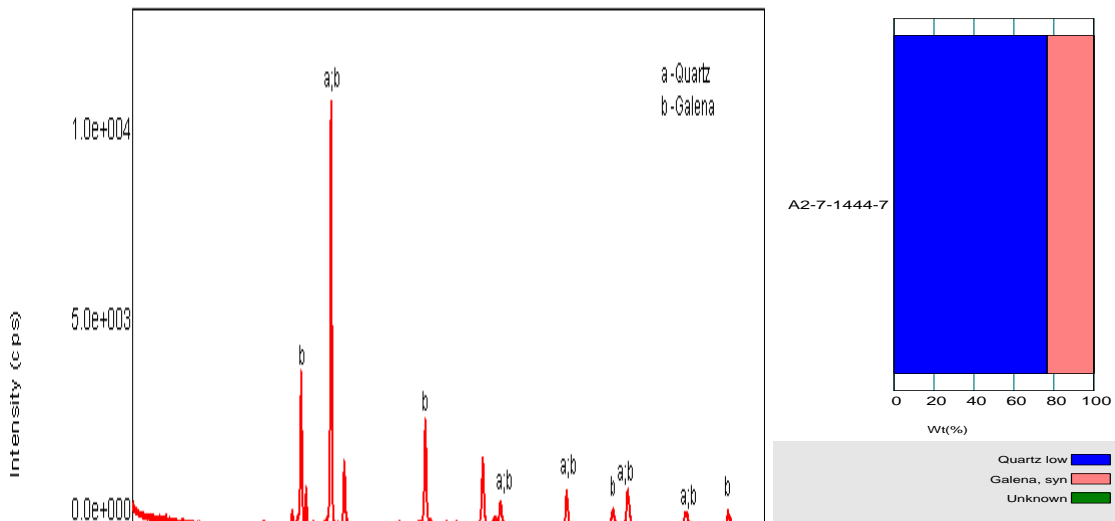


Figure 1a: XRD pattern of Ishiagu sulphide ore deposit.

Figure 1b: XRD Quantitative analysis Result of low grade sulphide from Ishiagu deposit

Figure 2 shows SEM/EDS micrographs which further established the mineralogical composition of the ore. The morphologies of the constituent minerals within ores are show the presence of galena, sphalerite, quartz and other minerals in low concentrations.

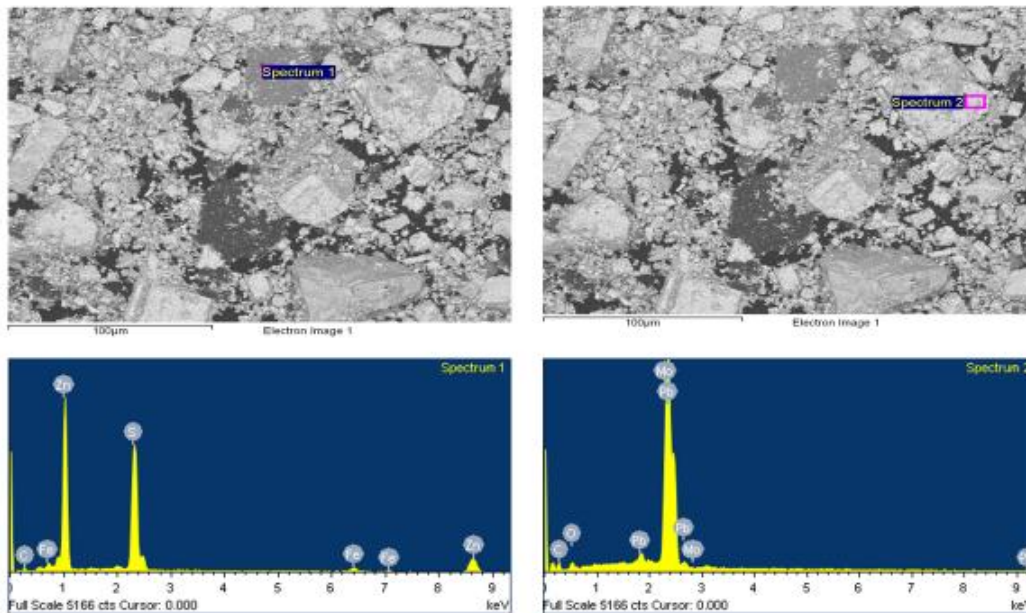


Figure 2: SEM/EDS Micrograph of "As mined" sulphide ore

Table 1: XRF Analysis of Ishiagu sulphide ore

Compound	Na <sub>2</sub> O	MgO	Al <sub>2</sub> O <sub>3</sub>	SiO <sub>2</sub>	P <sub>2</sub> O <sub>5</sub>	SO <sub>3</sub>	K <sub>2</sub> O	CaO	Cr <sub>2</sub> O <sub>3</sub>	MnO	Fe <sub>2</sub> O <sub>3</sub>	CuO	ZnO	PbO
Weight %	0.000	0.546	0.813	4.22	0.0355	16.4	0.152	1.11	0.0635	1.33	15.6	0.640	0.91	53.86

It was discovered that the low grade ore contains 0.91% zinc and 53.86% lead as seen in table 1. There are other unwanted minerals in various percentages.

### Effect of microwave treatment on the particle size

There were no particles retained on the 2000 $\mu\text{m}$  sieve for microwave treated sample unlike the untreated sample during sieve analysis. Figure 3 represents the cumulative % passing of microwave treated and untreated Ishiagu sulphide ore and figure 4 represents the size distribution patterns of the ore samples after Gate-Gaudin-Schuhmann law.

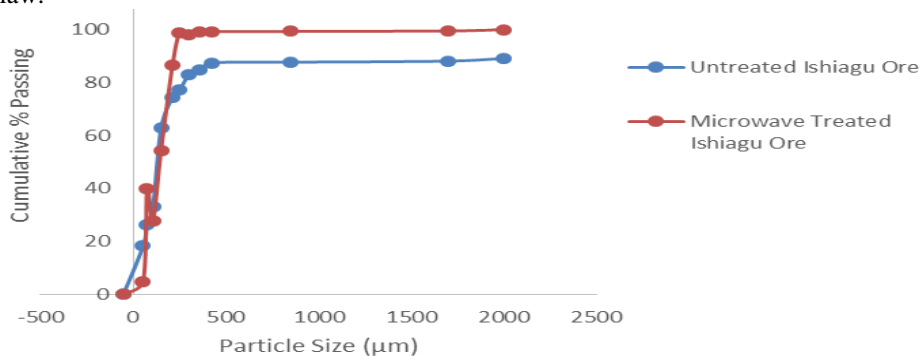


Figure 3: Graph of cumulative % passing of microwave treated ore

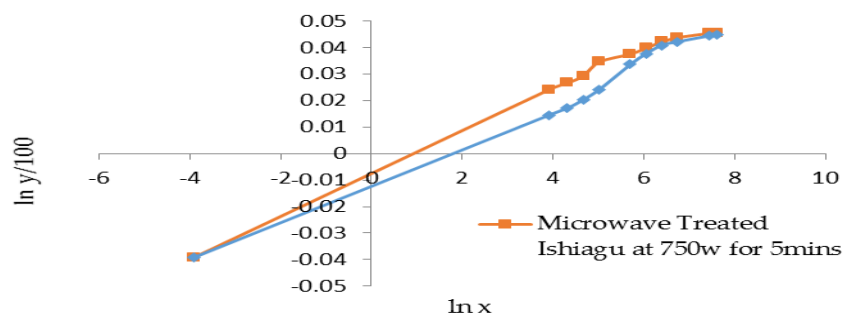


Figure 4: Gates-Gaudin-Schuhmann plot of particle size analysis

Cumulative % passing for 2000 $\mu\text{m}$  is equal to 89.13% while cumulative% passing for 2000 $\mu\text{m}$  of the microwave treated sample is equal to 100% no particles were retained on the 2000 $\mu\text{m}$  sieve. Hence,  $P_{80}$  for microwave treated sample is equal to  $-212\mu\text{m} + 150\mu\text{m}$  while for the untreated sample  $P_{80}$  corresponds to  $-250\mu\text{m} + 212\mu\text{m}$ . The implication of the results of particle size analysis as shown in figure 3 is that as a result of microwave treatment, enough required fine were produce and less energy is required to produce enough particle sizes because there will not be need to regrind and re-crush the ore, that mean less energy is required to produce enough particle sizes. Both microwave treated and untreated sample were comminuted under the same parameters. The energy expended on microwave is 17.85kwh/t because 3.5kg of the ore was microwaved for 5 minutes. If intensive grinding was to be done so as to get the same output as that of the microwave sample, more energy would be expended and too much fines would be generated. Intensive fine grinding reduces particles to fine sizes which make separation inefficient though froth flotation requires as much of the valuable mineral surface to be exposed.

### Effect of microwave treatment on the recovery of lead and zinc

Figure 5, 6,7and 8 show the effect of microwave treatment on the recovery of lead and zinc concentrates at various particle sizes and a power rating of 750W. Figures 5 shows that 88.48% of lead concentrate was recovered using SEX as collector and potassium dichromate as depressant. That of zinc was 17.9% (figure 6) with potassium dichromate as depressant and particle size 106 $\mu\text{m}$ . Meanwhile the untreated sample gave a recovery of 73.47% (figure 7) of lead and 11.72% (figure 8) of zinc. Microwave treatment has allowed most of the valuable minerals to be freed from the associated gangues. Recoveries are higher for all particle sizes of the microwave than for their unmicrowaved counterparts. For example, the values of lead recovery for microwave treated samples are higher in figure 5 when compare to the values of lead recovery in figure 7 of the unmicrowaved samples. Similarly, figure 6 and 8 followed the same trend of recovery of zinc. Potassium dichromate was the depressant which gave the best result though with higher particle size in each case, it may be because higher particle sizes are easily depressed because they are heavier than the finer sizes. Meanwhile, improvement in the recovery of zinc shows that using potassium dichromate to depress lead is the best out of the collectors.



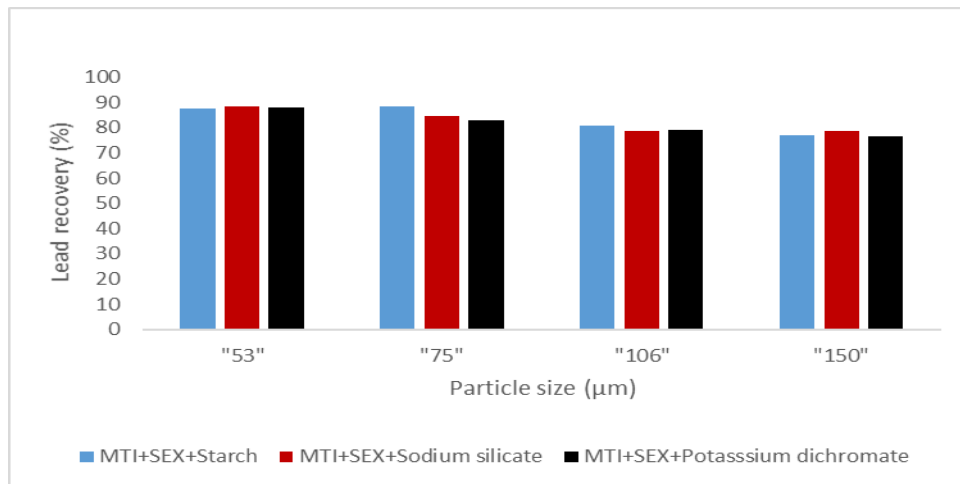


Figure 5: Recovery of lead microwave treated (MTI) Ishiagu sulphide ore using SEX as collector and varying depressants.

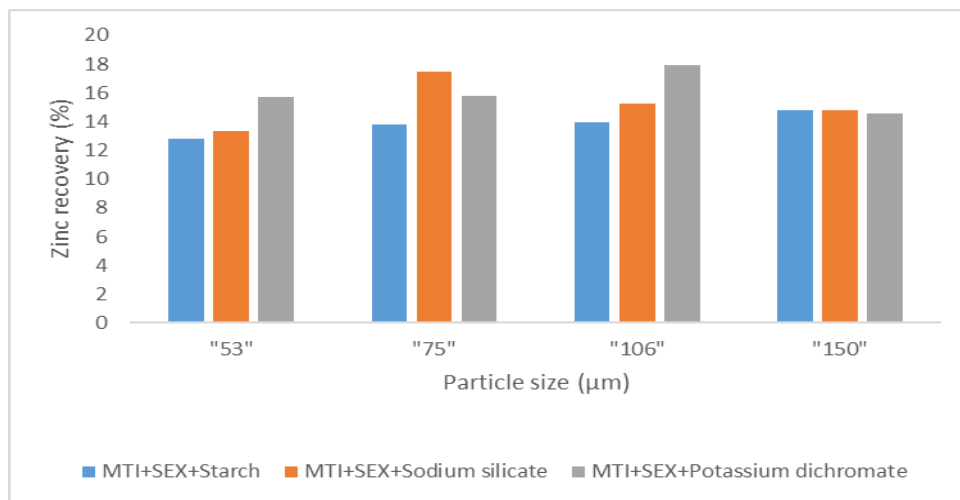


Figure 6: Recovery of zinc microwave treated (MTI) Ishiagu sulphide ore using SEX as collector and varying depressants.

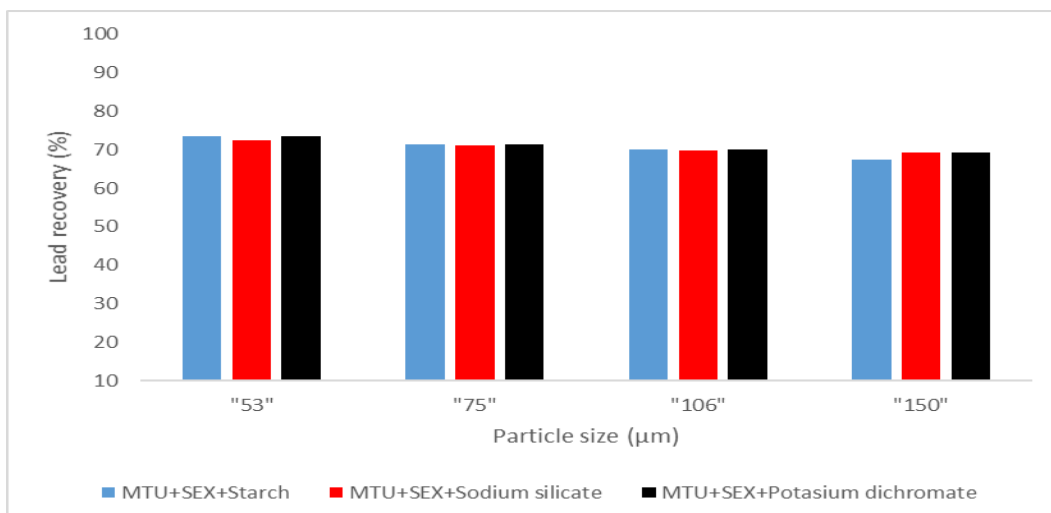


Figure 7: Recovery of lead from untreated (MTU) Ishiagu sulphide ore using SEX as collector and varying depressants.

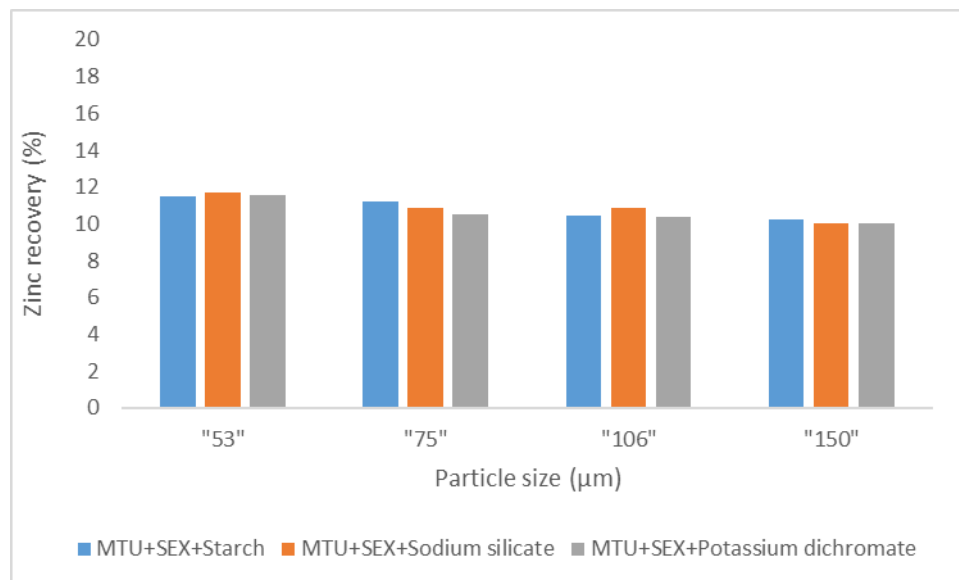


Figure 8: Recovery of zinc from untreated (MTU) Ishiagu sulphide ore using SEX as collector and varying depressants.

#### IV. CONCLUSION

Influence of microwave pre-treatment on the flotation of low-grade sulphide ore have been studied. From the results of sieve analysis for microwave treated and untreated samples it can be concluded that since more smaller particles were obtained from lower particle sizes microwave processing of minerals, especially sulphides, is beneficial for the recovery of the metals, since higher recoveries were obtained from fine particles sizes. Also, the results have shown that microwave pre-treatment has a significant effect on the recovery of lead and zinc concentrates from the sulphide ores. It can be concluded that with microwave treatment 53µm of Ishiagu galena-sphalerite ore gave a recovery of 88.48% using sodium ethyl xanthate as collector. The results have shown that microwave pre-treatment has a significant effect on the recovery of lead and zinc concentrates from the sulphide ores.

#### V. ACKNOWLEDGEMENT

The authors would like to acknowledge the Science Initiative Group at IAS, Regional Initiative in Science Education (RISE), African Materials Science and Engineering Network for financial support.

#### REFERENCES

- [1] Amankwah, R.K., Khan, A.U., Pickles, C.A., Yen, W.T.(2005). *Improved Grindability and Gold Liberation by Microwave Pretreatment of a Free-milling Gold Ore*. Mineral Processing and Extractive Metallurgy (Transactions of the Institute of Minerals and Metallurgy C), 114, pp. 30–36.
- [2] Haque, K. E., (1999). *Microwave Energy for Mineral Treatment Processes-a Brief Review*. International Journal of Mineral Processing, 57, pp. 1-24.
- [3] Kingman, S.W., and Rowson, N.A. (1998). *Mineral Treatment of Minerals a Review Minerals Engineering 11(11),pp. 1081-1087*
- [4] Kingman, S.W., 2006. *Recent Developments in Microwave Processing of Minerals*. International Materials Reviews 51, pp. 1–12.
- [5] Kingman, S.W., Vorster, W., Rowson, N.A., (1999). *The Influence of Mineralogy on Microwave Assisted Grinding*. Minerals Engineering 13(3), pp. 313–327
- [6] Xia D.K and Pickles C.A.(2000). *Microwave Caustic Leaching of Electric-arc Furnace Dust*. Miner Eng 2000; 13(1): pp. 79–97.
- [7] Olubambi, P.A., Potgieter, J.H., Hwang, J.Y, and Ndlovu, S., (2007). *Influence of Microwave Heating on the Processing and Dissolution Behaviour of Low-grade Complex Sulphide Ores*. Hydrometallurgy 89 (2007). Pp. 127-135.
- [8] Sahyoun, C., Rowson N.A, Kingman, S.W, Groves, L. and Bradshaw, S. M (2005). *The Influence of Microwave Pretreatment on Copper Flotation*. Journal of South African Institute of Mining and Metallurgy 2005. SA ISSN 00380-223X/3.00+0.00. pp. 7-13

## A Feasibility Study on Sustainable Management of Municipal Wastes in Ogbomoso

Olatunde Ajani Oyelaran<sup>1\*</sup>, Ibrahim Rufai<sup>2</sup>

<sup>1</sup>Department of Technology Business Development, Hydraulic Equipment Development Institute, Kano, Nigeria

<sup>2</sup>Department of Engineering and Technical Services, Hydraulic Equipment Development Institute, Kano, Nigeria

**ABSTRACT:** Solid waste characterization study is a basis to any proper planning of solid waste management in an area. This study was undertaken to assess the characteristics of the waste generated in the three zones of Ogbomoso, in Nigeria to enhance scientific management of solid wastes in the town. This study consists of carrying out survey, characterization of municipal solid waste (MSW) and exploring it's potential to be used for biogas production. The direct waste collection and sorting was applied to solid wastes collected from ninety (90) households, thirty (30) from each zone with different socio-economic characteristics for a period of four (4) weeks. The result shows that Ogbomoso solid waste consists to a large extent of organic and other biodegradable matter. They were dominated by food, vegetable, paper and animal waste (50.6 %), plastics (7.3%), metals (10.3%), glass (10.2%), ash and dirt (7.6%) suggesting that an integrated waste management approach supported by willingness to separate wastes from source could be the best option for the town. A questionnaire was designed for collecting information about waste generation in all the three zones. The questions asked, were so as to get a essential information about the two important qualities of the waste generated viz quantity and disposal. The study recommended the adoption of the biogas technology because of its potential to address both economic and sanitation challenges being faced by local authorities in developing countries.

**Keywords:** Biodegradable, Characteristics, Management, Municipal solid waste, Sustainability

### I. INTRODUCTION

Proper management of solid waste is critical to the health and well-being of urban residents [1]. Ogbomoso, like most towns in the developing countries is facing potential threat from unhealthy waste disposal practices prevailing in almost all the urban centers in the country. Though the living standard has significantly changed, the method of public health and sanitation still remains primitive. A vast quantity of waste generation in the town is one of the serious outcomes of unplanned development. Due to rapid population growth the town faces many problems. One of the major problems of the city is improper disposal of municipal solid waste. The management of municipal solid waste has become an acute problem due to enhanced economic activities and rapid urbanization. Urban population growths together with the development of markets resulted in the quantum of a huge amount of hazardous organic and inorganic waste daily. Proper management of the waste is a challenging issue that must be addressed adequately. The sources of waste are multiple and haphazard and disposal method is not scientific, as a result of it the environment is getting polluted day by day and gradually. The trace elements polluted the air and poses as a health risk to the people. Many tons of municipal solid waste is left uncollected, clogging drains, creating feeding ground for pests that spread disease and creating a numerous of related health and infrastructural complications. Municipal solid waste management is an important part of the urban infrastructure that ensures the protection of environment and human health [2]. The rising growth of urban population, increasing economic activities and lack of training in modern solid waste management practices in developing countries with unplanned urbanization complicates the efforts to improve solid waste services. Ludwig et al. [3] wrote that the changes in consumption patterns with alterations in the waste characteristics have also resulted in a quantum jump in solid waste generation. In their report, [1] wrote that solid waste management is hampered by a lack of data at all levels from the ward, district and municipality, and where available, is generally unreliable, scattered and unorganized. To this end, the planning of solid waste management has remained a difficult task.

Energy is one of the most significant factors for human development and to worldwide prosperity. Energy demand is a critical reason for extensive climate change, resource exploitation, and also restricts the living standards of humans [4]. [5] Reported that Cooking accounts for 90% of energy consumption in the households of developing countries. While 80% of the world's energy consumption still originates from combusting fossil fuels [6]. Yet the reserves are limited; means do not match with the fast population growth, and their burning substantially increases the greenhouse gas (GHG) concentrations that contributed for global warming and climate change [7]. The over dependence on fossil fuels as primary source of energy, has led to global climate change, environmental degradation, and consequently human health problems.

One technology that can successfully treat the organic fraction of wastes is anaerobic digestion; it has the advantages of producing energy, yielding high quality fertilizer and also preventing transmission of disease [8]. Harnessed biogas can either be processed and sold directly or used to generate energy, which can then be sold. Anaerobic digestion also produces savings by avoiding costs of synthetic fertilizers, soil conditioners and energy from other sources [9].

The classification of waste composition is thus, essential for the selection of the most appropriate technology for treatment, taking necessary health precautions and space needed for the treatment facilities. In spite of this acknowledgment, there has been no study on the analysis of municipal waste composition in Ogbomoso town and environ. This work attempts to fill this gap by providing pre-data on the composition, and sources of municipal waste in three different zones of the town with the aim of understanding the type of waste generated, waste flow, initiate and investigate a feasible sustainable waste disposal and implication for management.

## II. MATERIALS AND METHODS

This work was carried out in three stages. The first is direct sampling of solid waste from specific sources, secondly, questionnaire was designed for collecting information about waste generation in the town and lastly characterization of solid waste was carried out.

### 2.1 Sampling and data collection

The determination of the composition of unprocessed municipal solid waste during this study was done according to ASTM D5231 – 92 [10] Standard Test Method which involves the direct sampling of solid waste from specific sources, a labour-intensive manual process of sorting, classifying and weighing all items in each sampling unit and a detailed recording of the data. Composite solid waste samples were sorted into ten categories namely; food scrap, waste paper, textile material, plastic material, metal, glass, ash dirt, vegetable, animal waste (dung, etc) and others which comprise unidentified waste types. Each category was weighed and its percentage composition determined. A total 60 households were surveyed (20 from each zone), each of the households was visited every day for four (4) weeks in November, 2014 and the waste sorted and weighed at source. Statistical quantities such as the mean and standard deviation were used to summarize the findings in this study. Standard deviation showed variation in the values of variables from the mean.

### 2.2 The Questionnaire

A questionnaire was designed for collecting information about waste generation in the town. The questions included, were so as to obtain a basic idea about the two important qualities of the waste generated viz quantity and disposal. A total 300 questionnaire was distributed (100 for each zone).

### 2.3 Laboratory

The characterization of solid waste was done to by finding moisture content, organic matter (total solid (TS) and volatile solid components (VS)) of solid waste. These were done so as initiate and investigate a feasible sustainable waste disposal

**2.3.1 Determination of moisture content of samples:** The moisture content of the solid waste was determined using the method used by Cioabla et al. [11]. The samples were weighed in a dish and dried in an oven at 105°C overnight. The weight of the dried sample plus dish was noted and the percentage moisture content was calculated by this equation

$$\% \text{ moisture content} = \frac{(m_2 - m_1) - (m_3 - m_1)}{(m_2 - m_1)} \times 100 \quad (1)$$

Where,

$m_1$  = mass in grams of the empty dish,

$m_2$  = mass in grams of sample plus the empty dish before drying,

$m_3$  = mass in grams of sample plus empty dish after drying.

**2.3.2 Determination of total solids (TS):** The total solids (TS) were determined using the convection oven method which involved heating samples of 10g each of the biodegradable municipal solid waste and air dried at  $105 \pm 3^{\circ}\text{C}$  for three hours. The dried waste was then allowed to cool to room temperature in a desiccator after which it was weighed. The weight of the sample plus weighing dish was recorded. The sample was again heated in a convection oven at  $105 \pm 3^{\circ}\text{C}$ , until a constant weight change of  $\pm 0.1\%$  change was achieved upon one hour of re-heating the sample. The TS was then calculated from the formulae.

$$\text{TS} = \frac{\text{mass of dried sample remains}}{\text{initial mass of sample}} \quad (2)$$

**2.3.3 Determination of volatile solids (VS):** The volatile solids (VS) of the substrate was determined by igniting the dried samples from (a) in a muffle furnace for two hours at  $500^{\circ}\text{C}$ . The initial mass of the dried sample prior to ignition was recorded and the final mass of the solid remained after 2 hours of ignition was recorded. VS was then determined from the formulae.

$$\text{VS} = 1 - \frac{\text{mass of solid remains after igniting sample}}{\text{initial mass of dried sample}} \quad (3)$$

### III. RESULTS AND DISCUSSION

From the samples of solid wastes collected from the sampled households in the three zones, ten different types of wastes were categorized. These are food scrap, waste paper, textile material, plastic material, metal, glass, ash dirt, vegetable, animal waste (dung, etc) and others. Table 1 shows the different categories of waste observed in the three residential zones of Ogbomoso. Analysis of waste type shows that solid waste consists to a large extent of biodegradable matter (51.3 %) and the non biodegradable made up of substantially dirt, ash and other household trash typical of low income developing country [12, 13]. However, a closer look at the composition of municipal solid waste provides a description of the constituents of the waste and it differs widely from place to place [14]. The most remarkable difference is the difference in organic content which is much higher in the low income areas (metropolis) than the high income (lautech), while the metal and plastic content is much higher in high income areas than low income areas. It is a reflection of the difference in consumption pattern, cultural and educational differences. Due to the composition of the waste, especially the findings in this study of substantial presence of faecal matter and animal dung in the waste, many health and environmental issues are foreseen. The biodegradable wastes generated are in high quantity, these could be utilized by adopting appropriate technologies for processing it into a source of green energy and bio-fertilizer. While promoting sustainability, it would help prevent the degradation of the urban environment.

#### 3.1 Responses to Questionnaire

There were 248 respondents to the questionnaire from 300 distributed. The respondents consisted of male and female with various age, occupational and educational status. Of the 100 questionnaire distributed to each zone 79, 87 and 82 were returned from metropolis, lautech and suburban respectively.

**3.1.1 Type(s) of waste generated:** Identification of waste composition is crucial for the selection of the most appropriate technology for treatment, taking essential health precautions and space needed for the treatment facilities. The type of municipal solid waste generated varies according to the various sources within the town as shown in Table 1. In higher income areas disposable material and packaged food are used in higher quantities. In the case of lower income areas, the usage of fresh vegetables with lack of refrigeration, keeping of livestock like goats and waste food is responsible for the high decomposable material. The availability of space encourages the keeping of livestock in the suburban area of Ogbomoso hence has more animal dung as seen in Table 1.

Table 1: Waste type and composition (%) in the three residential zones of Ogbomoso

Categories	Metropolis (%)	Lautech (%)	Suburban (%)
Food scrap	23.2	12.8	18.4
Waste Paper	7.7	6.7	8.3
Textile material	10.7	9.8	11.1
Plastic material	5.1	12.1	3.9
Metal	6.4	18.4	6.2
Glass	7.2	16.7	6.7
Ash, dirt	6.4	4.7	11.5
Vegetable	14.3	10.5	7.9
Animal waste (dung, etc)	17.7	7.6	25.1
unidentified waste types	1.3	0.7	0.9

**3.1.2 Current method of disposal:** As shown in Table 2, the use of authorized dump site was highest among lautech resident 65.8%, followed by those in the metropolitan 33.7%, while it was least among those living in the suburban area of the town 26.9%. A reverse pattern was observed for unauthorized site dumping with lautech having the least 14.5%, followed by the metropolis with 61.4%, while suburban has the highest of 72.7% this could be as a result of availability of empty space which encourages indiscriminate disposal. For water ways disposal the practice is more pronounced in the metropolis 52.4%, suburban area recorded 38.7%, while lautech area has the least of 27.6% this could as a result of the area consisting of much higher percentage of educated people. Burning of refuse is higher in the metropolis area (49.3%) than the other two zones suburban 43.1% and lautech 23.4%. The lower percentage observed in the lautech area could be as a result of the knowledge of the effect of burning as will be seen later. Lack of space for disposal might be responsible for the high percentage of burning in the metropolis. The suburban area recorded the highest method of burying refuse (37.5%), followed by lautech with 8.1%, while the metropolis has the least of 3.6%. Availability of empty space could be responsible for this trend of waste disposal. The use of waste bin is highest in the lautech area with 62.7%, followed by suburban 21.1%, while metropolis is 6.3%. The trend could be as a result of the financial implication involved in this method.

Table 2: Current methods of disposal.

Place	Metropolis (%)	Lautech (%)	Suburban (%)
Authorized dump site	33.7	65.8	26.9
Unauthorized site	61.4	14.5	72.7
Water ways	52.4	27.6	38.7
Burning	49.3	23.4	43.1
Burying	3.6	8.1	37.5
Personal bin	6.3	62.7	21.1

Note: Multiple responses were allowed for disposal methods

**3.1.3 Awareness of waste separation and disposal options:** As shown in Table 3, Awareness of waste collection service (WCS) was highest in the lautech area 88.6%, followed by suburban area 72.9%, while it was least among metropolis 63.3%. The same pattern could be observed for awareness of waste management regulations (WMR). The percentage of those who used WCS was highest among lautech area 81.2% and least in metropolis 28.8%. The percentage of those who used WCR was higher among those resident in lautech 66.5% and lowest among those resident in the suburban area 22.1%. The separation of waste from source was also higher in the lautech area 52.3% , compared to metropolis 15.7 and 18.7% for suburban areas. The influence of education on solid waste management could then be inferred.

Table 4 shows reasons for not using WCS. Those who used other WDO like open dumping, open burning, dumping in drainages and burying gave the reason of being not been effective where the existed 67.8, 31.3 and 75.9% for metropolis, lautech and suburban respectively. The other reason gave was in availability of WCS in their area of residence 58.4, 12.3 and 76.7% for metropolis, lautech and suburban respectively. Furthermore 67.3, 45.3 and 73.2% for metropolis, lautech and suburban areas gave the reason of too far from dump sites. The awareness of WMR was highest among those who are educated. The percentages of those who used WCS seemed not to be influenced by educational status as the results did not follow an orderly pattern; the reasons could be the availability and effectiveness of WCS. As seen in Table 4.

Table: 3 Awareness of waste separation and disposal options

Question	Metropolis	Lautech	Suburban
Aware of WCS (%)	63.3	88.6	72.9
Aware of WCR (%)	28.8	81.2	41.3
Use of WCS (%)	33.1	66.5	22.1
Separate the waste at source (%)	15.7	52.3	18.7

Where,

Awareness of waste collection service (WCS)

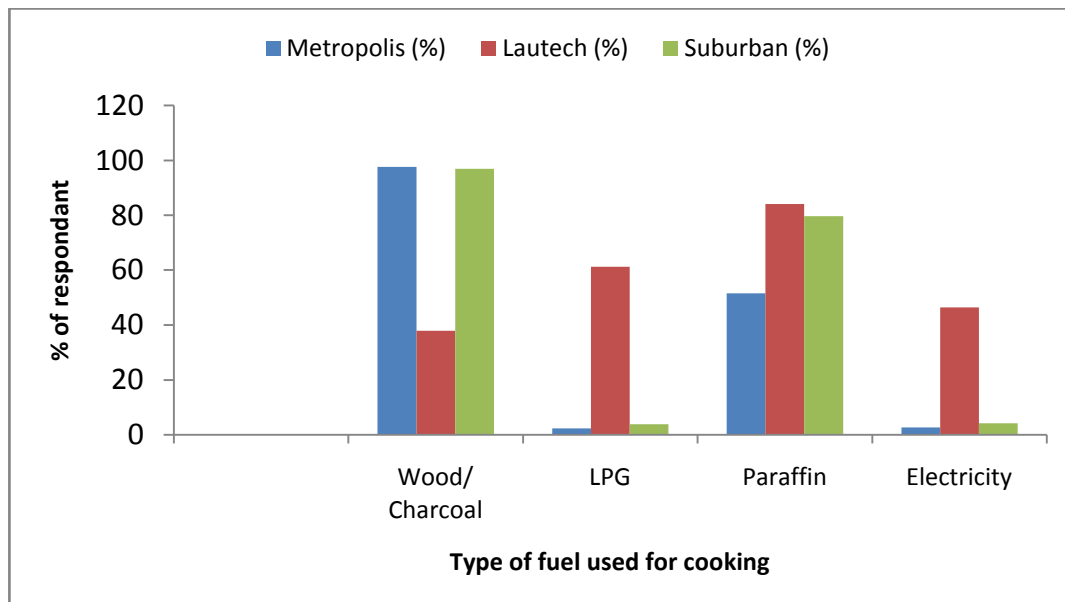
Awareness of waste management regulations (WMR)

Table 4: Reasons for not using WCS

Reasons	Metropolis (%)	Lautech (%)	Suburban (%)
Not effective in my area	67.4	31.3	75.9
Not available in my area	58.6	12.3	76.7
Collection service too costly	88.7	35.8	75.8
Dump site too far from home	67.5	45.3	73.2

Note: Multiple responses were allowed for sources of energy

**3.1.4 Type of cooking fuel used:** Figure 1 presents an aggregated view of the type of energy used for cooking in the three zones under study. It can be deduced that wood is the most used source of energy followed by paraffin with electricity and the use of LPG very small. The distribution of energy used in each zone shows that Metropolis and the suburban areas relied heavily on wood and charcoal for cooking 97.6 and 96.9% respectively. The used of LPG and electricity in the two zones of metropolis and suburban is less than 5% compared to lautech area which has 84.1 and 46.4% relying on LPG and electricity for their cooking respectively. The lack of usage of electricity for cooking in the metropolis could be as a result of lack of constant electricity supply in the areas compared to lautech areas that have almost 24 hours constant power supply per day. However the lower usage of LPG in the two areas of metropolis and suburban compared to lautech area might not be unconnected to the cost of LPG and its availability.



Note: Multiple responses were allowed for types cooking fuel

Figure 1: Type of cooking fuel used

**3.1.5 Daily cooking fuel requirement:** Most respondents in the metropolis, suburban and those that uses wood in lautech areas indicated that they consumed wood for 2-3 hours for cooking purposes. This was compared to less than 1 hour when paraffin was used for the same purpose. Heating about 2 litres of water using wood was generally observed to take slightly less than 1 hour. This probably indicates that the technology used for cooking with wood is less efficient when compared to the use of paraffin stoves. It might also reflect the relative cost of each source of energy for the various purposes as discussed above.

**3.1.6 Health impacts on the use of various sources of energy for cooking:** The study also sought to ascertain the perceptions of respondents on the knowledge of the various effect of usage of various sources of energy for cooking. Lautech areas resident 69.8% are aware of the hazards associated with burning of wood. Metropolis and suburban areas recorded 27.9 and 33.4% knowledge of the effect of the used wood for cooking. All respondent also perceived gas as being potentially dangerous because of their ability to cause accidental fires.

**3.1.7 Awareness of biogas technology:** The awareness of biogas technology as shown on Table 5, is very low in the metropolis (3.7%) and the suburban (6.8%) areas, while the knowledge of biogas technology is 53.6% in the lautech area. The high percentage awareness of the biogas technology in the lautech area might be due to higher educational level of the resident of the area.

Table 5: Awareness of biogas technology

Question	Metropolis (%)	Lautech (%)	Suburban (%)
Perception of health impact on the use of wood	27.9	69.8	33.6
Awareness of biogas	3.7	61.3	6.8
Ready to adopt to biogas technology if available	69.2	87.7	71.6

### 3.2 Laboratory tests results

As observed from Table 6, the moisture content of the waste varied from 70 to 75%. It is comparable to the moisture content obtained by Hafid et al., [15]. This can be a potential problem if we derive energy in the form of steam as a huge amount of fuel would be wasted in drying the waste. Biogas is a better option as there is a requirement of moisture in 50%. The findings from laboratory experiments carried out to determine solid content of solid waste are as shown in Table 6. A large fraction of this waste is biodegradable thus it can be used as a feedstock for methane production. The low percentage of total solids (TS) is due to the composition of food waste, vegetables, fruit remains and peels which had high moisture content (MC). The high percentage of the volatile solids (VS) 75% to 80% indicates the organic portion of the feedstock, which characterizes the digester systems input feedstock when expressed as a fraction of total sample (wet) weight. City of San Rafael Sanitation Agency [16] indicated that VS contents of 70% and above make solid wastes biodegradable.

Table 6: Characteristic of substrate

Substrates	Metropolis (%)	Lautech (%)	Suburban (%)
Moisture content (MC)	75±1.4	71±1.1	73 ±1.8
Total solids (TS)	15.3 ±0.7	16.2±0.4	15.8 ±0.9
volatile solids (VS)	87.1 ± 1.2	86.3±0.8	88.4±1.3

Due to the composition of the waste, especially the findings in this study of substantial presence of faecal matter in the waste, many health and environmental issues are foreseen. From the data presented in this work, it can be seen that biodegradable materials make up about half of the waste generated by households, therefore segregation at source should be encouraged, effectively reducing the bulk of municipal solid waste for disposal and the space required for the purpose causing a reduction in the expenses. The segregated organic waste could be utilized by adopting appropriate technologies for processing it into bio-fertilizers or as a source of green energy.

The characterization of MSW collected from three areas of Ogbomosho, the average moisture content of the samples was found to be between 70 and 75%. High moisture content makes thermal recovery from solid waste uneconomical as considerable fuel is used up by the latent moisture in the solid waste. Anaerobic digestion, which requires high moisture content for the sustenance of the methane bacteria, was the preferred alternative for energy recovery from organic waste in the Ogbomosho. Bioconversion processes are suitable for wastes containing moisture content above 50% than the thermo- conversion processes [17]. Waste-to-Energy transformation has been identified as a veritable option in the integrated waste management processing of MSW. A higher volatile matter content leads to a better biogas yield. The test samples contained an average of 87% of volatile matter, thus strengthening the case for the adoption of anaerobic digestion in Ogbomosho. Apart from biogas, the anaerobic digestion process produces byproduct (digested residual) which can have a value as a fertilizer or soil amendment. The bio-fertilizer enriches soil with no detrimental effects on the environment [18, 19]. However, if biogas is adopted, it should be accompanied by intensive awareness campaigns about the safety use of the fuel so as to take of the people's perception on the use of gas for cooking. For the respondents who use electricity for various purposes about 40% of them paid US\$ 21-55 in monthly bills. About 55% of the respondents spent between US\$11-40 on wood and 65 % spent between US\$1-50 on paraffin per month. This gives a daily average household energy expenditure of US\$1-50. It would seem most households will be able to pay for biogas and biodigester maintenance from the savings of buying wood and paraffin but this depends on the price visa vies cost

## IV. CONCLUSION

From this work, it is believed that no single waste management option can be employed in isolation for MSWM in Ogbomosho. Considering the nature and components of waste generated in Ogbomosho, a blend of certain management options in the waste management hierarchy would be more suitable in tackling the challenge of MSWM. These management options should be integrated in a sustainable agenda with adequate consideration be given to their hierarchical importance. In order that the desired result is accomplished, these options should



also be considered and employed based on local conditions rather than foreign methods. The backbone of most options in the waste management hierarchy is waste segregation at source. Other key aspects are proper storage, more efficient waste collection systems, sustainable recovery and disposal. Public education and properly planned waste management programs need to be introduced into the current waste management system. These are relevant because households should know and understand the importance of waste segregation and proper storage, as well as those of recycling and compost production. In order, to encourage and enhance cooperation of households, inclusion of incentives should not be overlooked when designing programs for waste management.

#### REFERENCES

- [1]. World Bank 2003. Thailand Environmental Monitor. A joint publication of the Pollution Control Department, Royal Thai Government. The World Bank, US Asia Environmental Partnership, 2003 .
- [2]. World Bank 2002. Data by country. Website <http://www.worldbank.org/data/countrydata/countrydata.html> (Retrieved June 11, 2003).
- [3]. C. Ludwig, S. Hellweg, S. Stucki (Eds.), Municipal Solid Waste Management: Strategies and Technologies for Sustainable Solutions. Berlin Heidelberg: Springer-Verlag, 2003.
- [4]. The World Bank Report 2009. Titled, "How we Classify Countries," in *Little Data Book*, Urban Development Series, 2009.
- [5]. A. Bandhu, Government of Uttar Pradesh, "Detailed Project Report for Solid Waste Management in Agra, Uttar Pradesh," RCUES, September 2008.
- [6]. J. Goldemberg, and T. B. Johansson, World energy assessment overview 2004 update. New York: UNDP. 2004, pp 88.
- [7]. W. Schamphelaire, G. Verstraete, Biological Energy Conversion, *Biotechnology. Bioeng.* 103(2) 2009
- [8]. B. Nirmala, S. Deepa, and K. Sunil, Biomethanation of Banana peel and Pineapple waste, *Bioresource Technology*, 58: 1996, 73-76.
- [9]. A. Kalantaifard and G. Yang, Energy potential from municipal solid waste in Tanjung Langsat landfill, Johor, Malaysia, *International Journal of Engineering Science and Technology (IJEST)*, 3( 12) 2011, 8560-8568.
- [10] ASTM D5231 – 92, Standard Test Method, 2008.
- [11] A. E. Cioabla, L. Lonel, G. A. Dumitrel, and F. Popescu, Comparative study of factors affecting anaerobic digestion of agricultural vegetal residues, *Biotechnology Biofuels.*, 5:39, 2012.
- [12] T. V. Ramachandra and S. Bachamanda, Environmental audit of Municipal Solid Waste Management. *International Journal Environmental Technology and Management*, 7(3/ 4), 2007, 369–391.
- [13] A. B. Nabegu, An Analysis of Municipal Solid Waste in Kano Metropolis, Nigeria, *Journal of Human Ecology*, 31(2) 2010, 111-119.
- [14] P. Kuruparan, O. Tubtimthai, C. Visvanathan, and J. Tränkler, Influence of Tropical Seasonal Variation, Operation Modes and Waste Composition on Leachate Characteristics and Landfill Settlement. Proceedings of the Workshop on Sustainable Landfill Management, December 3-5, 2003, Centre for Environmental Studies. Anna University, Chennai, India.
- [15] A. Apte, V. Cheernam, M. Kamat, S. Kamat, P. Kashikar and H. Jeswani, Potential of Using Kitchen Waste in a Biogas Plant *International Journal of Environmental Science and Development*, 4(4) 2013, 370 – 374.
- [16] G. Sibanda, D. Musademba, H. C. Chihobo and L. Zanamwe, A Feasibility Study of Biogas Technology to Solving Peri-urban Sanitation Problems in Developing Countries. A Case for Harare, Zimbabwe. *International Journal of Renewable Energy Development*, 2(2) 2013, 97-104.
- [17] M. Sharholi, K. Ahmed, G. Mahmood and R. C. Trivedi, Municipal solid waste management in Indian cities – A review, *Waste Management*, 28(2) 2008, 459–467.
- [18] E. I. Iyagba, I. A. Mangibo, and Y. S. Mohammad, The study of cow dung as co-substrate with rice husk in biogas production. *Science Research Essays* 4 (9) 2009, 861-866.
- [19] E. O. Uzodinma, A. U. Ofoefule, J. I. Eze, I. Mbaeyi and N. D. Onwuka, Effect of some organic wastes on the biogas yield from carbonated soft drink sludge. *Science Research Essays* 3 (9) 2008, 401-405.

## Data-Collection using Clustering Approach in Wireless Sensor Network Design based on Heuristic Algorithms

<sup>1</sup>Vishwaja B, <sup>2</sup>Mrs. Geetha

<sup>1</sup>M.TECH in Computer science CMR Institute of technology Bangalore, India

<sup>2</sup>Assistant professor CMR Institute of technology Bangalore, India

**Abstract**— Data-gathering wireless sensor networks (WSNs) are operated unattended over long time horizons to collect data in several applications such as those in climate monitoring and a variety of ecological studies. Typically, sensors have limited energy (e.g., an on-board battery) and are subject to the elements in the terrain. In-network operations, which largely involve periodically changing network flow decisions to prolong the network lifetime, are managed remotely, and the collected data are retrieved by a user via internet. In this paper, we study an integrated topology control and routing problem in cluster-based WSNs. To prolong network lifetime via efficient use of the limited energy at the sensors, we adopt a hierarchical network structure with multiple sinks at which the data collected by the sensors are gathered through the cluster heads (CHs). We consider a Particle Swarm Optimization model to optimally determine the sink and CH locations as well as the data flow in the network. Our model effectively utilizes both the position and the energy-level aspects of the sensors while selecting the CHs and avoids the highest-energy sensors or the sensors that are well-positioned sensors with respect to sinks being selected as CHs repeatedly in successive periods

**Keywords**—Wireless sensor networks, Data gathering, energy, Network lifetime, cluster head.

### I. INTRODUCTION

There is a rapid development of low cost, multifunctional and low power sensors through the recent advances in, embedded microprocessors, Wireless sensor networking, integration of micro electromechanical systems (MEMS), and nanotechnology. Sensors of very small size are capable of sensing, processing data and communicating with each other or with the data sinks. Wireless sensor network (WSN) is formed by the group of sensors which are communicating in a wireless medium in order to gather the data and transmit it to a user (sinks). The main purpose of Wireless sensor network applications is to monitor and collect data by the sensors and to transmit the data to the sinks. Wireless sensor networks are categorized into four types as time-driven, sink-initiated, event-driven and hybrid in terms of data delivery scheme. In the time-driven model, the sensors will send the data periodically to the sink by sensing the data continuously at a pre specified rate. For event-driven and sink-initiated models, when a certain event occurs or when a request is initiated by the sink, then the sensors report to the sink. These models are well suited to time-critical applications. A hybrid model is the combination of the all the above three methods.

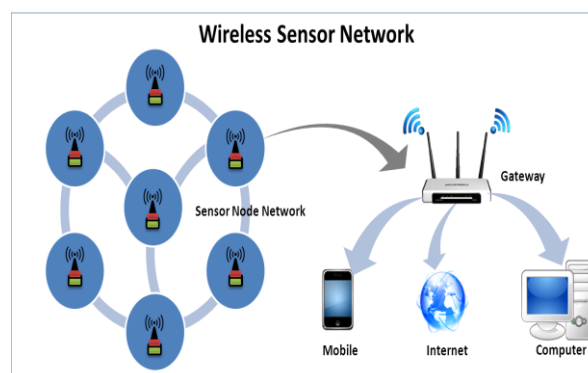


Fig 1 wireless sensor network

Wireless sensor network as shown in fig 1 gives an opportunity for ecological monitoring which was not possible before due to infeasibility of in-person attendance in data collection and the remoteness of areas of interest. Wireless sensor network make possible of eco-monitoring and also facilitates more frequent data collection. Wireless sensor network operations have the following framework. First a set of sensors with limited energy resource are equipped and as well as with the capabilities of sensing, processing and communication are deployed in a geographical region. Sensors forward the data collected by them to the designated sensors which are called as cluster heads ( CHs), which aggregate their received data through some processing. Cluster Heads then forward the data to sinks which are deployed at specific locations, either directly or through other Cluster heads. Determination of the cluster Head and sink locations is the design of the network, while routing of data from the sensors to the sinks in the network refers to the operation decisions

Network lifetime which is defined as the time between two sensor deployments is one of the main concerns in network design and operation. Having less number of operational sensors with enough remaining energy in the network may be one of the reason for the sensor redeployments. The lifetime is divided into periods which are of uniform length and each period is made with network design and operations decisions considering that the number of periods in deployment cycle is maximized.

The two fundamental problems in effective design and operation of Wireless sensor network are topology control and routing. The energy efficiency and computation-communication trade off are some design specific/ operation attributes which underlines the relation between the decisions and their relation to network lifetime. Energy efficiency is the main concern because each sensor has finite and nonrenewable energy resource. Communication-computation tradeoff means the fact that the energy consumed by the communication is more than the computations performed on board a sensor.

Despite the innumerable applications of WSNs, these networks have several restrictions, e.g., limited energy supply, limited computing power, and limited bandwidth of the wireless links connecting sensor nodes. One of the main design goals of WSNs is to carry out data communication while trying to prolong the lifetime of the network and prevent connectivity degradation by employing aggressive energy management techniques. The design of routing protocols in WSNs is influenced by many challenging factors. These factors must be overcome before efficient communication can be achieved in WSNs. In the following, we summarize some of the routing challenges and design issues that affect routing process in WSNs.

- **Node deployments:** Node deployment in WSNs is application dependent and affects the performance of the routing protocol. The deployment can be either deterministic or randomized.
- **Energy consumption without losing accuracy:** Sensor nodes can use up their limited supply of energy performing computations and transmitting information in a wireless environment.
- **Data Reporting Model:** Data sensing and reporting in WSNs is dependent on the application and the time criticality of the data reporting. Data reporting can be categorized as either time-driven (continuous), event-driven, query-driven, and hybrid.
- **Node/Link Heterogeneity:** In many studies, all sensor nodes were assumed to be homogeneous, i.e., having equal capacity in terms of computation, communication, and power. However, depending on the application a sensor node can have different role or capability.
- **Scalability:** The number of sensor nodes deployed in the sensing area may be in the order of hundreds or thousands, or more. Any routing scheme must be able to work with this huge number of sensor nodes.
- **Coverage:** In WSNs, each sensor node obtains a certain view of the environment. A given sensor's view of the environment is limited both in range and in accuracy; it can only cover a limited physical area of the environment. Hence, area coverage is also an important design parameter in WSNs.
- **Data Aggregation:** Since sensor nodes may generate significant redundant data, similar packets from multiple nodes can be aggregated so that the number of transmissions is reduced. Data aggregation is the combination of data from different sources according to a certain aggregation function, e.g., duplicate suppression, minima, maxima and average.
- **Quality of Service:** In some applications, data should be delivered within a certain period of time from the moment it is sensed, otherwise the data will be useless. Therefore bounded latency for data delivery is another condition for time-constrained applications. However, in many applications, conservation of energy, which is directly related to network lifetime, is considered relatively more important than the quality of data sent.
- Applications of Wireless Sensor Networks
  - **Area monitoring**  
Area monitoring is a common application of WSNs. In area monitoring, the WSN is deployed over a region where some phenomenon is to be monitored.
  - **Air quality monitoring**  
The degree of pollution in the air has to be measured frequently in order to safeguard people and the environment from any kind of damages due to air pollution.

➤ **Forest fire detection**

A network of Sensor Nodes can be installed in a forest to detect when a fire has started. The nodes can be equipped with sensors to measure temperature, humidity and gases which are produced by fire in the trees or vegetation.

➤ **Natural disaster prevention**

Wireless sensor networks can effectively act to prevent the consequences of natural disasters, like floods.

➤ **Machine health monitoring**

Wireless sensor networks have been developed for machinery condition-based maintenance (CBM) as they offer significant cost savings and enable new functionality. In wired systems, the installation of enough sensors is often limited by the cost of wiring.

➤ **Industrial sense and control applications**

In recent research a vast number of wireless sensor network communication protocols have been developed. While previous research was primarily focused on power awareness, more recent research have begun to consider a wider range of aspects, such as wireless link reliability, real-time capabilities, or quality-of-service.

➤ **Water/Waste water monitoring**

Monitoring the quality and level of water includes many activities such as checking the quality of underground or surface water and ensuring a country's water infrastructure for the benefit of both human and animal. The cluster based algorithms could be used for partitioning the sensor nodes into subgroups for task subdivision or energy management. A survey on clustering algorithms for WSNs can be found in [2].

Based on the set of sensors deployed and which are available at the beginning of a period, determining the sinks and Cluster Heads to employ and flow of data from sensors to sinks through Cluster Heads in the specified period is considered as the problem definition. Hence, the average usage of the energy and the variation in distributing the remaining energy in the network is minimized and the adoption of high-energy sensors as Cluster Heads is encouraged. There is a assumption that any sensor can be a Cluster Head while looking that whether there are special high-energy sensors deployed for this role.

The main aim of the project work is to optimize the energy possessed by each sensor node in wireless Sensor Networks that is to increase the lifetime of the sensor nodes deployed in various regions

## II. RELATED WORK

Grouping the sensors into clusters known as clustering has been shown effective in prolonging sensor network lifetime in the literature. The basic idea is organising the wireless sensor network into a set of clusters, sensors transmit the collected data to their Cluster Heads within each cluster. The received data is aggregated by each cluster head and forwards to the sink either directly or through other Cluster Heads.

There are three ways of benefits in terms of energy efficiency:

1) A multi-hop sensor-to-sink data transfer scheme that eliminates the quick energy drainage at the sensors which are away from the sink can be achieved by the hierarchical structure; 2) To reduce the redundancy of the data so that communication energy savings are realized, Cluster Heads will aggregate the data 3) Energy consumption can be balanced by reassigning the CHs and the sinks and adjusting the routing in the network by re-clustering in uniform time intervals.

Heinzelman et al. [18] develop a cluster-based data aggregating routing protocol Low Energy Adaptive Clustering Hierarchy (LEACH). In LEACH, a single-hop Cluster head-to-sink connection is assumed and the randomized rotation of Cluster Heads is adopted to ensure a balanced energy consumption.

LEACH (Low-Energy Adaptive Clustering Hierarchy), a clustering-based protocol that utilizes randomized rotation of local cluster base stations (cluster-heads) to evenly distribute the energy load among the sensors in the network. LEACH uses localized coordination to enable scalability and robustness for dynamic networks, and incorporates data fusion into the routing protocol to reduce the amount of information that must be transmitted to the base station. Simulations show that LEACH can achieve as much as a factor of 8 reduction in energy dissipation compared with conventional routing protocols. In addition, LEACH is able to distribute energy dissipation evenly throughout the sensors, doubling the useful system lifetime for the networks we simulated.

**Disadvantage**

These assumptions may not provide guarantee to network connectivity.

Younis and Fahmy [19] proposed a hybrid energy-efficient distributed clustering routing (HEED) protocol where the probabilistic selection of the cluster head is based on their remaining energy and the addition of sensors into the clusters such that the communication cost is minimized. A multihop connection between the CHs and to the sink is assumed in HEED.

HEED (Hybrid Energy-Efficient Distributed clustering), which has four primary goals: (i) prolonging network lifetime by distributing energy consumption, (ii) terminating the clustering process within a constant number of iterations/steps, (iii) minimizing control overhead (to be linear in the number of nodes), and (iv) producing well-distributed cluster heads and compact clusters. HEED does not make any assumptions about the distribution or density of nodes, or about node capabilities.

Liu et al. [20] suggested a distributed energy-efficient protocol known as EAP. In EAP, the selection of the cluster head is based on its ratio of the remaining energy to the average remaining energy of all the neighbor sensors within its cluster range. The Cluster heads are chosen based on a sensors' own remaining energy in EAP. To extend the network lifetime, the idea of "intracluster coverage" which allows a partial set of sensors to be active within clusters while maintaining an expected coverage is introduced by EAP.

**III. PROPOSED SYSTEM**

The Proposed System is a System which uses the particle swarm optimization heuristic algorithm to select the Cluster heads in various clusters formed by the large number of nodes. The cluster heads are selected based on the factors such as Energy, Density and Mobility. The node with the highest energy, density and lowest mobility is elected as the cluster head for that particular cluster and the nodes in that cluster gets informed about the cluster head. The nodes will collect the data from the deployed region and forward the data to the cluster head instead of base station and further the data is aggregated by the cluster head from all the nodes of that cluster and forwarded to the base station through the Gateways. The following are some of the advantages of the proposed system.

- Simple to understand and implement
- Convergence at the faster rate
- Adaptive towards the failure of any sensor node in the network.

**A. System Architecture**

The structure and behavior of a system are defined in the System Architecture. An architecture description is organized in a way to support reasoning about the system's structural properties and it provides a formal description of a system. It provides an overview from which products can be produced, and it defines the system components or building blocks and the systems developed, which will work together in the implementation of the overall system. The System architecture is shown below.

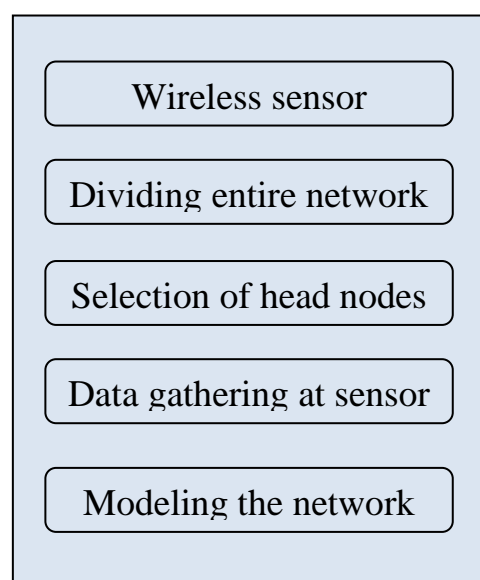


Fig 2 Architecture

Main Modules are:

- Network setup
- Clustering
- Selection of cluster head
- Data transmission to Base Station

### Network Setup

Large numbers of sensors are placed in the wireless sensor networks at remote places in order to gather the data from the clients to transfer to the destinations known as sinks. The sensor nodes are provided with the limited battery where its energy drains up to send the data to destination. All the nodes, Cluster heads and the sinks should have proper communication through the network.

### Clustering

As there are large number of sensors with limited energy, in order to have the energy efficiency the sensor nodes are divided into various clusters based on the energy obtained by them in order to select any one node from each cluster as cluster head to perform the data forwarding function on behalf of involvement of all nodes.

### Selection of Cluster Head

In order to optimize the energy among the nodes the nodes are grouped into various clusters. In Clusters the energy obtained by the nodes are compared with each other node using the particle swarm optimization technique. The node with the highest energy is elected as the cluster head of that particular cluster. The cluster head gathers all the data from its cluster's nodes, aggregates and forwards to the sink nodes through the network.

### Transmission of Data to Base Station

Sink Nodes are the destination nodes which are placed at a suitable distance from the cluster heads. The sink nodes receives the data from the clusters heads and acknowledges for receiving the data where there is no involvement of each node with the sink node. Hence the energy obtained by the nodes are effectively optimized.

## IV. SIMULATION RESULTS

Scenario 1:

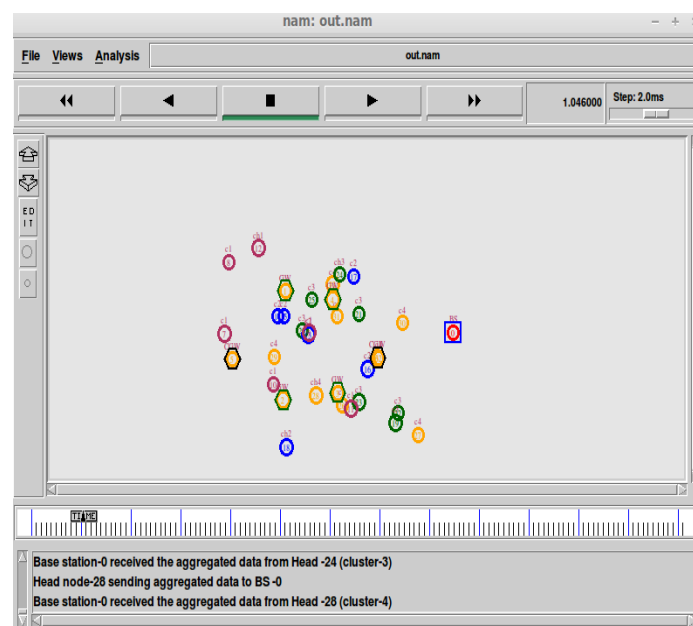


Fig 3 Communication between nodes and base station

The above scenario shows the sending of aggregated data from head node to the base station.

Scenario 2:

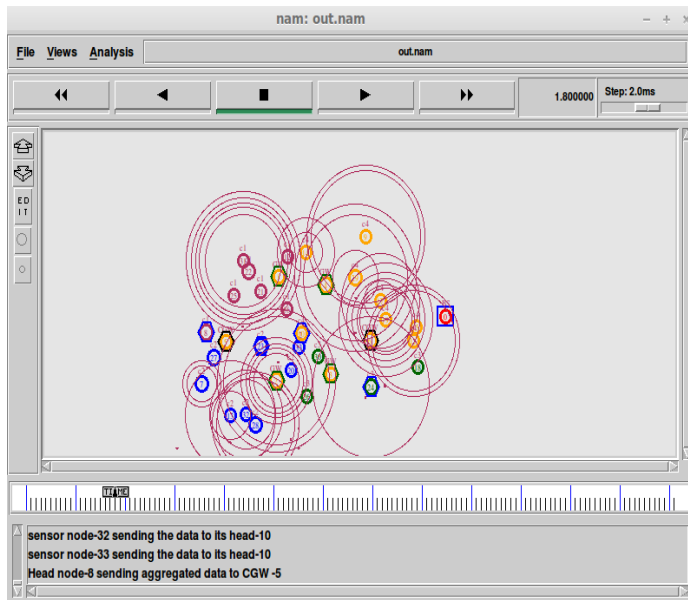


Fig 4 Communication between node and cluster head

The above scenario shows sending message between sensor node 32 to cluster head 10

Scenario 3:

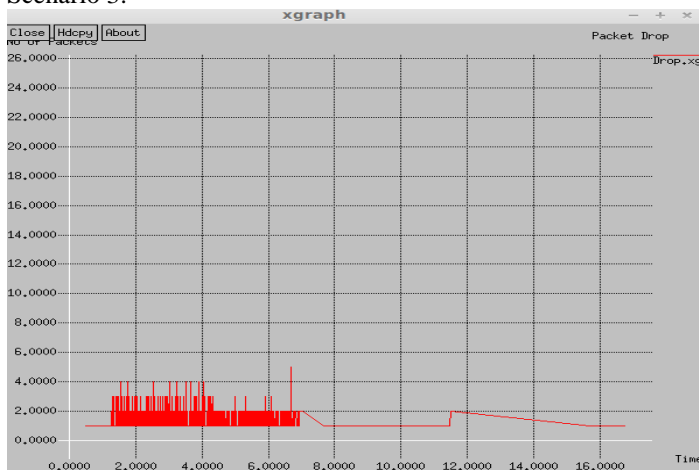


Fig 6 Packet drop

The above scenario shows the drop of packet graph

## V. RESULTS AND CONCLUSION

The Proposed System is a System which uses the particle swarm optimization heuristic algorithm to select the Cluster heads in various clusters formed by the large number of nodes. The cluster heads are selected based on the factors such as Energy, Density and Mobility. The node with the highest energy, density and lowest mobility is elected as the cluster head for that particular cluster and the nodes in that cluster gets informed about the cluster head. The nodes will collect the data from the deployed region and forward the data to the cluster head instead of base station and further the data is aggregated by the cluster head from all the nodes of that cluster and forwarded to the base station through the Gateways. The following are some of the advantages of the proposed system, Simple to understand and implement, Convergence at the faster rate, Adaptive towards the failure of any sensor node in the network. In future scope this system can also be implemented with ant bee colony technology.

### Acknowledgment

Vishwaja B thanks to Mrs. Geetha, who is always encouraging and motivating me to do research activities. I am also very thankful to my families and friends.

## REFERENCES

- [1] C. Y. Chong and S. P. Kumar, "Sensor networks: Evolution, opportunities, and challenges," *Proc. IEEE*, vol. 91, no. 8, pp. 1247–1256, Aug. 2003.
- [2] K. Sohraby, D. Minoli, and T. F. Znati, *Wireless Sensor Networks: Technology, Protocols, and Applications*. Hoboken, NJ, USA: Wiley, 2007.
- [3] S. Tilak, N. B. Abu-Ghazaleh, and W. R. Heinzelman, "A taxonomy of wireless micro-sensor network models," *Mobile Comput. Commun. Rev.*, vol. 6, no. 2, pp. 28–36, 2002.
- [4] J. Porter, P. Arzberger, H. Braun, P. Bryant, S. Gage, T. Hansen, P. Hanson, C. Lin, F. Lin, T. Kratz, W. Michener, S. Shapiro, and T. Williams, "Wireless sensor networks for ecology," *BioScience*, vol. 55, pp. 561–572, 2005.
- [5] A. Cerpa, J. Elson, D. Estrin, L. Girod, M. Hamilton, and J. Zhao, "Habitat monitoring: Application driver for wireless communications technology," in *Proc. ACM SIGCOMM Workshop Data Commun. Latin Amer. Carib.*, 2001, pp. 20–41.
- [6] A. Mainwaring, J. Polastre, R. Szewczyk, and D. Culler, "Wireless sensor networks for habitat monitoring," in *Proc. 1st ACM WSNA*, 2002, pp. 88–97.
- [7] E. Biagioni and K. Bridges, "The application of remote sensor technology to assist the recovery of rare and endangered species," *Int. J. High Perform. Comput. Appl.*, vol. 16, no. 3, pp. 315–324, 2002.
- [8] S. L. Collins, L. M. A. Bettencourt, A. Hagberg, R. F. Brown, D. I. Moore, G. Bonito, K. A. Delin, S. P. Jackson, D. W. Johnson, S. C. Burleigh, R. R. Woodrow, and J. M. McAuley, "New opportunities in ecological sensing using wireless sensor networks," *Frontiers Ecol. Environ.*, vol. 4, no. 8, pp. 402–407, 2006.
- [9] K. Martinez, J. K. Hart, and R. Ong, "Environmental sensor networks," *Computer*, vol. 37, pp. 50–56, 2004.
- [10] F. Al-Turjman, H. Hassanein, and M. Ibnkahla, "Connectivity optimization with realistic lifetime constraints for node placement in environmental monitoring," in *Proc. 34th IEEE LCN*, Oct. 2009, pp. 617–624.
- [11] F. Al-Turjman, H. Hassanein, and M. Ibnkahla, "Connectivity optimization for wireless sensor networks applied to forest monitoring," in *Proc. IEEE ICC*, Jun. 2009, pp. 1–6.
- [12] J. K. Hart and K. Martinez, "Environmental sensor networks: A revolution in the earth system science?," *Earth-Sci. Rev.*, vol. 78, no. 3–4, pp. 177–191, 2006.
- [13] P. W. Rundel, E. A. Graham, M. F. Allen, J. C. Fisher, and T. C. Harmon, "Environmental sensor networks in ecological research," *New Phytologist*, vol. 182, no. 3, pp. 589–607, 2009. [14] L. Selavo, A. Wood, Q. Cao, T. Sookoor, H. Liu, A. Srinivasan, Y. Wu, W. Kang, J. Stankovic, D. Young, and J. Porter, "Luster: Wireless sensor network for environmental research," in *Proc. 5th SenSys*, 2007.